FINAL REPORT

RADAR TARGET DISCRIMINATION AND IDENTIFICATION USING EXTINCTION-PULSES AND SINGLE-MODE EXTRACTION PULSES

Contract No. N00014 37-K-0336

Reporting Period: June 1, 1987 to January 31, 1991

Prepared for

Office of Naval Research
Defense Advanced Research Projects Agency
Office of Naval Technology

Prepared by

Kun-Mu Chen, Co-principal Investigator
Dennis P. Nyquist, Co-principal Investigator
Edward J. Rothwell, Co-principal Investigator

Division of Engineering Research
College of Engineering
Michigan State University
East Lansing, MI 48824

REPORT DOCUMENTATION PAGE

a. REPORT SECURITY CLASSIFICATION Unclassified	1b RESTRICTIVE MARKINGS N/A
a. SECURITY CLASSIFICATION AUTHORITY N/A	3 DISTRIBUTION / AVAILABILITY OF REPORT Approved for public release distribution unlimited.
b. DECLASSIFICATION / DOWNGRADING SCHEDULE N/A	
. PERFORMING ORGANIZATION REPORT NUMBER(S) N/A	5. MONITORING ORGANIZATION REPORT NUMBER(S)
a. NAME OF PERFORMING ORGANIZATION Division of Engr. Research Michigan State University 6b. OFFICE SYMBOL (If applicable)	7a. NAME OF MONITORING ORGANIZATION Office of Naval Research and Office of Naval Technology
ic. ADDRESS (City, State, and ZIP Code) East Lansing, MI 48824-1226	7b. ADDRESS (City, State, and ZIP Code) Electronics Division (Code 1114) Office of Naval Research Arlington, VA 22217-5000
Ja. NAME OF FUNDING / SPONSORING ORGANIZATION Defense Adv. Res. Proj. Agency Office of Naval Technology 8b. OFFICE SYMBOL (If applicable) DARPA & ONT	9. PROCUREMENT INSTRUMENT IDENTIFICATION NUMBER N00014-87-K-0336
ic. ADDRESS (City, State, and ZIP Code) DARPA, 1400 Wilson Blvd., Arlington, VA 22209 ONT, 800 N. Quincy St., Arlington, VA 22217	10. SOURCE OF FUNDING NUMBERS PROGRAM ELEMENT NO. / PROJECT NO. / TASK NO. / WORK UNIT ACCESSION NO.

11. TITLE (Include Security Classification)
Radar target discrimination and identification using Extinction-pulses and Single-mode extraction pulses

12. PERSONAL AUTHOR(S)
Kun-Mu Chen, Dennis Nyquist and Edward Rothwell

13a. TYPE OF REPORT	13b. TIME COVERED	14. DATE OF REPORT (Year, Month, Day)	15. PAGE COUNT
Final	FROM 6/1/87 TO 1/31/91	1991,1,31	234

16. SUPPLEMENTARY NOTATION

17. COSATI CODES			18 SUBJECT TERMS (Continue on reverse if necessary and identify by block number)
FIELD	GROUP	SUB-GROUP	Radar target discrimination and identification, Natural frequencies, E/S pulse technique, aspect-independence

19 ABSTRACT (Continue on reverse if necessary and identify by block number)

The goal of this research program is to develop an efficient new radar target discrimination and identification scheme based on the natural frequencies of the target. It consists of synthesizing aspect-independent discriminant signals including Extinction-pulse (E-pulses) and Single-mode extraction pulses (S-pulses) which, when convolved numerically with late-time transient response of an expected target, lead to zero or single-mode responses. When the synthesized discriminant signals for an expected target are convolved with the radar return from a different target, the resulting signals will be significantly different from the expected zero or single-mode responses, thus, the differing targets can be discriminated.

Major achievements on various topics under this research program are described in this report.

20 DISTRIBUTION / AVAILABILITY OF ABSTRACT ☒ UNCLASSIFIED/UNLIMITED ☐ SAME AS RPT ☐ OTIC USERS	21 ABSTRACT SECURITY CLASSIFICATION Unclassified
22a. NAME OF RESPONSIBLE INDIVIDUAL Dr. Rabinder Madan, Mr. James K. Hall	22b TELEPHONE (Include Area Code) (202)696-4217(202) 696-
	22c. OFFICE SYMBOL ONR (code 1114)

Table of Contents

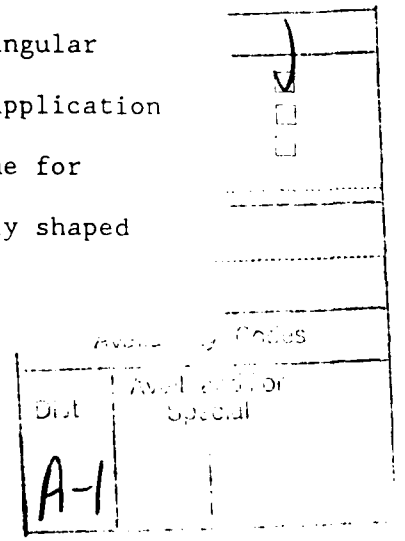

1. Introduction

This is the final report on the research program on "Radar Target Discrimination and Identification Using Extinction-Pulses and Single-Mode Extraction Pulses," supported by Defense Advanced Research Projects Agency, Office of Naval Research and Office of Naval Technology under Contract N00014-87-K-0336. This program was initiated on June 1, 1987 and ended on January 31, 1991.

The goal of this research program is to develop an efficient new radar target discrimination and identification scheme based on the natural frequencies of the target. It consists of synthesizing aspect-independent discriminant signals including Extinction-pulses (E-pulses) and Single-mode extraction pulses (S-pulses) which, when convolved numerically with late-time transient response of an expected target, lead to zero or single-mode responses. When the synthesized discriminant signals for an expected target are convolved with the radar return from a different target, the resulting signals will be significantly different from the expected zero or single-mode responses, thus, the differing targets can be discriminated.

In this program, we have firmly established the feasibility and efficiency of this E/S pulse scheme through experimental and theoretical studies. The unique characteristics of this scheme, the aspect-independence and noise-insensitivity, have been demonstrated. The scheme was also found to have potentiality of detecting and identifying low observable targets and rotating targets such as helicopters. For this program we have constructed new experimental facilities which include a new ground-plane time-domain scattering range and a new free-field anechoic chamber scattering range. These scattering ranges covering an area of 100' x 50' were constructed in a new Electromagnetics Laboratory in a newly built Engineering Research Complex. These scattering ranges have produced many good experimental results. We are now probably one of the few universities that are equipped with both types of scattering ranges.

We will describe in this report major accomplishments of this research program. They are (1) theory of E/S pulse techniques, (2) ground-plane time-domain scattering range, (3) free-field anechoic chamber scattering range, (4) noise-insensitivity of the E/S pulse scheme, (5) discrimination of helicopters with the E/S pulse scheme, (6) detection and identification of low observable targets, (7) effect of aspect variation on multi-pulse coherent processing, (8) discrimination of multiple targets in the same range cell, and (9) power

requirement for a pulsed radar system.

Some reprints of published papers and some preprints of submitted papers reporting details of various topics studied under this research program are included in Appendices. A list of publications and personnel participated in this research are also included.

2. Theory for E/S-pulse technique

In its broadest definition, an extinction pulse is a waveform of finite duration T_e which, upon interaction with a particular target, eliminates from its induced current, charge or scattered field response a preselected portion of the target's natural mode spectrum. If the remaining portion is a single damped sinusoid, the E-pulse is termed a "single-mode extraction signal" or "S-pulse".

Synthesis conditions for the E-pulse waveform can be easily established. The scattered field response of a conducting object can be written in the late-time as a sum of damped sinusoids

$$r(t) = \sum_{n=1}^{N} a_n e^{\sigma_n t}\cos(\omega_n t+\phi_n) \qquad t > T_L \tag{1}$$

where T_L is the beginning of the late-time response, a_n and ϕ_n are the aspect dependent amplitude and phase of the nth mode, $s=\sigma+j\omega$, and only N modes are assumed excited by the incident field waveform. The convolution of an E-pulse waveform e(t) with the above response is given by

$$c(t) = \sum_{n=1}^{N} a_n|E(s_n)|e^{\sigma_n t}\cos(\omega_n t+\psi_n) \tag{2}$$

where Ψ_n is dependent on e(t) and

$$E(s) = L\{e(t)\} = \int_0^{T_e} e(t)\,e^{-st}dt \tag{3}$$

is the Laplace transform of the E-pulse. Constructing an E-pulse to produce a null late-time convolved response, c(t)=0, is seen to require

$$E(s_n) = E(s_n^*) = 0 \tag{4}$$

In other words, the E-pulse must have zero spectral energy at the natural frequencies in the target response. A single mode extraction signal necessitates

$$E(s_n) = E(s_n^*) = 0 \qquad 1\le n\le N, \quad n\neq m \tag{5}$$

to leave the mth mode "unextinguished" in the convolved response. Alternatively, the conditions (5) can be applied along with

$$E(s_m) = E(s_m^*) \tag{6}$$

to give a "cosine" S-pulse or with

$$E(s_m) = -E(s_m^*) \tag{7}$$

to give a "sine" S-pulse.

To implement the above synthesis requirements, the E-pulse is represented as

$$e(t) = e^f(t) + e^e(t) \tag{8}$$

where $e^f(t)$ is a forcing component which excites the target's response, and $e^e(t)$ is an extinction component which extinguishes the response due to $e^f(t)$. The forcing component is chosen freely, while the extinction component is expanded in a set of basis functions

$$e^e(t) = \sum_{m=1}^{M} \alpha_m f_m(t) \tag{9}$$

and the synthesis conditions are applied. For an E-pulse designed to extinguish all the modes of a target response, (4) results in a matrix equation for the basis function amplitudes

$$\begin{bmatrix} F_1(s_1) & F_2(s_2) & \cdots & F_M(s_1) \\ \vdots & \vdots & & \vdots \\ F_1(s_N) & F_2(s_N) & \cdots & F_M(s_N) \\ F_1(s_1^*) & F_2(s_1^*) & \cdots & F_M(s_1^*) \\ \vdots & \vdots & & \vdots \\ F_1(s_N^*) & F_2(s_N^*) & \cdots & F_M(s_N^*) \end{bmatrix} \begin{bmatrix} \alpha_1 \\ \alpha_2 \\ \vdots \\ \alpha_M \end{bmatrix} = - \begin{bmatrix} E^f(s_1) \\ \vdots \\ E^f(s_N) \\ E^f(s_1^*) \\ \vdots \\ E^f(s_N^*) \end{bmatrix} \tag{10}$$

where

$$F_m(s) = L\{f_m(t)\}$$
$$E_f(s) = L\{e^f(t)\} \qquad (11)$$

and M=2N is chosen to make the matrix square. Note that if a DC offset artifact is present in the measured response the E-pulse can be synthesized to remove the DC by demanding, in addition to the above requirements, E(s=0)=0.

The matrix equation (10) has a solution for any choice of E-pulse duration. However, for some choices of T_e the determinant of the matrix vanishes and (1) has a solution only if $e^f(t)=0$. This type of E-pulse is termed a "natural" E-pulse, while all others are called "forced" E-pulses.

A variety of basis functions have been used in the expansion (8), including delta-functions, Fourier cosines, damped sinusoids and polynomials. While each choice has its own important motivation, perhaps the most versatile expansion is in terms of subsectional basis functions

$$f_m(t) = \begin{cases} g(t-[m-1]\Delta) & (m-1)\Delta \le t \le m\Delta \\ 0 & \text{elsewhere} \end{cases} \qquad (12)$$

so that $T_e=2N\Delta$ and

$$F_m(s) = F_1(s)\, e^{s\Delta}\, Z^m \qquad (13)$$

where

$$Z = e^{-s\Delta} \qquad (14)$$

giving a matrix of the Vandermonde type. The determinant of this matrix is zero when

$$\Delta = \frac{p\pi}{\omega_k} \qquad p=1,2,3,\ldots, \quad 1\le k\le N \qquad (15)$$

revealing that the duration of a natural E-pulse is only dependent upon the imaginary part of one of the natural frequencies. The minimum natural E-pulse duration is just

$$T_e = 2N\frac{\pi}{\omega_{max}} \qquad (16)$$

where ω_{max} is the la st radian frequency among the modes.

The proper cho e of T_e in the synthesis of an E-pulse is critical to its performance. Empirical results show that if T_e is chosen to be less than the minimum natural E-pulse duration (16) the resulting E-pulse waveform is highly oscillatory with a majority of its energy above ω_{max} and poor results are obtained in the presence of random noise.

Discrimination among radar targets is based upon the ability to differentiate the convolution of the correct E-pulse with a measured target waveform from the myriad of other convolutions. As the number of prospective targets becomes large, a visual inspection of the convolved outputs becomes more subjective, and eventually impractical. A scheme has therefore been devised to automate the discrimination decision.

Ideally, if the E-pulse convolutions were uncorrupted, the energy ratio

$$E = \frac{\int_{T_{LES}}^{T_{LEE}} c^2(t)\,dt}{\int_{0}^{T_e} e^2(t)\,dt} \qquad (17)$$

would be zero only for the correct E-pulse. Here c(t) is the convolution of the E-pulse e(t) with the measured response, and T_{LES} is the earliest time at which the unknown target convolution is certain to be a unique series of natural modes

$$T_{LES} = T_e + 2T_r \qquad (18)$$

where T_r is the one-way transit time of the largest dimension of the target corresponding to the E-pulse. (The largest dimension must be used unless the target aspect is known.) The end of the energy window, T_{LEE}, is chosen so that the window width, T_{LEE}-T_{LES}, is the same for all convolutions.

If the convolutions are corrupted with noise, the convolution with the smallest energy ratio corresponds to the correct target. The difference in dB between the smallest energy ratio and the next smallest gives a measure of the confidence of the discrimination decision, and is called the "E-pulse discrimination ratio" (EDR).

A similar approach can be applied to discrimination based on S-pulse waveforms. Here a discrimination decision is based on recognizing a pure single mode signal among a multitude of multi-mode signals.

Consider the convolution of an S-pulse with a return from the expected target. During a finite time period between the onset of late-time and the end of the measured return the convolved output will be a single damped sinusoid of unknown amplitude and phase (depending on target aspect) but known complex frequency. Using the outlined synthesis scheme it is possible to create both sine and cosine S-pulses which result in output convolutions $c_c(t)$ and $c_s(t)$ with identical unknown amplitudes and unknown phases differing by 90°

$$\begin{aligned} c_c(t) &= Ae^{\sigma_o t}\cos(\omega_o t+\psi) \\ c_s(t) &= Ae^{\sigma_o t}\sin(\omega_o t+\psi) \end{aligned} \tag{19}$$

which can be combined to form the complex exponential

$$C(t) = c_c(t) - jc_s(t) = Ae^{-j\psi}e^{\sigma_o t}e^{-j\omega_o t} \tag{20}$$

These outputs are analyzed for expected single-mode content in an approach inspired by the matched filtering concept. Define the S-Pulse energy ratio

$$E = \frac{\left[\int_{-\infty}^{\infty}|C(\omega)||F(\omega)|\,d\omega\right]^2}{\int_{-\infty}^{\infty}|C(\omega)|^2\,d\omega \int_{-\infty}^{\infty}|F(\omega)|^2 d\omega}$$

where $C(\omega)$ is the Fourier spectrum (obtained via the FFT) of $C(t)$, and $F(\omega)$ is the analytic spectrum of the expected complex exponential, taken over the same finite time interval. It is apparent that the energy ratio takes on a maximum of unity when the convolved output matches the expected signal. Thus, if the convolutions are corrupted with noise, the ratio closest to unity corresponds to the correct target. The difference in dB between the energy ratio closest to unity and the ratio next closest gives a measure of the confidence of the discrimination decision, and is called the "S-pulse discrimination ratio" (SDR).

Note that the unknown phase of the convolved output is inconsequential since only the spectral magnitude is involved.

Finally, the results from E-pulse and S-pulse discrimination can be combined into an overall confidence ratio DR=EDR(dB)+SDR(dB).

3. Ground-plane time-domain scattering range.

The layout of the ground-plane time-domain scattering range and the free-field anchoic chamber scattering range is shown schematically in Fig. 1. These two scattering ranges are located adjacent to each other and the arrangement of other instrumentations including a pulse generator, a sampling oscilloscope and a computer system are also depicted in Fig. 1.

The ground-plane time-domain scattering range implements antennas and target models imaged on a 20 by 32 ft. ground plane which was assembled from 4 by 8 ft. modules. A large monoconical antenna, with height 2.4 m, apex angle 16° and characteristic impedance 160 ohms, is used as the transmitting antenna to radiate narosecond EM pulses. A long wire antenna of length 2.4 m and diameter 1/4 inch. is used as the receiving antenna to receive the scattered fields form the targets. It is noted that a short monopole probe has been used previously as the receiving antenna. The replacement of a short monopole probe with a long wire antenna led to an improvement on the signal to noise ratio of the measured scattered fields from the targets. Scale models of various airplanes have been constructed, and they can be placed at various locations on the ground plane to be illuminated by the EM pulses radiated by the transmitting antenna, and their scattered fields received by the receiving antenna. A narosecond EM pulse generator (Tektronix 109 mercury-switched pulse generator) is used to excite the transmitting antenna. This pulse generator produces pulses of 100 ps risetime and duration between 1ns and 1 μs with amplitudes as great as 500 volts at 1 KHz repetition rate.

The scattered fields or pulse responses from the targets are sampled and measured using a Tektronix 7854 digital waveform processing sampling oscilloscope (DWPSO). The DWPSO automatically acquires and averages multiple target response waveforms, and implements intial signal processing operation such as interpolation, smoothing and integration. An IEEE GPIB interface links the DWPSO with an IBM-AT compatible microcomputer. Software programs executed on the microcomputer transfer data from the DWPSO waveform memories to computer RAM, and subsequently to hard-disk storage. After the measured scattered fields from the targets are transferred from the DWPSO to the computer, they are numerically convolved with the discriminant signals

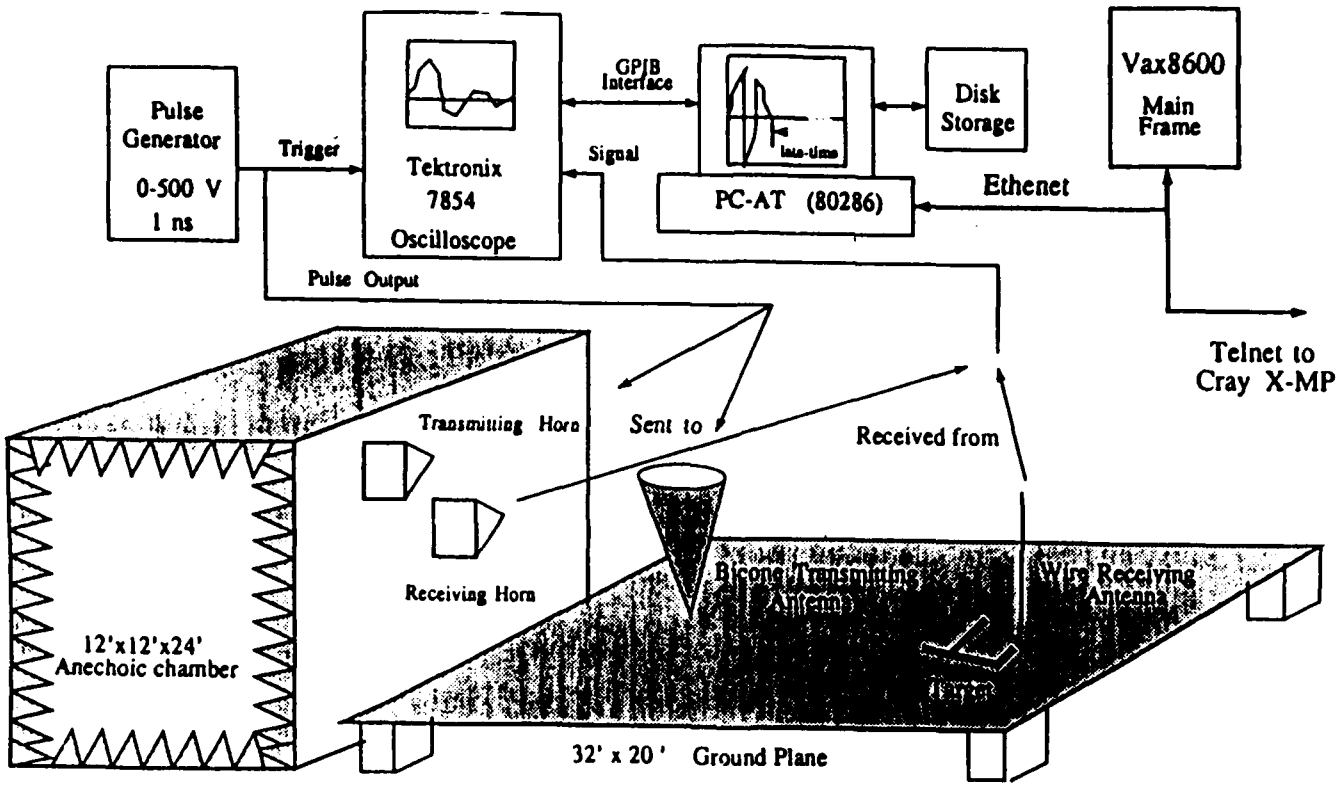

Fig. 1. Two scattering ranges with associated equipment in the Electromagnetics Laboratory of Michigan State University.

of the targets stored in the computer. The convolved outputs are then displayed on the computer monitor.

A photograph of the ground-plane scattering range is shown in Fig. 2. Using this improved ground-plane scattering range, numerous experiments have been conducted and very good results have been obtained. One set of typical results is described here.

We aimed to discriminate and then identify among four different target models; (1) a medium size B707 model of length 33 cm, (2) a medium size T-15 model (home made and arbitrarily named) of length 30 cm, (3) a big B707 model of length 64.5 cm and (4) a big F-18 model of length 72 cm as shown in Fig. 3. The E-pulses of these four models have been synthesized as shown in Fig. 4, and they were stored in the computer. The scattered fields or the pulse responses of these four targets measured at certain aspect angles are shown in Fig. 5. It is observed that these scattered fields consists of large early-time responses followed by oscillatory late-time responses. The shapes of these scattered fields are strongly dependent on the aspect angle and it is impossible to identify the targets from these scattered fields. However, when these scattered fields are convolved with the E-pulses of four different targets in such a way as depicted in Fig. 3, the targets can be easily and clearly identified.

Figure 6 shows the four convolved output signals when the scattered field of the medium B707 model was convolved with four E-pulses of the four different targets. It is observed that the convolved output of this scattered field with E-pulse of the medium B707 model (the same target) give a very small signal (almost a flat line) in the late-time period. On the other hand, the convolved outputs of this scattered field with the E-pulses of three other targets (wrong targets) all give large late-time responses. Thus, it is very easy to identify from these results that the scattered field belongs to the medium B-707 model.

Figure 7 shows the four convolved output signals when the scattered field of the medium T-15 model was convolved with four E-pulses of the four different targets. From the convolved output signal with a very small late-time response (almost a flat line), which is the convolved output of the scattered field with the E-pulse of the medium T-15 model, it is easy to identify that the measured target is the medium T-15 model.

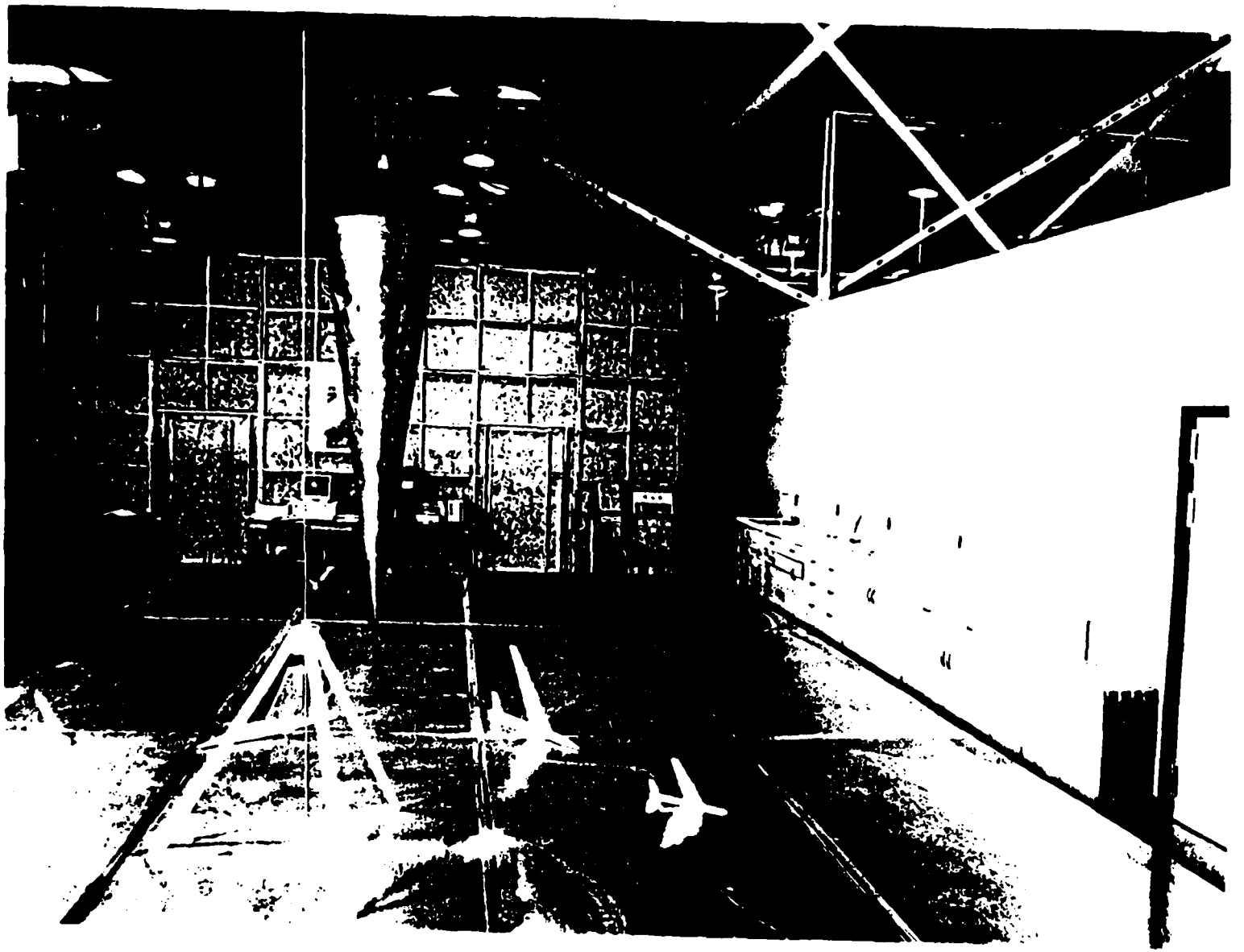

Fig. 2. MSU Ground-plane time-domain scattering range.

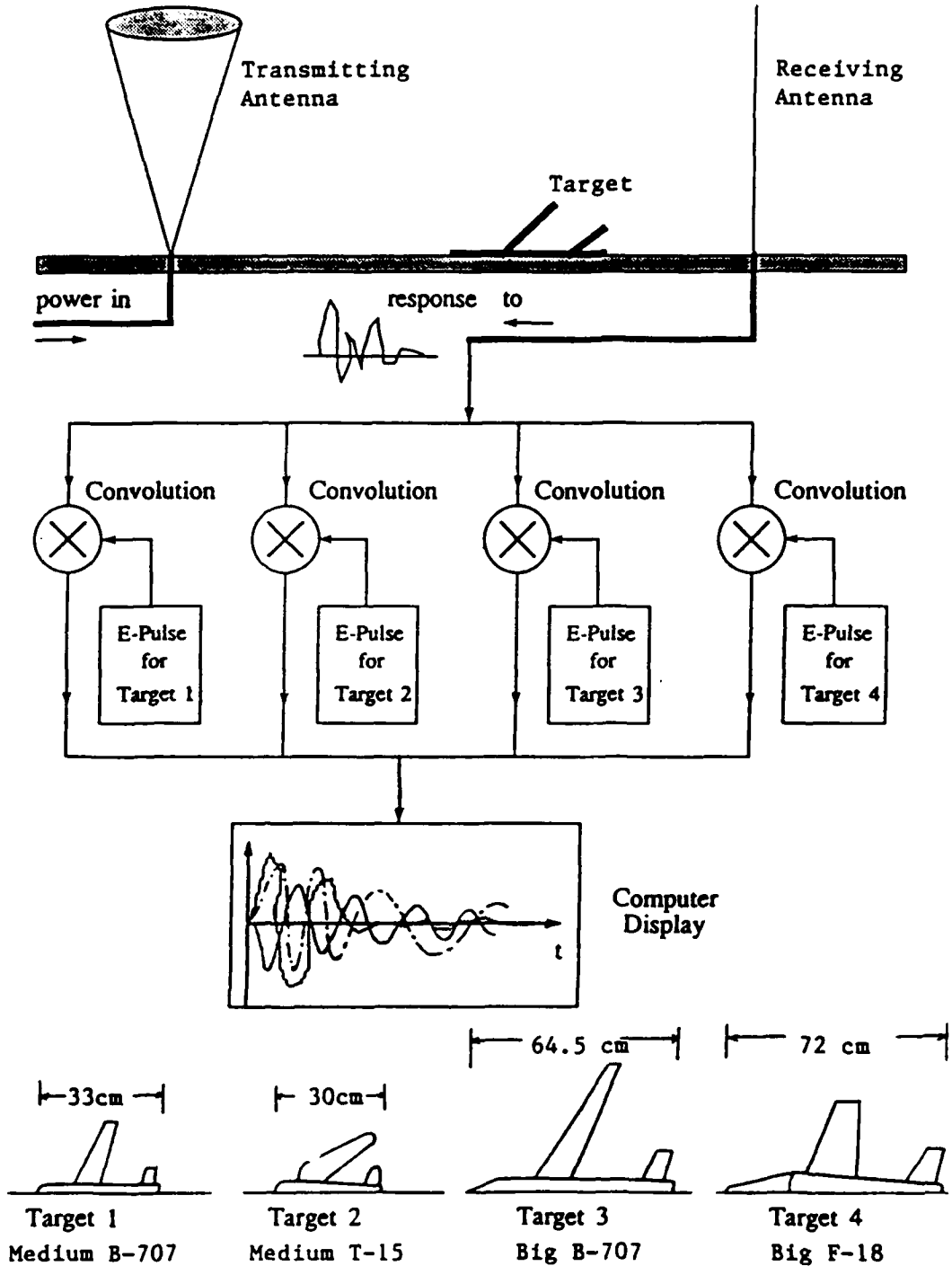

Fig. 3 Convolution process of a target response with the E-pulses of four different target models.

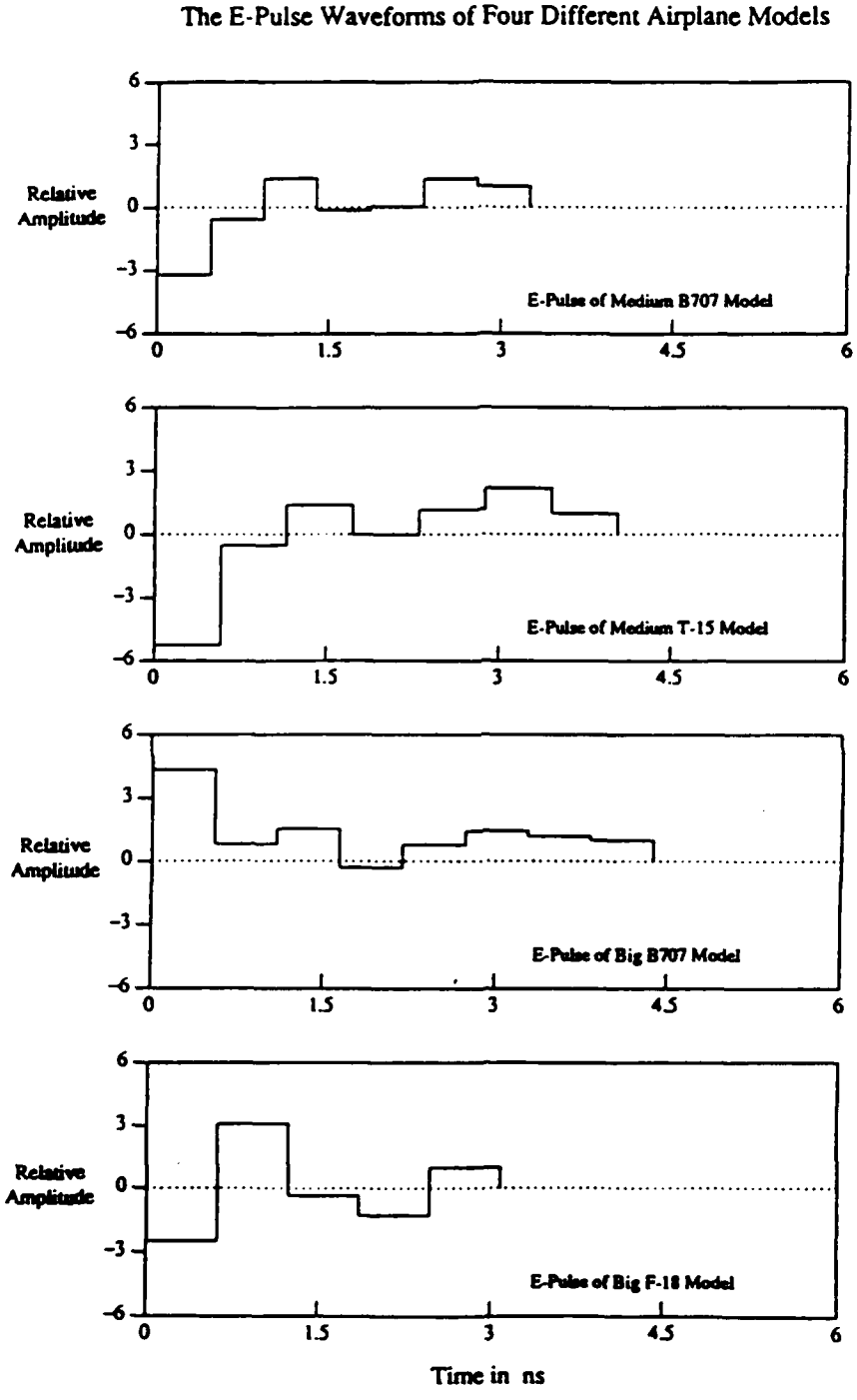

Fig. 4. E-pulses for the four target models: (1) a medium size B-707 model, (2) a medium size T-15 model, (3) a big B-707 model and (4) a big F-18 model.

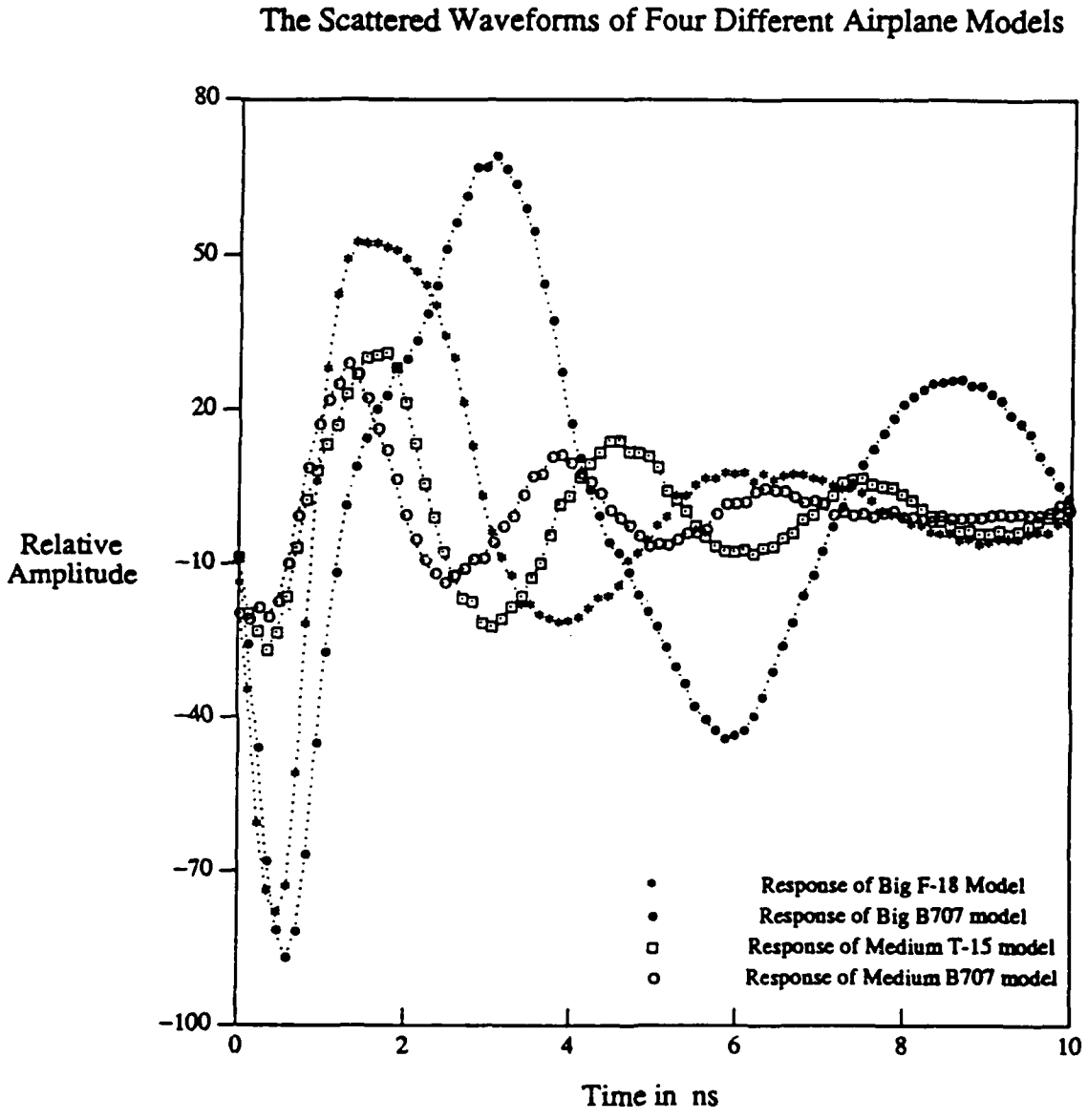

Fig. 5. The scattered fields or the pulse responses of the four target models measured at certain aspect angles.

The Scattered Waveform of Medium B707 Convolved with Different E-Pulses

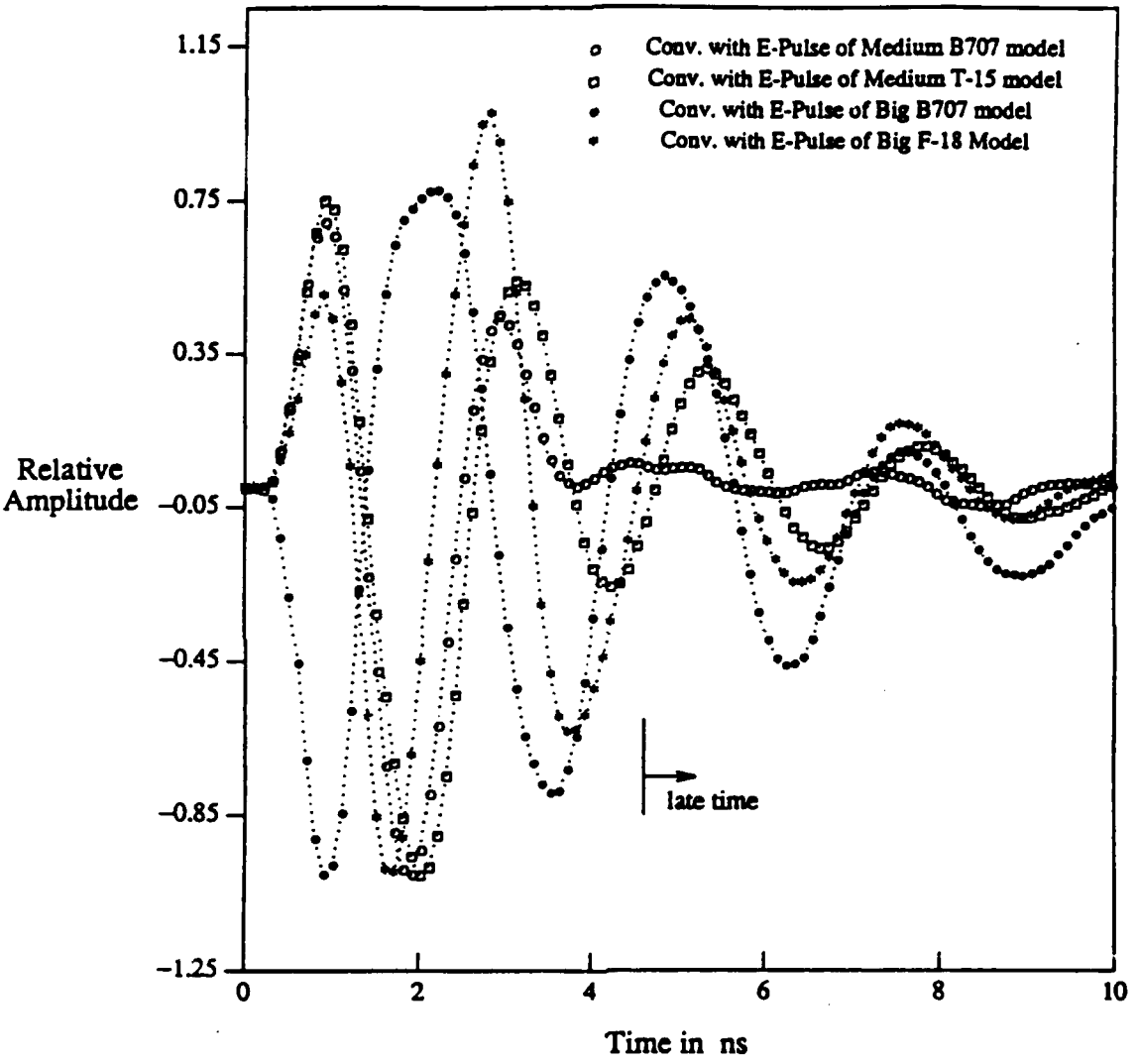

Fig. 6. Convolution of the scattered field of the medium B-707 model with the E-pulses of medium B-707 model, medium T-15 model, big B-707 model and big F-18 model.

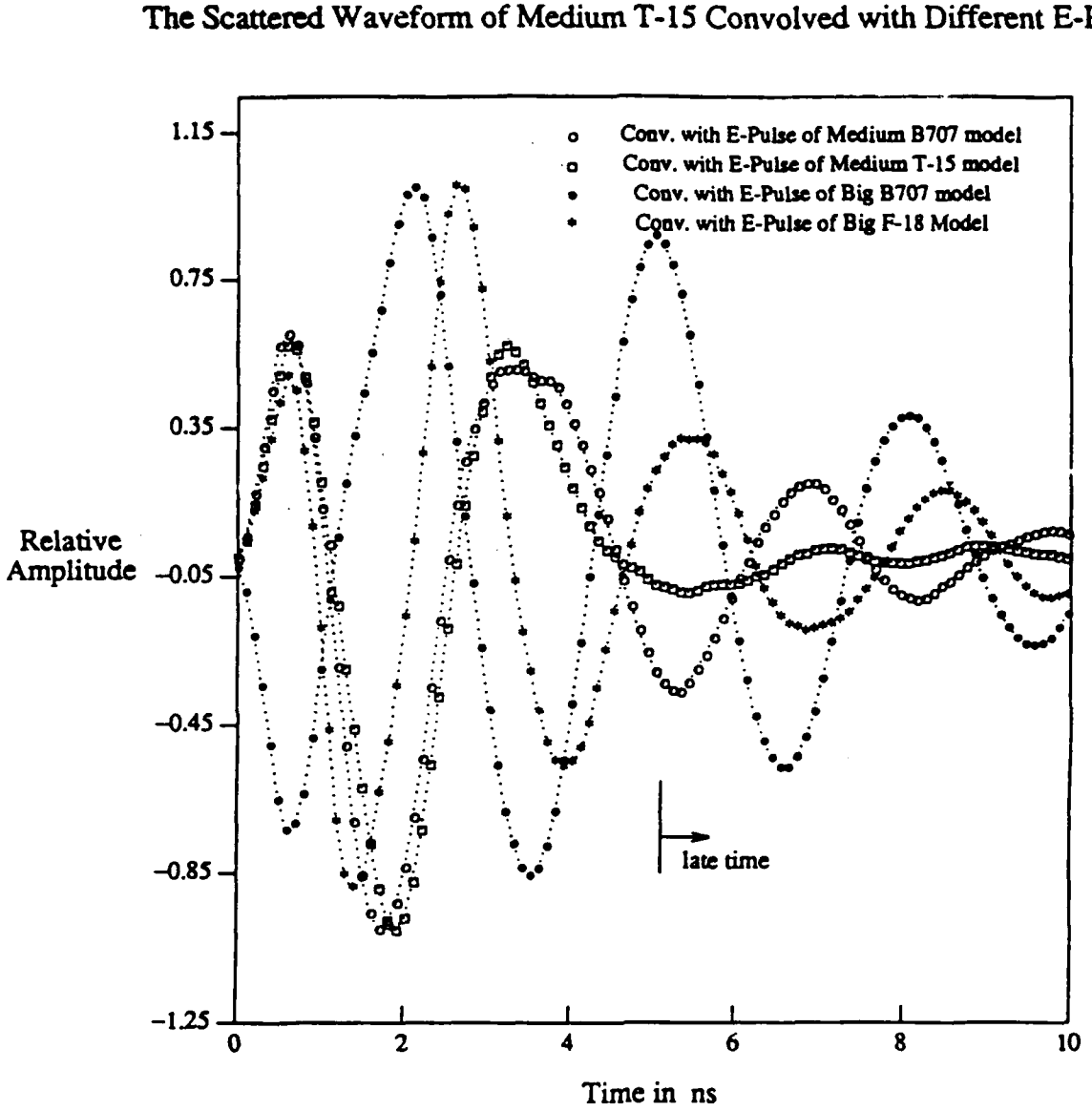

Fig. 7. Convolution of the scattered field of the medium T-15 model with the E-pulses of medium B-707 model, medium T-15 model, big B-707 model and big F-18 model.

Figure 8 shows the four convolved output signals when the scattered field of the Big B-707 model was convolved with the E-pulses of the four different targets. Again it is very easy to identify the target being measured as the big B-707 model from the convolved output of this scattered field with the E-pulse of the big B-707 model. Figure 9 shows the similar results when the scattered field of the big F-18 model was convolved with the E-pulses of the four different targets. From the convolved output signal with a flat late-time response, the target in question can be easily identified as the Big F-18 model.

We believe that these results are very convincing proofs for the feasibility and practicality of our target discrimination and identification scheme.

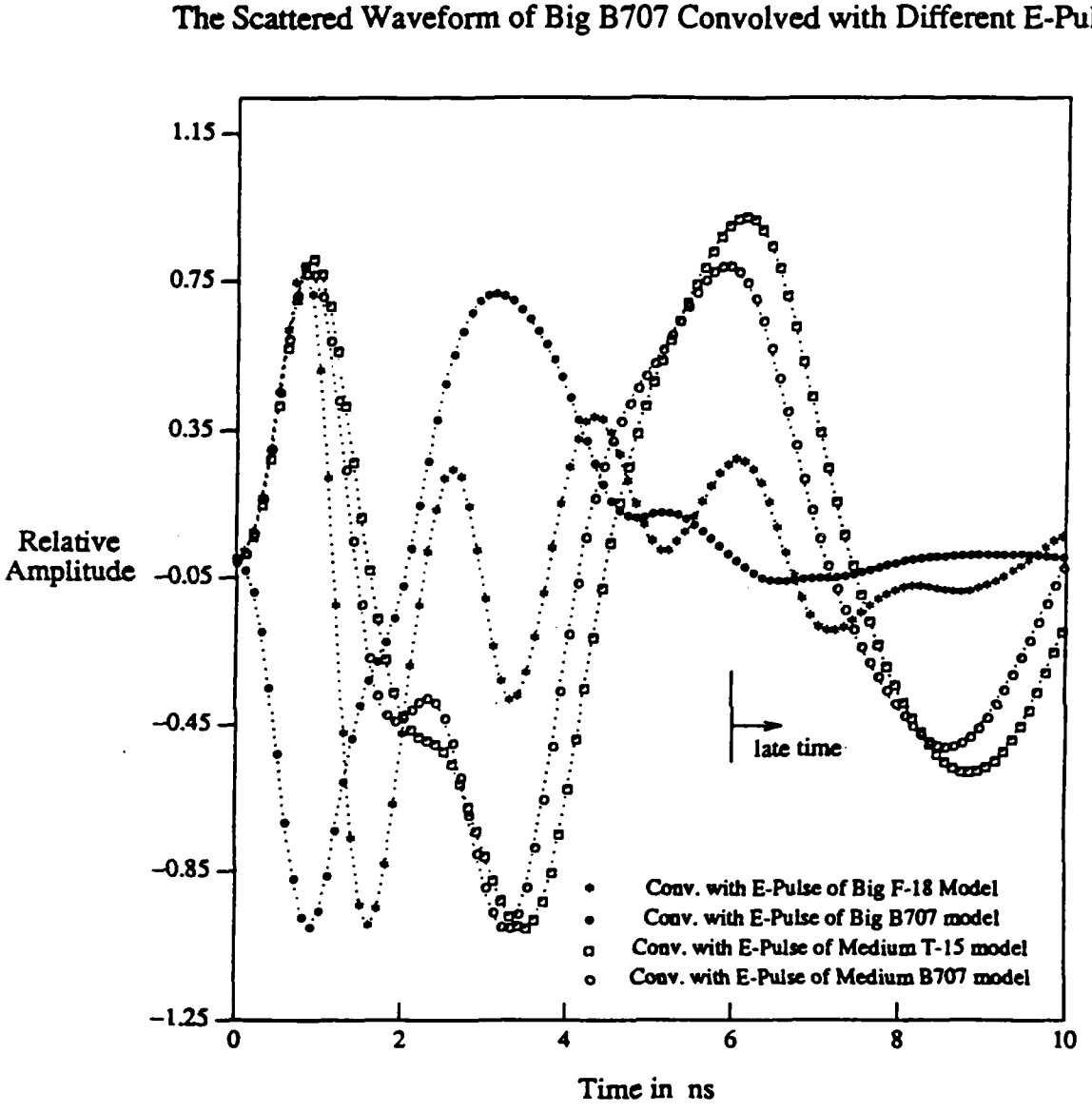

Fig. 8. Convolution of the scattered field of the big B-707 model with the E-pulses of medium B-707 model, medium T-15 model, big B-707 model and big F-18 model.

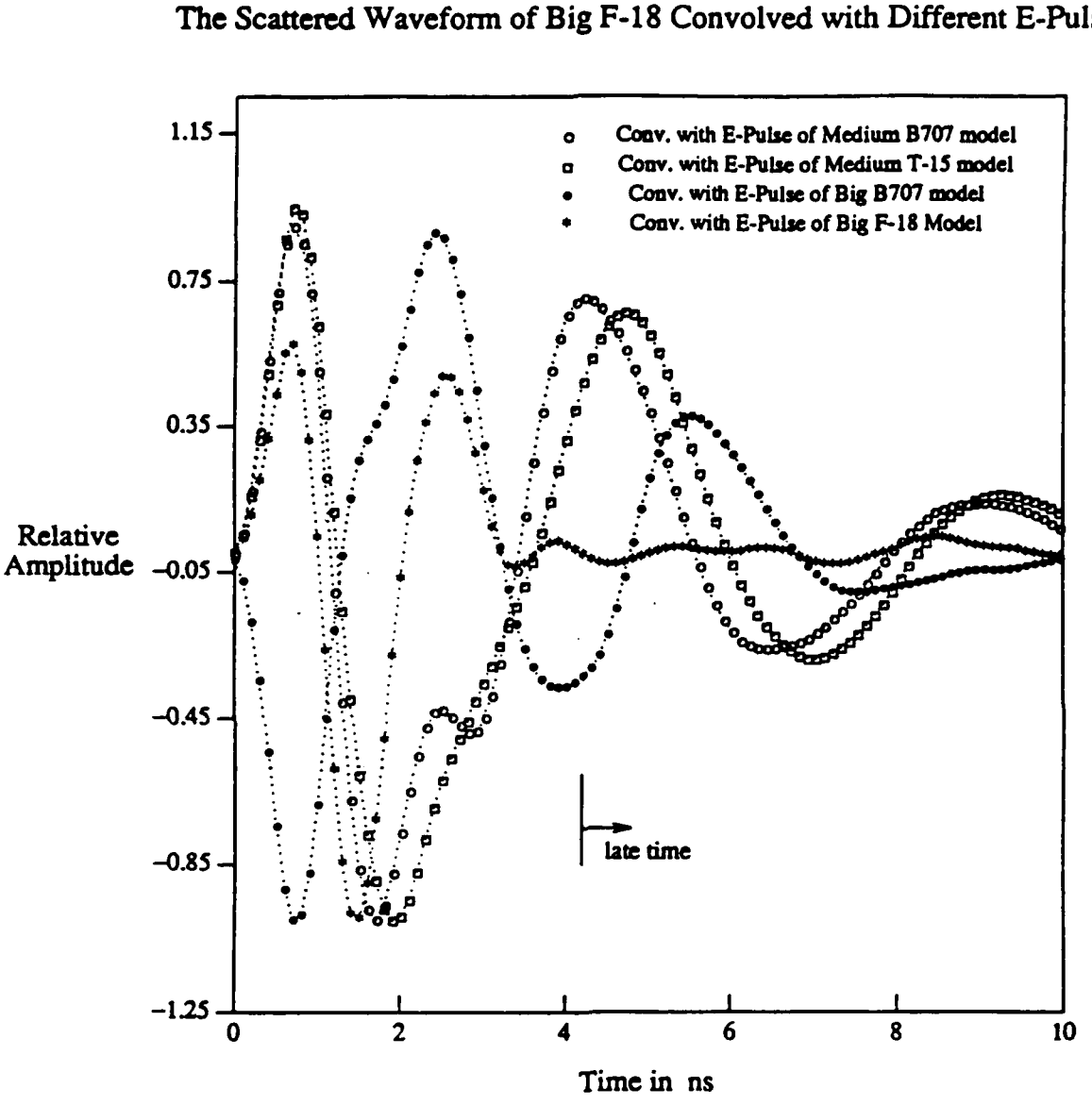

Fig. 9. Convolution of the scattered field of the big F-18 model with the E-pulses of medium B-707 model, medium T-15 model, big B-707 model and big F-18 model.

4. Free-field anechoic chamber scattering range.

A time domain chamber has been recently established at MSU for the purpose of demonstrating the E-pulse technique in a free-field environment. The chamber allows a simulation of the free-space radar environment where realistic scale-model targets can be illuminated at arbitrary aspect and polarization.

Figure 10 shows a schematic diagram of the MSU free field experimental facility. The chamber is 24' long by 12' wide by 12' high and is lined with 12" pyramidal absorber. A pulse generator provides a half nanosecond duration pulse to an American Electronic Laboratories model H-1734 wideband horn (0.5-6 Ghz) which has been resistively loaded to reduce inherent oscillations, and the field scattered from the radar target is received by an identical horn. A microcomputer controls a waveform processing oscilloscope which acquires the received signal and passes it to the computer for processing and analysis.

Accurate discrimination among eight different target models at a variety of aspects has been demonstrated using the free field range. The targets, shown in Figure 11, include simple aluminum models as well as detailed cast-metal models, and range in fuselage length of from six to eighteen inches. Figure 12 shows the responses of the big F-15 and A-10 target models measured at a 45° aspect angle (0° aspect is nose-on to the horn antennas), with the early and late-time portions of the responses indicated. Note that the late-time period begins at different times for the two targets, due to their dissimilar sizes. E-pulse waveforms have been constructed to eliminate all the modes of each target using the E-pulse mode extraction scheme (see Appendix I) with measurements from five different aspect angles. These waveforms are shown in Figure 13.

Discrimination between the big F-15 and the A-10 can be accomplished by convolving the E-pulses with the measured responses, and observing which E-pulse produces the smallest late-time output. First assume the 45° response of the big F-15 is from an unknown target. Figure 14 shows the convolutions of the two E-pulses with the response. Clearly the big F-15 E-pulse produces the smaller late-time signal, and thus the response is identified as coming from a big F-15 aircraft. For the complimentary situation, assume the 45° response of the A-10 is from an unknown target. Figure 15 shows the convolutions of the E-pulses with this response. In this case the A-10 E-pulse produces the smaller late-time signal, indicating the response is from an A-10 aircraft.

It is apparent that discrimination among radar targets is based on the

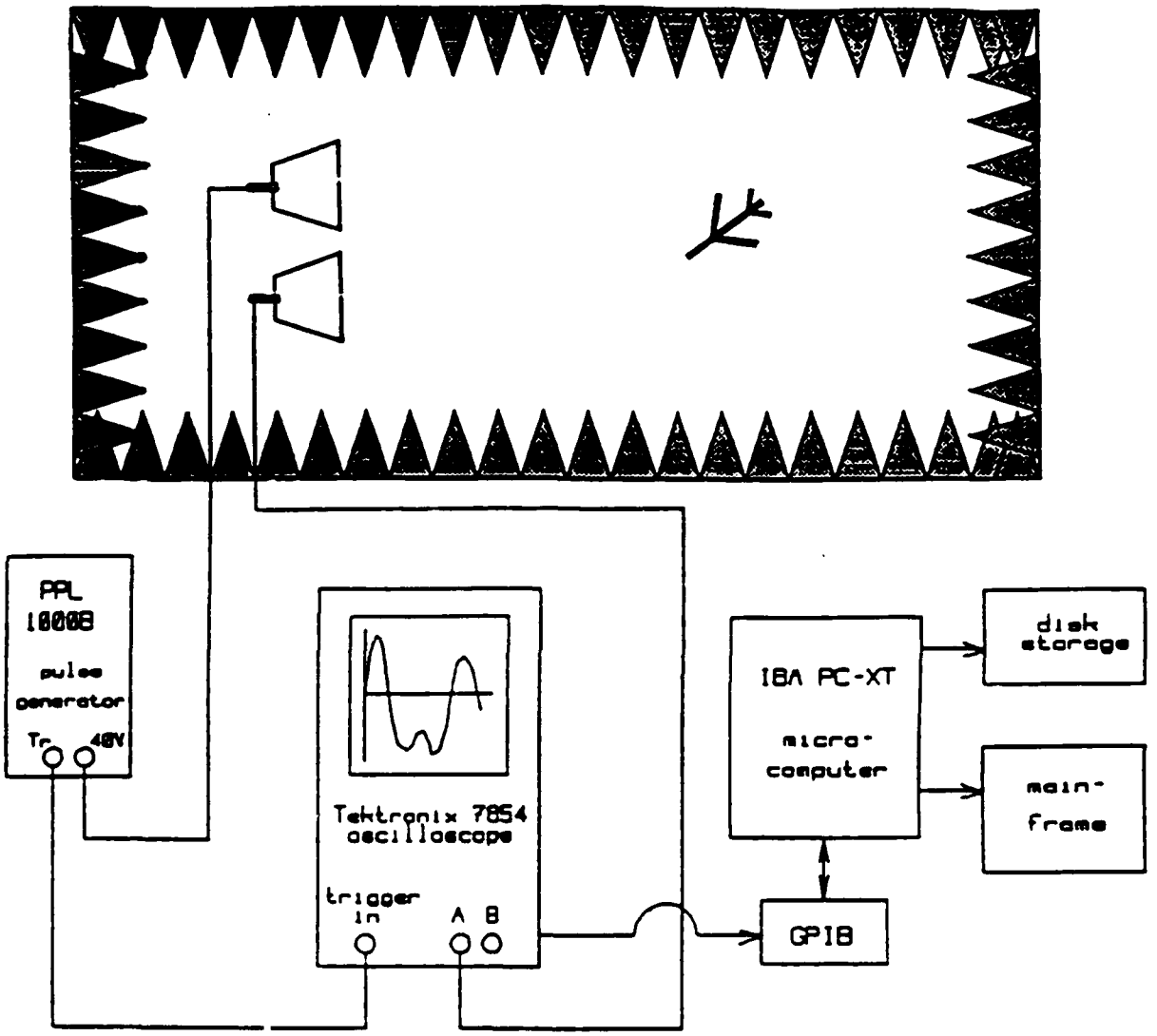

Figure 10 MSU free field experimental facility and associated equipment.

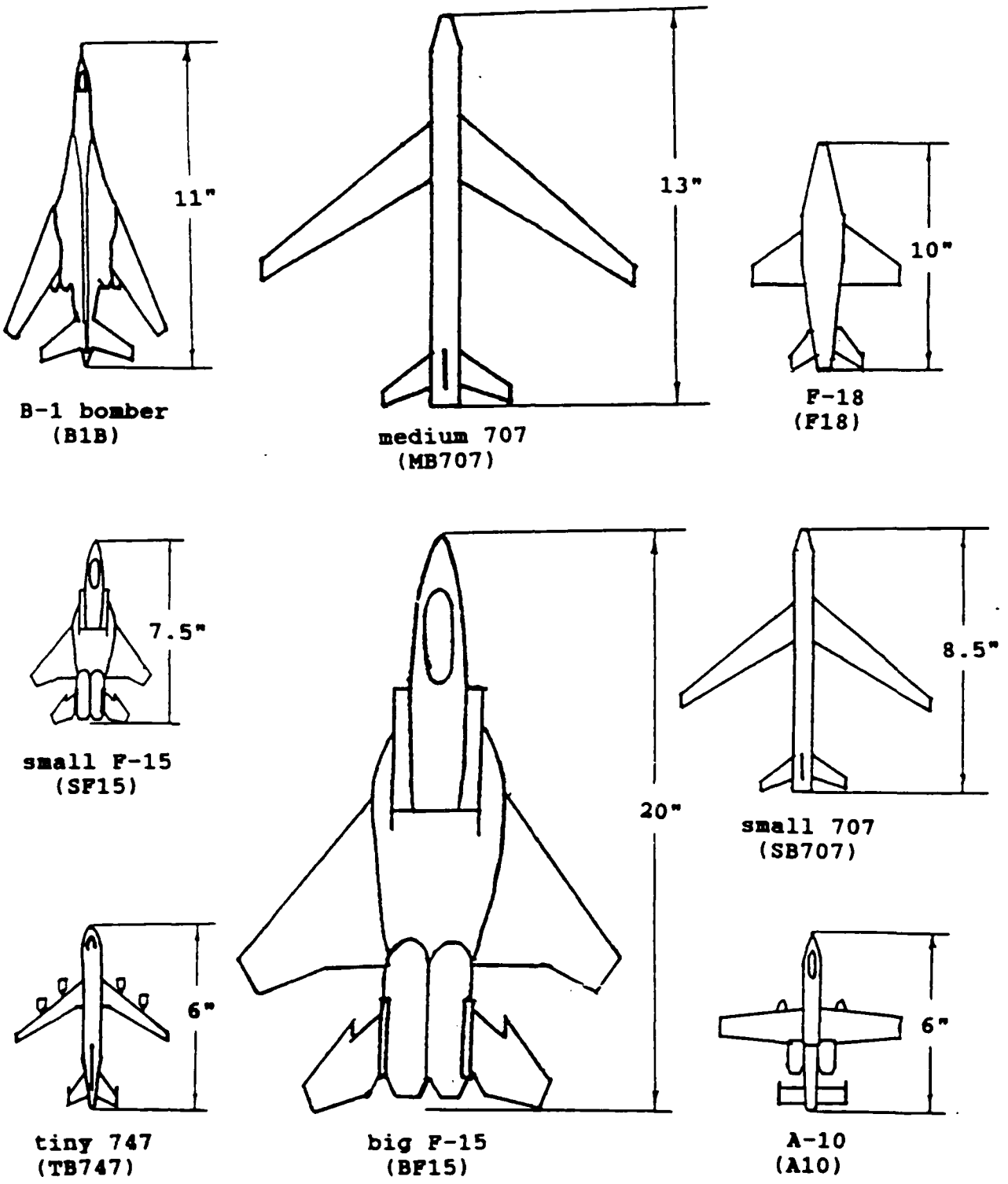

Figure 11. Eight target models used in discrimination experiments in the free-field chamber scattering range.

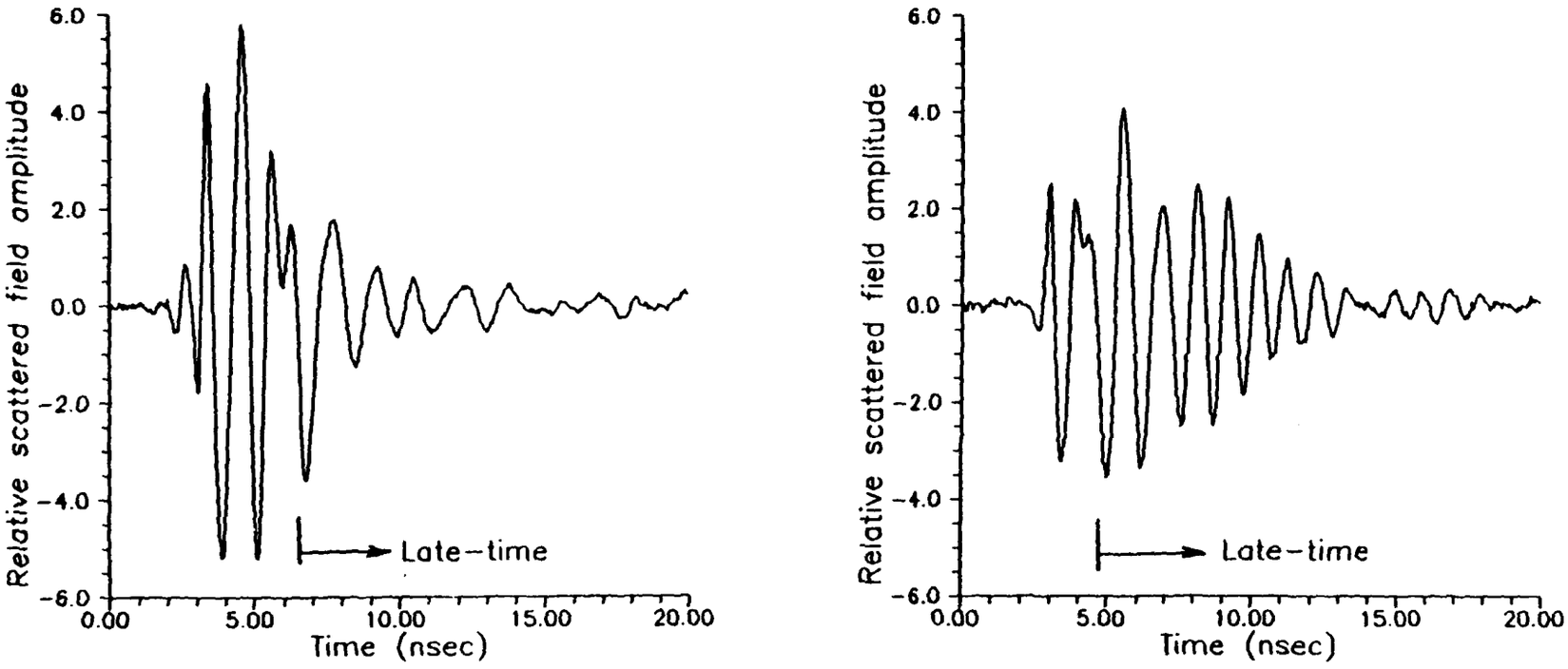

Figure 12. Scattered field pulse responses of (a) big F-15 and (b) A-10 target models measured at 45° aspect.

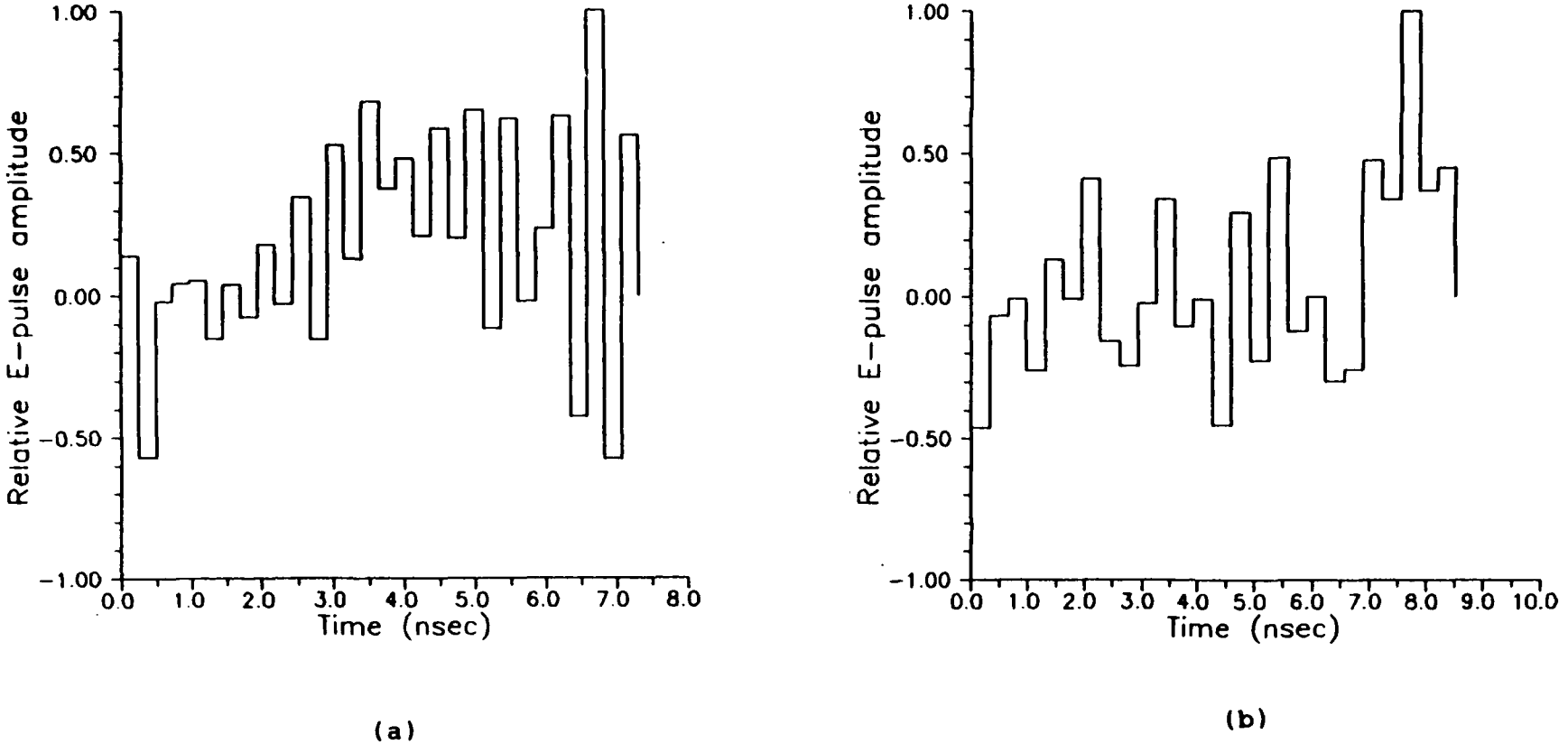

Figure 13. E-pulses constructed to eliminate the modes of the (a) big F-15 and (b) A-10.

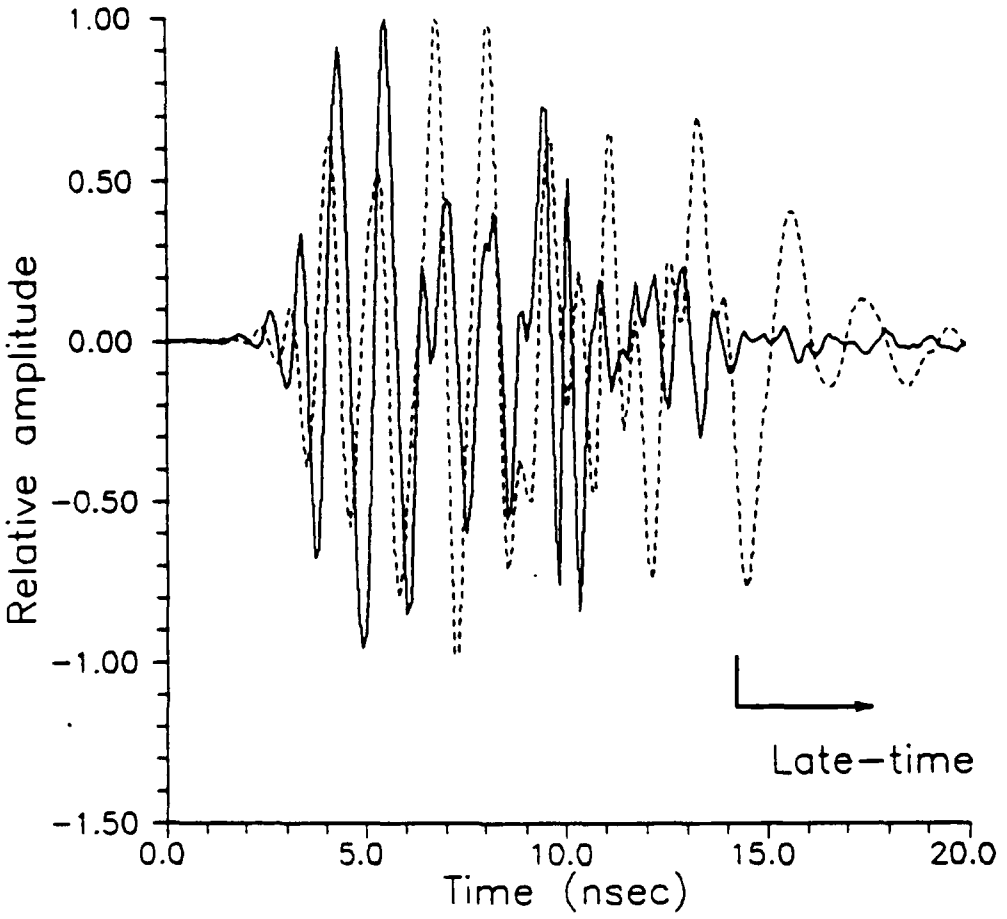

Figure 14 Convolution of the big F-15 E-pulse (solid line) and the A-10 E-pulse (dashed line) with the 45° response of the big F-15.

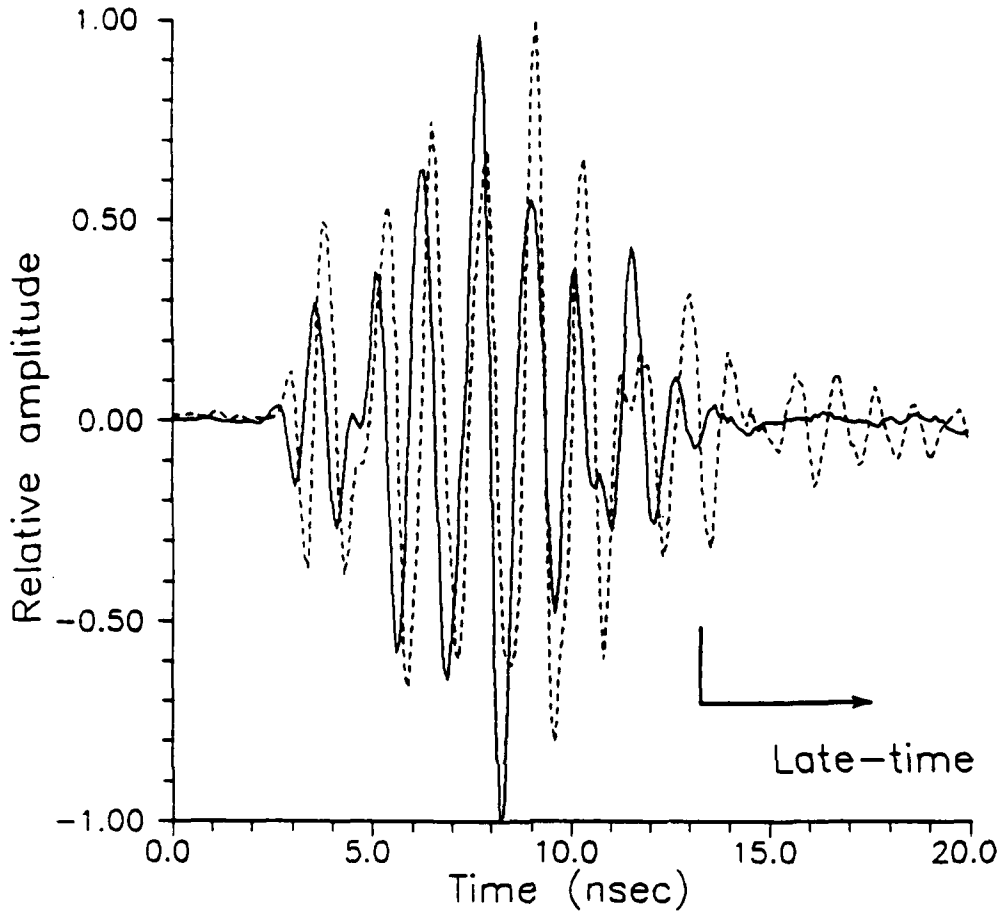

Figure 15. **Convolution of the big F-15 E-pulse (dashed line) and the A-10 E-pulse (solid line) with the 45° response of the A-10.**

ability to differentiate the convolution of the correct E-pulse with a measured target waveform from the myriad of other convolutions. As the number of prospective targets becomes large, a visual inspection of the convolved outputs becomes more subjective, and eventually impractical. A scheme has therefore been devised to automate the discrimination decision.

Ideally, if the E-pulse convolutions were uncorrupted by noise, the energy ratio

$$E = \frac{\int_{T_{LES}}^{T_{LEE}} c^2(t)\,dt}{\int_{0}^{T_e} e^2(t)\,dt} \qquad (1)$$

would be zero only for the correct E-pulse. Here c(t) is the convolution of the E-pulse e(t) with the measured response, T_e is the E-pulse duration and T_{LES} is the earliest time at which the unknown target convolution is CERTAIN to be a series of natural modes

$$T_{LES} = T_e + 2T_r \qquad (2)$$

where T_r is the one-way transit time of the largest dimension of the target corresponding to the E-pulse. (The largest dimension must be used if the target aspect is unknown.) The end of the energy window, T_{LEE}, is chosen so that the window width, T_{LEE}-T_{LES}, is the same for all convolutions.

Discrimination among all eight target models can now be demonstrated using the energy ratio (1) as the single discriminant factor. Begin by assuming the response of the big F-15 is from an unknown target. To show that successful discrimination is possible regardless of target aspect, E-pulses for the eight targets have been convolved with the responses of the big F-15 measured at five different aspect angles from 0° (nose-on) to 90° (broadside). The energy ratio (1) has been plotted as a function of aspect angle in Figure 16 for each expected target. It is obvious that for all aspects tested the big F-15 produces the smallest late-time convolved response, with a minimum 10 dB difference in late-time energy. Thus, the big F-15 is identified from among all the possible targets at each aspect angle.

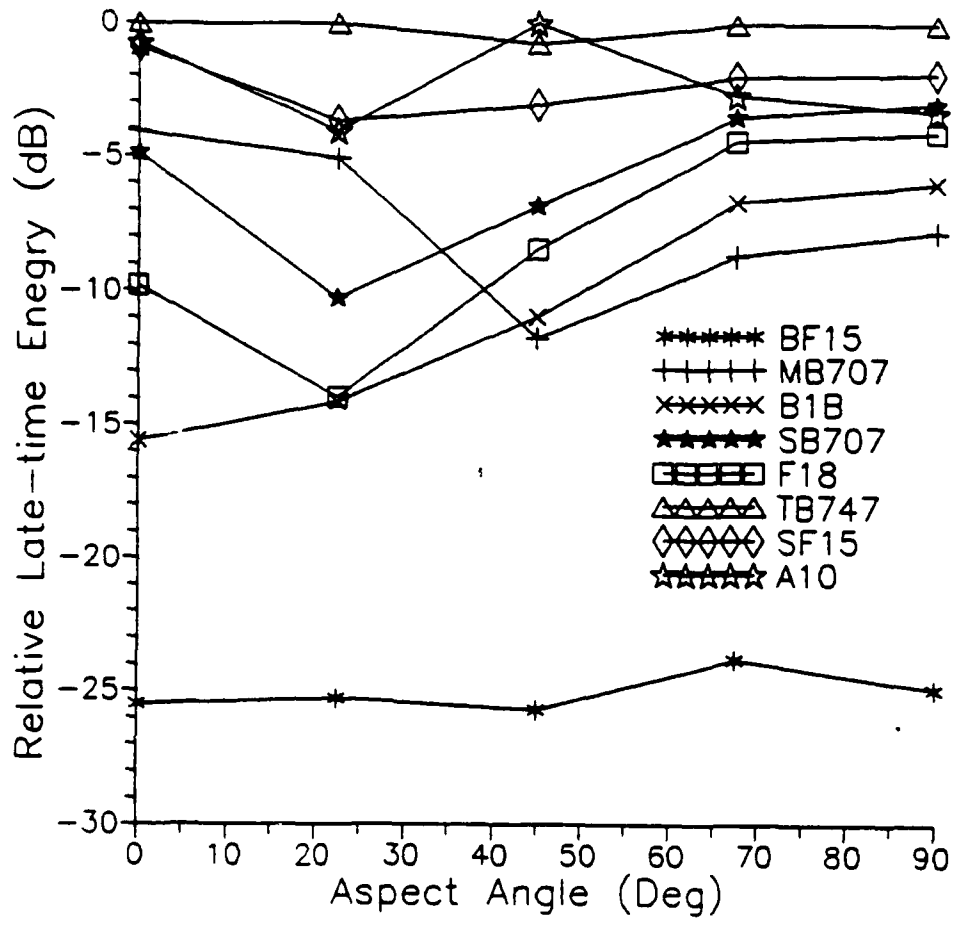

Figure 16. **Late-time energy from convolution of eight target E-pulses with responses of big F-15 measured at various aspect angles.**

Finally, discrimination among all eight targets can be demonstrated when any of the eight is the unknown target. Table 1 shows the energy ratios (1) obtained by assuming that each target is in turn the unknown target and convolving the E-pulses for each of the eight expected targets with the response of the unknown target. Here the target responses were all measured at 45° aspect. Accurate discrimination for each target is indicated by the minimum energy ratio being due to the E-pulse of the unknown target. For example, the convolution of the F-18 E-pulse with the F-18 response produces a late-time energy 29.8 dB below that produced by the convolution of the medium 707 E-pulse with the F-18 response, and 15.3 dB below that produced by the convolution of the B-1 bomber E-pulse with the F-18 response.

E-Pulse / Target Response	BF15	MB707	B1B	SB707	F18	TB747	SF15	A-10
BF15	**-25.7 dB**	-11.8	-11.0	- 6.9	- 8.5	- 0.8	- 3.1	0
MB707	-20.0	**-32.0**	-16.9	- 9.1	- 9.6	- 3.3	- 4.8	0
B1B	-11.2	0	**-23.4**	- 7.7	- 7.0	- 4.5	- 3.1	- 1.3
SB707	-16.7	- 0.8	-20.1	**-25.1**	- 8.0	0	- 2.5	- 3.8
F18	- 7.1	0	-14.5	- 2.6	**-29.8**	-11.8	- 1.9	- 4.6
TB747	-10.5	- 0.1	- 5.0	0	- 6.0	**-21.5**	- 3.0	- 1.5
SF15	-4.5	- 1.7	- 6.2	- 4.3	- 5.5	- 2.2	**-11.4**	0
A-10	-9.2	-2.9	- 0.8	0	- 4.9	-10.9	- 6.8	**-17.5**

Table 1. Late-time energy in the convolutions of various E-pulses with responses of various targets at 45° aspects.

5. Noise-insensitivity of the E/S pulse scheme.

For the purpose of demonstrating that the E/S/ pulse scheme is also noise-insensitive, in addition to being aspect-independent, the following experimental results are presented.

To prove the noise insensitivity of our scheme, we have created very noisy radar responses of complex targets by intentionally adding a large random noise to the measured radar responses of the targets. These noisy responses were then used to convolve with the discriminant signals, the E-pulse and the S-pulses of the targets. We have found that the discriminant signals f the targets are very powerful and effective in rejecting a large random noise and are capable of discriminating between the right and the wrong targets from their very noisy radar responses. The following figures will demonstrate this finding.

Figure 17 shows the pulse response of B707 model measured at 90° aspect angle without an extra random noise added. Figure 18 is the convolved output of the pulse response of Fig. 17 with the E-pulse of B707 model. As expected, a very small output was obtained in the late-time period of the convolved output. This indicates that the pulse response of Fig. 17 came from the right target of B707 model. Next, a very noisy pulse response was created by intentionally adding a large random noise (created by a computer) to the measured pulse response of B707 model shown in Fig. 17. This random noise amounted to 30% of the maximum amplitude of the measured response of Fig. 17. It is noted that the added random noise has a flat wide frequency spectrum and it can not be simply filtered out by a low-pass filter. The created noisy pulse response is shown in Fig. 19. When this noisy pulse response of Fig. 19 was convolved with the E-pulse of B707 model, a very satisfactory convolved output was obtained, as shown in Fig. 20. This convolved output resembles that of Fig. 18; the early-time response stayed nearly unchanges and, more importantly, the late-time response still remained small. This indicates that the E-pulse of B707 model was capable of identifying the noisy pulse response of Fig. 19 belonged to B707 model. Next, we tried to discriminate a wrong target, a F-18 model, with the E-pulse of B707 model using noisy pulse responses of the wrong target. Figure 21 is the pulse response of F-18 model measured at 90° aspect angle without a random noise added. When the response of Fig. 21 was convolved with the E-pulse of B707, the convolved output is shown in Fig. 22. In Fig. 22, it is seen that a large late-time response was obtained. This indicates that the response of Fig. 21 came from a wrong target other than B707 model. Next, a very noisy pulse response of F-18 model was

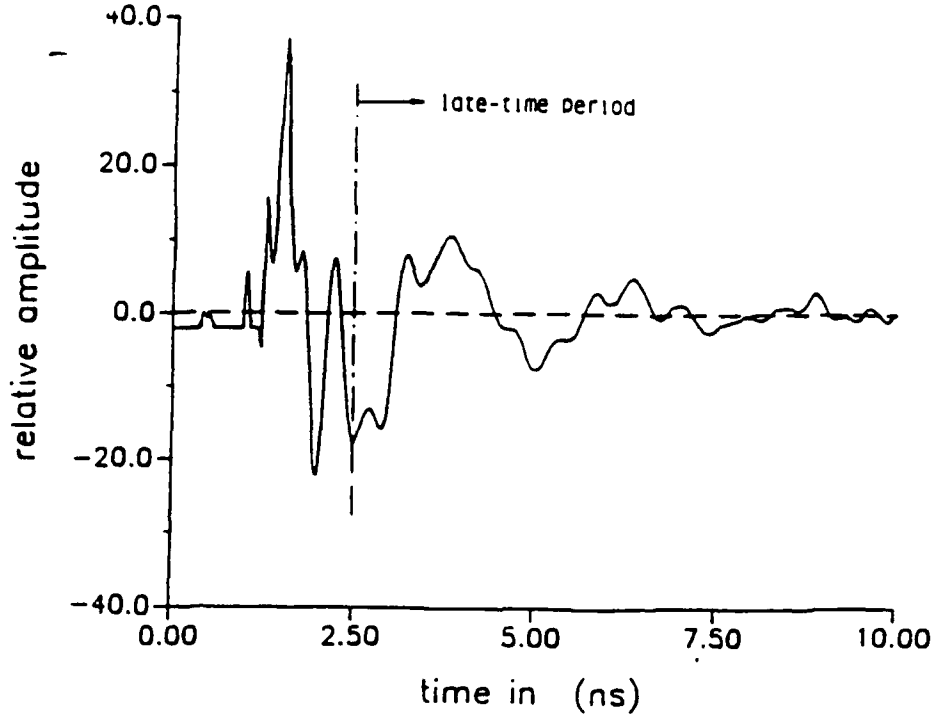

Figure 17 Pulse response of B707 model measured at 90^0 aspect angle without an extra noise added.

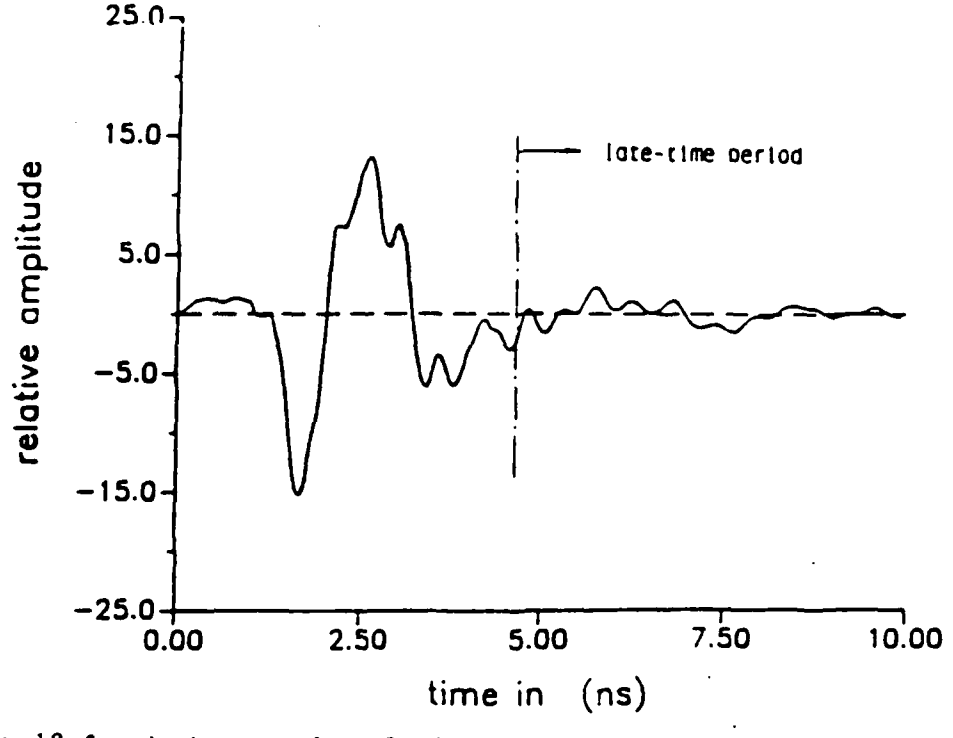

Figure 18 Convolved output of the E-pulse of B707 model with the pulse response of B707 model measured at 90^0 aspect without an extra noise added. A very small late-time response was obtained.

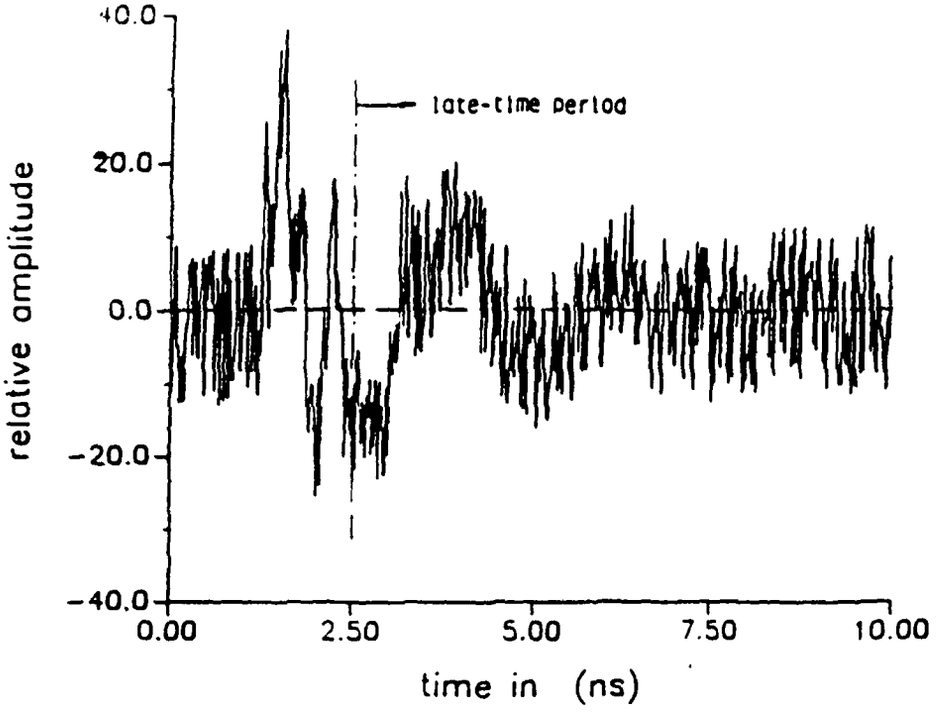

Figure 19 Pulse response of B707 model measured at 90^0 aspect angle with an extra random noise (30% of the maximum waveform amplitude) added.

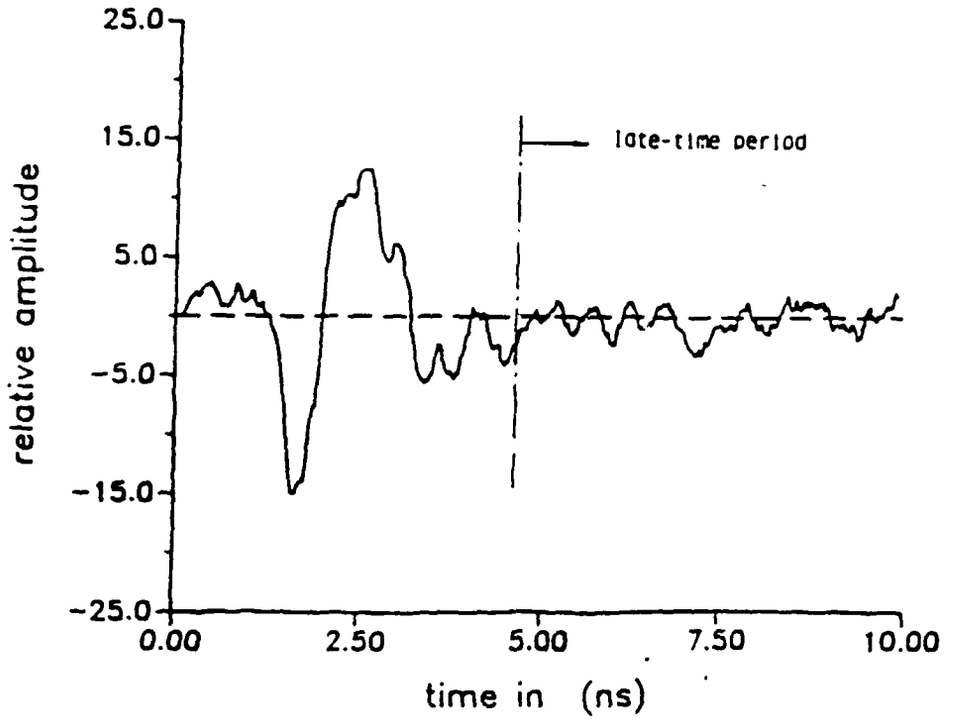

Figure 20 Convolved output of the E-pulse of B707 model with the pulse response of B707 model measured at 90^0 aspect angle with an extra random noise (30% maximum amplitude) added. The late-time response was still very small.

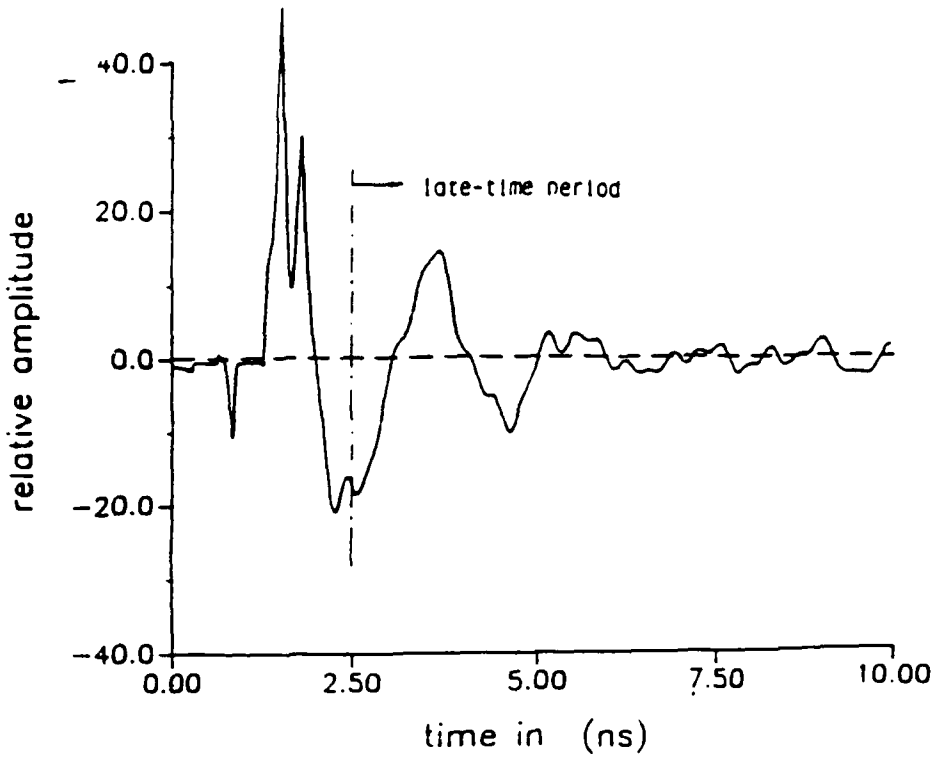

Figure 21 Pulse response of F-18 model measured at 90^0 aspect angle without an extra noise added.

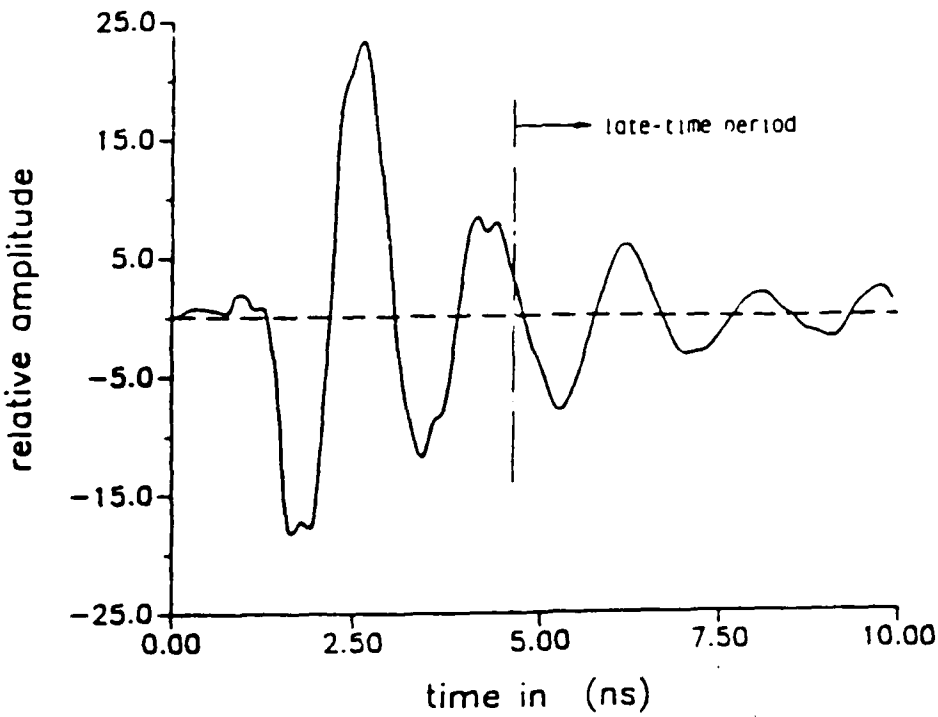

Figure 22 Convolved output of the E-pulse of B707 model with the pulse response of F-18 model measured at 90^0 aspect angle without an extra noise added. A large late-time response was obtained.

created by intentionally adding a large random noise, 30% of the maximum amplitude of the response of Fig. 21, to the measured response of Fig. 21. This noisy pulse response of F-18 model is shown in Fig. 23. The noisy pulse response of Fig. 23 was then used to convolve with the E-pulse of B707, and the convolved output is shown in Fig. 24. The convolved output of Fig. 24, as compared with the result of Fig. 22, shows a relatively unchanged early-time response followed by a still large and some-what noisy late-time response. This large late-time response is sufficient to indicate that the noisy pulse response of Fig. 23 belonged to a wrong target other than B707 model.

We have also convolved noisy pulse responses of complex targets with the S-pulses of the targets. Similar results as those described in Figs. 17 to 24 were obtained; the S-pulses of a complex target are capable of discriminating between the right target and wrong targets based on very noisy pulse responses of the targets.

Based on this study, we can conclude that our target discrimination scheme of using the E-pulse and the S-pulses of the target is very noise insensitive.

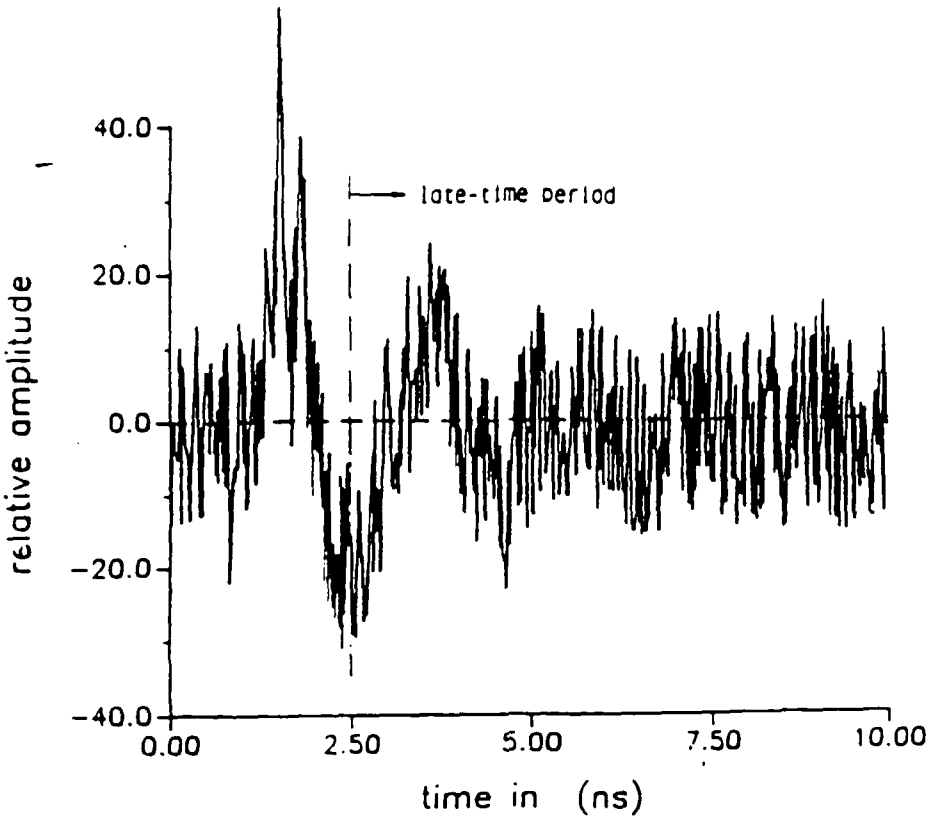

Figure 23 Pulse response of F-13 model measured at 90^0 aspect angle with an extra random noise (30% of the maximum waveform amplitude) added.

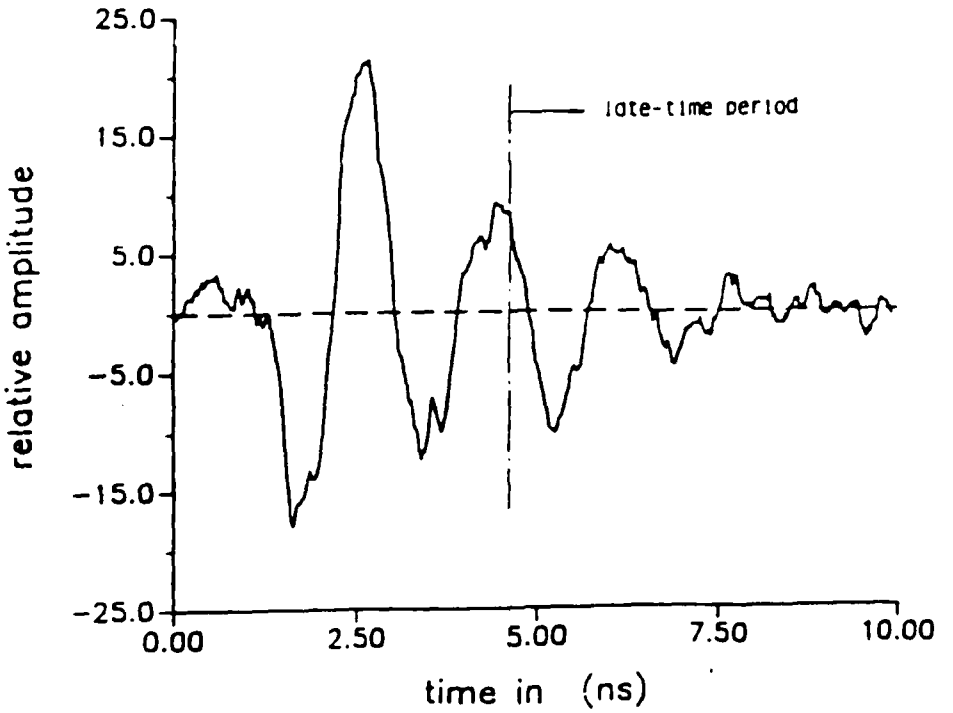

Figure 24 Convolved output of the E-pulse of B707 model with the pulse response of F-18 model measured at 90^0 aspect angle with an extra random noise (30% maximum amplitude) added. The late-time response remained large.

6. Discrimination of helicopters with the E/S pulse scheme.

The successful discrimination of helicopters is complicated by the rapid motion of the rotor blades. During the measurement of a transient response of a helicopter, the blades are caught in different positions during different pulse transits with the precise blade location unknown. If the dominant natural frequencies of the helicopter depend heavily on coupling between the blades and the fuselage, and thus upon blade position, accurate discrimination will depend on an unlikely fortuitous measurement.

Preliminary experiments have been conducted using a crude helicopter model which suggests that coupling between the rotors and the fuselage is minimal. Thus, discrimination between disimilar helicopters is possible regardless of the rotors' positions at the times of interrogation.

The helicopter model is constructed using a 12" length of 4" diameter aluminum cylinder for the fuselage, and two sets of perpendicular blades of lengths 12" and 16" attached to the cylinder by a perpendicular post. Discrimination between the helicopter with 12" blades and the helicopter with 16" blades has been accomplished with the blades in two different positions. In the first position, the blades are mutually perpendicular, with one blade parallel to the fuselage. In the second position, the blades are still mutually perpendicular, but are rotated so that each makes a 45° angle with the fuselage.

Measurements have been made both within the free-field chamber (simulating a helicopter flying in air) and on the ground plane range (simulating a helicopter hovering above the ground).

Results from the ground plane range are shown in Figures 25 to 28, with the helicopter being illuminated at broadside (90° aspect angle). In Figure 25, the energy plots (time domain) are calculated from the convolution of the response of the 45° oriented short-blade helicopter (H90D45S) with the E-pulses constructed for the 0° oriented (parallel to fuselage) short blade helicopter (EPHD0S), the 45° oriented short-blade helicopter (EPHD45S), the 0° oriented, long-blade helicopter (EPHD0L), and the 45° oriented long-blade helicopter (EPHD45L). As expected, the convolution of the 45° short-blade E-pulse with the 45° short-blade response gives the smallest late-time energy (most dB down). However, convolution of the 0° oriented E-pulse with

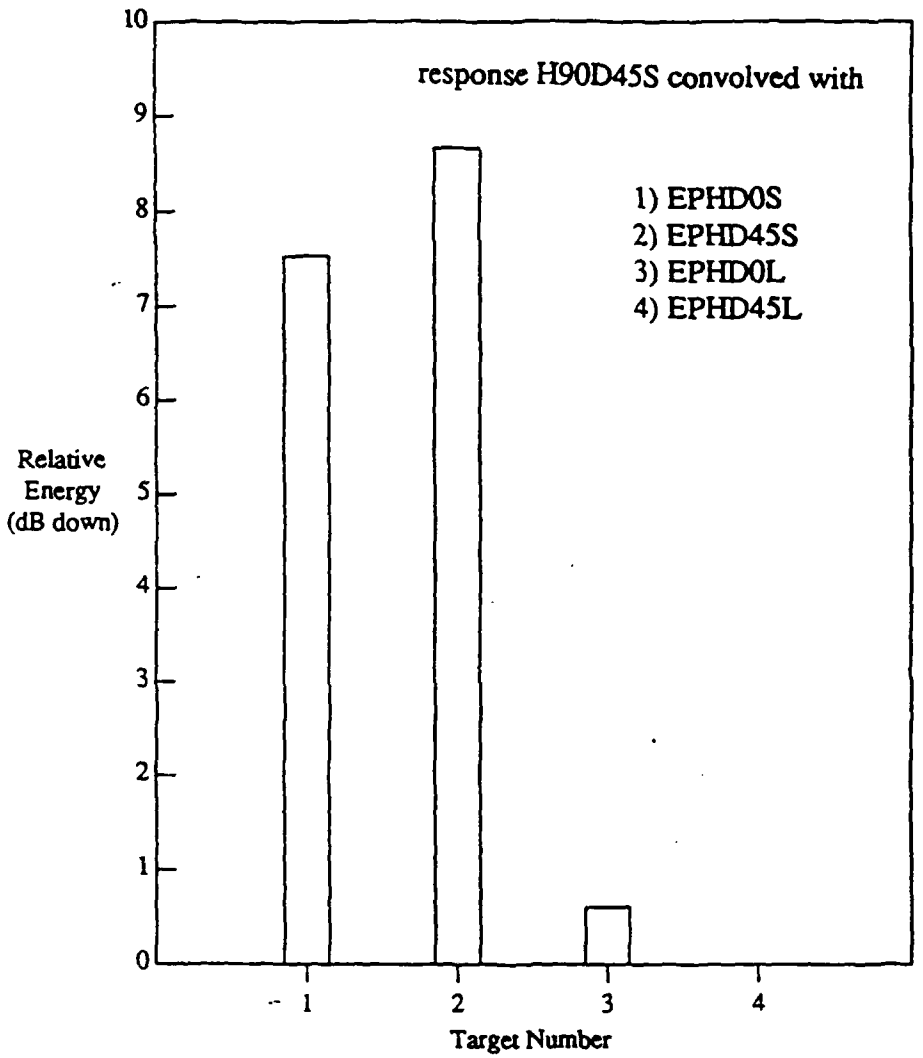

Fig. 25. Late-time energy from convolution of 45° oriented short-blade helicopter response and E-pulses for long and short-blade helicopters.

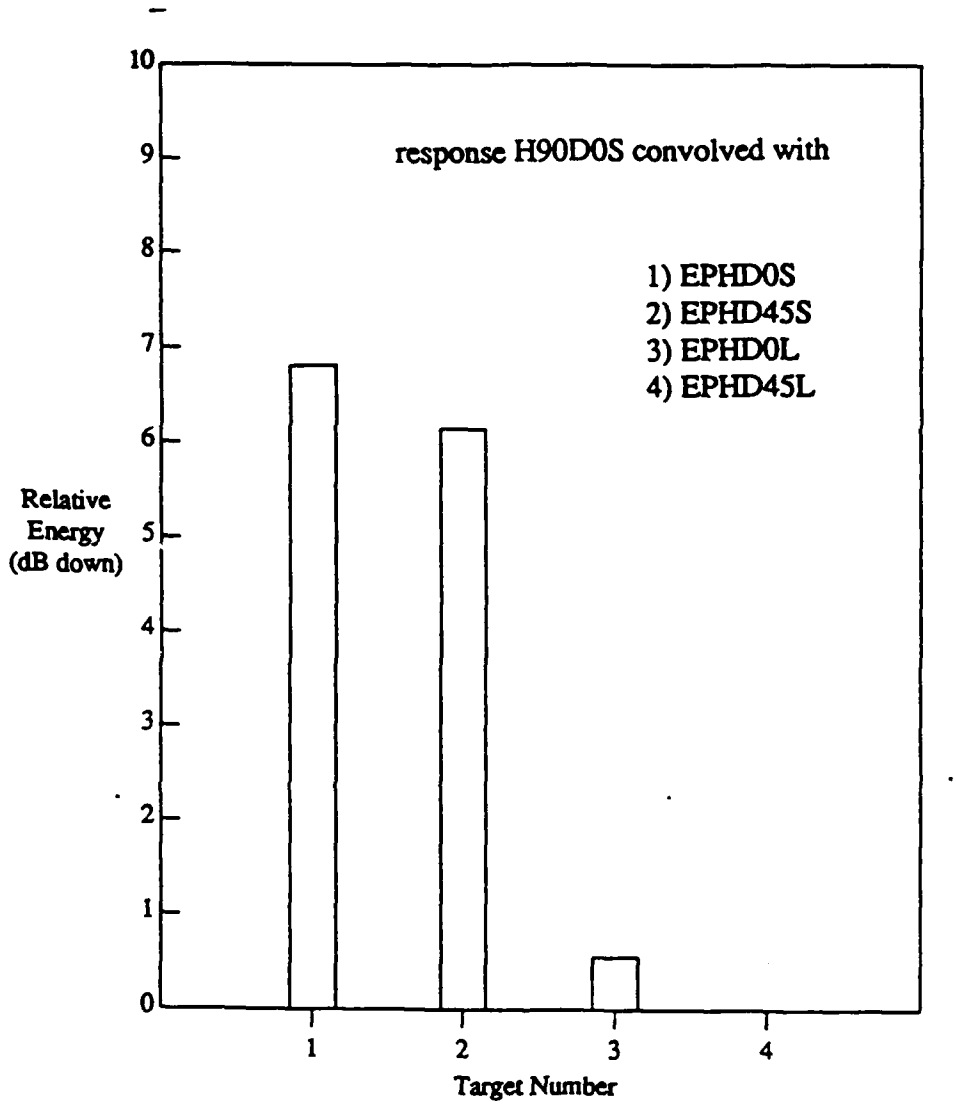

Fig. 26. Late-time energy from convolution of 0° oriented short-blade helicopter response and E-pulses for long and short-blade helicopters.

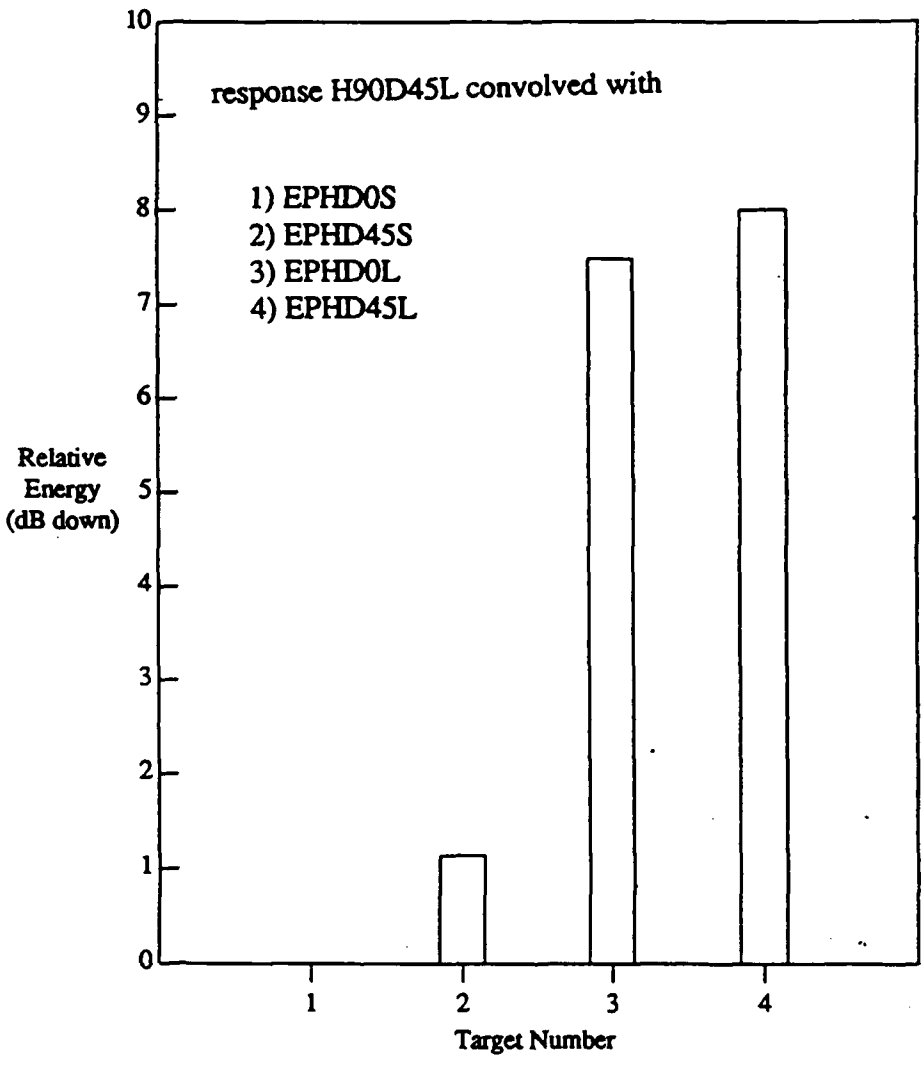

Fig. 27. Late-time energy from convolution of 45° oriented long-blade helicopter response and E-pulses for long and short-blade helicopters.

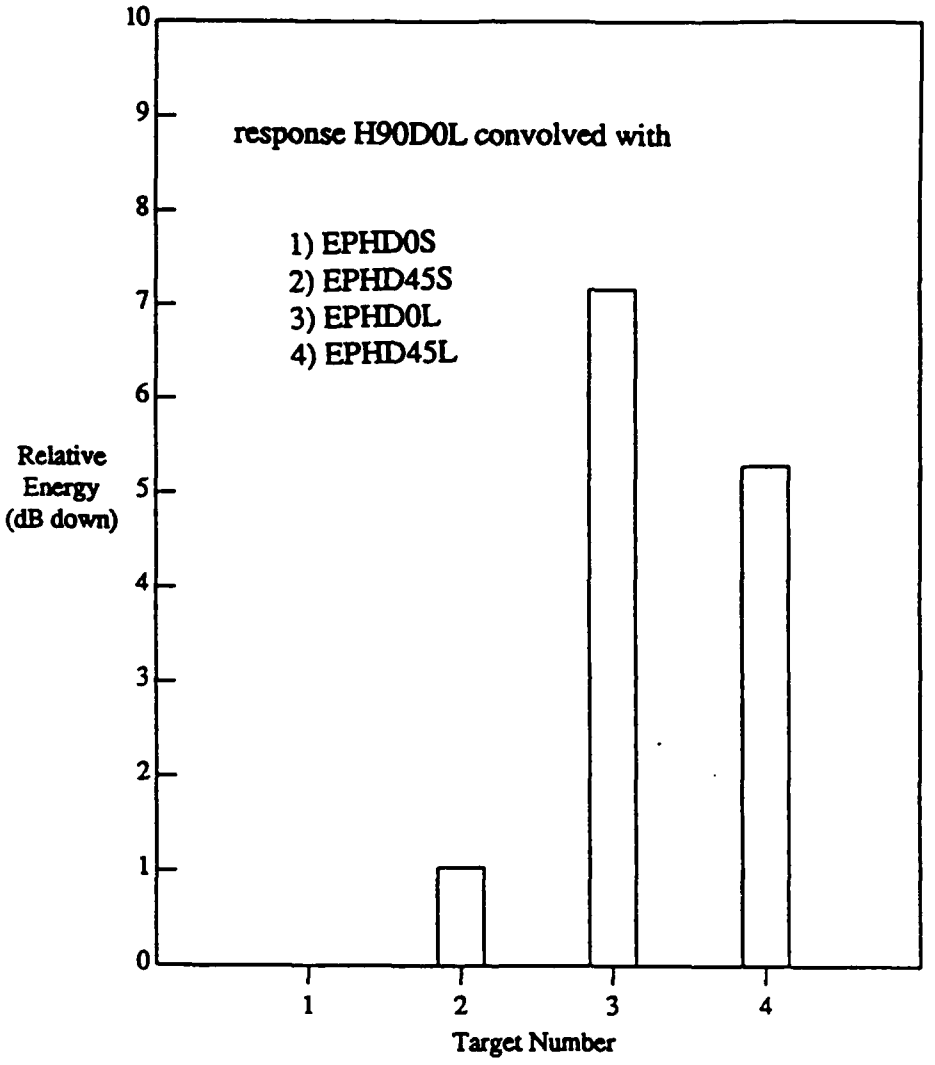

Fig. 28. Late-time energy from convolution of 0° oriented long-blade helicopter response and E-pulses for long and short-blade helicopters.

the 45° short-blade response also gives small energy, while convolution with the two long-blade E-pulses gives much larger energy.

Similar results are shown in Fig. 26 where the response of the 0° short-blade helicopter is convolved with all four E-pulses. Thus, it is possible to discriminate the long-blade helicopter from the short-blade helicopter regardless of the blade orientation with respect to the fuselage.

This conclusion is enhanced by the results shown in Figures 27 and 28 which show the convolutions of the long-blade helicopter responses with all four E-pulses. Here, the long-blade E-pulses produce little late-time energy when convolved with long-blade responses, but the short-blade E-pulses produce large late-time energy when convolved with long-blade responses. This occurs regardless of blade orientation.

Figures 29-33 show results obtained from measurements performed using the free-field range. In this case, an experiment was performed to determine if the aspect angle of the helicopter would affect the discrimination performance. In this sequence of plots, the response of a 0° oriented long-blade helicopter (HOWCL) measured at five aspect angles (0°-90°) is convolved with E-pulses constructed for a 0° oriented short-blade helicopter (HOWCS), a 45° oriented short-blade helicopter (H45WCS), a 0° oriented long-blade helicopter (HOWCL), and a 45° oriented long-blade helicopter (H45WCL), and the late-time energy calculated. It is seen that regardless of the target aspect angle, both the 0° oriented and 45° oriented long-blade helicopters are easily discriminated from the 0° oriented and 45° oriented short-blade helicopters.

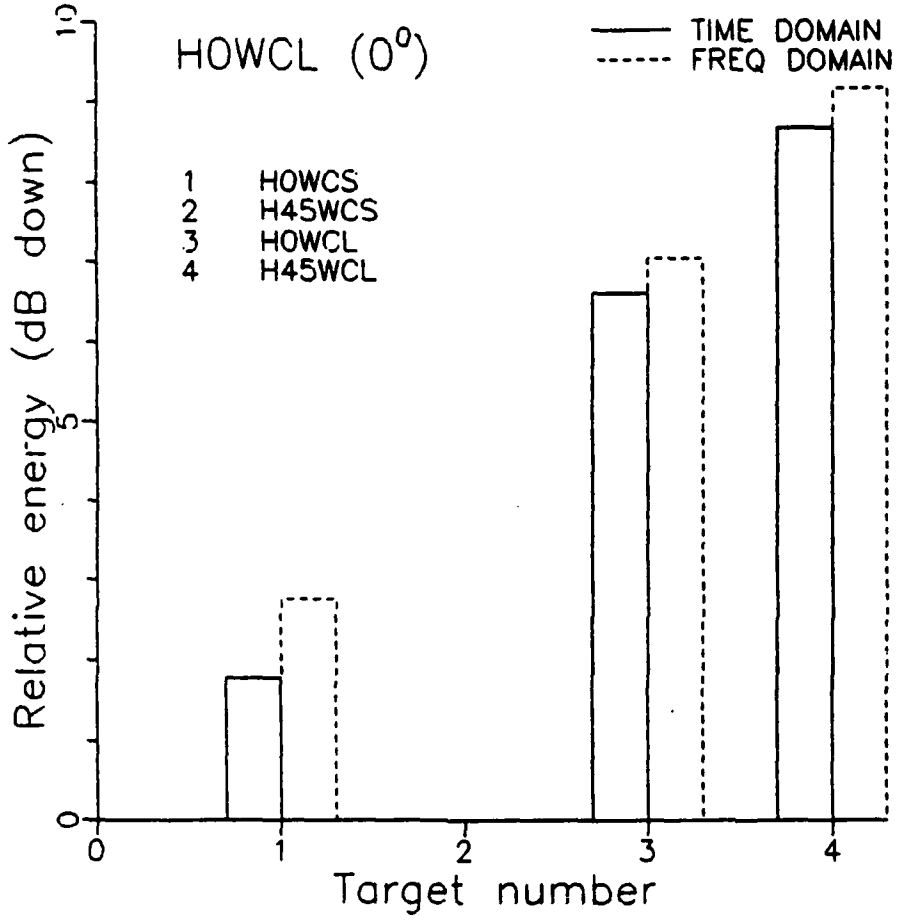

Fig. 29. Late-time energy from convolution of 0° oriented long-blade helicopter response measured at 0° aspect and E-pulses for long and short-blade helicopters.

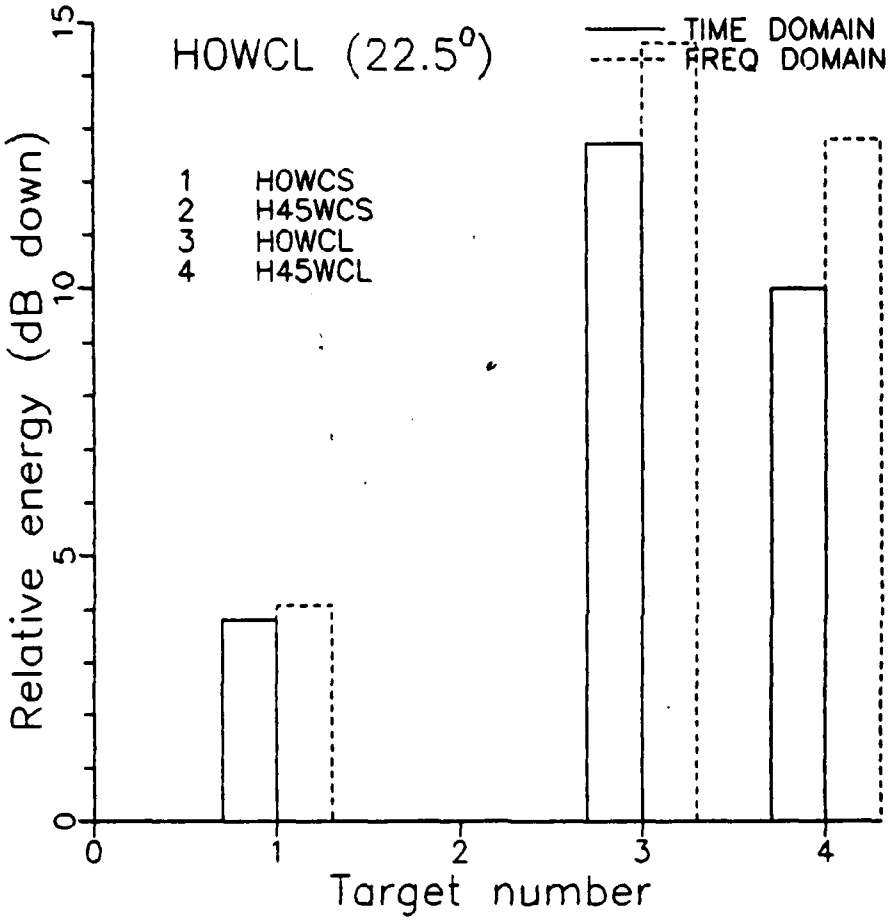

Fig. 30. Late-time energy from convolution of 0° oriented long-blade helicopter response measured at 22.5° aspect and E-pulses for long and short-blade helicopters.

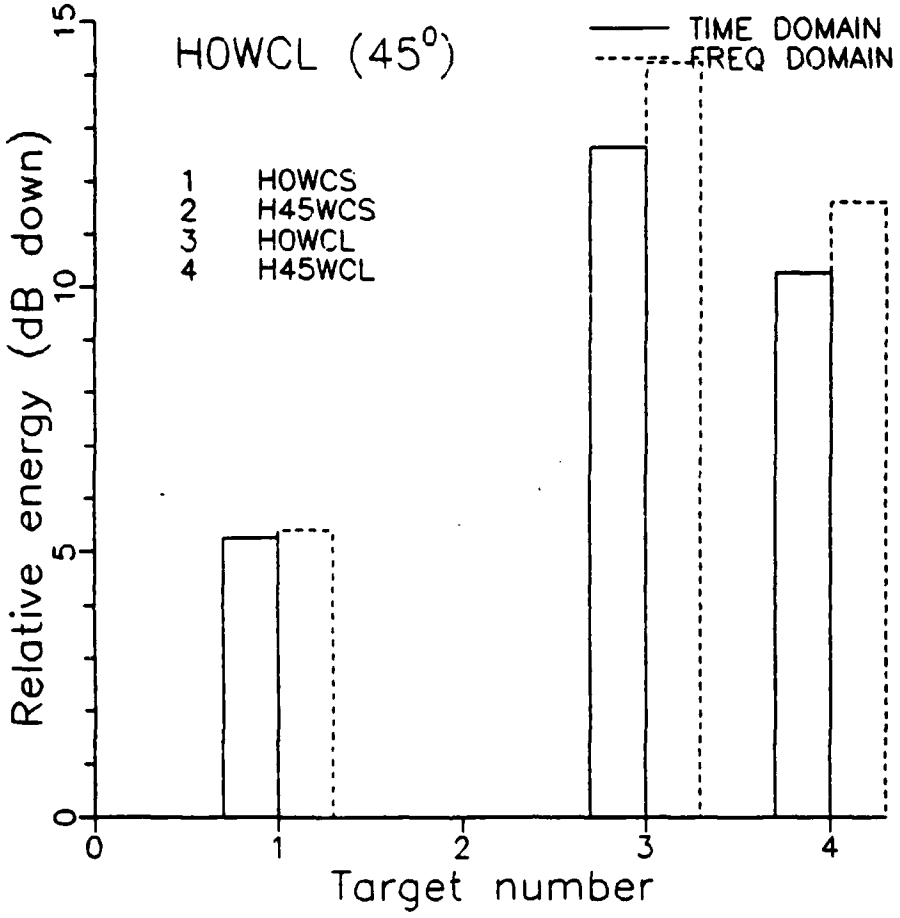

Fig. 31. Late-time energy from convolution of 0° oriented long-blade helicopter response measured at 45° aspect and E-pulses for long and short-blade helicopters.

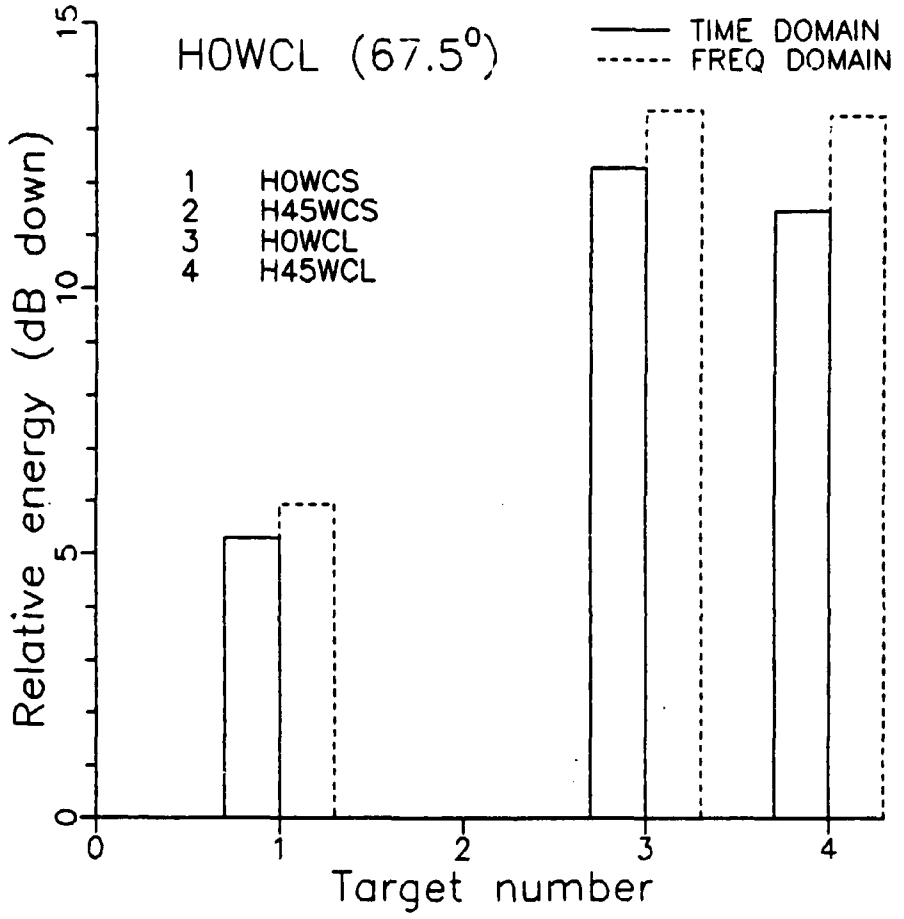

Fig. 32. Late-time energy from convolution of 0° oriented long-blade helicopter response measured at 67.5° aspect and E-pulses for long and short-blade helicopters.

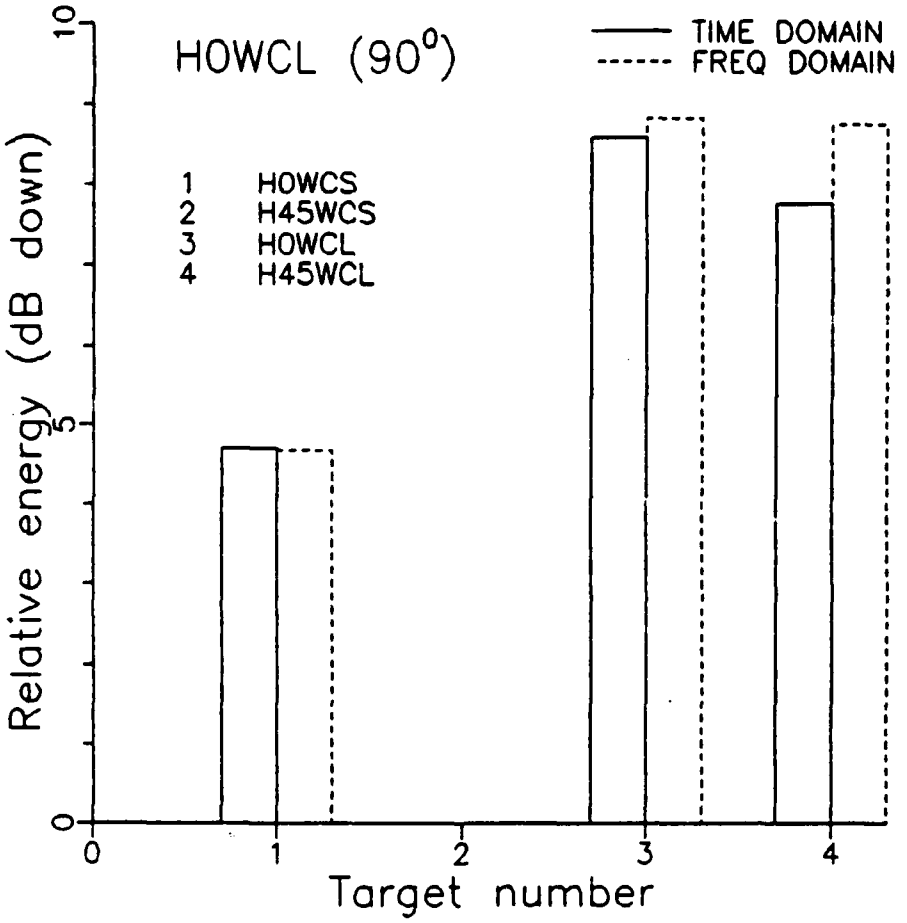

Fig. 33. Late-time energy from convolution of 0° oriented long-blade helicopter response measured at 90° aspect and E-pulses for long and short-blade helicopters.

7. Detection and identification of low observable targets.

In the course of our research, it was observed that the E/S pulse technique can be utilized to detect a low observable target and also to identify the target even though it is covered by a lossy material which absorbs microwave radar signal. The reason for this unique capability is that the E/S pulse technique uses an interrogating EM pulse which excites low order natural resonant modes of the target. These natural modes are due to the oscillation of free electrons in the target's main structures such as the wing and the fusilage, and these oscillations are not significantly affected by the coating of lossy material on the target.

To show that the E/S pulse technique can be used to detect a low observable target, the pulse response of a 4" x 12" aluminum plate (a simulated wing structure) and that of the same plate covered by a one half inch thick layer of microwave absorber were measured at various aspect angles. The measured responses at the normal incidence are shown in Figs. 34 and 35. It is observed that the pulse response of the lossy coated plate is somewhat lower in magnitude and quite different in waveform when compared with that of the uncoated plate. The fact that a lossy coated plate still give a significant return to an interrogating EM pulse will make the detection of a low observable target possible with the E/S pulse technique. Furthermore, we will show that the lossy coated plate can be discriminated from other plates of different dimensions based on its late-time pulse response using the E/S pulse scheme.

We have attempted to discriminate a 6" x 15" plate from the lossy coated 4" x 12" plate, assuming information is only available for the 4" x 12" plate without loss. Figure 36 shows the convolved response of the 6" x 15" plate E-pulse with the response of the coated 4" x 12" plate. As expected, the late-time portion of the convolved response exhibits a large amplitude. In contrast, Figure 37 shows the convolved response of the E-pulse synthesized for the UNCOATED 4" x 12" plate with the measured response of the COATED 4" x 12" plate. The small amplitude of the late-time component demonstrates that the coating has little effect on the pulse discrimination. Lastly, Figure 38 shows the convolution of the E-pulse for

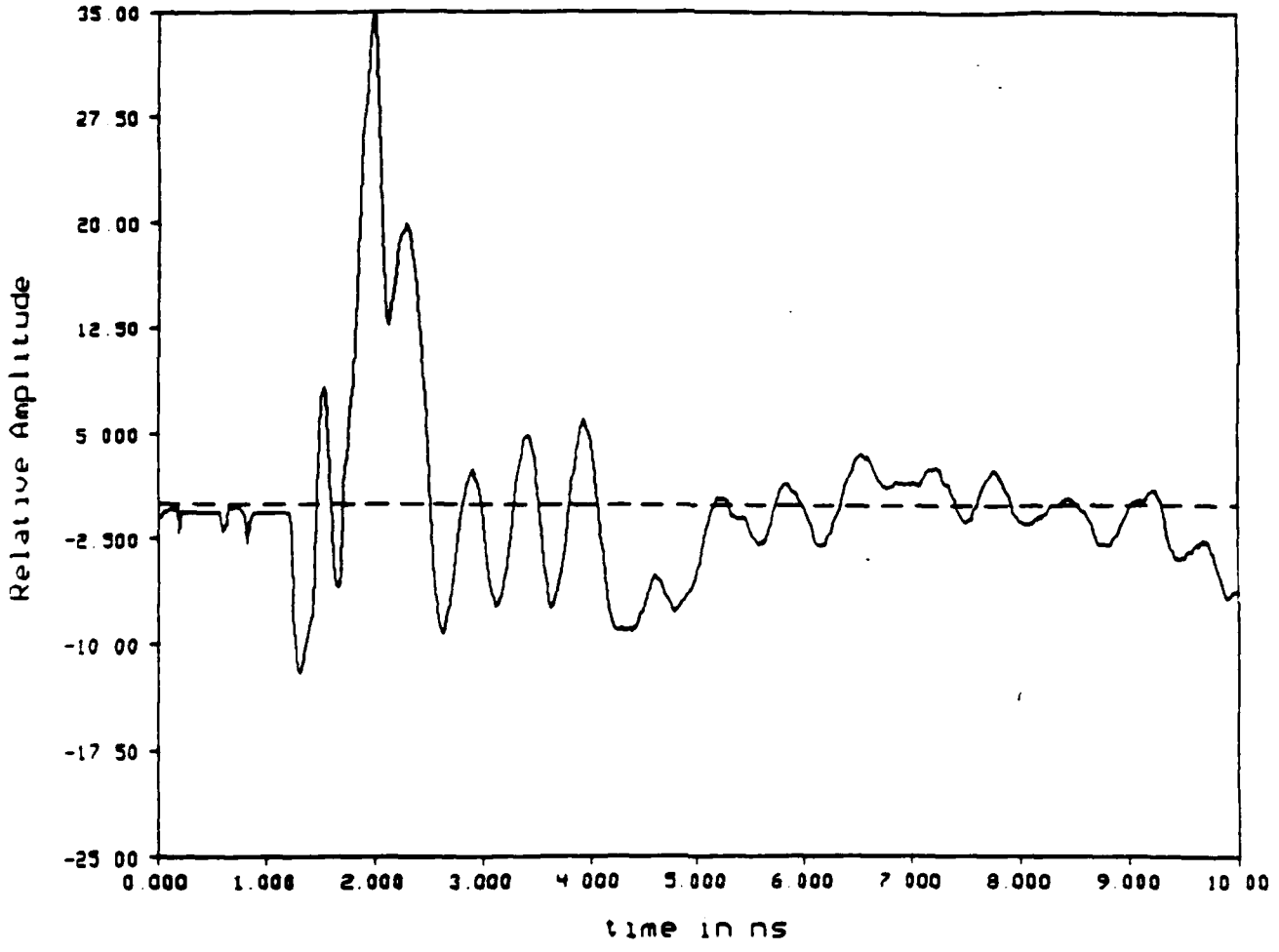

Figure 34. Radar Response of A Conducting Plate (4" x 12") at Normal Incidence

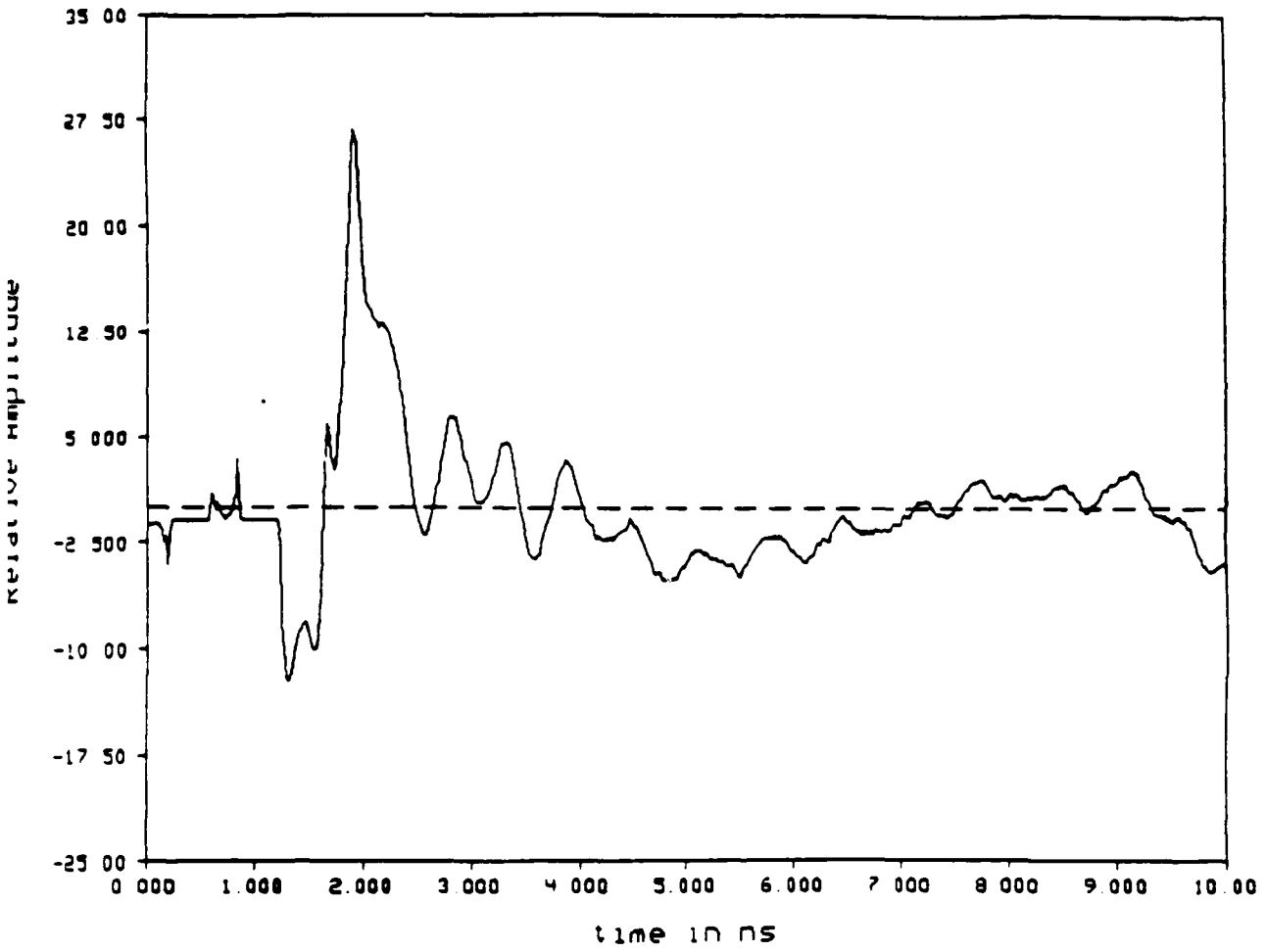

Figure 35. Radar Response of A Conducting Plate (4" x 12") Covered with A Lossy Layer at Normal Incidence

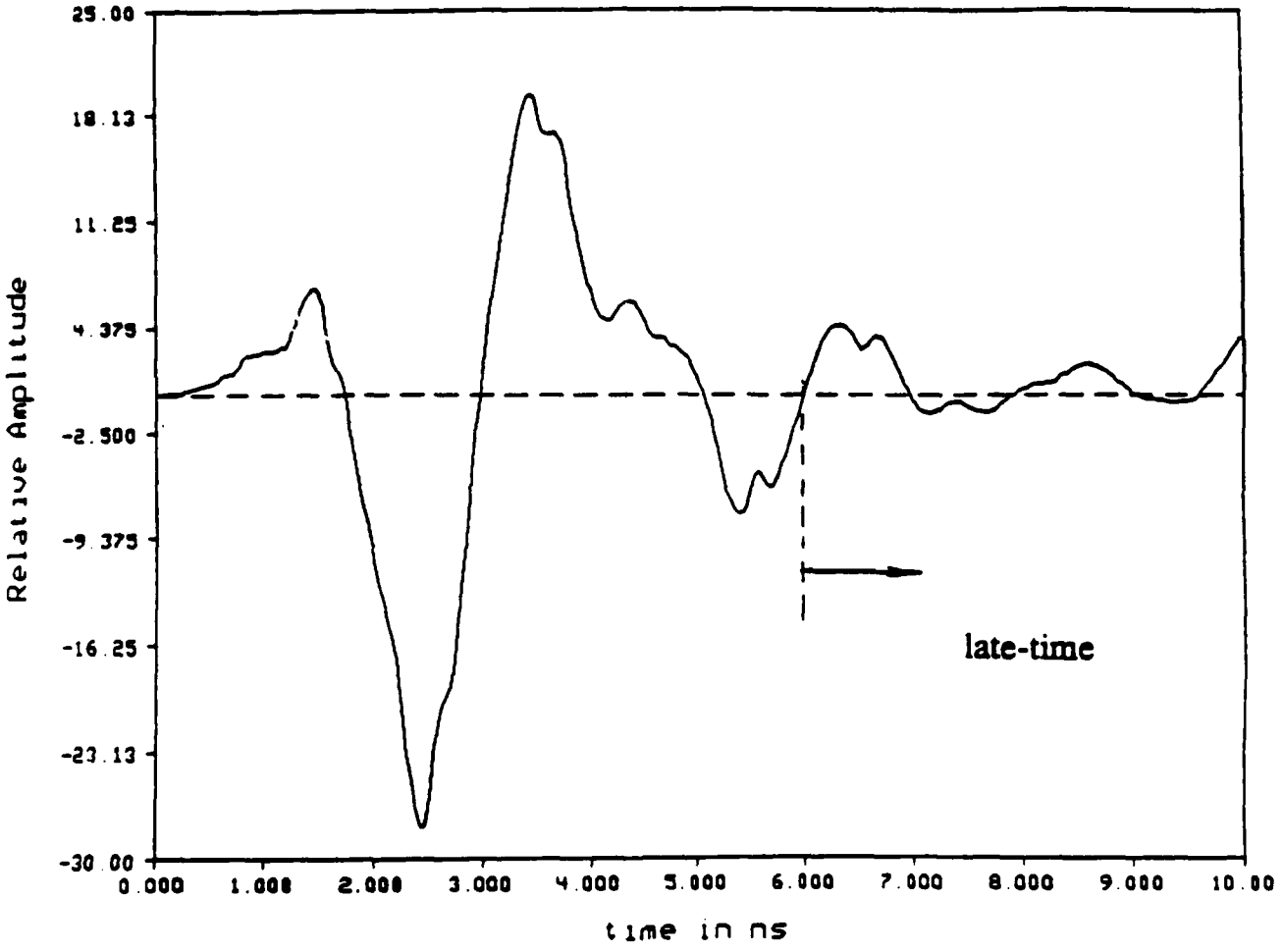

Figure 36. Output of the Convolution Between the E-Pulse Synthesized for Conducting Plate (6" x 15") and Radar Response from the Conducting Plate (4" x 12") Covered with A Lossy Layer

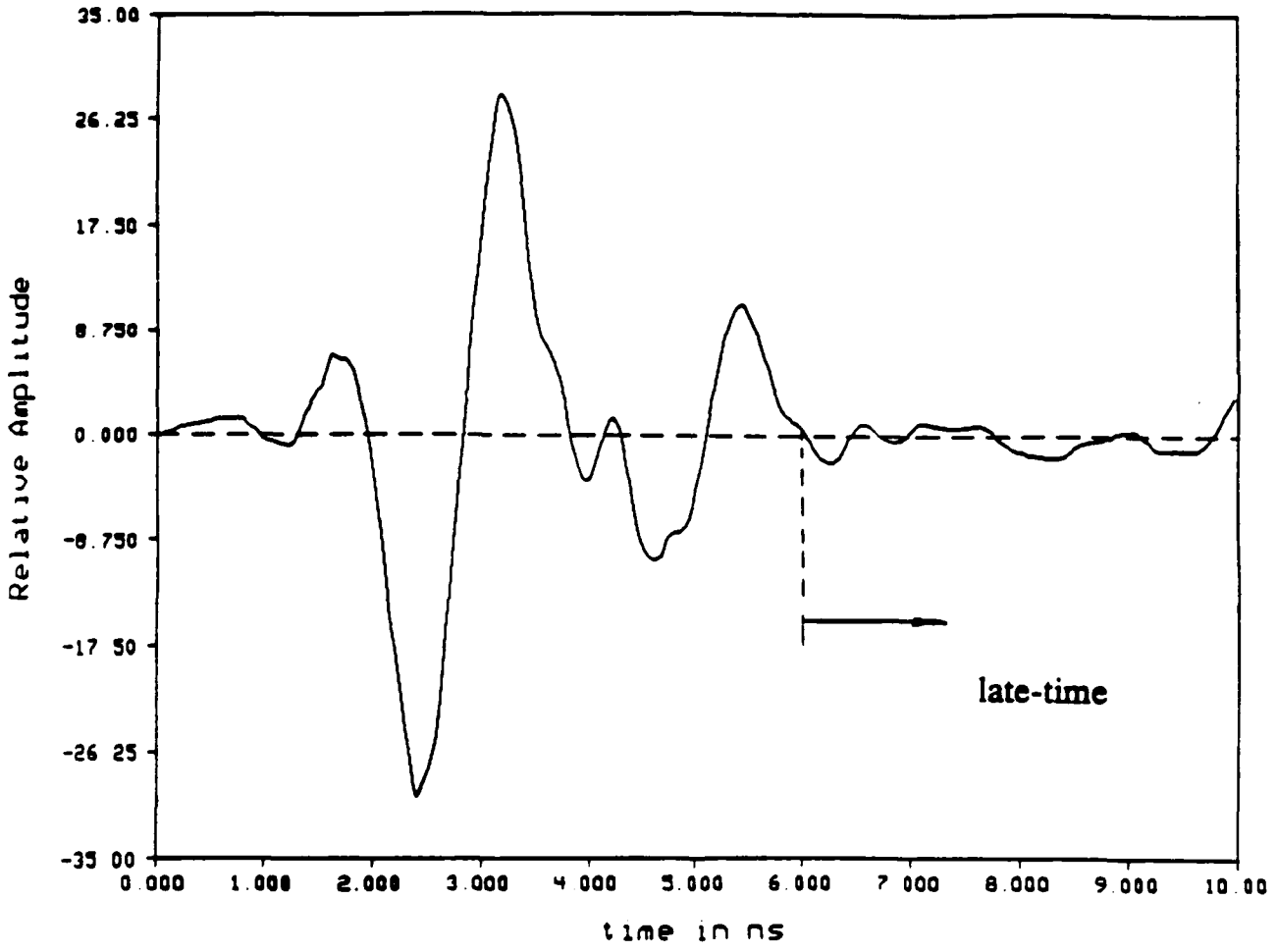

Figure 37. Output of the Convolution Between the E-Pulse Synthesized for Conducting Plate (4" x 12") and Radar Response from the Same Conducting Plate (4" x 12") Covered with A Lossy Layer

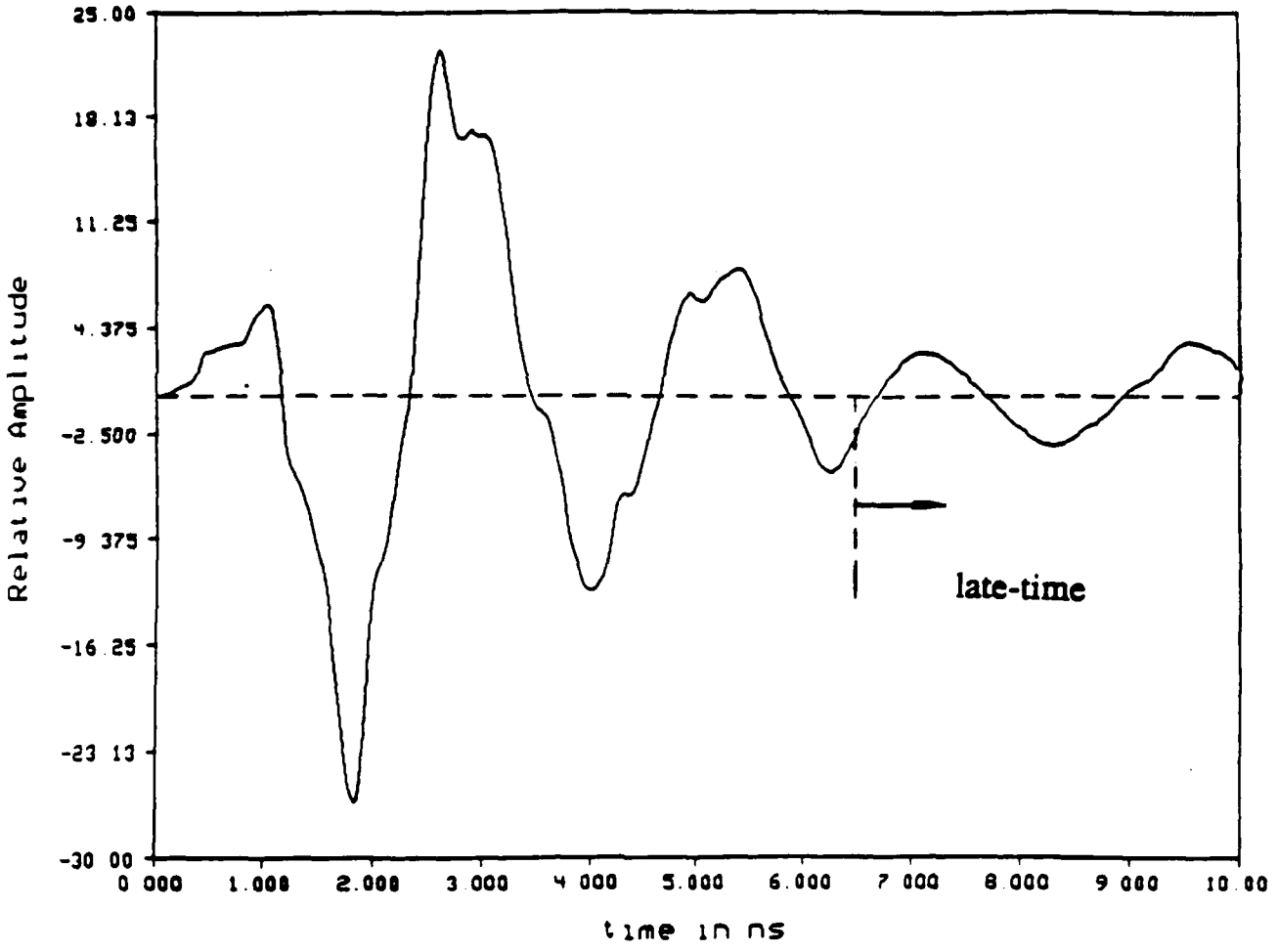

Figure 38. Output of the Convolution Between the E-Pulse Synthesized for Conducting Plate (4" x 12") and Radar Response from the Conducting Plate (6" x 15")

the uncoated 4" x 12" plate with the response of the 6" x 15" plate. Here the late-time portion has a large amplitude. Similar results have been obtained using waveforms measured at end-on and oblique incidence.

The implication of these results is that discrimination between radar targets using E-pulses is possible even if the targets are coated by lossy material, but information is available only for the uncoated targets. The reason for this is that E-pulse waveforms are based entirely on the natural frequencies of the targets, and the natural frequencies of resonance region are not perturbed greatly by addition of the lossy layer; the imaginary parts of the natural frequencies are determined primarily by the geometry of the underlying conducting plate. It is interesting to note that although the measured waveforms of the 4" x 12" plate and the 4" x 12" coated plate (Figures 34 and 35) are quite different, the natural frequencies contained in each are nearly identical. Thus, the presence of the lossy layer serves mostly to perturb the amplitudes and phases of the natural modes. An obvious scenario is as follows. The natural frequencies of a group of aircraft are determined by a scale model measurements, and a set of E-pulses constructed. However, in acturality, each of the aircraft is operated carrying an additional coating of lossy material, for the purpose of thwarting high frequency radar. Since the E-pulse technique is based on resonance region frequencies, the presence of the coating does not affect the ability to accurately discriminate the targets in practical situations.

These preliminary results tend to indicate that a pulsed radar or an ultrawideband radar operated on the E/S pulse scheme has good potentiality of detecting and identifying low observable targets such as Stealths if more research is conducted on this effort.

8. Effect of aspect variation on multi-pulse coherent processing.

For multi-pulse coherent processing, it is important to know the effect of aspect angle changes on the modal amplitudes of typical target modes. If the changes are severe, then pulse-to-pulse coherent processing would not be practical.

To get a feeling for the possible range of aspect changes in a realistic situation, consider a missile travelling at Mach 5 (1630 m/s) perpendicular to the radar line of sight, at a range of 10 km. If the pulse repetition rate is 10 kHz, then the missile will travel a distance of 165 m during a 1000 pulse interrogation. This corresponds to an aspect angle change of about $\tan^{-1}$ (165/10000) = 0.9°. It is anticipated that a change of aspect of less than a degree will produce an unimportant change in the amplitudes of the dominant natural modes.

An experimental verification of this prediction has been performed using the free-field target range. The response of a detailed model of an F-15 fighter aircraft (18" fuselage length) has been measured at angles of 0°, 5°, 10°, and 15° from head-on (a much larger range of aspect angles than anticipated above). The total responses are shown in Figure 39 while the late-time portions of these resp ·ses are shown in Fig. 40. It is apparent from the late-time plots that the modal amplitudes change relatively little over this range of aspects, and thus the responses should add constructively.

Evidence for the coherence of the different aspect angle waveforms is given in Figure 40 which shows the sum of the individual waveforms. All the waveforms add in phase, as the resulting signal has approximately four times the amplitude of a single waveform.

Additional evidence for the coherence of the four waveforms is obtained by extracting the dominant modal frequencies and examining the energy in each individual mode as a function of aspect angle. Table 2 shows the natural frequencies of the first two modes of the F-15 extracted from the measured waveforms, as well as the modal energies. It is seen that the energy is nearly constant with aspect. Also shown in Table 2 are the frequencies and energy obtained from the sum of the waveforms. The energy in each of the modes of the sum is about 16 times as large as the energy in

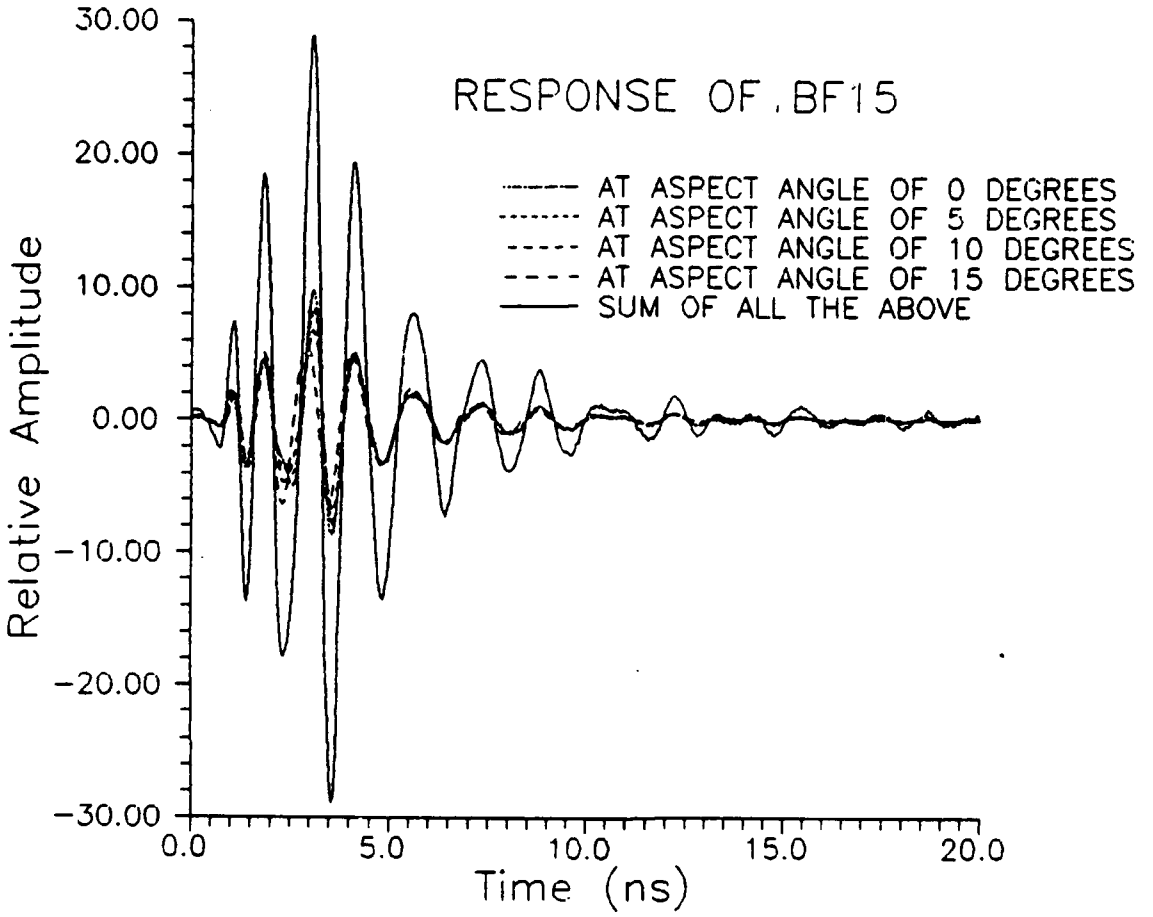

Figure 39. Measured responses of big F-15 at four aspect angles, and sum of responses.

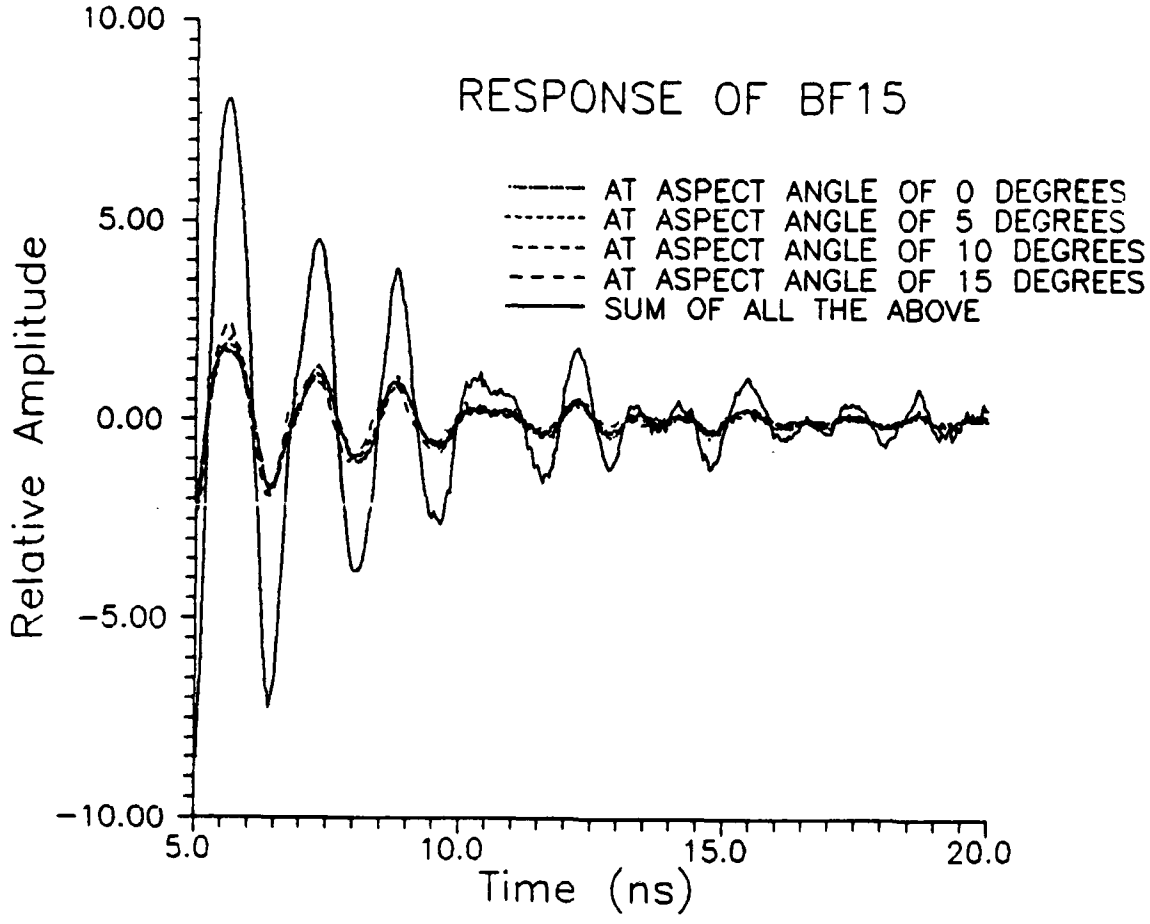

Figure 40. Late-time portions of measured responses of big F-15 at four aspect angles, and sum of responses.

each individual waveform, again indicating that the signals have added constructively.

Table 2 Modes extracted from measured response of big F-15 at various aspects

Aspect Angle	Mode Number	Damping Coefficient	Radian Frequency	Modal Energy
0°	1	-0.261	3.91	3.66
	2	0.072	5.69	0.096
5°	1	-0.290	3.91	3.60
	2	0.056	5.80	0.144
10°	1	-0.356	3.93	3.79
	2	0.071	5.69	0.096
15°	1	-0.433	3.99	4.37
	2	0.133	5.77	0.097
SUM	1	-0.330	3.93	60.79
	2	0.039	5.73	2.02

9. Discrimination of multiple targets in the same range cell.

Discrimination of individual targets using the E-pulse technique has been effectively demonstrated both in a free space environment and on a ground plane. A more complicated problem is performing discrimination when multiple targets are present.

Many target configurations are possible, including identical or disimilar targets in or out of the same range cell. If identical targets are located within the same range cell, it is anticipated that the E-pulse for a single target will remain effective. This assumes that mutual coupling of the targets will produce a negligible shift in target natural resonance frequencies, and must be demonstrated experimentally.

An experiment using the free-field range has been conducted to test discrimination of multiple groups of identical targets. Measurements were made of a single 11 cm (fuselage length) Boeing 747 and a single 15 cm (fuselage length) Boeing 747. Measurements were also made of two 11 cm 747's in the same range cell, separated by 10 cm, 20 cm, 40 cm, and 60 cm. An E-pulse was then constructed for the single 11 cm 747, and convolved with each of the measured waveforms. The discrimination ratios, calculated using (1) and (2), are shown in Figure 41. It can be seen that the single 11 cm 747 is easily discriminated from the single 15 cm 747 (the energy ratio of the correct 11 cm 747 is the smallest--the most dB down). It can also be seen that the set of two 11 cm 747's are easily discriminated from the single 15 cm 747 using the E-pulse for the single 11 cm 747. Note that as the targets are brought closer together, the discrimination level lessens, but still remains high.

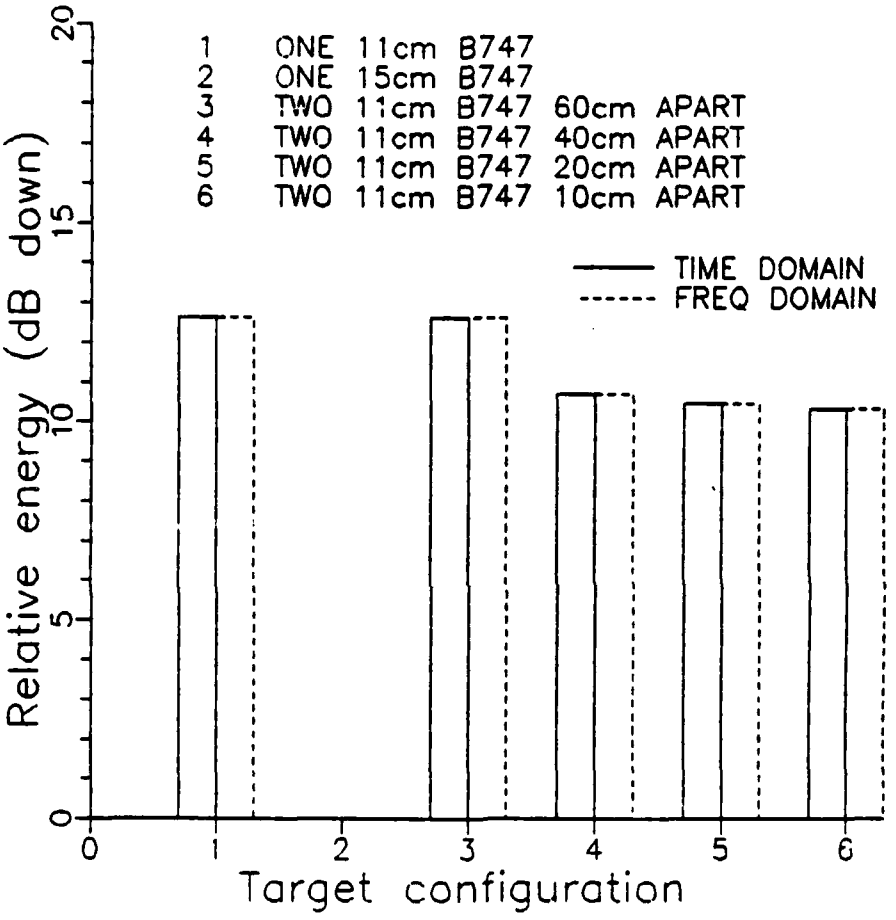

Figure 41. Energy ratios for convolutions of single 11 cm Boeing 747 E-pulse with responses of single and multiple target configurations.

10. Power Requirement for a Pulsed Radar System

It is essential to know how much power needs to be transmitted in order to have the signal above the noise level in the late-time of the scattered field. This is very important for the E/S-pulse discrimination technique since it uses the late-time of the returned signal of a target. A simple analysis is done for a thin cylinder illuminated by an arbitrary time-dependent spherical wavefront at oblique incidence. From this analysis, a rough estimate will be made as to how much power must be transmitted in order to keep the late-time signal above the noise level. Figure 42 is a geometrical configuration of a thin cylinder illuminated by the impressed field $\vec{E}^i(\vec{r},s)$ and the cylinder, in turn, maintained the scattered field $\vec{E}^s(\vec{r},s)$.

Assume an incident electric field with an arbitrary time-dependent spherical wavefront propagating in the u direction makes an angle θ with cylinder axis having the following expression:

$$\vec{E}^i(r,t) = \hat{v}\,\frac{r_o}{r}\,E_o P\left(t - \frac{r+u}{c}\right),$$

where r is the distance between the antenna and the target, r_o is the distance between the antenna phase center and an antenna aperture, $u = z\cos\theta$ and P(t) is the time-dependent function describing the incident electric field which has an amplitude of E_o at antenna aperture.

In transform domain the incident field is:

$$\vec{E}^i(r,s) = \hat{v}\,\frac{r_o E_o P(s)}{r}\,\exp\left(\frac{-su}{c}\right)\,\exp\left(\frac{-sr}{c}\right).$$

The general electric field integral equation (EFIE) for the transform induced current $\vec{K}(\vec{r},s)$ excited on a surface of an arbitrary perfectly conducting body is:

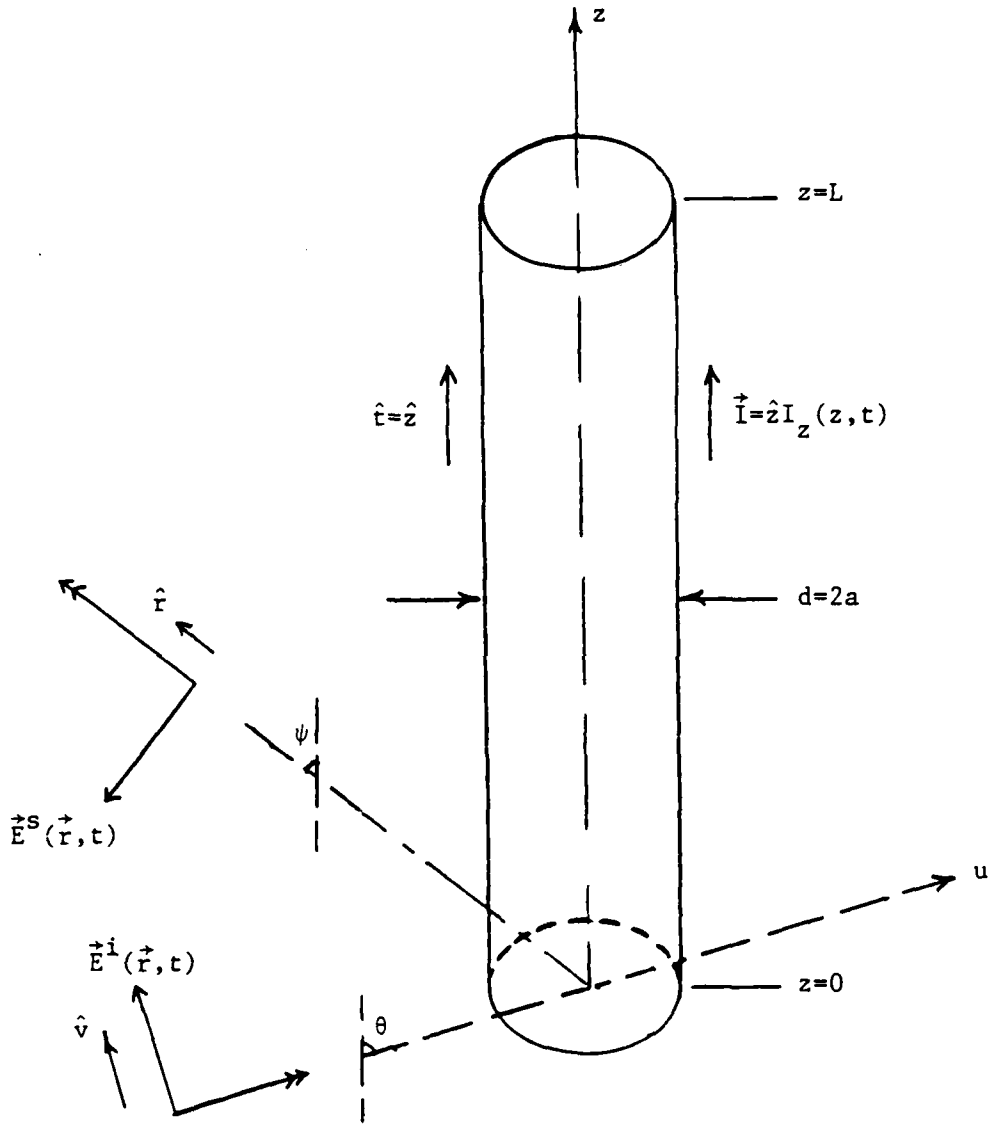

Figure 42. A wire target is illuminated by an interrogating EM pulse, $\vec{E}^i$, and it, in turn, produces a scattered wave, $\vec{E}^s$.

$$\frac{1}{s\epsilon_o}\int_s \left[\nabla'\cdot\vec{K}(\vec{r}',s)(\hat{t}\cdot\nabla) - \frac{s^2}{c^2}\hat{t}\cdot\vec{K}(\vec{r}',s)\right]\frac{e^{\frac{-sR}{c}}}{4\pi R}\,dS = -\hat{t}\cdot\vec{E}^i(\vec{r},s),$$

for all r in the space S, and $R = |\vec{r} - \vec{r}'|$ is the distance between source and field points on the body surface. Specializing the EFIE to a thin cylinder gives:

$$\int_o^L I(z',s)\left[\frac{\partial^2}{\partial z^2} - \frac{s^2}{c^2}\right]K(z,z',s)dz' = -\epsilon_o s E_z^i(z,s),$$

where:

$$E_z^i(z,s) = \frac{r_o E_o P(s)}{r}\sin\theta e^{-\frac{szcos\theta}{c}} e^{-\frac{sr}{c}},$$

$$K(z,z',s) = \frac{e^{-\frac{sR}{c}}}{4\pi R} \qquad \text{with} \qquad R = \sqrt{(z-z')^2 + a^2}.$$

Rewriting the EFIE in SEM notation gives:

$$\int_o^L I(z',s)\Gamma(z,z',s)dz' = -\epsilon_o s E_z^i(z,s) \quad \text{----} \quad \text{for } 0\le z\le L$$

with $$\Gamma(z,z',s) = \left[\frac{\partial^2}{\partial z^2} - \frac{s^2}{c^2}\right]\frac{e^{-\frac{sR}{c}}}{4\pi R}.$$

The SEM solution for the induced current, I(z,s), for the excitation $E^i{}_z(z,s)$ is:

$$I(z,s) = \sum_{\alpha=1}^{N} \eta_\alpha(s)\nu_\alpha(z)(s - s_\alpha)^{-1} + W(z,s).$$

The first term of I(z,s) is the SEM expansion due to first order simple pole singularities while the other terms are due to complex singularities such as higher order poles, branch points, essential singularities, and an entire function. It is important to note that the coupling coefficients η_α are dependent on the incident field illumination.

The natural mode current distribution $\nu_\alpha(z)$ which can exist at complex frequencies $s = s_\alpha$ when the impressed field vanishes, $E_z^i(z,s) = 0$, is defined through:

$$\int_o^L \nu_\alpha(z')\Gamma(z,z',s_\alpha)dz' = 0.$$

Substituting the I(z,s) into the EFIE yields the coupling coefficient at $s = s_\beta$:

$$\eta_\beta(s_\beta) = \frac{\int_o^L \nu_\beta(z)S(z,s_\beta)dz}{\int_o^L\int_o^L \nu_\beta(z)\nu_\beta(z')\Gamma_{1\beta}(z,z',s_\beta)dzdz'},$$

where:

$$S(z,s_\beta) = -\epsilon_o s_\beta E_z^i(z,s_\beta) \text{ and,}$$

$$\Gamma_{\ell\beta} = \frac{1}{\ell!}\frac{\partial^\ell}{\partial s^\ell}\Gamma(z,z',s)\bigg|_{s=s_\beta}.$$

An important assumption made in obtaining the coupling coefficient is that W(z,s) has no simple pole or higher order poles at $s = s_\beta$. The coupling coefficients are categorized into two types, class-1, which is best suited for late-time calculations, and class-2, which is best suited for early-time calculations. Since E/S-pulse discrimination uses the late-time

scattered field component, attention is given to the class-1 coupling coefficients.

Assume the modal current distribution, $\nu_\alpha(z)$, can be approximated as a sinusoid with an amplitude a_α defined as:

$$a_\alpha^2 = \left[\int_o^L\int_o^L \sin\left(\frac{\alpha\pi z}{L}\right)\sin\left(\frac{\alpha\pi z'}{L}\right)\Gamma_{1\alpha}(z,z',s_\alpha)dzdz'\right]^{-1},$$

then

$$\eta_\alpha(s) \approx - a_\alpha \epsilon_o s \frac{r_o E_o P(s)}{r} \sin\theta \; e^{-\frac{sr}{c}} \int_o^L \sin(\frac{\alpha\pi z}{L}) e^{-\frac{sz\cos\theta}{c}} dz.$$

To calculate the impulse response of the thin cylinder, the $E_o P(t)$ function is chosen as a delta function with a Laplace Transform of 1. Simply substituting this into the above equations gives the following results.

After going through several approximations the amplitude of the αth current distribution is found to be:

$$a_\alpha^2 = - \frac{4\pi c^2}{s_\alpha L}\left[2 \ln (\frac{L}{a}) - 1\right]^{-1},$$

while the coupling coefficient is:

$$\eta_\alpha(s) = \frac{sr_o a_\alpha \epsilon_o s \sin\theta \; e^{-\frac{sr}{c}}}{r\left[(s/c\cos\theta)^2 + \left(\frac{\alpha\pi}{L}\right)^2\right]} \left(\frac{\alpha\pi}{L}\right)\left[e^{-\frac{sL}{c}\cos\theta} - 1\right].$$

Combining these results gives:

$$I(z,s) \approx \sum_{\alpha=1}^{N} a_\alpha \eta_\alpha(s)(s - s_\alpha)^{-1} \sin\left(\frac{\alpha\pi z}{L}\right),$$

and

$$a_\alpha \eta_\alpha(s) \approx \frac{r_o\left[\frac{-4\pi}{\mu_o L}\right] \sin\theta \; e^{-\frac{sr}{c}\left[\frac{s}{s_\alpha}\right]\left[\frac{\alpha\pi}{L}\right]}}{r\left[\left(\frac{s}{c}\cos\theta\right)^2 + \left(\frac{\alpha\pi}{L}\right)^2\right]\left[2\ln\left(\frac{L}{a}\right) - 1\right]} \left[\cos(\alpha\pi)\, e^{-\frac{sL}{c}\cos\theta} - 1\right],$$

---- for class-2

while for class-1, $a_\alpha \eta_\alpha = a_\alpha \eta_\alpha(s \to s_\alpha)$.

Once the induced current on the thin cylinder is known, the scattered field maintained by this current in the far zone can be calculated. The scattered field maintained by general current $\vec{J}(\vec{r},t)$ is given by:

$$\vec{E}^s(\vec{r},t) = -\nabla\Phi^s(\vec{r},t) - \frac{\partial}{\partial t}\vec{A}^s(\vec{r},t),$$

where Φ^s and $\vec{A}^s$ are scalar and vector potentials maintained by the induced current, and they are defined in the Laplace transform domain as:

$$\Phi^s(\vec{r},s) = \frac{1}{4\pi\epsilon_o}\int_v \rho(\vec{r}',s)\,\frac{e^{-\frac{sR}{c}}}{R}\,dv',$$

$$\vec{A}^s(\vec{r},s) = \frac{\mu_o}{4\pi}\int_v \vec{J}(\vec{r}',s)\,\frac{e^{-\frac{sR}{c}}}{R}\,dv'.$$

After some manipulation, the scattered field in the far zone ($sR/c \gg 1$) is found to be:

$$\vec{E}^s(r,s) \simeq -\frac{\mu_o s}{4\pi}\int_v \left[\vec{J}(\vec{r}',s) - \hat{R}c\rho(\vec{r}',s)\right]\frac{e^{-\frac{sR}{c}}}{R}\,dv'.$$

Using the continuity equation $\nabla\cdot\vec{J}(\vec{r},s) = -s\rho(\vec{r},s)$, and using the approximation for distance $R \approx r$, and for phase $R \approx r - \hat{r}\cdot\vec{r}'$, the scattered field is simplified to:

$$\vec{E}^s(\vec{r},s) \simeq -\frac{\mu_o s}{4\pi}\frac{e^{-\frac{sr}{c}}}{r}\hat{r}\times\left[\hat{r}\times\int_v \vec{J}(\vec{r}',s)\, e^{\frac{s(\hat{r}\cdot\vec{r}')}{c}}\, dv'\right].$$

In the thin cylinder case $\vec{J}(\vec{r}',s)$ is $\hat{z}\, I(z',s)\delta(x')\delta(y')$, while $\vec{r}' = z'\hat{z}$, $\hat{r}\cdot\vec{r}' = z'\cos\psi$, where ψ is shown in Fig. 42.

The backscattered field is given when $\psi = \pi - \theta$:

$$\vec{E}_b^s(\vec{r},s) = -\hat{\theta}\,\frac{r_o s^2\sin^2\theta}{L[2\ln\left(\frac{L}{a}\right) - 1]}\,\frac{e^{-\frac{2sr}{c}}}{r^2}\sum_{\alpha=1}^{N}\left(\frac{\alpha\pi}{L}\right)^2\frac{(s - s_\alpha)^{-1}}{s_\alpha}\cdot$$

$$\cdot\left[\frac{1 - (-1)^\alpha e^{-\frac{sL}{c}\cos\theta}}{\left(\frac{s\cos\theta}{c}\right)^2 + \left(\frac{\alpha\pi}{L}\right)^2}\right]^2.$$

As we can clearly see that the scattered field depends on the class-1 or class-2 coefficients and they both depend on the aspect of incident wavefront.

Since the back scattered field was calculated for an impulsive incident field, the system transfer function in the Laplace transform domain can be easily evaluated:

$$H(\theta,s) = K_1 e^{-\frac{2sr}{c}}\sum_{\alpha=1}^{N}\frac{1}{\alpha^2 s_\alpha}\,\frac{s^2}{(s - s_\alpha)}\left[\frac{1 - (-1)^\alpha e^{-sT}}{1 + \left(\frac{T}{\alpha\pi}\right)^2 s^2}\right]^2,$$

with $K_1 = -\, r_o L \sin^2\theta / r^2\pi^2 [2\ln(\frac{L}{a}) - 1]$, and $T = L\cos\theta/c$ is the one way transit-time delay parameter depending on the aspect of incidence.

To get the expressions in the time domain simply do the inverse Laplace transform, and the scattered field for any incident wavefront can be obtained by the convolution.

The transfer function can be manipulated into the form below:

$$H(\theta,s) = K_1 e^{-\frac{2sr}{c}} \sum_{\alpha=1}^{N} H_\alpha(\theta,s),$$

and $$H_\alpha(\theta,s) = \frac{a_c^4}{\alpha^2 s_\alpha} \frac{s^2}{(s-s_\alpha)} \left[\frac{1 - (-1)^\alpha e^{-sT}}{\left(s^2+a_c^2\right)}\right]^2, \text{ with } a_c = \frac{\alpha\pi}{T}.$$

The impulse response $h(\theta,t)$ is simply obtained as:

$$h(\theta,t) = L^{-1}\{H(\theta,s)\}$$

$$= K_1 \sum_{\alpha=1}^{N} h_\alpha(\theta,\tau), \text{ where } \tau = t - \frac{2r}{c}.$$

After significant effort $h_\alpha(\theta,\tau)$ is found to be:

$$h_\alpha(\theta,\tau) = A_\alpha(s_\alpha)\left[u(\tau)e^{s_\alpha\tau} - 2(-1)^\alpha u(\tau - T)e^{s_\alpha(\tau-T)} + u(\tau - 2T)e^{s_\alpha(\tau-2T)}\right]$$

$$- [B_\alpha(s_\alpha)f_1(\tau) - C_\alpha(s_\alpha)f_2(\tau)]\sin(a\tau)$$

$$- [D_\alpha(s_\alpha)f_1(\tau) - E_\alpha(s_\alpha)f_2(\tau)]\cos(a\tau),$$

with:

$$f_1(\tau) = u(\tau) - 2u(\tau - T) + u(\tau - 2T)$$

$$f_2(\tau) = \tau u(\tau) - 2(\tau - T)2u(\tau - T) + (\tau - 2T)u(\tau - 2T)$$

$u(\tau)$ is a unit step function.

$$A_\alpha(s_\alpha) = \frac{a_c^4 s_\alpha}{\alpha^2(s_\alpha^2 + a_c^2)^2}, \qquad B_\alpha(s_\alpha) = \frac{a_c^3(s_\alpha^2 - a_c^2)}{2\alpha^2(s_\alpha^2 + a_c^2)^2},$$

$$C_\alpha(s_\alpha) = \frac{a_c^5}{2\alpha^2 s_\alpha(s_\alpha^2 + a_c^2)} \qquad D_\alpha(s_\alpha) = \frac{a_c^4 s_\alpha}{\alpha^2(s_\alpha^2 + a_c^2)^2},$$

$$E_\alpha(s_\alpha) = \frac{a_c^4}{2\alpha^2(s_\alpha^2 + a_c^2)}$$

Considering only the late-time, the contribution by $f_1(t)$ and $f_2(t)$ vanishes. The impulse response in the late-time then becomes:

$$h_\alpha(\theta,\tau) = A_\alpha(s_\alpha)e^{s_\alpha\tau}\left[1 - (-1)^\alpha e^{-s_\alpha T}\right]^2, \qquad \text{when } \tau \geq 2T.$$

If a rectangular pulse of width T_p with unit amplitude is chosen as the incident field $E_o P(t)$, then the backscattered field $\vec{E}_b^s$ is obtained by the convolution as:

$$r^2\vec{E}_b^s(\tau,\theta) = \hat{\theta}\, Q_1 \sum_{\alpha=1}^{N} Q_2(s_\alpha)e^{s_\alpha\tau}\left[1 - (-1)^\alpha e^{-s_\alpha T}\right]^2 \left[1 - e^{-s_\alpha T_p}\right],$$

where

$$Q_1 = \frac{r_o L \sin^2\theta}{\pi^2[2\ln(\frac{L}{a}) - 1]}, \qquad Q_2 = \frac{a_c^4}{\alpha^2(s_\alpha^2 + a_c^2)^2}.$$

The complex natural frequencies are always in complex conjugate pairs, so to get the total backscattered field, contribution due to $s = s_\alpha^*$ is added with the contribution of $s = s_\alpha$. The contribution by $s = s_\alpha^*$ is simply evaluated by substituting s_α^* wherever s_α exists. An important observation is that the coefficient $Q_2(s_\alpha^*)$ is a ratio of polynomials in s with real coefficients. Therefore $Q_2(s_\alpha^*) = Q_2^*(s_\alpha)$, so the backscattered field can be simplified to:

$$r^2\vec{E}_b^s(\tau,\theta) = \hat{\theta}\, Q_1 \sum_{\alpha=1}^{N} \Big\{ g_\alpha(\tau) - g_\alpha(\tau - T_p) - 2(-1)^\alpha g_\alpha(\tau - T)$$

$$+ 2(-1)^\alpha g_\alpha(\tau - T - T_p) + g_\alpha(\tau - 2T) - g_\alpha(\tau - 2T - T_p) \Big\}, \qquad (1)$$

and $g_\alpha(\tau) = 2e^{\sigma_\alpha \tau}[\text{Real}(Q_2(s_\alpha))\cos\omega_\alpha\tau - \text{Im}(Q_2(s_\alpha))\sin\omega_\alpha\tau]$, with $s_\alpha = \sigma_\alpha + j\omega_\alpha$.

The quantity $\vec{E}_b^s$ given in eq. (1) is the backscattered electric field at the receiving antenna maintained by a thin wire target which is excited by a rectangular electric field pulse having a duration of T_p.

In summary, when illuminated by an incident electric field pulse of:

$$\vec{E}^i(\vec{r},t) = \hat{v}\,\frac{r_o}{r}\,E_o P\left(r - \frac{r+u}{c}\right),$$

the backscattered electric field maintained by a wire target at the receiving antenna can be expressed as:

$$\vec{E}_b^s(\tau,\theta) = \hat{\theta}\,\frac{E_o}{r^2}\,f(\tau,\theta) \qquad \text{where } \tau = t - 2R/c,$$

and

$$f(\tau,\theta) = Q_1 \sum_{\alpha=1}^{N} \Big\{ g_\alpha(\tau) - g_\alpha(\tau - T_p) - 2(-1)^\alpha g_\alpha(\tau - T) + 2(-1)^\alpha g_\alpha(\tau - T - T_p) + g_\alpha(\tau - 2T) - g_\alpha(\tau - 2T - T_p) \Big\}. \qquad (2)$$

The power density of the radiated pulse at the aperture of the transmitting antenna is $P_t = E_o^2/2\zeta_o$ where ζ_o is the impedance of free space. The power density of the backscattered wave by the target at the location of the receiving antenna is $P_s = |\vec{E}_b^s|^2/2\zeta_o$. We can define the normalized power density of the backscattered wave as:

$$\frac{P_s}{P_t} = \frac{|\vec{E}_b^s|^2}{E_o^2} = \frac{f^2(\tau,\theta)}{r^4} \qquad (3)$$

Some numerical results have been calculated for a wire target with a length of 10 m and a radius of 5 cm being illuminated by a 1 nanosecond rectangular pulse. Figure 43 shows the normalized late-time pulse response of the target, $f(\tau,\theta)$, when the pulse is normally incident upon the target, $\theta = 90°$. This pulse response was constructed with 600 points in time and using 10 natural frequencies of the target. We have shown only the late-time pulse response because in the E/S pulse discrimination technique we have no use for the early-time pulse response which is usually difficult to calculate numerically. Figures 44 and 45 show the late-time pulse responses

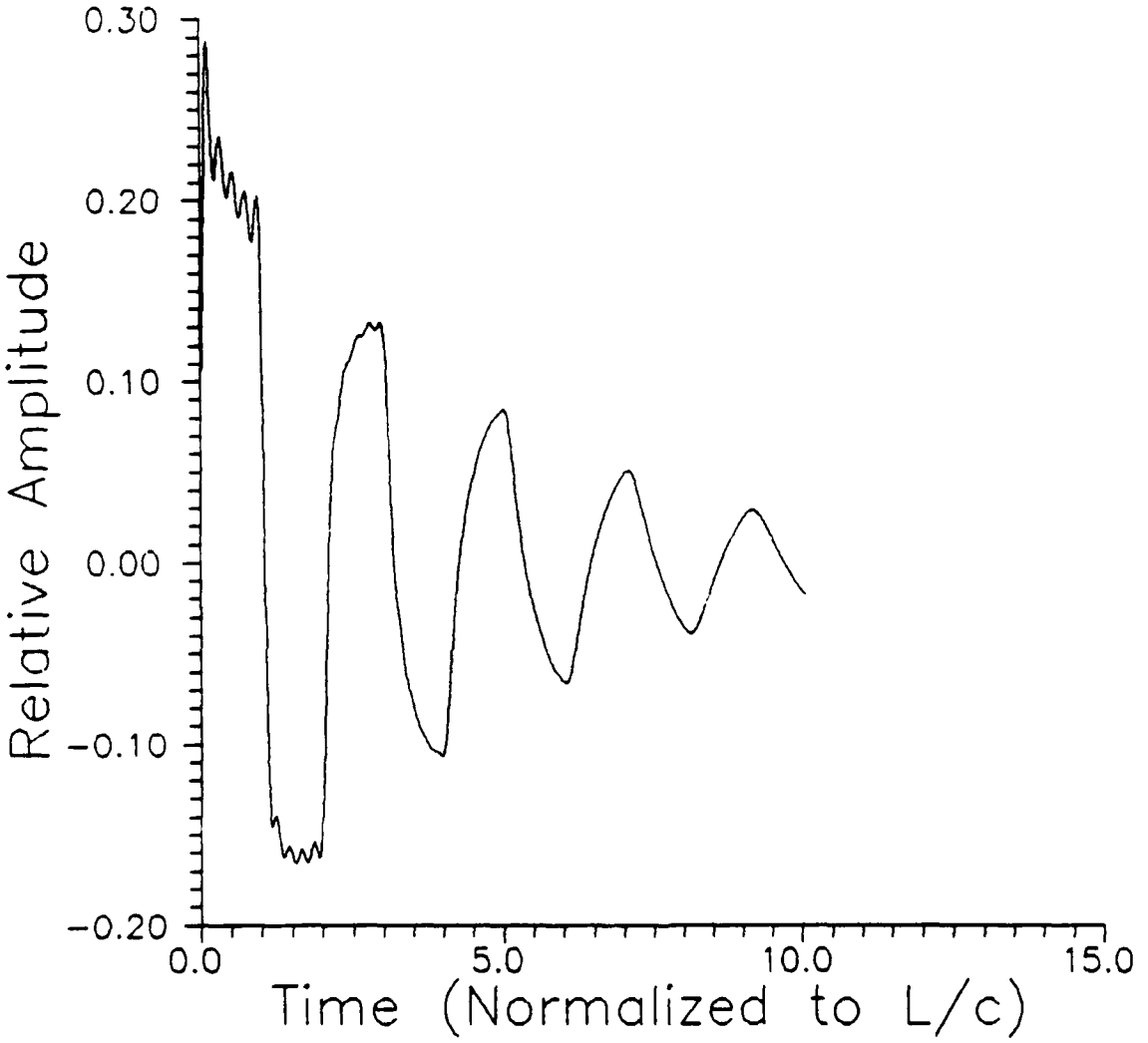

Figure 43. Normalized pulse response of a wire target (10 m in length and 5 cm in radius) illuminated by an incident pulse (1 ns duration) at an aspect angle of $\theta = 90°$.

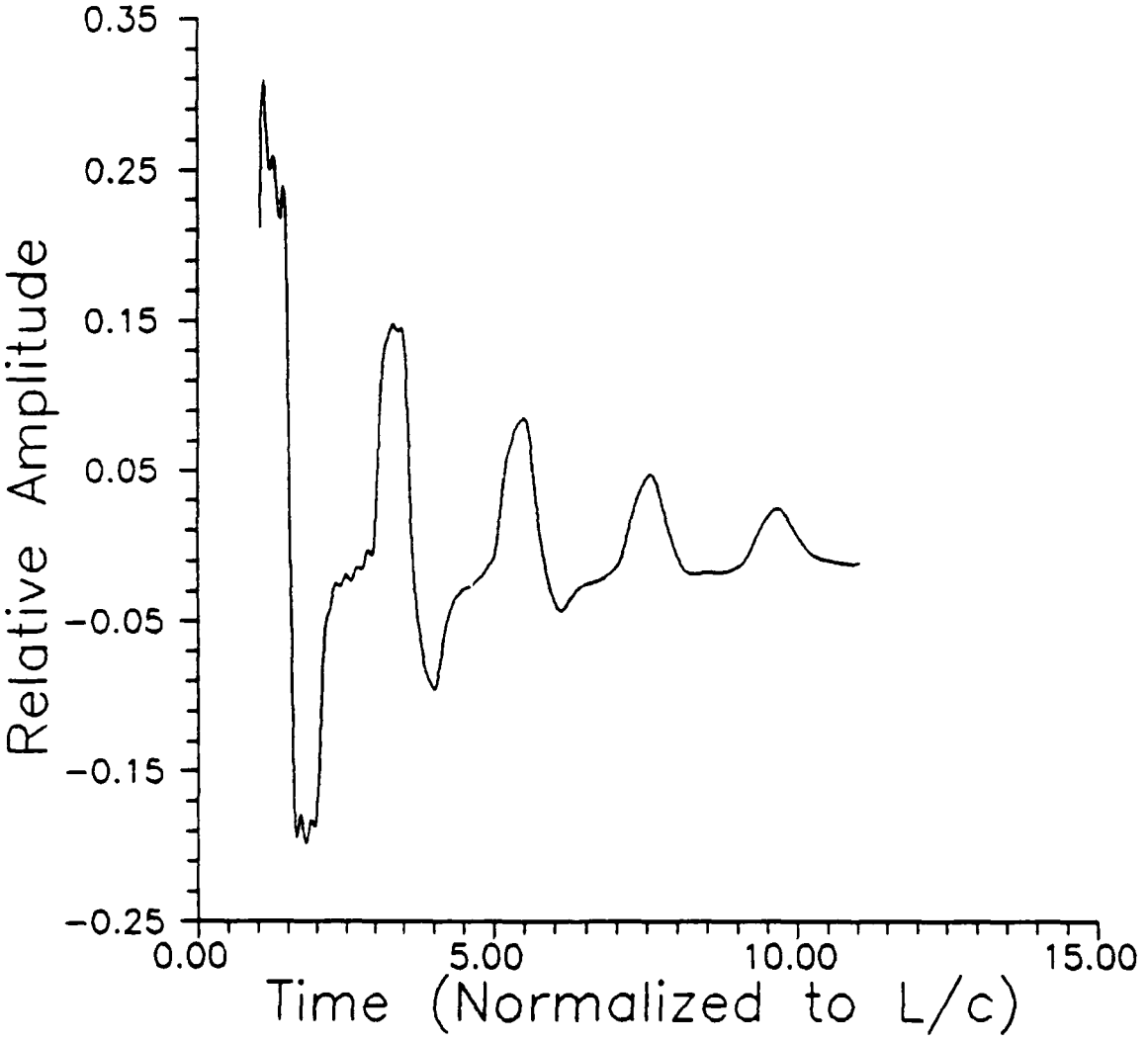

Figure 44. Normalized pulse response of a wire target (10 m in length and 5 cm in radius) illuminated by an incident pulse (1 ns duration) at an aspect angle of $\theta = 60°$.

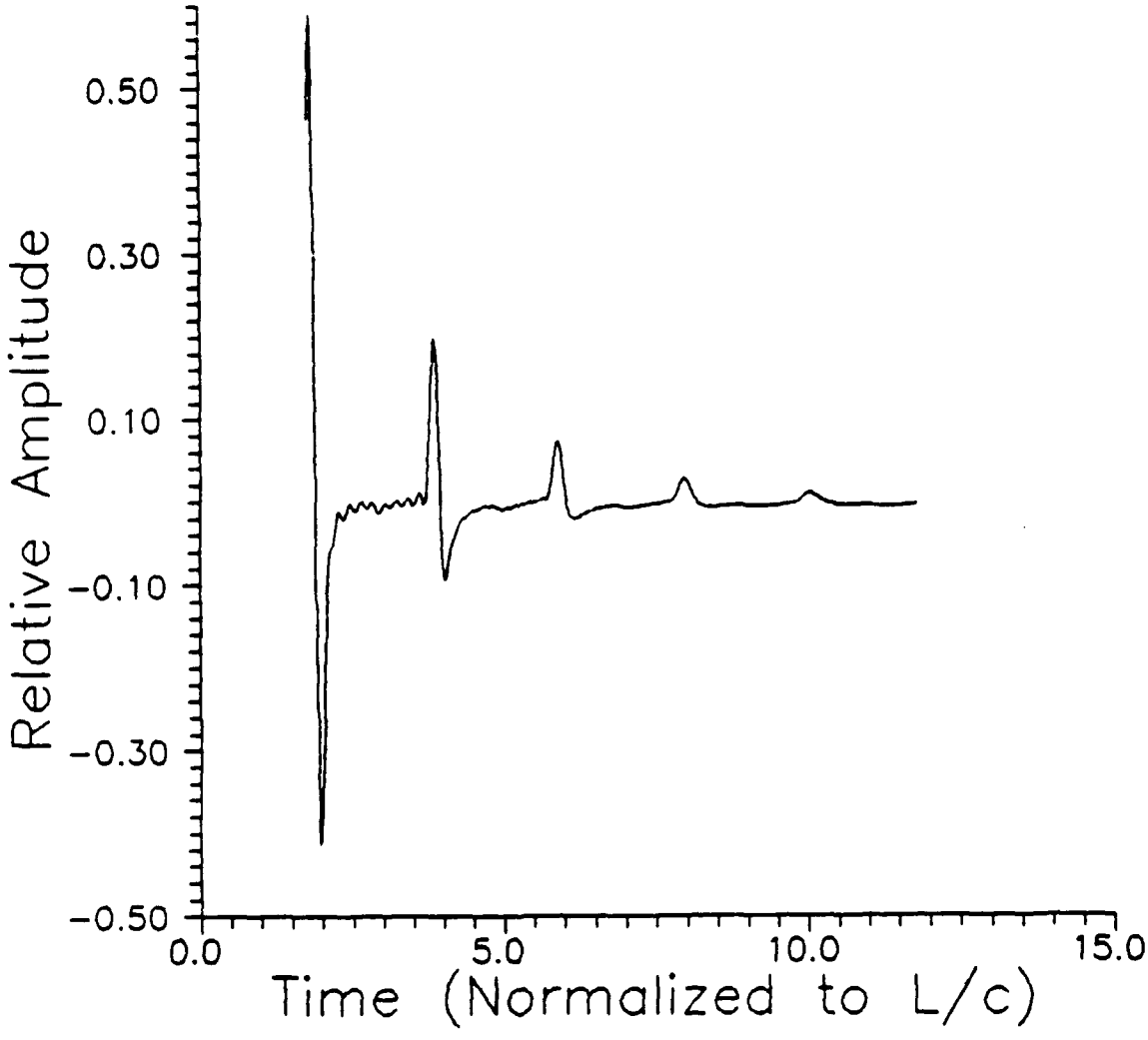

Figure 45. Normalized pulse response of a wire target (10 m in length and 5 cm in radius) illuminated by an incident pulse (1 ns duration) at an aspect angle of $\theta = 30°$.

of the same target when the radiated pulse is incident upon the target at an aspect angle of 60° and 30°, respectively.

Figure 46 shows the normalized power density of the backscattered wave at the receiving antenna multiplied by r^4, or the quantity of $f^2(\tau,\theta)$, for the case of normal incidence, $\theta = 90°$. Figures 47 and 48 show the corresponding results for the cases of $\theta = 60°$ and 30°, respectively. Physical meaning of the normalized power density is given as follows. For example, in Fig. 46 at the normalized time of $\tau/(L/C) = 1$, the normalized power density, $f^2(\tau,\pi/2)$, is 0.02. This means that if the power density of the incident pulse is 1 watt/m^2 and the wire target is located at 1 m away from the transmitting and receiving antennas, the power density of the backscattered wave at the receiving antenna is 0.02 watt/m^2.

We can now estimate the required radiated power of the transmitting antenna to produce a backscattered wave from a wire target with sufficient amplitude to be received by the receiving antenna.

Assuming that the effective radiating area of transmitting antenna is A_t and the effective receiving area of receiving antenna is A_r.

The total radiated power of the interrogating pulse is:

$$W_t = P_t A_t,$$

and the total power of the backscattered wave received by the receiving antenna is:

$$W_r = P_r A_r.$$

If we require the received power to be 10 dB higher than the noise power:

$$(W_r)_{req} = 10\, W_{noise}.$$

Thus, the required power density of the backscattered wave is:

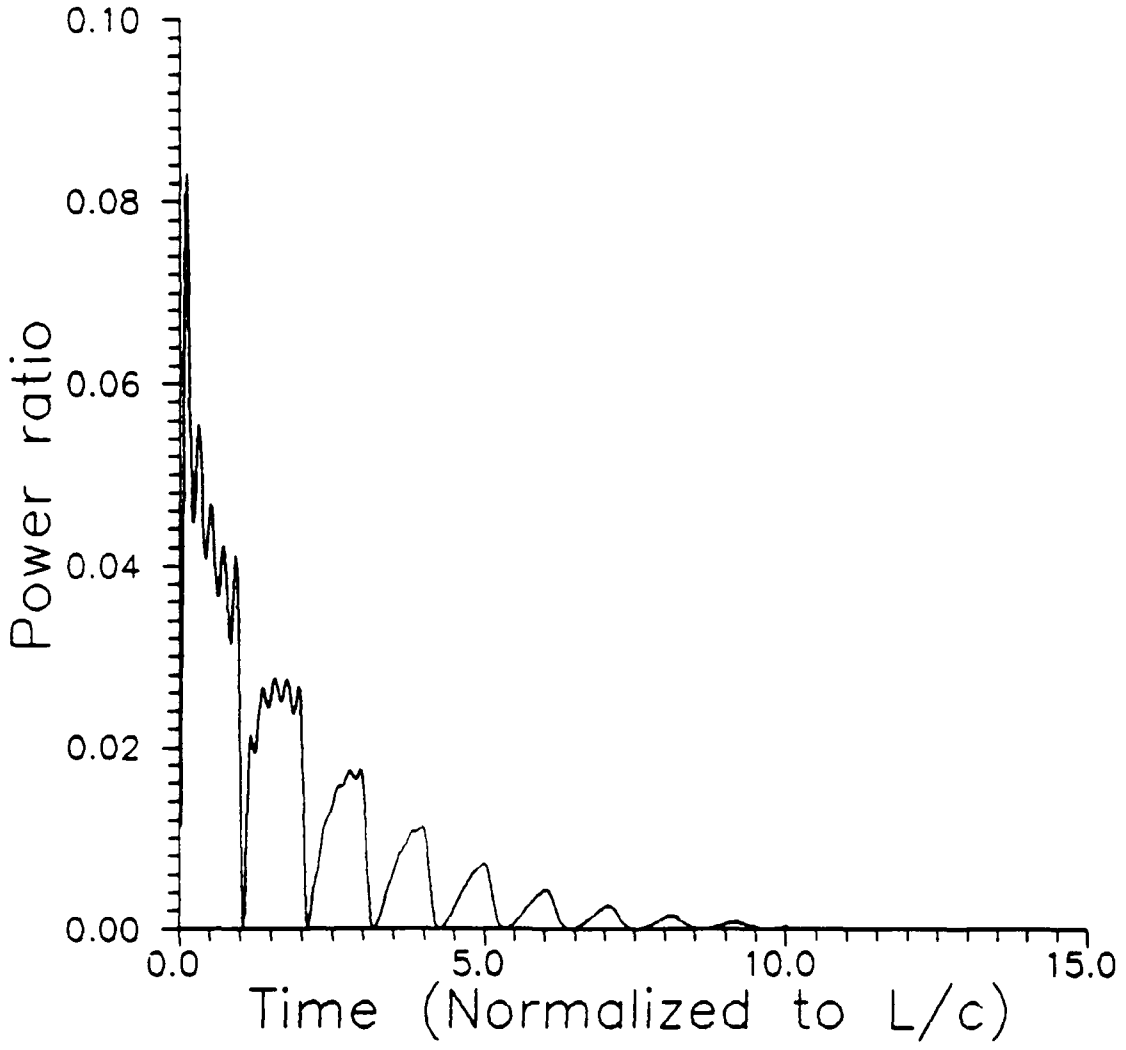

Figure 46. Normalized power density of the backscattered wave multiplied by r^4, or $f^2(\tau,\theta)$, of a wire target (10 m in length and 5 cm in radius) illuminated by an incident pulse (1 ns duration) at an aspect angle of $\theta = 90°$.

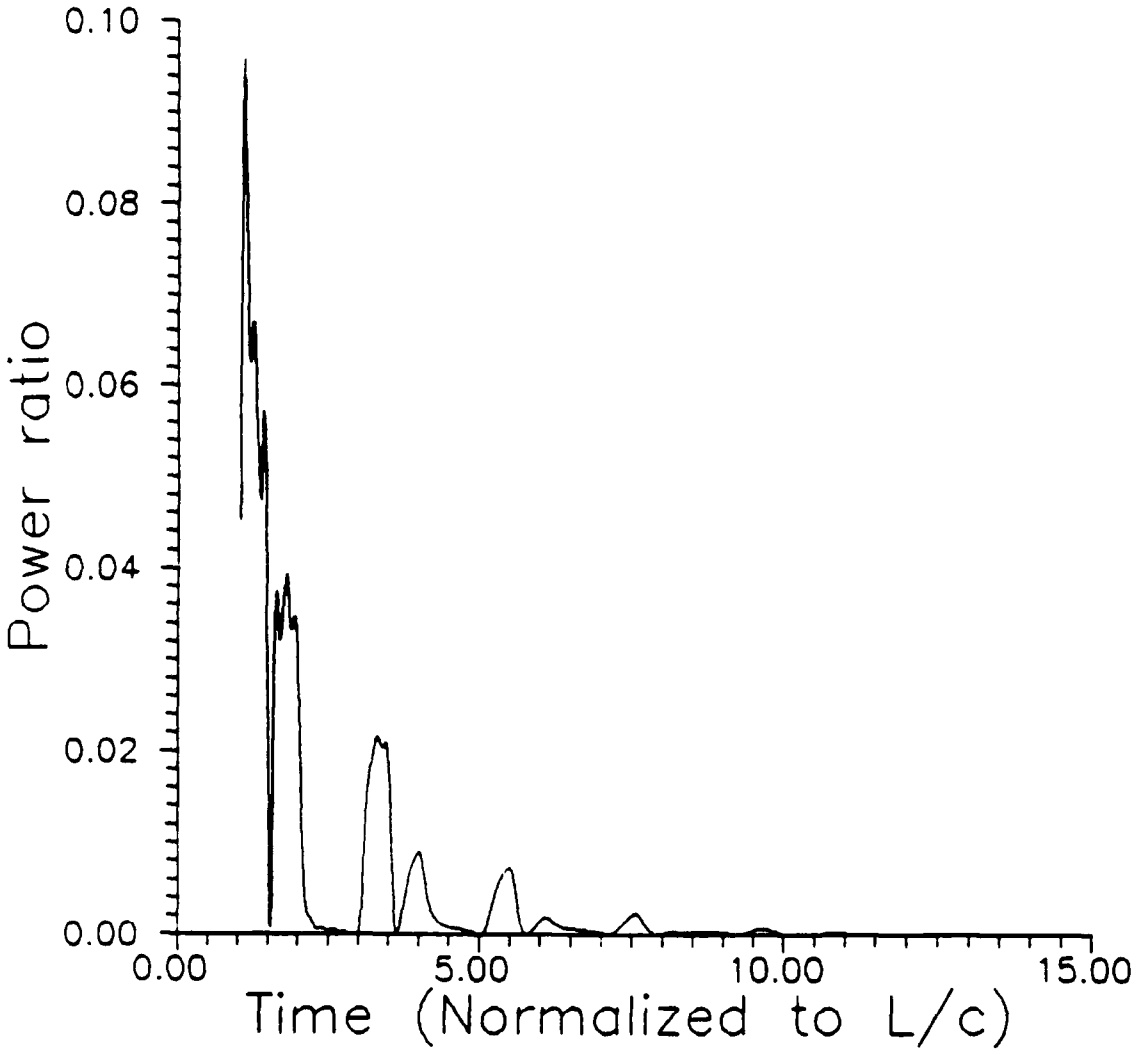

Figure 47. Normalized power density of the backscattered wave multiplied by r^4, or $f^2(\tau,\theta)$, of a wire target (10 m in length and 5 cm in radius) illuminated by an incident pulse (1 ns duration) at an aspect angle of $\theta = 60°$.

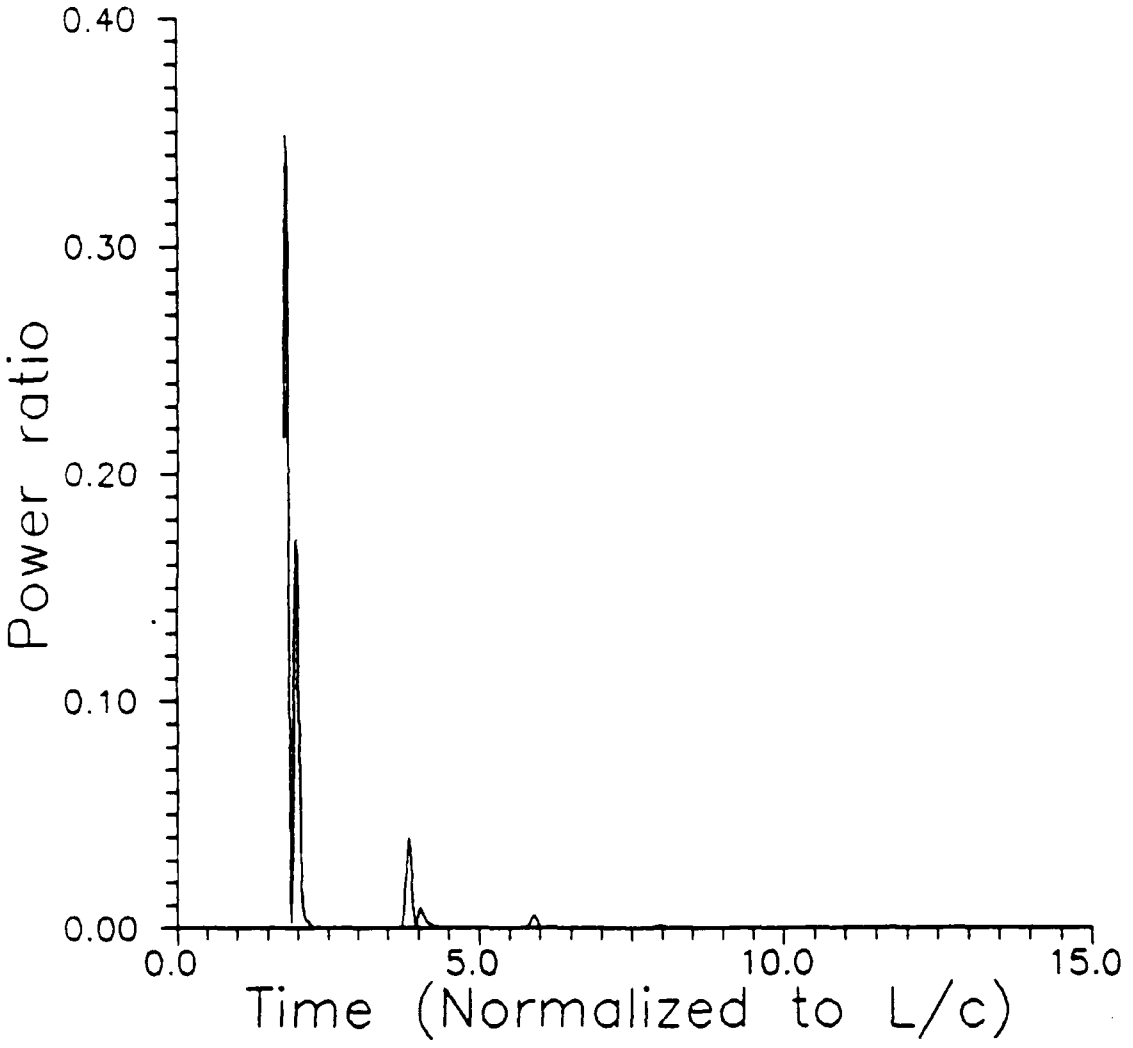

Figure 48. Normalized power density of the backscattered wave multiplied by r^4, or $f^2(\tau,\theta)$, of a wire target (10 m in length and 5 cm in radius) illuminated by an incident pulse (1 ns duration) at an aspect angle of $\theta = 30°$.

$$(P_s)_{req} = \frac{(W_r)_{req}}{A_r}.$$

As a result, the required power density of the interrogating pulse can be found from eq. (2) to be:

$$(P_t)_{req} = (P_s)_{req} r^4 / f^2(\tau_1, \theta),$$

where $f^2(\tau_1, \theta)$ is the normalized power density evaluated at an appropriate time τ_1 in the late-time period.

The total required power needs to be radiated by the transmitting antenna is:

$$(W_t)_{req} = (P_t)_{req} A_t$$

$$= (W_r)_{req} \frac{r^4}{f^2(\tau_1, \theta)} \frac{A_t}{A_r}. \qquad (4)$$

As a numerical example, let's consider the same wire target (10 m in length and 5 cm in radius) located at a distance of 10 Km from the antennas. Assuming that the noise level is roughly 5 μV or the noise power is 5×10^{-13} watts using a 50 ohm transmission line. To have the received power of the backscattered wave be 10 dB above the noise power:

$$(W_r)_{req} = 10(5 \times 10^{-13}) = 5 \times 10^{-12} \text{ watts}.$$

From Figs. 46 to 48, let's choose $f^2(\tau_1, \theta)$ to be 0.02, an average value of $f^2(\tau, \theta)$ in the late-time period. If the same antenna or the same type of antennas are used for transmitting and receiving purposes, we can assume that $A_t = A_r$.

For this example, the total required power to be radiated by the transmitting antenna is:

$$(W_t)_{req} = (5 \times 10^{-12}) \frac{(10^4)^4}{0.02} = 2.5 \times 10^6 \text{ watts.}$$

Since the interrogating pulse is 1 nanosecond (T_p), the energy of the pulse is:

$$E = (W_t)_{req} T_p = 2.5 \times 10^{-3} \text{ Joule.}$$

The radiated power for sending a single 1 ns pulse is in the order of Megawatt. This value appears to be very high. However, the energy contained in the interrogating pulse is quite small. If it is necessary to reduce the power density of the radiating pulse or the electric field intensity of the radiating pulse, a train of pulses should be radiated and the multi-pulse coherent processing scheme, as discussed in Section 8, applied in receiving the backscattered wave from the target. Another easy solution is to use antennas with large effective areas.

11. List of Publications

The following papers reporting research results of this research program have been published in Journals or presented in professional meetings.

1. W. Sun, K.M. Chen, E. Rothwell, and D.P. Nyquist, "Target discrimination using the E-pulse technique and high gain antennas," presented at 1987 IEEE AP-S/URSI Symposium, Virginia Tech., June 15-19, 1987.

2. N. Gharsallah, K.M. Chen, E. Rothwell, and D.P. Nyquist, "Experimental characterization of transient EM response of a sphere," presented at 1987 IEEE AP-S/URSI Symposium, Virginia Tech., June 15-19, 1987.

3. E. Rothwell, K.M. Chen, and D.P. Nyquist, "Extraction of the natural frequencies of a radar target from a measured response using E-pulse techniques," IEEE Transactions on Antennas and Propagation, Vol. AP-35, No. 6, pp. 715-720, June 1987.

4. E. Rothwell, K.M. Chen, D.P. Nyquist, and P. Ilavarasan, "Time domain deconvolution of transient radar data," presented at the National Radio Science Meeting, Boulder, CO, January 5-8, 1988.

5. E. Rothwell, K.M. Chen, D.P. Nyquist, and W. Sun, "A hybrid E-pulse/least squares technique for natural resonance extraction," presented at the National Radio Science Meeting, Boulder, CO, January 5-8, 1988.

6. W.M. Sun, K.M. Chen, D.P. Nyquist, and E. Rothwell, "Discrimination of conducting plates by E-pulse technique," presented at the National Radio Science Meeting, Boulder, CO, January 5-8, 1988.

7. E. Rothwell and K.M. Chen, "Hybrid E-pulse/least squares technique for natural resonance extraction," Proceedings of the IEEE, Vol. 76, No. 3, pp. 296-298, March 1988.

8. K.M. Chen, D.P. Nyquist, E. Rothwell, W.M. Sun, P. Ilavarasan, and W. Gesang, "New development in the study of radar target discrimination using E-pulses and S-pulses," presented at 1988 International IEEE AP-S/URSI Symposium, Syracuse University, June 6-11, 1988.

9. W.M. Sun, K.M. Chen, D.P. Nyquist, and E. Rothwell, "Extraction of natural frequencies of a rectangular plate from measured responses," presented at 1988 International IEEE AP-S/URSI Symposium, Syracuse University, June 6-11, 1988.

10. W.M. Sun, K.M. Chen, D.P. Nyquist, and E. Rothwell, "Natural oscillations of an infinitely long cylinder coated with lossy materials," presented at 1988 International IEEE AP-S/URSI Symposium, Syracuse University, June 6-11, 1988.

11. P. Ilavarasan, E. Rothwell, K.M. Chen, and D.P. Nyquist, "Travelling-wave antennas for transient illumination of radar targets," presented at 1988 International IEEE AP-S/URSI Symposium, Syracuse University, June 6-11, 1988.

12. K.M. Chen, D.P. Nyquist, E. Rothwell, W.M. Jun and P. Ilavarasan, "New progress on radar target discrimination using E-pulses and S-pulses," presented at 1989 International IEEE AP-URSI Symposium, San Jose, June 26-30, 1989.

13. M. Deford, E. Rothwell, D.P. Nyquist and K.M. Chen, "Experimental investigation of the presence of natural mode information in the early time current response of a thin wire," presented at 1989 International IEEE AP-/URSI Symposium, San Jose, June 26-30, 1989.

14. W.M. Sun, K.M. Chen, D.P. Nyquist, and E.J. Rothwell, "The natural oscillation of an infinitely long cylinder coated with lossy material," Radio Science, Vol. 24, No. 3, pp. 369-380, May-June 1989.

15. K.M. Chen, D.P. Nyquist, and E.J. Rothwell, "Radar target discrimination using E-pulses and S-pulses," an invited paper presented at The First Progress in Electromagnetic Research Symposium, Boston, July 25-26, 1989.

16. N. Gharsallah, E.J. Rothwell, K.M. Chen, and D.P. Nyquist, "Identification of the natural resonance frequencies of a conducting sphere from a measured transient response," IEEE Trans. on Antennas and Propagation, Vol. 38, No. 1, pp. 141-143, January 1990.

17. P. Ilavarasan, E.J. Rothwell, K.M. Chen, D.P. Nyquist, and J. Ross, "Radar target discrimination of nearly identical targets using free-field measurements," presented at 1990 IEEE AP-S International Symposium and URSI National Radio Science Meeting, Dallas, May 6-11, 1990.

18. E.J. Rothwell, J. Baker, D.P. Nyquist and K.M. Chen, "Approximate natural response of an arbitrarily shaped thin wire scatterer," presented at 1990 IEEE AP-S International Symposium and URSI National Radio Science Meeting, Dallas, May 6-11, 1990.

19. J. Ross, E.J. Rothwell, D.P. Nyquist, and K.M. Chen, "Multiple target discrimination using E-pulse technique," presented at 1990 IEEE AP-S International Symposium and URSI National Radio Science Meeting, Dallas, May 6-11, 1990.

20. W. Sun, K.M. Chen, D.P. Nyquist, and E.J. Rothwell, "Determination of the Natural Modes for a Rectangular Plate," IEEE Trans. on Antennas and Propagation, Vol. 38, No. 5, pp. 643-652, May 1990.

12. Personnel

The following researchers have participated in this research program.

1. Kun-Mu Chen, Professor of Electrical Engineering, Principal Investigator.
2. Dennis P. Nyquist, Professor of Electrical Engineering, Co-Principal Investigator.
3. Edward Rothwell, Associate Professor of Electrical Engineering, Co-Principal Investigator.
4. W.M. Sun, Graduate Research Assistant, graduated with Ph.D. in 1989.
5. Neila Gharsallah, Graduate Research Assistant, graduated with M.S. in 1987.
6. Ponniah Ilavarasan, Graduate Research Assistant.
7. John Ross, Graduate Research Assistant.
8. W. Gesang, Graduate Research Assistant.
9. J. Baker, Graduate Assistant.
10. M. Deford, Undergraduate Assistant.
11. M. Christensen, Undergraduate Assistant.
12. J. Veihl, Undergraduate Assistant.

Some of these students were not financially supported by the contract.

13. List of Appendices

Appendix 1:

"Radar target discrimination by convolution of radar return with extinction-pulses and single-mode extraction signals."

This paper presents basic theory on the E/S pulse technique with some experimental verification. It also proposes a target identification system based on the E/S pulse technique.

Appendix 2:

"Radar target discrimination using extinction-pulse technique."

This paper studies the application of the E-pulse technique to wire targets and single airplane models.

Appendix 3:

"Frequency domain E-pulse synthesis and target discrimination."

This paper synthesized E-pulses of targets using frequency-domain approach. It also shows experimental proof of the aspect-independence of the E-pulse technique.

Appendix 4:

"Extraction of the natural frequencies of a radar target from a measured response using E-pulse technique."

This paper introduces a new scheme of extracting natural frequencies of a target from a measured pulse response of the target based on the E-pulse technique.

Appendix 5:

"A hybrid E-pulse/least squares technique for natural resonance extraction"

This paper presents another new technique to exact the resonant frequencies of a target by combining the E-pulse technique and the least squares technique.

Appendix 6:

"The natural oscillation of an infinitely long cylinder coated with lossy material."

The purpose of this paper is to study the effect on the natural frequencies of a metallic body due to a coating of lossy material on the body surface.

Appendix 7:

"Identification of the natural resonance frequencies of a conducting sphere from a measured transient response."

In this paper the natural frequencies of a sphere are determined from the measured transient scattered field and surface charge response.

Appendix 8:

"Determination of the natural modes for a rectangular plate."

A new theoretical method for determining the natural modes of a rectangular plate is presented in this paper.

Appendix 9:

"The singularity expansion method and its application to target identification.

This paper reviews the singularity expansion method and shows its application leading to the development of the E/S pulse technique.

Appendix 10:

"Noise characteristics of the E-pulse technique for target discrimination."

This paper provides theoretical analysis of the noise-sensitivity of the E/S pulse technique.

Appendix 11:

"Approximate natural response of an arbitrarily shaped thin wire scatter."

This paper introduces an approximate but computationally simple technique for calculating the transient response of an arbitrarily shaped wire target.

Radar Target Discrimination by Convolution of Radar Return with Extinction-Pulses and Single-Mode Extraction Signals

KUN-MU CHEN, FELLOW, IEEE, DENNIS P. NYQUIST, MEMBER, IEEE, EDWARD J. ROTHWELL, MEMBER, IEEE, LANCE L. WEBB, MEMBER, IEEE, AND BYRON DRACHMAN

Abstract—**A new method of radar target discrimination and identification is presented. This new method is based on the natural frequencies of the target. It consists of synthesizing *aspect-independent* discriminant signals, called extinction-pulses (E-pulses) and single-mode extraction signals which, when convolved numerically with the late-time transient response of an expected target, lead to zero or single-mode responses. When the synthesized, discriminant signals for an expected target are convolved with the radar return from a different target, the resulting signal will be significantly different from the expected zero or single-mode responses, thus, the differing targets can be discriminated. Theoretical synthesis of discriminant signals from known target natural frequencies and experimental synthesis of them for a complex target from its measured pulse response are presented. The scheme has been tested with measured responses of various targets in the laboratory.**

I. Introduction

A NEW RADAR discrimination scheme has been investigated by our group over the past few years, and this paper describes the basic principle of the scheme and reports some recent results. The present scheme is based on the finding [1]–[5] that for a specific target there exist *aspect-independent* discriminant signals, called the extinction-pulses (E-pulses[1]) and single-mode extraction signals, which can be used to excite the target to produce desirable late-time radar returns. When these aspect-independent discriminant signals with particular waveforms are used to excite the target, they will produce zero response or single-mode responses in the late-time period. On the other hand, if the late-time response of the target radar return, which is excited by a convenient radar pulse and is the sum of target's natural modes, is convolved with the discriminant signals, the convolved output will yield zero response or single-mode responses. The former scheme is a transmitting scheme and the latter a receiving scheme. Since it is difficult to physically synthesize and radiate the discriminant signals with particular waveforms without suffering distortion, the latter receiving scheme is preferred. The synthesized signals with particular waveforms are now stored in the computer; they are convolved with the received radar return inside the computer. Thus, we can sidestep the difficulty of synthesizing and radiating the discriminant signals.

The synthesized discriminant signals can be used to discriminate targets because when the radar return of a wrong target is convolved with the synthesized discriminant signals of the expected target, the convolved outputs will be significantly different from the expected zero response or single-mode responses. Thus the wrong target can be discriminated.

The complex natural resonant frequencies of a radar target are aspect independent features of its transient electromagnetic response. A number of researchers have recently attempted to discriminate among various targets by extracting those natural frequencies from late-time transient radar returns. Since extraction of natural frequencies from late-time target responses is an inherently ill-conditioned numerical procedure, very large signal-to-noise (S/N) ratios are required in the transient return. It has therefore been concluded that this method for the direct discrimination of differing targets is impractical. Our discrimination scheme differs significantly. Synthesis of the discriminant signals requires only knowledge of the natural frequencies of various expected targets. The latter natural frequencies are measured in the laboratory where they are extracted from the late-time pulse responses of target scale models. The numerically ill-conditioned natural frequency extraction procedure need therefore be applied only to target responses measured in a controlled (S/N) environment. Synthesized discriminant signals based upon those laboratory measurements are stored as computer data files, and subsequently convolved numerically with actual transient target radar returns. Since the latter convolution operation is numerically well conditioned (a smoothing integral operator), the (S/N) requirements for the actual radar return are significantly relaxed.

Another observation made in the course of our study is worth noting. It is common thinking among many researchers that radar detection utilizing the late-time transient radar return may not be practical because it contains little energy; most energy is associated with the early-time part of that return. This thinking may be true for very low-Q targets.

Manuscript received June 22, 1985, revised September 5, 1985. This work was supported by the Naval Air Systems Command under Contract N00019-83-C-0132.

K. M. Chen, D. P. Nyquist, and E. J. Rothwell are with the Department of Electrical Engineering and Systems Science, Michigan State University, East Lansing, MI 48824.

L. L. Webb was with the Department of Electrical Engineering and Systems Science, Michigan State University, East Lansing, MI. He is now with Northrop Aircraft Division, One Northrop Avenue, Hawthorne, CA 90250.

B. Drachman is with the Department of Mathematics, Michigan State University, East Lansing, MI 48824.

IEEE Log Number 8608850.

[1] The E-pulse is similar to the K pulse studied by other workers [5], [10].

0018-926X/86/0700-0896$01.00

Fortunately, for most space vehicles, such as rockets and aircrafts, these targets are not exactly low-Q structures. There is sufficient energy contained in the late-time returns of such targets, as can be evidenced from our measured responses of complex targets as discussed in this paper.

In Sections II and III, we will demonstrate how to synthesize theoretically and experimentally E − 0, E − 1, —, E − n pulse or the zero mode, the first mode, —, the nth-mode extraction signal. E − 0 pulse (extinguishing all the modes) or the zero-mode extraction signal can be used to produce a zero-response in the convolved output while E − n pulse (extinguishing all but the nth-mode) or the nth-mode extraction signal will produce a nth-mode response in the convolved output.

In Section IV, examples are given to show the convolution of the synthesized discriminant signals with the measured radar returns of various targets. The effectiveness of target discrimination by the present method is also discussed.

Finally, a potential radar detection system based on the present scheme is suggested in Section V.

II. Synthesis of Discriminant Signals Based on Known Natural Frequencies

The zero-mode and other single-mode extraction signals or E − 0 pulse and E − n pulses of a given target can be synthesized theoretically based on the prior knowledge of natural frequencies of the target.

The late-time radar return of a target is the sum of natural modes, assuming the absence of noise, and it can be expressed as

$$h(t)=\sum_{n=1}^{N} a_n(\theta,\ \phi)e^{\sigma_n t}\ \cos\ (\omega_n t+\phi_n(\theta,\ \phi)) \tag{1}$$

where σ_n is the damping coefficient and ω_n is the angular frequency of the nth natural mode, and $a_n(\theta,\ \phi)$ and $\phi_n(\theta,\ \phi)$ are the amplitude and the phase angle of the nth natural mode. It is noted that σ_n and ω_n are independent of the aspect-angle (θ and ϕ), but $a_n(\theta,\ \phi)$ and $\phi_n(\theta,\ \phi)$ are usually strong functions of the aspect angle. N is the total number of natural modes which have significant amplitudes to be considered. In practice, N can be estimated based on the frequency spectrum of the interrogating radar pulse.

We aim to synthesize an extraction signal of duration T_e which can be convolved with the radar return $h(t)$ to produce a single-mode or zero-mode output in the late-time period ($t > T_e$):

$$\mathrm{E}^0(t)=\int_0^{T_e} \mathrm{E}^e(t')h(t-t')\ dt',\qquad \text{for } t>T_e \tag{2}$$

where $\mathrm{E}^0(t)$ is the convolved output signal, $\mathrm{E}^e(t)$ is the extraction signal to be synthesized. The substitution of (1) in (2) leads to

$$\mathrm{E}^0(t)=\sum_{n=1}^{N} a_n(\theta,\ \phi)e^{\sigma_n t}[A_n\ \cos\ (\omega_n t+\phi_n(\theta,\ \phi)) + B_n\ \sin\ (\omega_n t+\phi_n(\theta,\ \phi))],\quad \text{for } t>T_e \tag{3}$$

where

$$A_n=\int_0^{T_e} \mathrm{E}^e\ (t')e^{-\sigma_n t'}\ \cos\ \omega_n t'\ dt' \tag{4}$$

$$B_n=\int_0^{T_e} \mathrm{E}^e\ (t')e^{-\sigma_n t'}\ \sin\ \omega_n t'\ dt'. \tag{5}$$

The coefficients A_n and B_n which determine the amplitudes of the natural modes of the convolved output are independent of the aspect angle (θ and ϕ). This makes it possible to synthesize the aspect-independent $\mathrm{E}^e(t)$ for producing single-mode or zero-mode $\mathrm{E}^0(t)$. It is noted that A_n and B_n are numerically stable because they are finite integrals over a short period of time T_e, even though there is a time growing factor of $e^{-\sigma_n t'}$ in them.

Now for example, if we synthesize $\mathrm{E}^e(t)$ in such a way that $A_1 = 1$ and all other A_n and B_n go to zero, then the output signal will be a cosine first natural mode as

$$\mathrm{E}^0(t)=a_1(\theta,\ \phi)e^{\sigma_1 t}\ \cos\ (\omega_1 t+\phi_1(\theta,\ \phi)),\qquad \text{for } t>T_e.$$

If we choose $\mathrm{E}^e(t)$ in such a way that $B_3 = 1$ and all other A_n and B_n go to zero, then the output signal will be a sine third natural mode such as

$$\mathrm{E}^0(t)=a_3(\theta,\ \phi)e^{\sigma_3 t}\ \sin\ (\omega_3 t+\phi_3(\theta,\ \phi)),\qquad \text{for } t>T_e.$$

If we synthesize $\mathrm{E}^e(t)$ in such a way that all A_n and B_n vanish, then the zero-mode output is obtained:

$$\mathrm{E}^0(t)=0,\qquad \text{for } t>T_e.$$

This $\mathrm{E}^e(t)$ is the E − 0 pulse or the zero-mode extraction signal because it extinguishes the late-time response completely.

The next task is to synthesize $\mathrm{E}^e(t)$. Construct $\mathrm{E}^e(t)$ with a set of basis function $f_m(t)$ as

$$\mathrm{E}^e(t)=\sum_{m=1}^{2N} d_m f_m(t) \tag{6}$$

where $\{f_m(t)\}$ can be pulse functions, impulse functions or Fourier cosine functions, etc. and $\{d_m\}$ are the unknown coefficients to be determined. We need $2N$ of $f_m(t)$ because there are $2N$ of A_n and B_n to be specified,

$$A_n=\sum_{m=1}^{2N} M^c_{nm}d_m \tag{7}$$

$$B_n=\sum_{m=1}^{2N} M^s_{nm}d_m \tag{8}$$

where

$$M^c_{nm}=\int_0^{T_e} f_m(t')e^{-\sigma_n t'}\ \cos\ \omega_n t'\ dt' \tag{9}$$

$$M^s_{nm}=\int_0^{T_e} f_m(t')e^{-\sigma_n t'}\ \sin\ \omega_n t'\ dt'. \tag{10}$$

Equations (7) and (8) can be expressed in a matrix form as

$$\begin{bmatrix} A_n \\ B_n \end{bmatrix} = \begin{bmatrix} M^c_{nm} \\ M^s_{nm} \end{bmatrix} [d_m] \qquad \begin{matrix} n=1, 2, \cdots, N \\ m=1, 2, \cdots, 2N. \end{matrix} \tag{11}$$

The coefficient d_m for constructing $E^e(t)$ can then be obtained from

$$[d_m] = \begin{bmatrix} M^c_{nm} \\ M^s_{nm} \end{bmatrix}^{-1} \begin{bmatrix} A_n \\ B_n \end{bmatrix}. \tag{12}$$

To synthesize $E^e(t)$ for the jth-mode extraction, we can assign $A_j = 1$ or $B_j = 1$ and let all other A_n and B_n go to zero, and then calculate $[d_m]$ from (12) accordingly. Using this approach, we select an appropriate value for the signal duration T_e which is short and also leads to a well behaved waveform for $E^e(t)$.

To synthesize the E−0 pulse or the extraction signal for zero response, all A_n and B_n are set to be zero. For this case $[d_m]$ will have nontrivial solutions only when the determinant of $\begin{bmatrix} M^c_{nm} \\ M^s_{nm} \end{bmatrix}$ vanishes. That is

$$\det \begin{bmatrix} M^c_{nm} \\ M^s_{nm} \end{bmatrix} = 0. \tag{13}$$

This condition can be met because all the elements of M^c_{nm} and M^s_{nm} are functions of the signal duration T_e, and it is possible to numerically search for the optimum value of T_e which makes (13) valid. Usually we use the Newton method for this purpose. Once the optimum T_e is determined, $[d_m]$ can be easily determined from a set of homogeneous equations generated from (11) by setting A_n and B_n to be zero.

Single-mode extraction signals or E−n pulses can also be synthesized in a similar way as that for the E−0 pulse. For example, if we aim to synthesize the cosine first mode extraction signal, we drop the first equation involving A_1 in (11). We then have a new set of $(2N-1)$ simultaneous equations as

$$\begin{bmatrix} A_2 \\ \vdots \\ A_N \\ B_1 \\ \vdots \\ B_N \end{bmatrix} = \begin{bmatrix} M^c_{nm} \\ M^s_{nm} \end{bmatrix}' [d_m] \qquad \begin{matrix} n=2, 3, \cdots, N, & \text{for } M^c_{nm} \\ n=1, 2, \cdots, N, & \text{for } M^s_{nm} \\ m=1, 2, \cdots, 2N-1 & \end{matrix} \tag{14}$$

where $\begin{bmatrix} M^c_{nm} \\ M^s_{nm} \end{bmatrix}'$ is a $(2N-1) \times (2N-1)$ matrix and it is the original $\begin{bmatrix} M^c_{nm} \\ M^s_{nm} \end{bmatrix}$ matrix with its first row and its last column removed. We now force $A_2, \cdots, A_N, B_1, \cdots, B_N$ to be zero. This requires that

$$\det \begin{bmatrix} M^c_{nm} \\ M^s_{nm} \end{bmatrix}' = 0. \tag{15}$$

Equation (15) can be solved numerically to determine the optimum T_e for the cosine first mode extraction signal. After that $[d_m]$ can be determined from a corresponding set of homogeneous equations from (14).

It has been found that the signal duration T_e for various discriminant signals is not unique but there exists an optimum value of T_e for which the waveform of the discriminant signal is best behaved and it possesses a maximal sensitivity in discriminating the target [6]. This optimum value of T_e is numerically found to be slightly longer than twice the transit time of the target or 2 L/C where L is the longest dimension of the target and C is the speed of light.

III. Synthesis of Discriminant Signals Based on Experimental Pulse Response

In the preceding section, discriminant signals for zero response or single-mode responses were synthesized based on the prior knowledge of target's natural frequencies. In the case of complex targets, this information is difficult to obtain, and the synthesis of the discriminant signals will be based on an experimental measurement of the pulse response or the late-time response of the scale model of the target combined with some theoretical techniques described below.

A. Application of Continuation Method to a Measured Pulse Response

The first method we have employed to synthesize the discriminant signals for a target is to apply a recently developed, continuation method [7] to extract major natural frequencies of the target from its measured pulse response. This method is to regularize the ill-conditioned problem. After the natural frequencies are determined, the theoretical technique of the preceding section is used to synthesize the discriminant signals. The following steps are used in the process.

1) Measure the pulse response of the scale model of the target at various aspect ang
2) Use the fast Fourier tran[illegible] to obtain approximate values of natural frequencies from the measured pulse response.
3) Employ the continuation method and the natural frequencies obtained from FFT as the initial guesses to calculate accurate values of natural frequencies of the target. At each step of the algorithm, the condition number of the regularized problem is checked.
4) The theoretical technique of the preceding section is then applied to synthesize the discriminant signals for the target.

B. Application of Fast Prony's Method to a Measured Pulse Response

The second method we have used to synthesize the discriminant signals for a target is mainly based on the fast Prony's method [3], [8] and a measured pulse response. This method in discrete-time basis consists of the following steps.

1) The fast Prony's method is applied to the sampled data of the measured pulse response of the target. The coefficients of Prony polynomial are obtained. The time-ordered sequence of these coefficients can be shown to become the E−0 pulse [E−0] of the target [8], which eliminates the natural modes of the target and other noise.

2) Find roots of the Z-transform of the sequence which represents [E−0]. From those roots in the proper locations of the complex plane, the complex natural frequencies $[S_m]$ of the target can be calculated.
3) At this step, E−0 pulse [E−0] which extinguishes N natural modes of the target can be constructed by convolving N couplets $(1, -z_m)$ for $m = 1, 2, \cdots, N$ where $z_m = \exp(S_m \Delta T)$ and ΔT is the sampling interval:

$$[E-0] = (1, -z_1)*(1, -z_2)*, \cdots, *(1, -z_N).$$

4) The jth-mode extraction signal $[E_j^e]$ can be obtained by removing the couplet $(1, -z_j)$ from [E−0] as

$$[E_j^e] = (1, -z_1)*, \cdots, *(1, -z_i)*(1, -z_k)*, \cdots, *(1, -z_N).$$

IV. Convolution of Synthesized Discriminant Signals with Experimental Radar Returns

To demonstrate the applicability of the present target discrimination method in practice, we have convolved the measured radar returns of various targets with the corresponding synthesized signals for extracting zero-response and single-mode responses. We have tested many targets and produced many interesting results but only a few examples will be given here for brevity.

Experimental pulse responses of various radar targets used in the present study were either measured recently in the time-domain scattering range at Michigan State University (MSU) or have been published previously [3]. The MSU scattering range uses a biconical transmitting antenna (2.5 m long, 16° cone angle) and as a receiving probe it uses a short monopole field probe on the ground plane (6 m × 5 m), a current probe or a charge probe on the target surface. The transmitting antenna is excited either by a mercury-switched nanosecond pulser (Tektronix-109), which produces pulses of about 100 pS risetime and variable duration 1 ns $< t_p <$ 1 μs with amplitude as great as 500 V at a 1 kHz rate, or by another picosecond pulser (Picosecond Lab-1000B) which produces a narrower but a lower amplitude pulse. The signal from the receiving probe is measured by a sampling scope and the signal processing, including averaging and clutter subtraction, is performed by a computer controlled system.

Fig. 1 shows the measured impulse response of a thin cylinder target, having length l = 12.5 in = 31.75 cm and length-to-radius ratio l/a = 400, illuminated obliquely by a nanosecond plane-wave pulse at θ = 60° aspect and the synthesized E−0 pulse. This E−0 pulse was synthesized in terms of pulse functions with the first three natural modes, indicated in the figure, extracted by the continuation method as described in Section III-A. The bandlimited frequency spectrum of the 1−nS incident pulse precluded the identification of higher natural frequencies. Fig. 2 shows the convolved result of the E−0 pulse of Fig 1 with the pulse response of the correct cylinder along with the similar convolved results with the pulse responses of cylinders 5 and 25 percent longer. The correct cylinder yields a low-amplitude late-time response

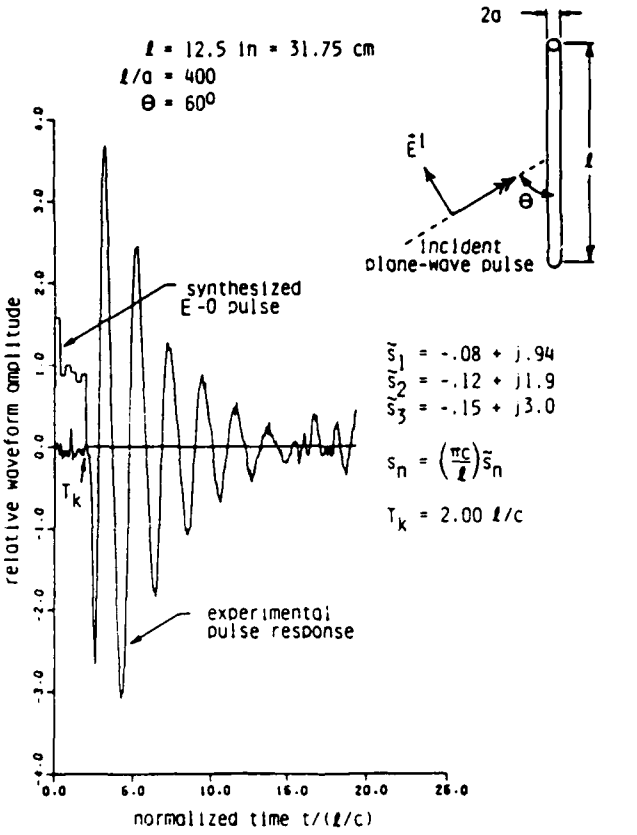

Fig. 1. Synthesis of thin-cylinder E−0 pulse from experimentally measured pulse response; dominant natural frequencies extracted by the continuation method.

which approximates the expected zero response; failure to achieve a perfect zero response is the result of imperfect experimental data having content other than the assumed sum of pure natural modes (the latter may be artifacts introduced by the measurement system). Longer targets lead to responses which can be discriminated from an expected zero response. Discrimination of the 5 percent longer cylinder is marginal while that of the 25 percent longer target is clear.

The next example was given to show the convolution of single-mode extraction signals with the measured radar return of a target. Fig. 3 shows the results of the convolution of the measured pulse response of a wire target with 18.6 in length and 0.0465 in radius with the synthesized signal for the third mode extraction. Fig. 3(a) shows the synthesized signal for extracting the cosine third mode, constructed in terms of impulse basis functions using the fast Prony's method described in Section III-B, and the convolved output. It is observed that a cosine third mode is produced in the late-time period of the convolved output. Fig. 3(b) shows the synthesized signal for extracting the sine third mode (in terms of impulse basis functions) and convolved output. A sine third mode is produced in the late-time period. To demonstrate that these late-time responses are indeed that of the third mode, a complex convolved output is constructed as

$$C(t) = A(t) - jB(t)$$

where $A(t)$ is the convolved output of Fig. 3(a) and $B(t)$ is the

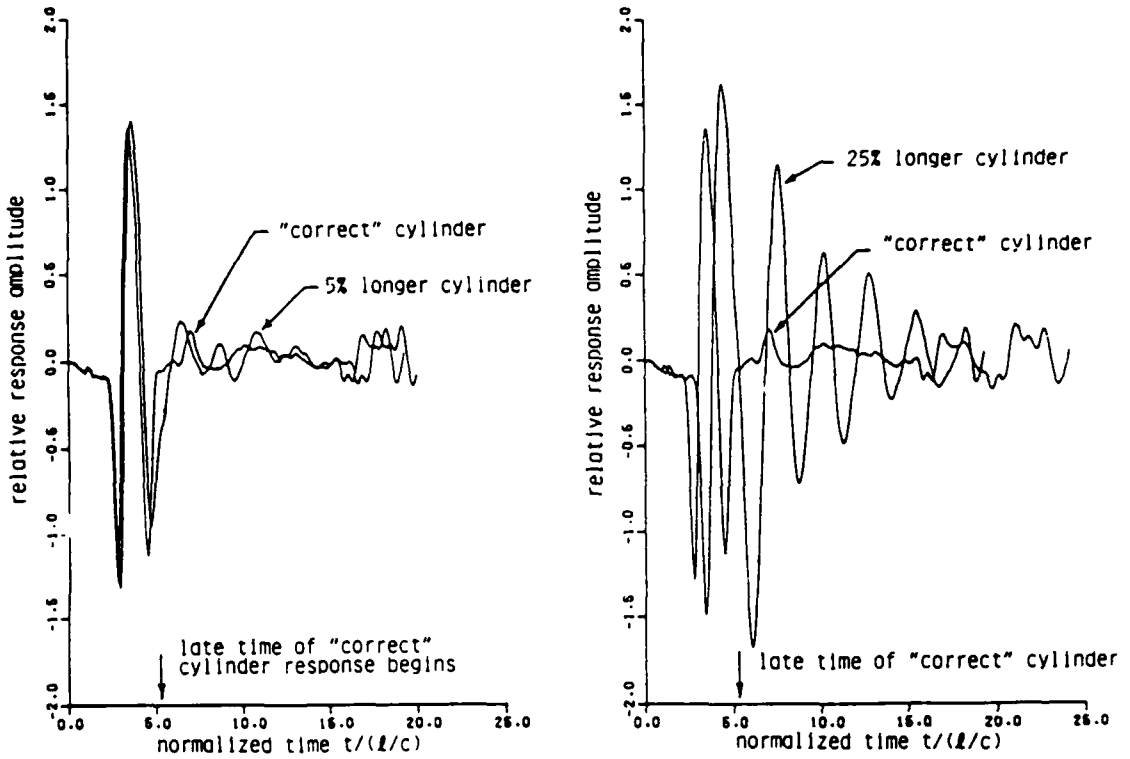

Fig. 2. Convolution (target response) of thin-cylinder E – 0 pulse synthesized from measured pulse response with the responses of the same "correct" cylinder and those of 5 and 25 percent greater length.

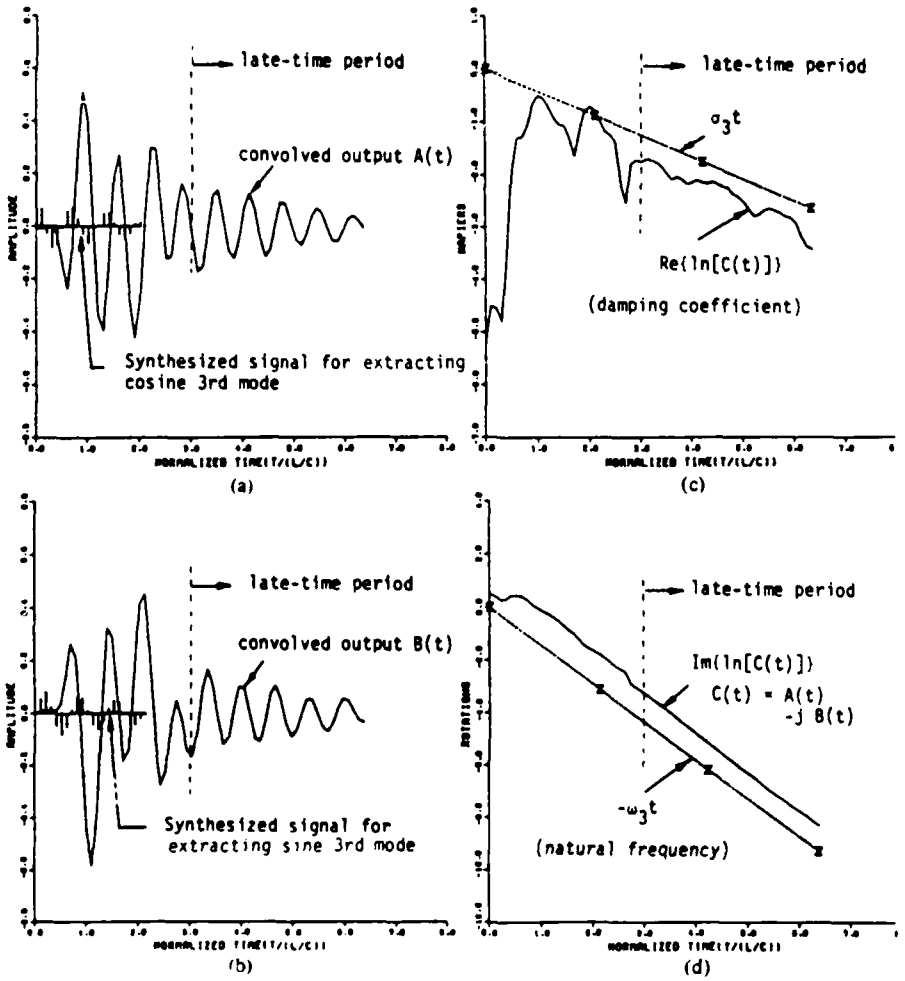

Fig. 3. Convolution of the impulse response of a 18.6 in (length) wire with the synthesized signal for the third mode extraction of the 18.6 in wire.

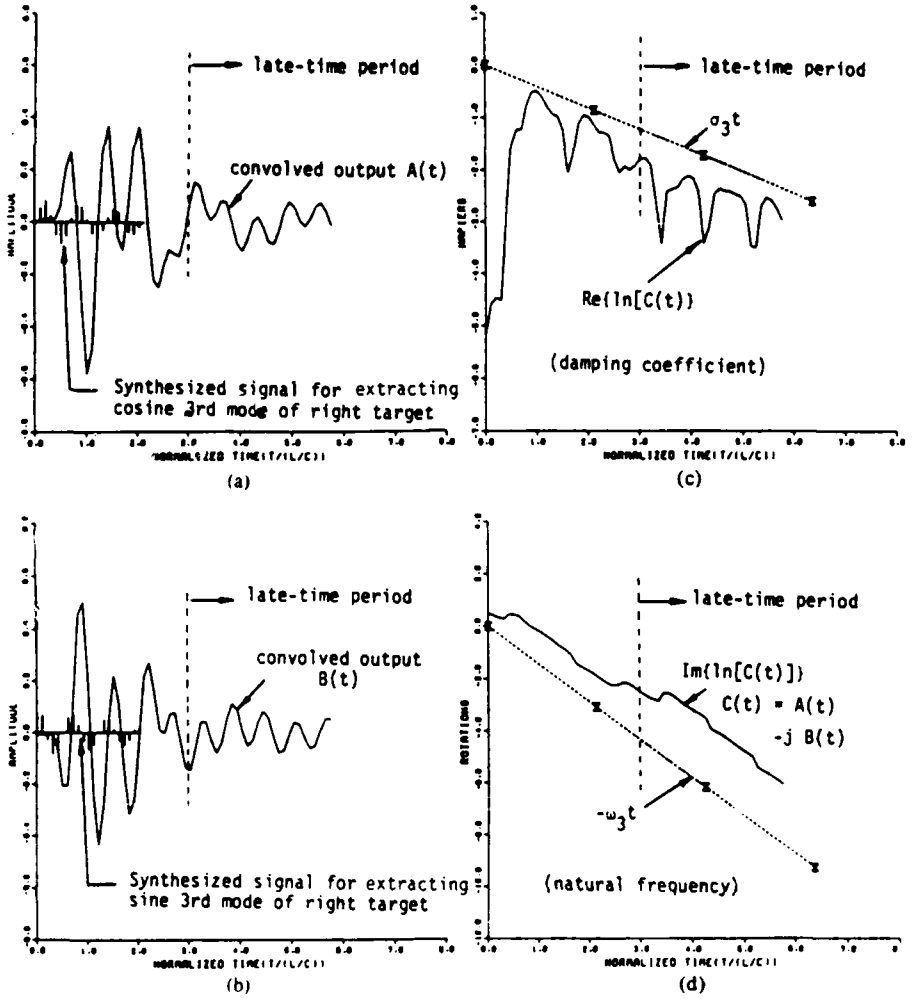

Fig. 4. Convolution of the impulse response of a wrong target, a 16.74 in wire, with the synthesized signal for extracting the third mode of the right target, a 18.6 in wire.

convolved output of Fig. 3(b). If the late-time response of $A(t)$ is a pure cosine third mode, it can be expressed as

$$[A(t)]_{\text{late}} = a_3 e^{\sigma_3 t} \cos(\omega_3 t + \phi_3).$$

Similarly, if the late-time response of $B(t)$ is a pure sine third mode, it can be expressed as

$$[B(t)]_{\text{late}} = a_3 e^{\sigma_3 t} \sin(\omega_3 t + \phi_3).$$

Thus, the late-time response of the complex convolved output should be

$$[C(t)]_{\text{late}} = a_3 e^{\sigma_3 t} e^{-j(\omega_3 t + \phi_3)}.$$

The logarithm of the late-time response of $C(t)$ yields

$$\ln [C(t)]_{\text{late}} = \ln a_3 + \sigma_3 t - j(\omega_3 t + \phi_3)$$

and

$$\text{real part of } \ln [C(t)]_{\text{late}} = \sigma_3 t + \ln a_3$$

$$\text{imaginary part of } \ln [C(t)]_{\text{late}} = -\omega_3 t - \phi_3.$$

Fig. 3(c) shows the real part of $\ln [C(t)]$ in comparison with the line of $(\sigma_3 t)$. It is observed that the late-time response of Re $\{\ln [C(t)]\}$ is nearly in parallel with the line of $(\sigma_3 t)$ for the late-time period of $t/(L/C) > 3$ where $t/(L/C)$ is the normalized time with L as the wire length and C as the speed of light. Fig. 3(d) shows the imaginary part of $\ln [C(t)]$ in comparison with the line of $(-\omega_3 t)$. It is again observed that the late-time response of Im $\{\ln [C(t)]\}$ is in parallel with the line of $(-\omega_3 t)$ for the late-time period of $t/(L/C) > 3$. Figs. 3(c) and 3(d) give a positive indication that the late-time response of the convolved outputs of Figs. 3(a) and 3(b) contain only (or predominantly) the third mode of the target.

An example is also given to show the capability of target discrimination provided by the present method. Fig. 4 shows the results of the convolution of the radar return of a wrong target, a 16.74 in wire, with the synthesized signal for extracting the third mode of the right target, a 18.6 in wire. In Figs. 4(a) and 4(b), the convolved outputs are significantly different from the expected third mode of the right target. Furthermore, the late time response of Re $\{\ln [C(t)]\}$ deviates greatly from the line of $(\sigma_3 t)$ and the late-time response of Im $\{\ln [C(t)]\}$ also differs significantly from the line of $(-\omega_3 t)$ as shown in Figs. 4(c) and 4(d). The results given in Fig. 4 give a positive discrimination of the wrong target, implying

that the radar return does not belong to the right target of 18.6 in wire.

We have also applied the present method to discriminate between complex radar targets. Two targets, experimental models of the F-18 plane and the 707 plane which have similar sizes but different geometrics, were used for this purpose. In the experiment, the half of each model was placed on the ground plane (image effect), and was illuminated by a pulsed electric field polarized perpendicularly to the ground plane. Results on these two targets are depicted in the following figures.

Fig. 5(a) shows the convolution of the E – 0 pulse for the F-18 plane with the measured radar response of the F-18 plane. The convolved outputs shows a strong early-time response followed by a "extinguished" (almost zero) late-time response as expected. Fig. 5(b) shows the convolved output of the E – 0 pulse for the 707 plane with the measured radar response of the F-18 plane. This convolved output shows a significant, "unextinguished" late-time response implying that the 707 E – 0 pulse was convolved with the radar response of a wrong target other than the 707 plane.

Fig. 6 shows the convolved results of the measured radar response of the 707 plane with the fourth-mode extraction signal for the 707 plane. In this figure, the extracted angular frequency line is almost parallel to the $\omega_4 t$ line (of the 707) and the extracted damping coefficient line closely parallel to the $\sigma_4 t$ line (of the 707) in the late-time period. This implies that the radar response belongs to the right target of the 707 plane.

Fig. 7 shows the convolved results of the measured radar response of the F-18 plane with the fourth-mode extraction signal for the 707 plane. The extracted angular frequency line deviates from the ($\omega_4 t$) line of the 707 plane and the extracted damping coefficient line also differs from the ($\sigma_4 t$) line of the 707 plane. These results imply that the radar response belongs to a wrong target other than the 707 plane.

It is noted that the synthesized E – 0 pulses and single-mode extraction signals for these targets are available elsewhere [9].

V. A Potential Radar Detection System Based on the Present Convolution Method

Fig. 8 depicts a potential radar detection system based on the present scheme of convolving the target radar return with the synthesized discriminant signals. The system consists of a network of computers and each of them is assigned to store the synthesized signals for extracting various single-mode or zero-mode response for a particular friendly target. All the relevant friendly targets are assumed to be covered in the network of computers. When an approaching target is illuminated by an interrogating radar signal, the radar return is divided and fed to each computer after amplification and signal processing. Inside each computer the stored discriminant signals are convolved with the radar return. In principle, only one of the computers will produce various single-mode and zero-mode outputs in the late-time period; the rest of the computers should produce irregular outputs. The computer producing the single-mode and zero-mode outputs will then be identified with the target. If none of the computers produces single-mode and zero outputs in the late-time period, the approaching targets will not be friendly.

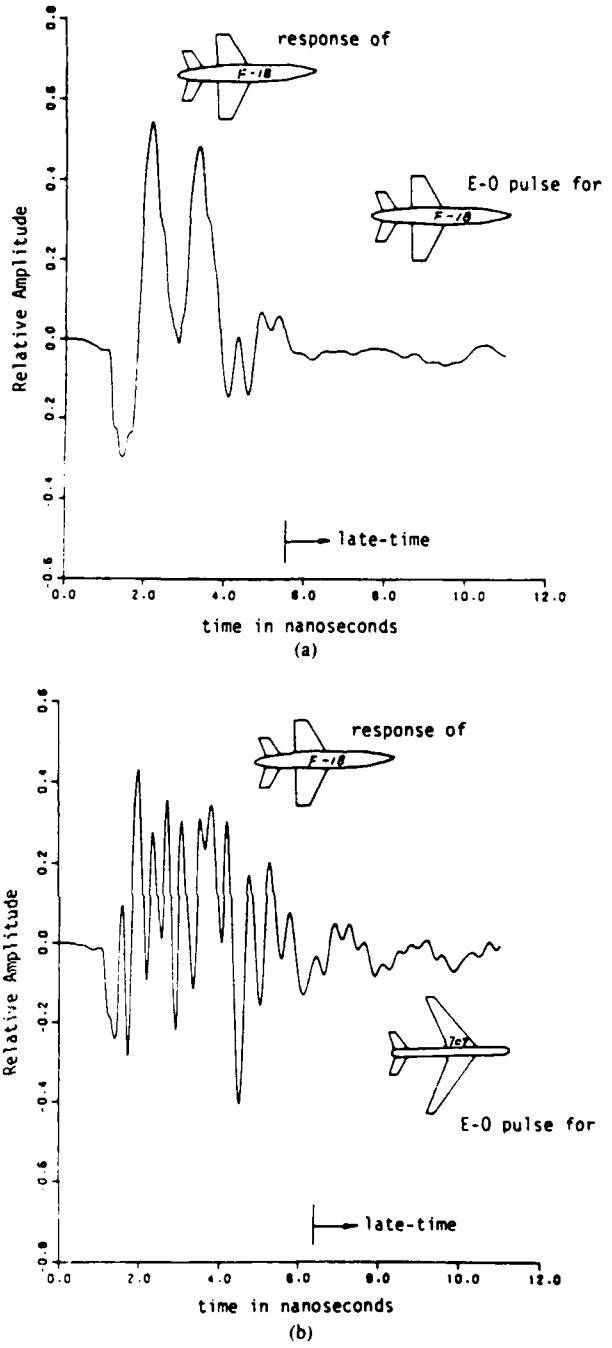

Fig. 5. (a) Convolution of the F-18 E – 0 pulse with the F-18 measured response showing "extinguished" late-time response. (b) Convolution of the 707 E – 0 pulse with the F-18 response showing a significant late-time response.

VI. Discussion

The present radar discrimination scheme is not a conventional correlation method because the measured radar return is convolved with synthesized discriminant signals which possess particular waveforms. The present scheme is basically different from the matched filtering scheme. A fundamental difference between the E-pulse scheme and the matched

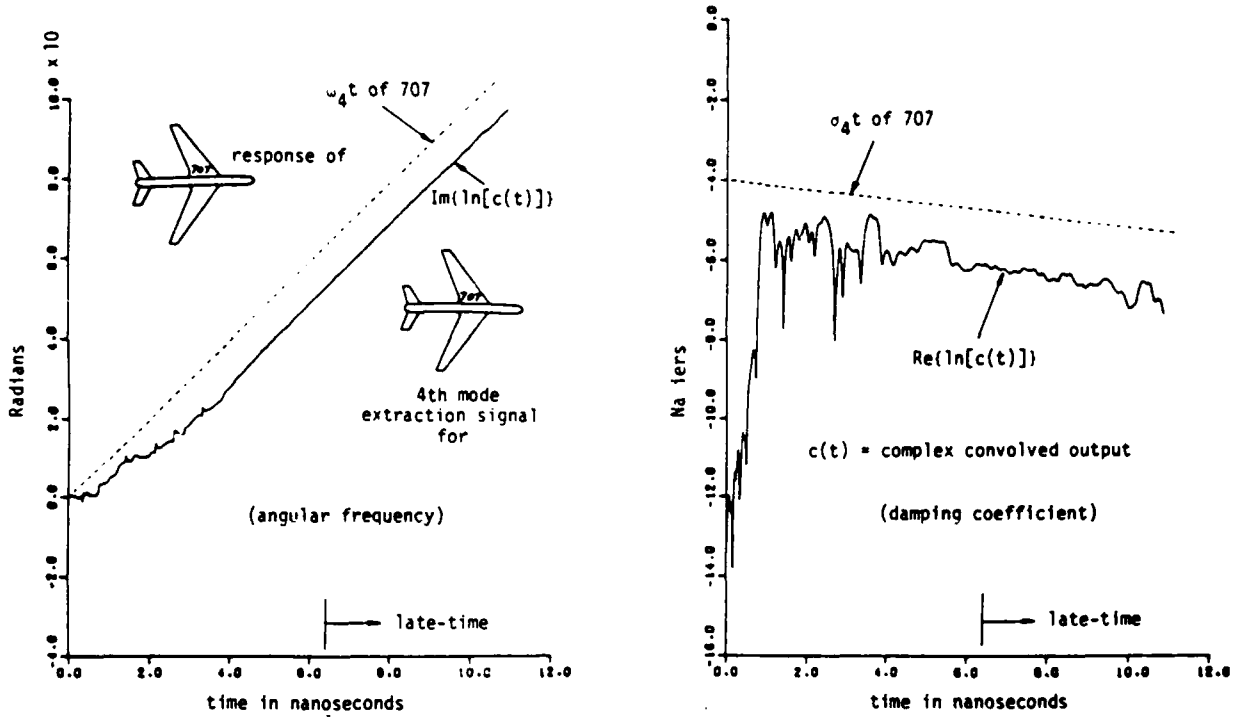

Fig. 6. Angular frequency and damping coefficient extracted from the complex convolved output of the fourth mode extraction signal for the 707 target and the 707 measured response.

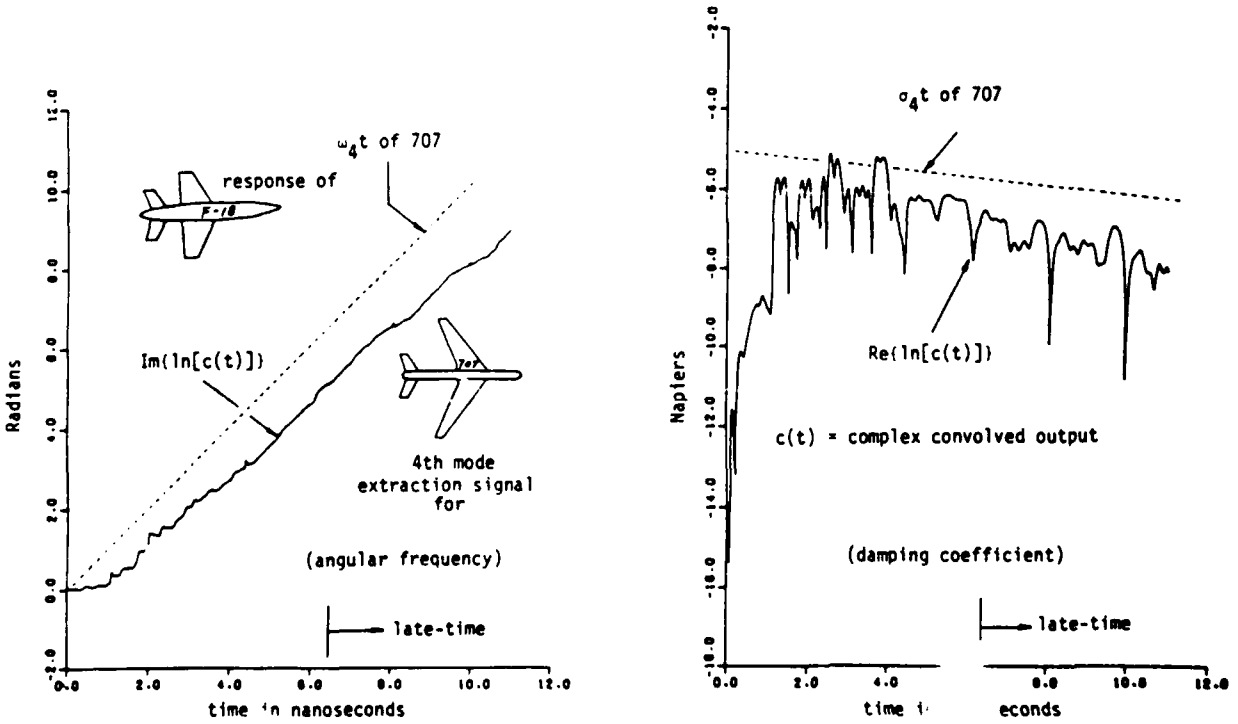

Fig. 7. Angular frequency and damping coefficient extracted from the complex convolved output signal for the 707 target and the F-18 measured response.

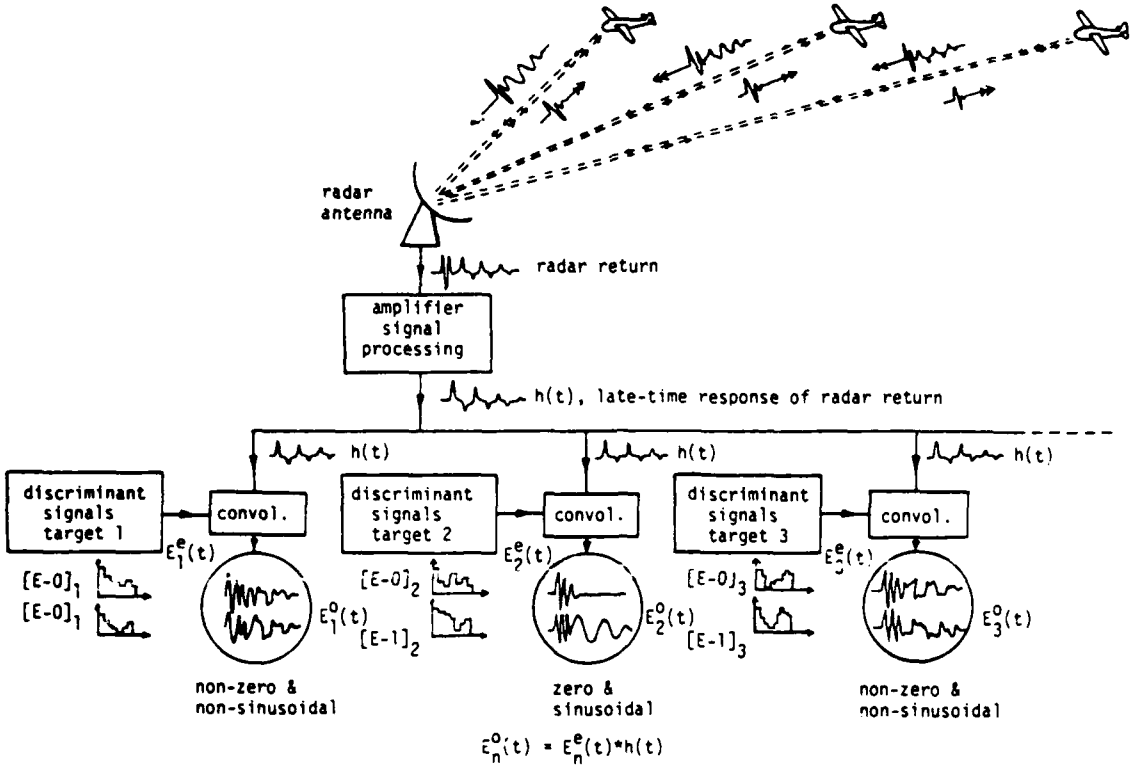

Fig. 8. A proposed target discrimination and identification system.

filtering scheme is as follows: the E-pulse scheme is to nullify a selected natural mode set, and does not deal with maximizing a specific modal content. For example, the E − 0 pulse eliminates all the modes in the late time. The single-mode extraction signal eliminates all but one mode. We do not consider maximization of responses in the presence of noise at specific times as in the matched filtering scheme. A further difference between these two schemes is the following: The natural modes are not, in general, orthogonal. Maximizing the response of a particular mode will not nullify the other modes. Also note that the E-pulse scheme is aspect-independent, whereas the matched filtering is not.

We have not attempted to compare the performance of the E-pulse scheme with that of a matched filtering scheme.

References

[1] K. M. Chen, D. P. Nyquist, D. Westmoreland, C. I. Chuang, and B. Drachman, "Radar waveform synthesis for single-mode scattering by a thin cylinder and application for target discrimination," *IEEE Trans. Antennas Propagat.*, vol. AP-30, no. 5, pp. 867-880, Sept. 1982.

[2] K. M. Chen and D. Westmoreland, "Radar waveform synthesis for exciting single-mode backscatters from a sphere and application for target discrimination," *Radio Sci.*, vol. 17, no. 3, pp. 574-588, June 1982.

[3] L. Webb, K. M. Chen, D. P. Nyquist, and B. Hollmann, "Extraction of single-mode backscatters by convolving synthesized radar signal with a radar return," presented at 1983 Int. IEEE/Antennas Propagat. Soc. Symp., Univ. Houston, Houston, TX, May 23-26, 1983, *Symp. Dig.*, pp. 676-679.

[4] E. Rothwell, D. P. Nyquist, and K. M. Chen, "Synthesis of Kill-pulse using time-domain SEM," presented at 1983 Int. IEEE/Antennas Propagat. Soc. Symp., Univ. Houston, Houston, TX, May 23-26, 1983, *Symp. Dig.*, pp. 672-675.

[5] E. M. Kennaugh, "The K-pulse concept," *IEEE Trans. Antennas Propagat.*, vol. AP-20, no. 2, pp. 327-331, Mar. 1981.

[6] E. Rothwell, D. P. Nyquist, and K. M. Chen, "Synthesis of Kill-pulse to excite selected target models," presented at 1984 Int. IEEE/Antennas Propagat. Soc. Symp., Boston, June 25-29, 1984, *Symp. Dig.*, pp. 15-18.

[7] B. Drachman and E. Rothwell, "A continuation method for identification of the natural frequencies of an object using a measured response," *IEEE Trans. Antennas Propagat.*, vol. AP-33, no. 4, pp. 445-450, Apr. 1985.

[8] L. Webb, "Radar target discrimination using K-pulse from a "fast" Prony's method," Ph.D dissertation, Dept. Elec. Eng. Sys. Sci., Michigan State Univ., 1984.

[9] K. M. Chen, "Radar waveform synthesis for target identification," Naval Air Sys. Command, Div. of Eng. Res., Michigan State Univ., Final Rep., 1983.

[10] I. Gerst and J. Diamond, "The elimination of intersymbol interference by input signal shaping," *Proc. IRE*, pp. 1195-1203, July 1961.

Kun-Mu Chen (SM'64-F'76), for a photograph and biography please see page 936 of the September 1985 issue of this TRANSACTIONS.

Dennis P. Nyquist (S'63-M'67), for a photograph and biography please see page 936 of the September 1985 issue of this TRANSACTIONS.

Edward J. Rothwell (S'84-M'85), for a photograph and biography please see page 936 of the September 1985 issue of this TRANSACTIONS.

Lance L. Webb (S'62-M'66-S'76-M'78-S'80-M'84) was born in Eaton Rapids, MI, on April 21, 1941. He received the B.S.E.E. degree from Massachusetts Institute of Technology, Cambridge, in 1963, the M.S.E.E. degree from Georgia Institute of Technology, Atlanta, in 1980, and the Ph.D. degree in electrical engineering from Michigan State University, East Lansing, in 1984.

He has worked on radar, jammer, missile, and Satcom antenna programs for Raytheon, Sylvania, Martin Marietta, Harris and Georgia Tech. He currently works on antennas and radomes for Northrop Aircraft Division.

Byron Drachman, for a photograph and biography please see page 937 of the September 1985 issue of this TRANSACTIONS.

IEEE TRANSACTIONS ON ANTENNAS AND PROPAGATION, VOL. AP-33, NO. 9, SEPTEMBER 1985

Radar Target Discrimination Using the Extinction-Pulse Technique

EDWARD ROTHWELL, STUDENT MEMBER, IEEE, D. P. NYQUIST, MEMBER, IEEE, KUN-MU CHEN, FELLOW, IEEE, AND BYRON DRACHMAN

Abstract—**An aspect independent radar target discrimination scheme based on the natural frequencies of the target is considered. An extinction-pulse waveform upon excitation of a particular conducting target results in the elimination of specified natural modal content of the scattered field. Excitation of a dissimilar target produces a noticeably different late-time response. Construction of appropriate extinction-pulse waveforms is discussed, as well as the effects of random noise on their application to thin cylinder targets. Also presented is experimental verification of this discrimination concept using simplified aircraft models.**

I. Introduction

RADAR TARGET identification methods using the time-domain response of a target to a transient incident waveform have generated considerable interest recently [1]–[4]. One of the most intriguing schemes involves the so-called "kill-pulse" technique as first described by Kennaugh [5]. A Kill-pulse (K-pulse) is an excitation waveform synthesized in such a way as to minimize a transient scattered field response. Target discrimination results from the unique correspondence of a K-pulse to a particular target; excitation of a dissimilar target yields a "larger" response.

This paper describes a related "extinction-pulse" (E-pulse) concept, based on the natural resonance of a conducting radar target via the singularity expansion method (SEM) [6]. The time domain electric field scattered by the target is divided into an early-time, forced response period when the excitation waveform is traversing the target, and a late-time, free oscillation period that exists after the excitation waveform has passed [7], [8]. The early-time response is not utilized due to its complicated nature. The late-time response can be decomposed into a sum of damped sinusoids oscillating at frequencies determined entirely by the geometry of the target. An E-pulse is then viewed as a transient, finite duration waveform which annihilates the contribution of a select number of these natural resonances to the late-time response. A related target identification scheme based on natural target resonances has been examined by Chen [9].

Target discrimination using this SEM viewpoint is easily visualized. Each target can be described by a set of natural frequencies. An E-pulse designed to annul certain natural resonances of one target will excite those of a target with different natural frequencies, resulting in a different scattered field. Also made apparent is the aspect-independent nature of the E-pulse. Since the values of the target resonance frequencies are independent of the excitation waveform, the E-pulse will eliminate the desired natural modal content of the late-time scattered field regardless of the orientation of the target with respect to the transmitting and receiving antennas.

It is important to note that the E-pulse waveform need not be transmitted to employ this concept. It is assumed that an excitation waveform with finite usable bandwidth will be used to excite the target, resulting in a measured scattered field with the desired (finite) modal content. The E-pulse can then be convolved numerically with the measured target response, yielding results analogous to E-pulse transmission. If the maximum modal content of the target scattered field can be estimated from the frequency content of the excitation pulse, then the E-pulse waveform can be constructed to yield a null late-time convolved response.

After an initial presentation of the SEM representation of the backscattered field excited by a transient incident wave and calculation of the corresponding impulse response, two types of E-pulses, forced and natural, will be discussed. The results are then specialized to a thin cylinder target, which has an impulse response amenable to analytic calculation. Target discrimination using the natural thin cyclinder E-pulse, as well as the effects of random noise are also investigated. Lastly, experimental verification of the E-pulse concept is presented.

II. Backscattered Field Excited By Transient Incident Wave

A perfectly conducting radar target is illuminated by a plane electromagnetic wave as shown in Fig. 1. The electric field associated with this transient wave can be written in the Laplace transform domain as

$$\vec{E}^i(\vec{r},\ s) = \hat{\xi} e(s) e^{-(s/c)\hat{k}\cdot\vec{r}} \tag{1}$$

where $\vec{r}$ is a position vector in a coordinate system local to the target, $\hat{\xi}$ is a constant vector specifying the polarization of the wave, $\hat{k}$ is a unit vector in the direction of propagation, and $e(t)$ represents the time dependence of the incident field. The current $\vec{k}$ induced on the surface of the target is given by the solution to the transform domain E-field integral equation

$$\int_S \left[\nabla' \cdot \vec{k}(\vec{r}',\ s)(\hat{t}\cdot\nabla) - \frac{s^2}{c^2}\hat{t}\cdot\vec{k}(\vec{r}',\ s) \right] \frac{e^{-(sR/c)}}{4\pi R}\, ds' = -s\epsilon_0 \hat{t}\cdot\vec{E}^i(\vec{r},\ s) \tag{2}$$

Manuscript received February 8, 1985; revised July 10, 1984. This work was supported by the Naval Air Systems Command under Contract N00019-83-C-0132.

The authors are with the Department of Electrical Engineering, Michigan State University, East Lansing, MI 48824.

0018-926X/85/0900-0929$01.00

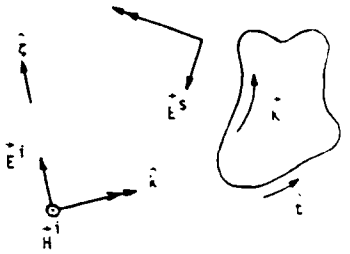

Fig. 1. Illumination of a conducting target by an incident electromagnetic wave.

where $\hat{t}$ is a unit vector tangent to the surface of the target at the point $\vec{r}$ on S, and $R = |\vec{r} - \vec{r}'|$. The surface current can also be expanded using the SEM representation

$$\vec{K}(\vec{r}, s) = \sum_{\alpha=1}^{N} a_\alpha \vec{K}_\alpha(\vec{r})(s - s_\alpha)^{-1} + \vec{W}(\vec{r}, s) \tag{3}$$

where $\vec{W}(\vec{r}, s)$ represents any entire function contribution to the current, and it is assumed that only a finite number of natural modes are substantially excited by the incident field. It is further assumed that the only singularities of $\vec{K}(\vec{r}, s)$ in the finite complex s-plane are simple poles at natural frequencies $s_\alpha = \sigma_\alpha + j\omega_\alpha$. Then, $\vec{K}_\alpha(\vec{r})$ represents the current distribution of the αth natural mode, and a_α is the "class-1" coupling coefficient given by Baum [10].

The far-zone backscattered electric field can be computed by integrating the current distribution over the surface of the target. The ζ component of backscattered field can then be written as

$$E_\zeta^s(r, s, \hat{k}) = \frac{e^{-(sr/c)}}{r} e(s) H(s, \hat{k}, \hat{\zeta}) \tag{4}$$

where $r = |\vec{r}|$ and $H(s, \hat{k}, \hat{\zeta})$ is the aspect dependent transfer function of the target. Using (3) to represent the surface current, the transfer function can be inverse transformed to determine the backscatter impulse response of the target.

Because of the entire function contribution to the current, the impulse response will exhibit two distinct regions. The early-time, forced component represents the backscattered field excited by currents during the time when the impulse is traversing the target; it has a duration equal to twice the one-way maximal transit time of the target T. The late-time free oscillation component is composed purely of a sum of constant amplitude natural modes and exists for all time $t > 2T$ as

$$h(t, \hat{k}, \hat{\zeta}) = \sum_{n=1}^{N} a_n(\hat{k}, \hat{\zeta}) e^{\sigma_n t} \cos(\omega_n t + \phi(\hat{k}, \hat{\zeta})), \quad t > 2T \tag{5}$$

where it has been assumed that the entire function makes no contribution to the late-time component [6]. Thus, the component of the far-zone backscattered field is given simply by the convolution of the time domain incident field and the impulse response, and is also composed of forced and free oscillating portions.

III. Incident E-Pulse Waveform Synthesis

To synthesize an E-pulse for a particular target, the convolutional representation of the backscattered field is written in integral form using the impulse response of (5) as

$$\begin{aligned} E_\zeta^s(t, \hat{k}) &= \int_0^{T_e} e(t') h(t - t', \hat{k}, \hat{\zeta})\, dt' \\ &= \int_0^{T_e} e(t') \sum_{n=1}^{N} a_n(\hat{k}, \hat{\zeta}) e^{\sigma_n (t - t')} \cos[\omega_n (t - t') \\ &\quad + \phi_n(\hat{k}, \hat{\zeta})]\, dt'. \end{aligned} \tag{6}$$

This response is valid for the late-time portion of the scattered field, $t > T_L = T_e + 2T$, where T_e is the duration of $e(t)$. The excitation waveform becomes an E-pulse when the scattered field is forced to vanish identically in the late-time. Rewriting (6) and employing this condition yields a defining equation for the E-pulse.

$$\begin{aligned} &\sum_{n=1}^{N} a_n(\hat{k}, \hat{\zeta}) e^{\sigma_n t} [A_n(T_e) \cos(\omega_n t + \phi_n(\hat{k}, \hat{\zeta})) \\ &\quad + B_n(T_e) \sin(\omega_n t + \phi_n(\hat{k}, \hat{\zeta}))] = 0, \qquad t > T_L = T_e + 2T \end{aligned} \tag{7}$$

where the coefficients $A_n(T_e)$ and $B_n(T_e)$ are given by

$$\begin{Bmatrix} A_n(T_e) \\ B_n(T_e) \end{Bmatrix} = \int_0^{T_e} e(t') e^{-\sigma_n t'} \begin{Bmatrix} \cos \omega_n t' \\ \sin \omega_n t' \end{Bmatrix} dt'. \tag{8}$$

The linear independence of the damped sinusoids in (7) requires $A_n(T_e) = B_n(T_e) = 0$ for all $1 \le n \le N$.

It is important to note that $A_n(T_e)$ and $B_n(T_e)$ are independent of the aspect parameters $\hat{k}$ and $\hat{\zeta}$, verifying the aspect independence of the E-pulse. This is a direct consequence of the separability of the terms of the impulse response.

A physical interpretation of the E-pulse can be facilitated by decomposing the excitation waveform as shown in Fig. 2 as

$$e(t) = e^f(t) + e^e(t) \tag{9}$$

where $e^f(t)$ is an excitatory component, nonvanishing during $0 \le t < T_f$, the response to which is subsequently extinguished by $e^e(t)$ which follows during $T_f \le t \le T_e$. Substituting (9) into (8) and using $A_n(T_e) = B_n(T_e) = 0$ yields

$$\begin{aligned} &\int_{T_f}^{T_e} e^e(t') e^{-\sigma_n t'} \begin{Bmatrix} \cos \omega_n t' \\ \sin \omega_n t' \end{Bmatrix} dt' \\ &\quad = -\int_0^{T_f} e^f(t') e^{-\sigma_n t'} \begin{Bmatrix} \cos \omega_n t' \\ \sin \omega_n t' \end{Bmatrix} dt'. \end{aligned} \tag{10}$$

The excitation component of the E-pulse necessary to eradicate the response due to a preselected excitatory component can be constructed as an expansion over an appropriately chosen set of linearly independent basis functions as

$$e^e(t) = \sum_{m=1}^{2N} c_m g_m(t). \tag{11}$$

Equation (10) then becomes

$$\sum_{m=1}^{2N} M_{l,m}^{c,s}(T_e) C_m = -F_l^{c,s}, \qquad 1 \le l \le N \tag{12}$$

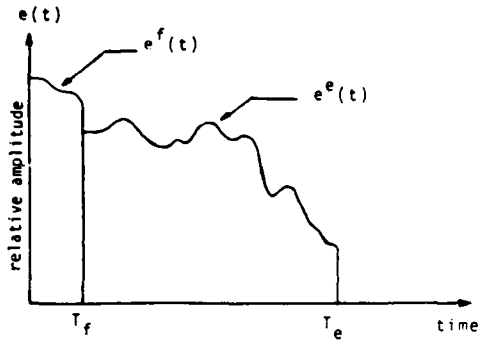

Fig. 2. Decomposition of E-pulse into forcing and extinction components.

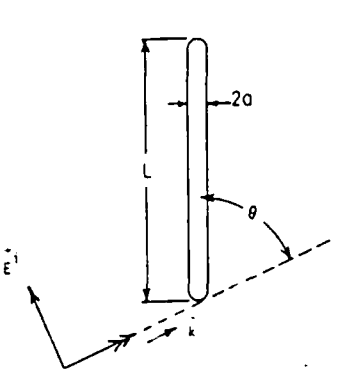

L/a = 200

n	S_n
1	-0.0828 + j0.9251
2	-0.1212 + j1.912
3	-0.1491 + j2.884
4	-0.1713 + j3.874
5	-0.1909 + j4.854
6	-0.2080 + j5.845
7	-0.2240 + j6.829
8	-0.2383 + j7.821
9	-0.2522 + j8.807
10	-0.2648 + j9.800

Fig. 3. Orientation for thin-cylinder excitation and first ten natural frequencies.

where

$$M^{c,s}_{l,m}(T_e) = \int_{T_f}^{T_e} g_m(t') e^{-\sigma_l t'} \begin{Bmatrix} \cos \omega_l t' \\ \sin \omega_l t' \end{Bmatrix} dt' \tag{13a}$$

$$F^{c,s}_{l} = \int_{0}^{T_f} e^f(t') e^{-\sigma_l t'} \begin{Bmatrix} \cos \omega_l t' \\ \sin \omega_l t' \end{Bmatrix} dt'. \tag{13b}$$

This can be written using matrix notation as

$$\begin{bmatrix} M^c_{l,m}(T_e) \\ \hline M^s_{l,m}(T_e) \end{bmatrix} \begin{bmatrix} C_1 \\ \vdots \\ C_{2N} \end{bmatrix} = - \begin{bmatrix} F_1 \\ \vdots \\ F_{2N} \end{bmatrix}. \tag{14}$$

Solving this equation for $C_1, \cdots, C_{2N}$ determines the extinction component via (11) and thus the E-pulse.

It is convenient at this point to identify two fundamental types of E-pulses. When $T_f > 0$ the forcing vector on the right side of (14) is nonzero and a solution for $e^e(t)$ exists for almost all choices of T_e. This type of E-pulse has a nonzero excitatory component and is termed a "forced" E-pulse. In contrast, when $T_f = 0$ the forcing vector vanishes and solutions for $e^e(t)$ exist only when the determinant of the coefficient matrix vanishes, i.e., when det $[M(T_e)] = 0$. These solutions correspond to discrete eigenvalues for the E-pulse duration T_e, which are determined by rooting the determinantal characteristic equation. Since there is no excitatory component, this type of E-pulse is viewed as extinguishing its own excited field and is called a "natural" E-pulse.

IV. Thin Cylinder E-Pulse Analysis

A theoretical analysis of a thin wire target has been undertaken by various authors [11], [12]. Target natural frequencies are determined from the homogeneous solutions to the integral equation (2). The geometry of the target and its orientation with respect to the excitation field are given in Fig. 3 along with the first ten natural frequencies. The frequencies are normalized by $\pi c/L$ where L is the length of the wire and c is the speed of light, and correspond to a wire of radius given by $L/a = 200$.

The thin cylinder impulse response can be calculated by inverting (4) [12] and becomes a pure sum of natural modes in the late time. Fig. 4 shows the impulse responses of thin cylinders oriented at $\theta = 30°$ and $\theta = 60°$, generated by using the first ten modes of the target. Note the distinct early and late-time regions. An E-pulse to extinguish the first ten modes of the target is created by solving (14) using the corresponding frequencies.

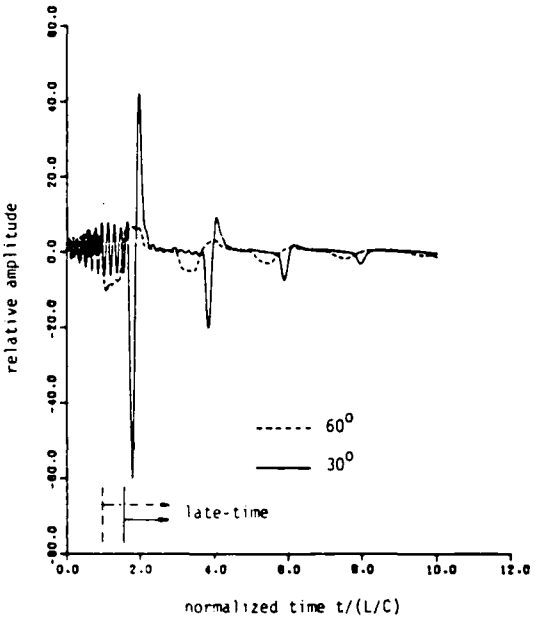

Fig. 4. Thin cylinder impulse responses for $\theta = 30°$ and $\theta = 60°$ generated using the first ten natural modes.

Fig. 5 shows a natural E-pulse synthesized to kill the first ten natural modes of the thin wire target, using a pulse function basis set. The duration of the waveform, $T_e = 2.0408L/c$, corresponds to the first root of the resulting determinantal equation. Superimposed with this is Kennaugh's original K-pulse. The similarlity is striking, with the major difference being the finite duration of the E-pulse. Also shown in Fig. 5 is a forced pulse function E-pulse constructed to extinguish the first ten modes of the target. The duration has been chosen as $T_e = 2.3$ and the excitation component has been chosen as a pulse function of width equal to that of the basis functions.

Numerical verification of the thin wire E-pulse is given in Fig. 6. The natural E-pulse waveform of Fig. 5 is convolved with the 30° and 60° impulse responses of Fig. 4 and the resulting backscattered field representations are observed to be zero in the late time. Note also the expected nonzero early-time response. This portion is useful since it provides a

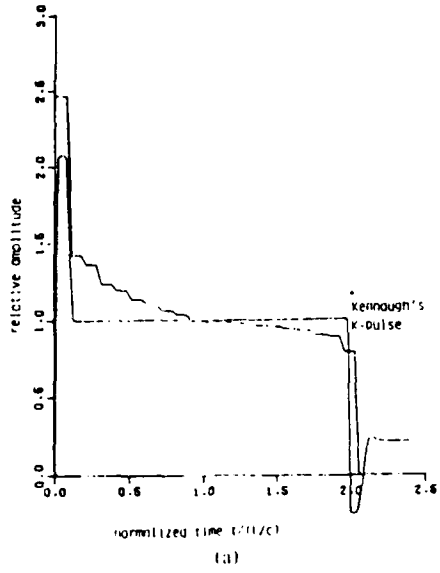

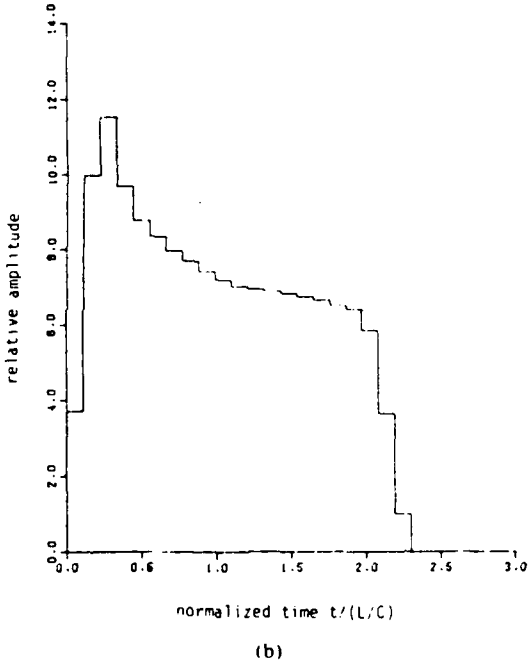

Fig. 5. Pulse function based E-pulse synthesized to eliminate first ten modes of thin cylinder target. (a) Natural E-pulse compared to Kennaugh's K-pulse. (b) Forced E-pulse of duration $T_f = 2.3\ L/c$.

comparative benchmark assessing the quality of the annulled component of the response; this is important when imperfect "extinction" is evident (due to noise, errors in the natural frequencies, etc.).

The question of E-pulse waveform uniqueness as the number of natural frequencies extinguished N is taken to infinity has not been resolved. For the thin cylinder target there appears to be such a unique waveform. Evidence is provided by Fig. 7 which shows natural E-pulses of minimum duration designed to extinguish various numbers of natural modes, using both Fourier cosine and pulse function basis sets. It is apparent that these waveforms are nearly identical and they appear to be converging to a particular shape.

The most critical parameter necessary for E-pulse unique-

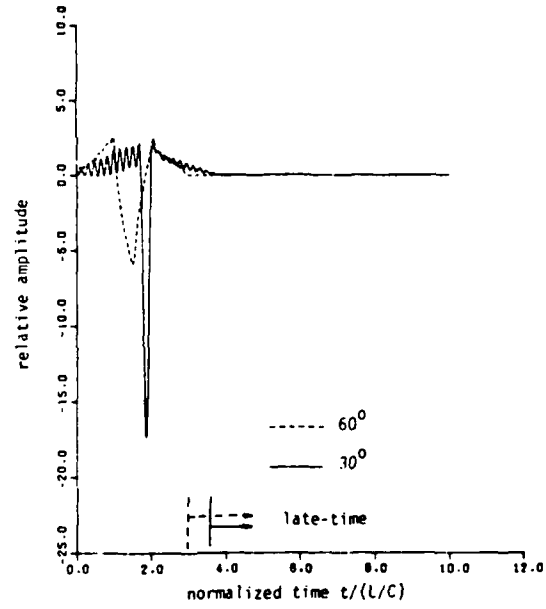

Fig. 6. Convoltuion of ten mode natural E-pulse with 30° and 60° ten mode impulse responses showing null late-time response.

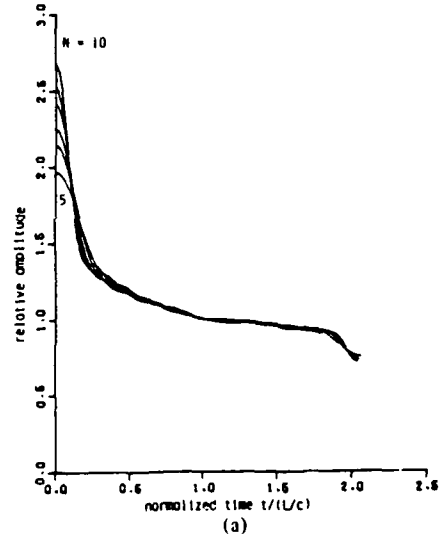

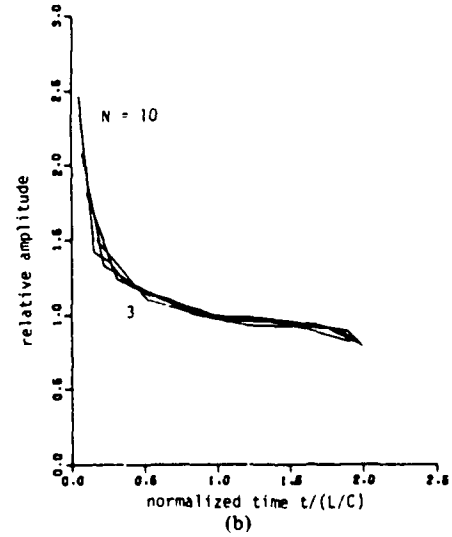

Fig. 7. Natural E-pulse constructed using (a) Fourier cosine basis functions to eliminate 5, 6, 7, 8, 9, and 10 modes. (b) Pulse function basis functions to eliminate 3, 5, 7, and 10 modes.

ness is the finite E-pulse duration T_e. This must converge to a distinct value as $N \to \infty$. For the pulse function basis set it can be shown that the natural E-pulse durations are given by

$$T_e = 2\pi N \frac{p}{\omega_l}, \qquad p = 1, 2, \cdots, \quad 1 \le l \le N \tag{15}$$

where ω_l is the imaginary part of the lth natural frequency. If this is written for the thin cylinder as

$$\omega_l = \pi [l - \delta(l)] \frac{c}{L} \tag{16}$$

where $\delta(l)/l$ decreases asymptotically to zero with increasing l, then the minimum E-pulse duration converges to

$$(T_e)_{\min} = \lim_{N \to \infty} \frac{2\pi N}{\pi [N - \delta(N)]} \frac{L}{c} = 2 \frac{L}{c}. \tag{17}$$

V. Target Discrimination With E-Pulse Waveforms

Discrimination between different thin cylinder targets is demonstrated by convolving the natural E-pulse of Fig. 5, which has been constructed to extinguish the first ten modes of a target of length L, with the impulse response of the expected target and a target 5 percent longer. The result is shown in Fig. 8. The late-time response of the expected target has been successfully annulled, while the response of the differing target is nonzero over the same period. The difference in target natural frequencies provides the basis for discrimination based on the comparison of adequately dissimilar late-time responses of differing targets.

Sensitivity of E-pulse performance to the presence of uncorrelated random noise is investigated by perturbing each point of the thin cylinder impulse response of Fig. 4 by a random amount not exceeding 10 percent of the maximum waveform amplitude. The result is shown in Fig. 9. An attempt is then made to extinguish this noisy response by convolving it with the natural E-pulse of Fig. 5. As expected, the convolution, shown in Fig. 10, does not exhibit a null late-time response, but results in a distribution of noise about the zero line. Also plotted in this figure is the convolution of the E-pulse with a noisy waveform representing a target 5 percent longer. It is quite easy to separate the effects of noise and target length sensitivity, suggesting that random noise will not interfere with target discrimination.

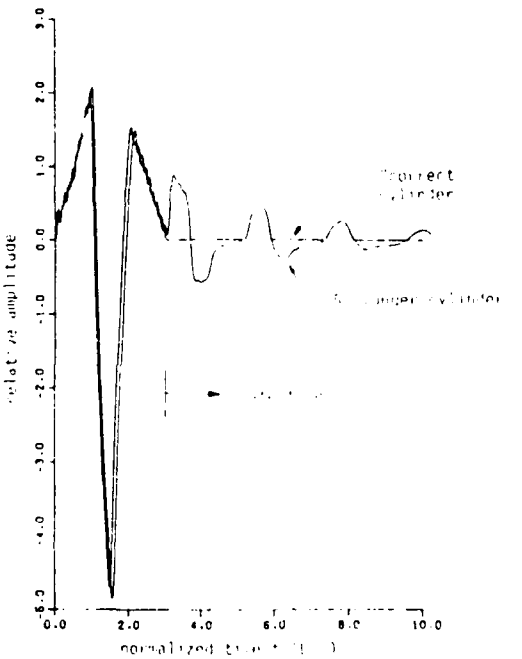

Fig. 8. Convolution of 10 mode natural thin cylinder E-pulse with 60° thin cylinder impulse response and 60° response of a cylinder 5 percent longer.

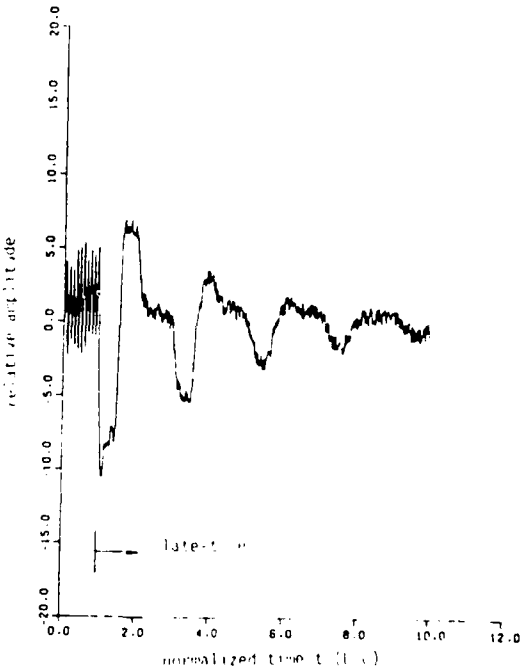

Fig. 9. Thin cylinder 60° impulse response generated from first ten natural modes, with 10 percent random noise added.

VI. Experimental Verification Of The E-Pulse Concept

Time domain measurements of complex conducting target responses provide the means for a practical test of the E-pulse concept. The present experiment involves measuring the near scattered field response of a simplified aircraft model to transient pulse excitation. A Tektronix 109 pulse generator is used to provide a quasirectangular 400 V incident pulse of nanosecond duration. Transmission of the pulse over a 5 × 6 m conducting ground screen is accomplished by using an (imaged) biconical antenna of axial height 2.5 m, half-angle of 8° and characteristic impedance of 160 Ω, while reception is implemented using a short monopole E-field probe of length 1.6 cm. Although the receiving probe is not positioned in the far field region of the scatterer, the resulting measurements have the desired modal content in the late-time period, providing the small probe purely differentiates the waveform. Lastly, discrete sampling of the time domain waveform is accomplished by using a Tektronix sampling oscilloscope (S2 sampling heads, 75 ps risetime) coupled to a Radio Shack model III microcomputer.

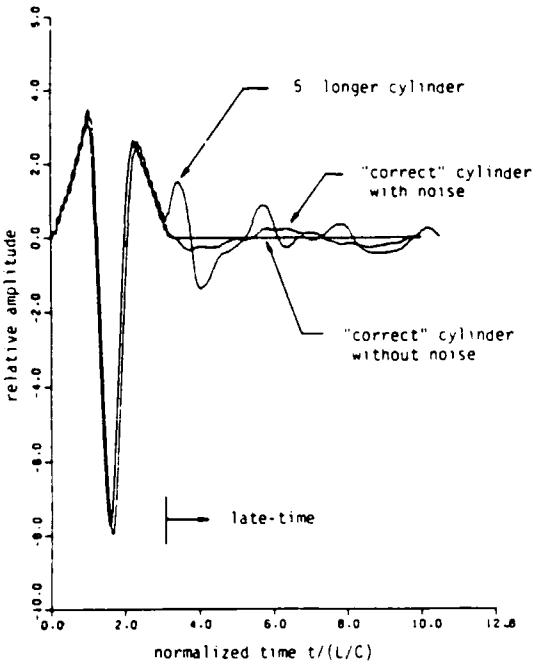

Fig. 10. Convolution of natural ten mode E-pulse with noisy ten mode 60° impulse response.

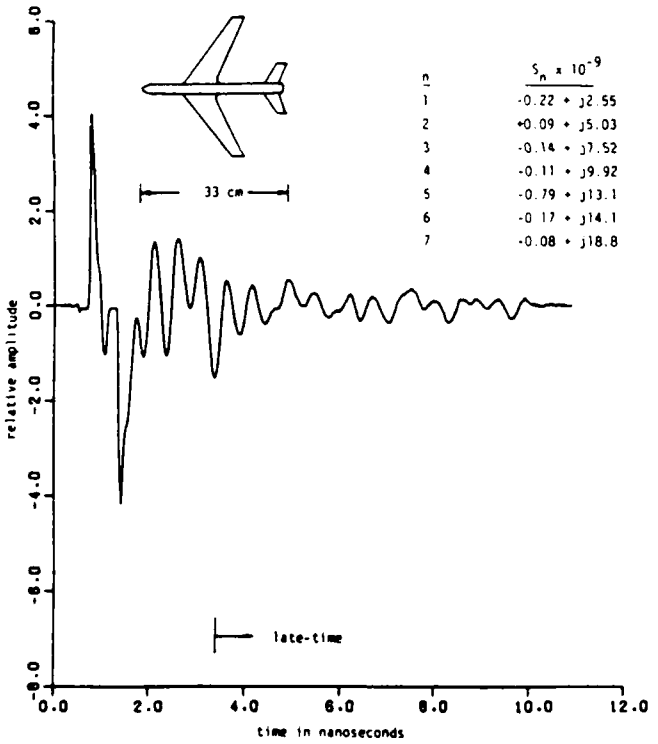

Fig. 11. Measured response of a Boeing 707 aircraft model and seven dominant natural frequencies.

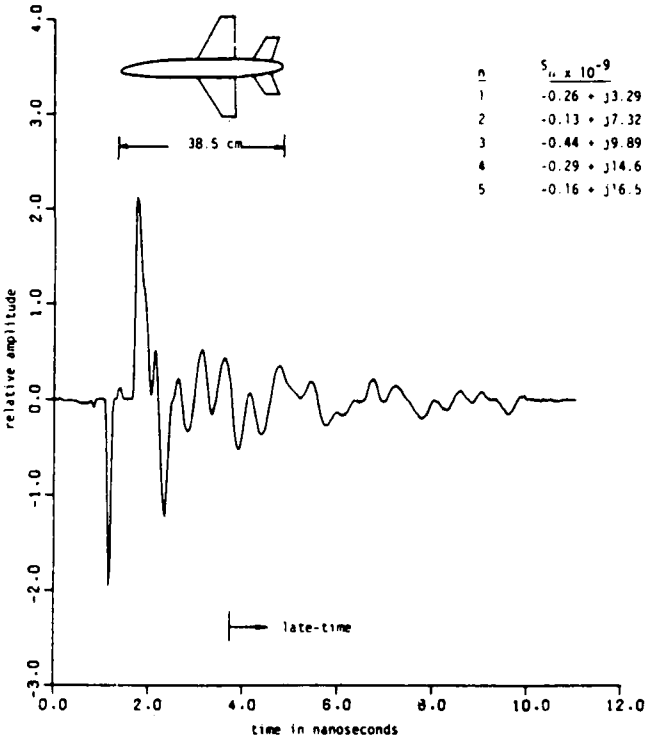

Fig. 12. Measured response of a McDonnel Douglas F-18 aircraft model and give dominant natural frequencies.

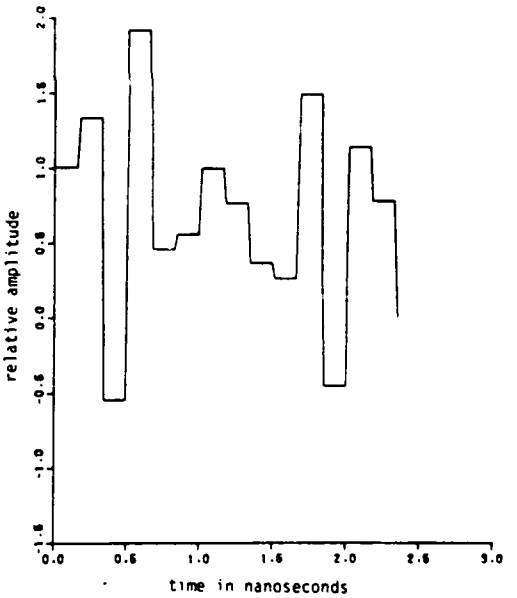

Fig. 13. Natural E-pulse constructed to eliminate the seven dominant modes in the 707 measured response.

In this experiment, an attempt is made to discriminate between two aircraft models by employing the E-pulse technique. Figs. 11 and 12 show the measured pulse responses of simplified Boeing 707 and McDonnell Douglas F-18 aircraft models, respectively. Each model is constructed of aluminum and has a geometry as indicated in the figures. Also shown in the figures are the dominant natural frequencies extracted from the late-time portion of the response using a nonlinear least squares curve fitting technique [13]. E-pulse waveforms can then be constructed to annul these frequencies.

Pulse function based natural E-pulses constructed to annul each of the two target responses are shown in Figs. 13 and 14. Discrimination between the targets is accomplished by convolving these waveforms with the measured responses of Figs. 11 and 12. Fig. 15 shows the convolution of the F-18 E-pulse

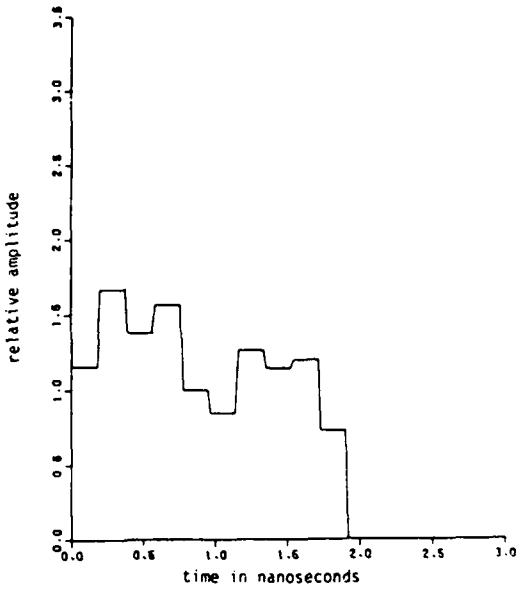

Fig. 14. Natural E-pulse constructed to eliminate the five dominant modes in the F-18 measured response.

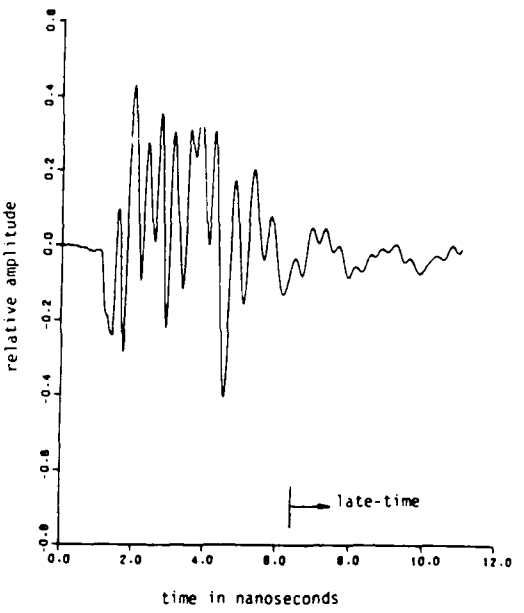

Fig. 16. Convolution of the 707 E-pulse with the F-18 measured response.

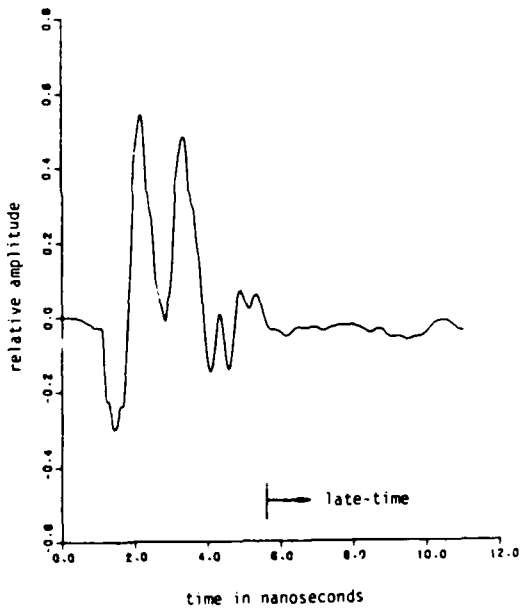

Fig. 15. Convolution of the F-18 E-pulse with the F-18 measured response showing "extinguished" late-time region.

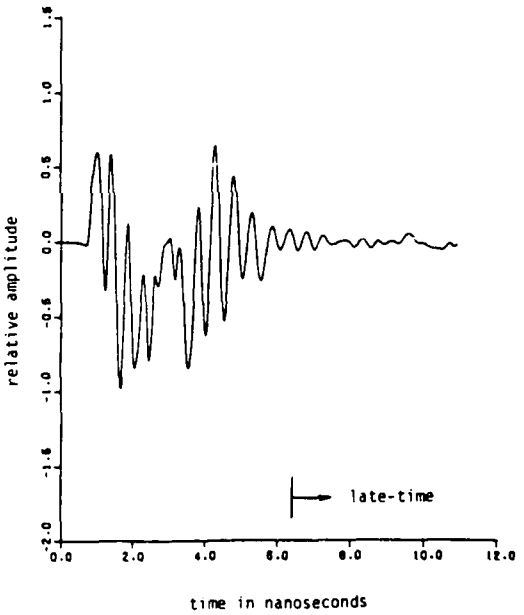

Fig. 17. Convolution of the 707 E-pulse with the 707 measured response showing "extinguished" late-time region.

with the F-18 measured response. Compared to early time, the late-time region has been effectively annulled. In contrast, Fig. 16 shows the convolution of the 707 E-pulse with the F-18 measured response. The result is a relatively larger late-time amplitude. Similarly, Fig. 17 displays the convolution of the 707 E-pulse with the 707 measured response. Again, the late-time region of the convolution exhibits small amplitude. Lastly, Fig. 18 shows the convolution of the F-18 E-pulse and the measured response of the 707 model. As before, the "wrong" target is exposed by its larger late-time convolution response.

VII. Summary And Conclusion

Radar target discrimination based on the natural frequencies of a conducting target has been investigated. The response of targets to a particular class of waveforms known as "E-pulses" has been demonstrated to provide an effective means for implementing a discrimination process in the presence of random noise.

Two types of E-pulses have been identified, natural and forced. Discrimination based on natural E-pulses and the response of a thin cylinder target has been demonstrated theoretically.

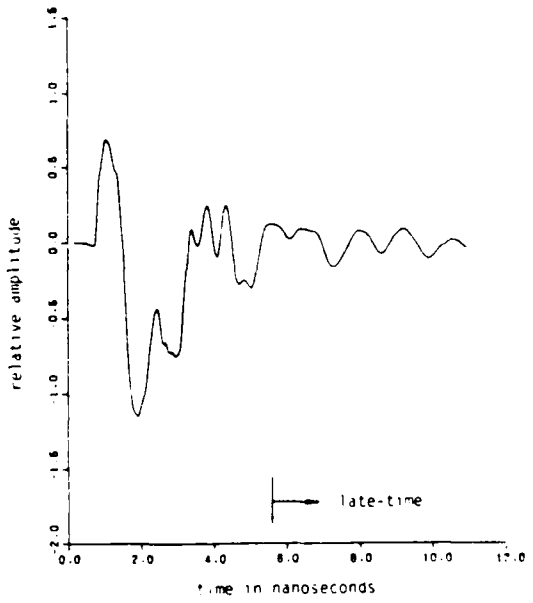

Fig. 18. Convolution of the F-18 E-pulse with the 707 measured response.

Most encouraging are the experimental results which reveal that two quite complicated, similar sized targets can be adequately and convincingly discriminated using natural E-pulse waveforms. Further experimentation using more accurate aircraft models is currently being undertaken.

References

[1] K. M. Chen, "Radar waveform synthesis method—a new radar detection scheme," *IEEE Trans. Antennas Propagat.*, vol. AP-29, no. 4, pp. 553-566, July 1981.

[2] D. L. Moffatt and R. K. Mains, "Detection and discrimination of radar targets," *IEEE Trans. Antennas Propagat.*, vol. AP-23, no. 3, pp. 358-367, May 1975.

[3] A. J. Berni, "Target identification by natural resonance estimation," *IEEE Trans. Aerospace Electron. Syst.*, vol. AES-11, no. 2, pp. 147-154, Mar. 1975.

[4] C. W. Chuang and D. L. Moffatt, "Natural resonances of radar targets via Prony's method and target discrimination," *IEEE Trans. Aerospace Electron. Syst.*, vol. AES-12, no. 5, pp. 583-589, Sept. 1976.

[5] E. M. Kennaugh, "The K-pulse concept," *IEEE Trans. Antennas Propagat.*, vol. AP-29, no. 2, 327-331, Mar. 1981.

[6] C. E. Baum, "The singularity expansion method," in *Transient Electromagnetic Fields*, L. B. Felson, Ed. New York: Springer-Verlag, 1976, ch. 3, pp. 129-179.

[7] M. A. Morgan, "Singularity expansion representation of fields and currents in transient scattering," *IEEE Trans. Antennas Propagat.*, vol. AP-32, no. 5, pp. 466-473, May 1984.

[8] L. W. Pearson, "A note on the representation of scattered fields as a singularity expansion," *IEEE Trans. Antennas Propagat.*, vol. AP-32, no. 5, pp. 520-524, May 1984.

[9] K. M. Chen and D. Westmoreland, "Radar waveform synthesis for exciting single-mode backscatter from a sphere and application for target discrimination," *Radio Sci.*, vol. 17, no. 3, pp. 574-588, May-June, 1982.

[10] C. E. Baum, "Emerging technology for transient and broad-band analysis of antennas and scatterers," *Proc. IEEE*, vol. 64, no. 11, pp. 1598-1616, Nov. 1982.

[11] K. M. Chen *et al.*, "Radar waveform synthesis for single-mode scattering by a thin cylinder and application for target discrimination," *IEEE Trans. Antennas Propagat.*, vol. AP-30, no. 5, pp. 867-880, Sept. 1982.

[12] F. M. Tesche, "On the analysis of scattering and antenna problems using the singularity expansion technique," *IEEE Trans. Antennas Propagat.*, vol. AP-21, no. 1, pp. 53-62, Jan. 1973.

[13] B. Drachman and E. Rothwell, "A continuation method for identification of the natural frequencies of an object using a measured response," *IEEE Trans. Antennas Propagat.*, vol. AP-33, no. 4, pp. 445-450, Apr. 1985.

Edward J. Rothwell (S'84) was born in Grand Rapids, MI, on September 8, 1957. He received the B.S. degree in electrical engineering with high honors from Michigan Technological University, Houghton, MI, in 1979 and the M.S. in electrical engineering and the degree of Electrical Engineer from Stanford University, Stanford, CA, in 1980 and 1982.

He worked for Raytheon Company, Microwave and Power Tube Division, Waltham, ME, from 1979 to 1982 on low power traveling-wave tubes. Since 1982, he has been a Ph.D. candidate at Michigan State University, East Lansing, where he is involved in transient electromagnetic scattering analysis.

Mr. Rothwell is a member of Phi Kappa Phi.

Dennis P. Nyquist (S'63-M'67) was born in Detroit, MI, on August 18, 1939. He received the B.S.E.E. and M.S.E.E. degrees in 1961 and 1964, respectively, and the Ph.D. degree in electrical engineering from Michigan State University, East Lansing, in 1966.

Prior to obtaining the Ph.D. degree, he was a Research Engineer at the Ford Research Laboratories. He held an Engineering College Predoctoral Fellowship during his doctoral program at Michigan State University, East Lansing. He joined the Electrical Engineering Faculty at Michigan State University as an Instructor in 1966, became Assistant Professor in 1967, Associate Professor in 1970 and Professor in 1979. He has published a number of papers on electromagnetic radiation, antennas, and scattering. His current research interests include target discrimination with transient waveforms and guided-wave optics.

Dr. Nyquist is a member of Commission B of the International Union of Radio Science, the American Association for the Advancement of Science, Sigma Xi, and Phi Kappa Phi. He was the recipient of the Michigan State University Teacher-Scholar Award in 1969.

Kun-Mu Chen (SM'64-F'76) was born in Taipei, Taiwan, China, on February 3, 1933. He received the B.S.E.E. degree from the National Taiwan University, Taipei, Taiwan, in 1955, and the M.S. and Ph.D. degrees in applied physics from Harvard University, Cambridge MA, in 1958 and 1960, respectively.

While at Harvard University, he held the C. T. Loo and Gordon McKay Fellowships. From 1956 to 1957 he was a Teaching Assistant at the National Taiwan University, and from 1959 to 1960 he was a Research Assistant and Teaching Fellow at Harvard University. From 1960 to 1964 he was associated with the Radiation Laboratory, University of Michigan, Ann Arbor, where he was engaged in studies of electromagnetic theory and plasma. In 1962, while on leave from the University of Michigan, he was a Visiting Professor of Electronics at Chao-Tung University, Taiwan. Since 1964 he has been with Michigan State

University, East Lansing, first as Associate Professor of Electrical Engineering, and since 1967 as Professor of Electrical Engineering. From 1968 to 1973 he was the Director of the Electrical Engineering Program of the Department of Electrical Engineering and Systems Science. He has published numerous papers on electromagnetic radiation and scattering, plasmas, and the interaction of electromagnetic radiation with biological systems.

Dr. Chen is a fellow of the American Association for the Advancement of Science, a member of U.S. Commissions A, B, and C of the International Scientific Radio Union, Sigma Xi, Phi Kappa Phi and Tau Beta Pi. He is the recipient of Distinguished Faculty Award from Michigan State University in 1976. He is also the recipient of Achievement Award in Science and Engineering from Taiwanese American Foundation in 1984.

Byron Drachman received the B.S. degree in electrical engineering from the University of Illinois, Urbana, the M.S. degree in applied mathematics from the University of Arizona, Tucson, and the Ph.D. degree in pure mathematics (algebraic topology) from Brown University, Providence, RI, in 1960, 1962, 1966, respectively.

He was at the Centro de Investigacion del IPN, Mexico City from 1966 to 1970. He has been at Michigan State University, East Lansing, since 1971, where he is currently a Professor of Mathematics.

Appendix 3

Frequency Domain *E*-Pulse Synthesis and Target Discrimination

EDWARD J. ROTHWELL, MEMBER, IEEE, KUN-MU CHEN, FELLOW, IEEE, DENNIS P. NYQUIST, MEMBER, IEEE, AND WEIMIN SUN

Abstract—**A frequency domain approach to the *E*-pulse radar target discrimination scheme is introduced. This approach is shown to allow easier interpretation of *E*-pulse convolutions via the *E*-pulse spectrum, and leads to a simplified calculation of pulse basis function amplitudes in the *E*-pulse expansion. Experimental evidence obtained using aircraft models verifies the single-mode discrimination scheme, as well as the aspect-independent nature of the *E*-pulse technique. This leads to an integrated technique for target discrimination combining the *E*-pulse with single mode extraction waveforms.**

I. Introduction

THE TIME-DOMAIN scatte ' field response of a conducting arget has been observed to be composed of an early-time forced period, when the excitation field is interacting with the scatterer, followed immediately by a late-time period during which the target oscillates freely [1], [2]. The late-time portion can be decomposed into a finite sum of damped sinusoids (excited by an incident field waveform of finite usable bandwidth), oscillating at frequencies determined purely by target geometry. The natural resonance behavior of the late-time portion of the scattered field response can be utilized to provide an aspect-independent means for radar target discrimination [3]–[7].

An extinction pulse (*E*-pulse) is defined as a finite duration waveform which, upon interaction with a particular target, eliminates a preselected portion of the target's natural mode spectrum. By basing *E*-pulse synthesis on the target natural frequencies, the *E*-pulse waveform is made aspect-independent.

Discrimination is accomplished by convolving an *E*-pulse waveform with the measured late-time scattered field response of a target. If the scattered field is from the anticipated target, the convolved response will be composed of an easily interpreted portion of the expected natural mode spectrum. If the target is different from that expected, a portion of its dissimilar natural mode spectrum will be extracted, resulting in an unexpected convolved response.

This paper will consider the construction of two types of *E*-pulse waveforms. The first is designed to eliminate the entire finite expected natural mode spectrum of the target, and the second to extract just a single mode. Both time and frequency domain analyses will be used to develop a set of defining *E*-pulse equations. The frequency domain approach will be shown to be of significant value not only for providing a much more convenient way of viewing *E*-pulse discrimination, but also for constructing certain *E*-pulse waveforms.

Lastly, experimental results using aircraft models will be presented, demonstrating single mode discrimination and verifying the aspect independence of the *E*-pulse technique.

Manuscript received December 26, 1985; revised April 24, 1986. This work was supported by Naval Air Systems Command under Contract N00019-84-C-0190.

The authors are with the Department of Electrical Engineering and Systems Science, Michigan State University, East Lansing, MI 48824.

IEEE Log Number 8613188

II. Time Domain Synthesis

Assume that the measured time domain scattered field response waveform of a conducting radar target can be written during the late-time period as a finite sum of damped sinusoids

$$r(t)=\sum_{n=1}^{N} a_n e^{\sigma_n t}\cos(\omega_n t+\phi_n), \qquad t>T_l \tag{1}$$

where a_n and ϕ_n are the aspect dependent amplitude and phase of the n'th mode, T_l describes the beginning of late time, and only N modes are assumed to be excited by the incident field waveform. Then, the convolution of an *E*-pulse waveform $e(t)$ with the measured response waveform becomes

$$\begin{aligned} c(t) &= e(t)*r(t) \\ &= \int_0^{T_e} e(t')r(t-t')\,dt' \\ &= \sum_{n=1}^{N} a_n e^{\sigma_n t}[A_n\cos(\omega_n t+\phi_n)+B_n\sin(\omega_n t+\phi_n)], \\ & \qquad t>T_L=T_l+T_e \end{aligned} \tag{2}$$

where

$$\begin{Bmatrix} A_n \\ B_n \end{Bmatrix} = \int_0^{T_e} e(t')e^{-\sigma_n t'}\begin{Bmatrix} \cos\omega_n t' \\ \sin\omega_n t' \end{Bmatrix} dt' \tag{3}$$

and T_e is the finite duration of $e(t)$.

Two interesting waveforms are now considered. Constructing $e(t)$ to result in $c(t)=0$, $t>T_L$, requires

$$A_n=B_n=0, \qquad 1\le n\le N. \tag{4}$$

This approach was considered in [3]. In addition, $e(t)$ can also be constructed so that $c(t)$ is composed of just a single mode.

0018-926X/87/0400-0426$01.00

In this case $e(t)$ is termed a "single mode extraction signal," as discussed in [5]–[7]. If the specific value of the phase constant of $c(t)$ is unimportant, $e(t)$ can be synthesized by demanding

$$A_n = B_n = 0, \qquad 1 \le n \le N, \quad n \ne m \tag{5}$$

to excite the m'th natural mode. On the other hand, requiring

$$A_n = B_n = 0, \qquad 1 \le n \le N, \quad n \ne m$$
$$A_m = 0 \tag{6}$$

results in

$$c(t) = c_s(t) = a_m e^{\sigma_m t} B_m \sin(\omega_m t + \phi_m) \tag{7}$$

and requiring

$$A_n = B_n = 0, \qquad 1 \le n \le N, \quad n \ne m$$
$$B_m = 0 \tag{8}$$

yields

$$c(t) = c_c(t) = a_m e^{\sigma_m t} A_m \cos(\omega_m t + \phi_m). \tag{9}$$

The E-pulse resulting from (5) is termed a "sin/cos" single mode extraction waveform, since $c(t)$ contains both sine and cosine components. Similarly (6) results in a "sine" and (8) a "cosine" single mode extraction waveform. With the proper normalization of $e(t)$ (giving $A_m = B_m$), the convolved waveforms (7) and (9) can be combined to yield plots of the m'th mode frequencies versus time, via

$$\omega_m t + \phi_m = \tan^{-1} \frac{c_s(t)}{c_c(t)}$$

$$\sigma_m t + \log |a_m A_m| = \frac{1}{2} \log [c_c^2(t) + c_s^2(t)]. \tag{10}$$

III. Frequency Domain Synthesis

The convolution of the E-pulse waveform with the measured response waveform can also be written in the form

$$c(t) = \sum_{n=1}^{N} a_n |E(s_n)| e^{\sigma_n t} \cos(\omega_n t + \psi_n), \qquad t > T_l \tag{11}$$

where

$$E(s) = \mathcal{L}\{e(t)\} = \int_{t_0}^{t_0 + T_e} e(t) e^{-st}\, dt \tag{12}$$

is the Laplace transform of the E-pulse waveform, and

$$\psi_n = \phi_n + \tan^{-1}\left(-\frac{E_{rn}}{E_{in}}\right) \tag{13}$$

where

$$E_{in} = \mathrm{Im}\{E(s_n)\} \quad E_{rn} = \mathrm{Re}\{E(s_n)\}. \tag{14}$$

Now, $c(t) = 0$ for $t > T_l$ requires

$$E_{in} = E_{rn} = 0, \qquad 1 \le n \le N \tag{15}$$

or, equivalently,

$$E(s_n) = E(s_n^*) = 0, \qquad 1 \le n \le N. \tag{16}$$

In addition, a sin/cos m'th mode extraction waveform can be synthesized via

$$E(s_n) = E(s_n^*) = 0, \qquad 1 \le n \le N, \quad n \ne m \tag{17}$$

while a sine m'th mode extraction waveform requires

$$E(s_n) = E(s_n^*) = 0, \qquad 1 \le n \le N, \quad n \ne m$$
$$E(s_m) = -E(s_m^*) \tag{18}$$

and a cosine m'th mode extraction waveform necessitates

$$E(s_n) = E(s_n^*) = 0, \qquad 1 \le n \le N, \quad n \ne m$$
$$E(s_m) = E(s_m^*). \tag{19}$$

It is easily shown that the frequency domain and time domain requirements for synthesizing an E-pulse are identical. By expanding the exponential in (12), one can show that (17), (18), and (19) are equivalent to (5), (6), and (8), respectively.

A significant benefit of using a frequency domain approach comes via the increased intuition allowed by (11). When an E-pulse waveform is convolved with the measured response of an unexpected target, the amplitudes of the resulting natural mode components are determined by evaluating the magnitude of the spectrum of $e(t)$ at the natural frequencies of the target (a result of the Cauchy residue theorem). Thus, the E-pulse spectrum becomes the key tool in predicting the success of E-pulse discrimination.

IV. E-Pulse Synthesis Using Frequency Domain Approach

To implement the E-pulse requirements, it becomes necessary to represent the waveform mathematically. Let $e(t)$ be composed of two components

$$e(t) = e^f(t) + e^e(t). \tag{20}$$

Here $e^f(t)$ is a forcing component which excites the target, and $e^e(t)$ is an extinction component which extinguishes the response due to $e^f(t)$. The forcing component is chosen freely, while the extinction component is determined by first expanding in a set of basis functions

$$e^e(t) = \sum_{m=1}^{M} \alpha_m f_m(t) \tag{21}$$

and then employing the appropriate E-pulse conditions from Section III. For an E-pulse designed to extinguish all of the modes of the measured response, using (16) results in the matrix equation

$$\begin{bmatrix} F_1(s_1) & F_2(s_1) & \cdots & F_M(s_1) \\ \vdots & \vdots & & \vdots \\ F_1(s_N) & F_2(s_N) & \cdots & F_M(s_N) \\ F_1(s_1^*) & F_2(s_1^*) & \cdots & F_M(s_1^*) \\ \vdots & \vdots & & \vdots \\ F_1(s_N^*) & F_2(s_N^*) & \cdots & F_M(s_N^*) \end{bmatrix} \begin{bmatrix} \alpha_1 \\ \alpha_2 \\ \\ \vdots \\ \\ \alpha_M \end{bmatrix} = \begin{bmatrix} -E^f(s_1) \\ \vdots \\ -E^f(s_N) \\ -E^f(s_1^*) \\ \vdots \\ -E^f(s_N^*) \end{bmatrix} \tag{22}$$

where

$$F_m(s) = \mathcal{L}\{f_m(t)\}$$
$$E^f(s) = \mathcal{L}\{e^f(t)\} \tag{23}$$

and $M = 2N$ is chosen to make the matrix square. Similar equations can be constructed to accomodate the requirements given by (17), (18), or (19).

As in [3], two types of E-pulses can be easily identified. When $e^f(t) \neq 0$, the forcing vector on the right-hand side of (22) is nonzero, and solutions for the basis function amplitudes exist for any choice of E-pulse duration, T_e, which does not cause the matrix to be singular. In contrast, when $e^f(t) = 0$ the matrix equation becomes homogeneous, and solutions for $e^e(t)$ exist only for specific durations T_e, which are calculated by solving for the zeros of the determinantal equation. The former type of E-pulse is termed "forced" and the latter "natural." Since a natural E-pulse has no forcing component, it is viewed as extinguishing its own excited response.

The frequency domain approach makes it possible to visualize an improved E-pulse waveform whose spectrum has been shaped to accentuate the response of a known target. For example, by using damped sinusoids or Fourier cosines as basis functions in the E-pulse expansion, it is possible to concentrate the energy of the E-pulse near prechosen frequencies, and enhance the single mode response of a particular target [4].

V. Calculation of Pulse Basis Function Amplitudes

A very useful application of the frequency domain approach results from using subsectional basis functions in (21). Let

$$f_m(t) = \begin{cases} g(t-[m-1]\Delta), & (m-1)\Delta \le t \le m\Delta \\ 0, & \text{elsewhere} \end{cases} \tag{24}$$

where $g(t)$ is an arbitrary (but Laplace transformable) function, and Δ is the pulse width. Then

$$F_m(s) = \int_0^{T_e} g(t-[m-1]\Delta)e^{-st}\,dt$$
$$= F_1(s)e^{s\Delta}e^{-sm\Delta} \tag{25}$$

and the matrix equation (22) can be written for the case of the natural E-pulse as

$$\begin{bmatrix} 1 & z_1 & z_1^2 & \cdots & z_1^{2N-1} \\ \vdots & \vdots & \vdots & & \vdots \\ 1 & z_N & z_N^2 & \cdots & z_N^{2N-1} \\ 1 & z_1^* & (z_1^*)^2 & \cdots & (z_1^*)^{2N-1} \\ \vdots & \vdots & \vdots & & \vdots \\ 1 & z_N^* & (z_N^*)^2 & \cdots & (z_N^*)^{2N-1} \end{bmatrix} \begin{bmatrix} \alpha_1 \\ \alpha_2 \\ \vdots \\ \alpha_{2N} \end{bmatrix} = 0 \tag{26}$$

where

$$z_n = e^{-s_n\Delta}. \tag{27}$$

Equation (26) is homogeneous, and thus has solutions only when the determinant of the matrix is zero. As the determinant is of the Vandermonde type [8], the condition for a singular matrix can be calculated easily as

$$\Delta = \frac{p\pi}{\omega_k}, \qquad p = 1, 2, 3, \cdots, \quad 1 \le k \le N. \tag{28}$$

Thus, the duration of the E-pulse depends only on the imaginary part of one of the natural frequencies. With Δ determined, the basis function amplitudes can be calculated using Cramer's rule and the theory of determinants [9] as

$$\alpha_m = (-1)^m P_{(2N-1)(m-1)} \tag{29}$$

where $P_{n,i}$ is the sum of the products $n - i$ at a time, without repetitions, of the quantities $z_1, z_1^*, z_2, \cdots, z_N^*$.

Note that $g(t)$ does not appear in this analysis, and thus the resulting pulse amplitudes are independent of the individual pulse shapes. However, when discriminating between different targets, $g(t)$ manifests itself through the term $F_1(s)$.

Fig. 1. Aluminum aircraft models of Boeing 707 (left) and McDonnell Douglas F-18 used in the experiment. Note that the models are not to the same scale, but rather are of similar physical size.

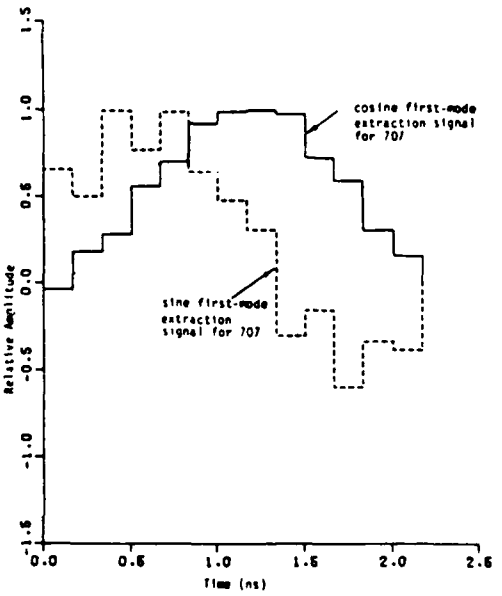

Fig. 2. Natural rectangular pulse function based first mode extraction waveforms for the Boeing 707 aircraft model.

VI. Experimental Results

This section will address two important topics. First discrimination between two similar aircraft models will be

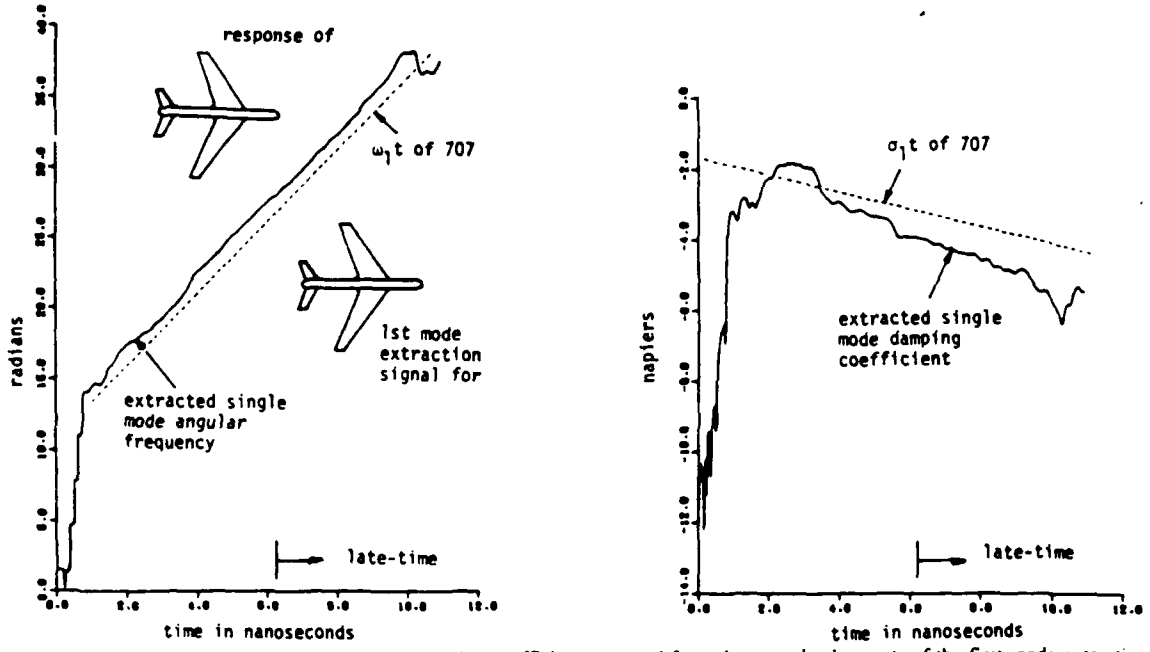

Fig. 3. Single mode angular frequency and damping coefficient extracted from the convolved outputs of the first mode extraction signals for the 707 target and the 707 measured response.

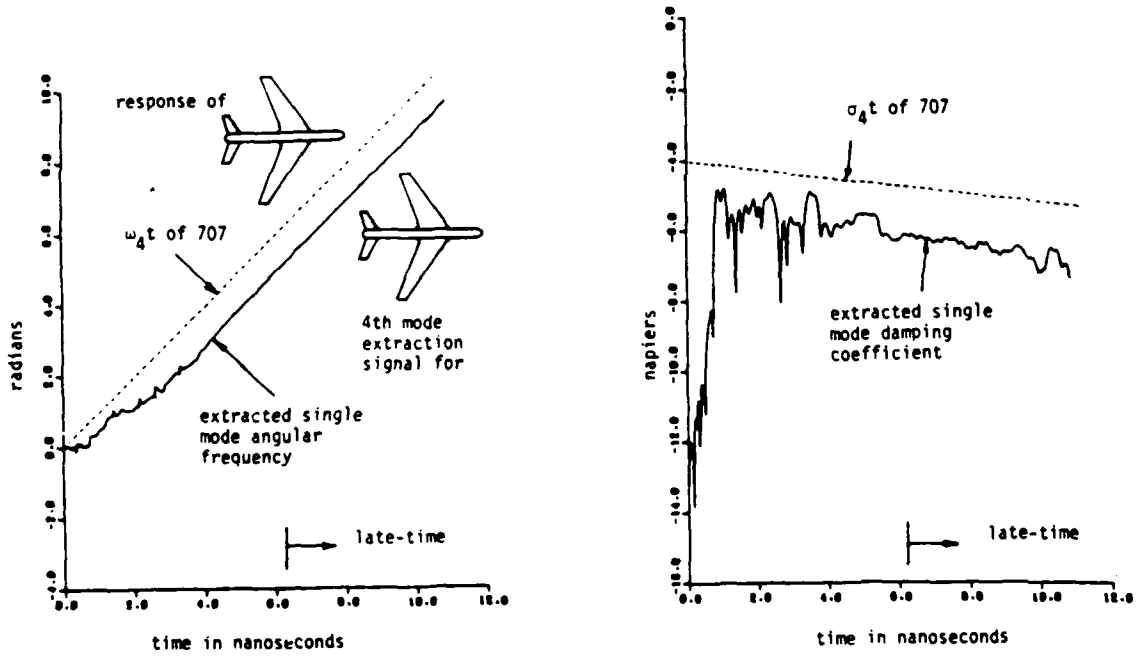

Fig. 4. Singular mode angular frequency and damping coefficient extracted from the convolved outputs of the fourth mode extraction signals for the 707 target and the 707 measured response.

demonstrated using single mode extraction waveforms. Second, the aspect independence of the *E*-pulse technique will be confirmed using the same two models.

The measured near field responses of simplified McDonnel Douglas F-18 and Boeing 707 aircraft models have been published previously [3]. The models are constructed of aluminum, and are shown in Fig. 1. The dominant natural frequencies have been extracted from the late-time portions of the responses using a continuation method [10]. With these, pulse function based natural sine and cosine single mode extraction waveforms of minimum duration can be constructed using (18) and (19) together with (24) to extract the first and fourth modes of the 707. The first mode waveforms are shown in Fig. 2. Discrimination between the F-18 and the 707 can be accomplished by convolving the *E*-pulse waveforms with each of the measured aircraft responses. If the *E*-pulses are convolved with the expected (707) response, the result should be either a pure first or fourth mode damped sinusoid. If the *E*-pulses are convolved with the unexpected (F-18) response, the result will be an unrecognizable conglomeration of the modes of the unexpected target.

Figs. 3–6 show the results of convolving the 707 *E*-pulses

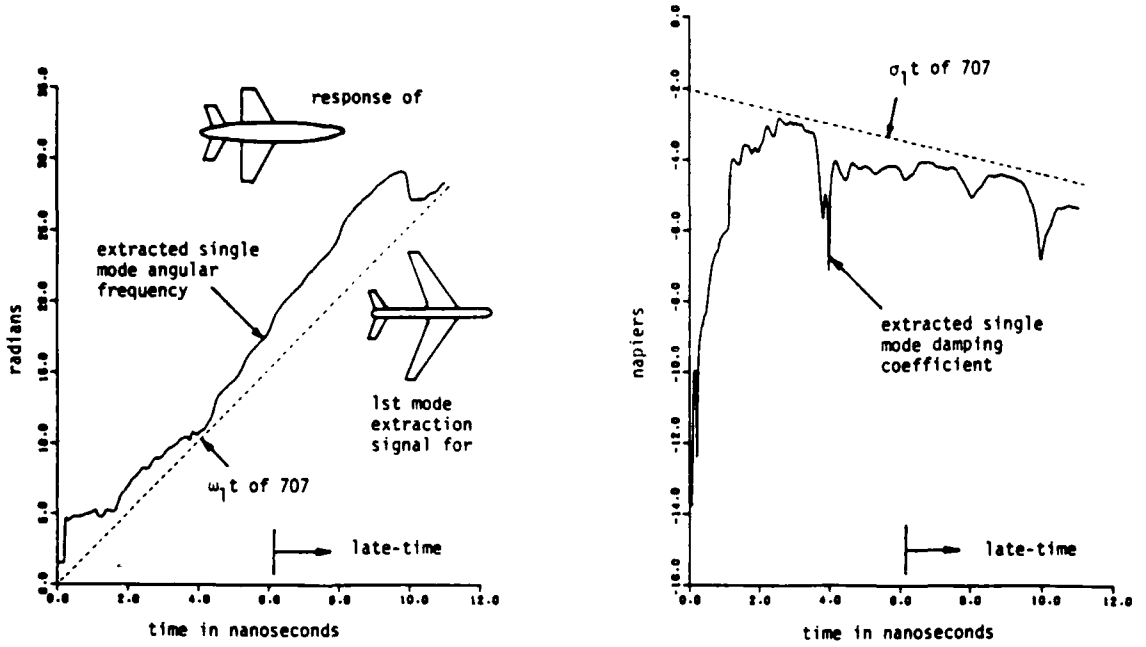

Fig. 5. Single mode angular frequency and damping coefficient extracted from the convolved outputs of the first mode extraction signals for the 707 target and the F-18 measured response.

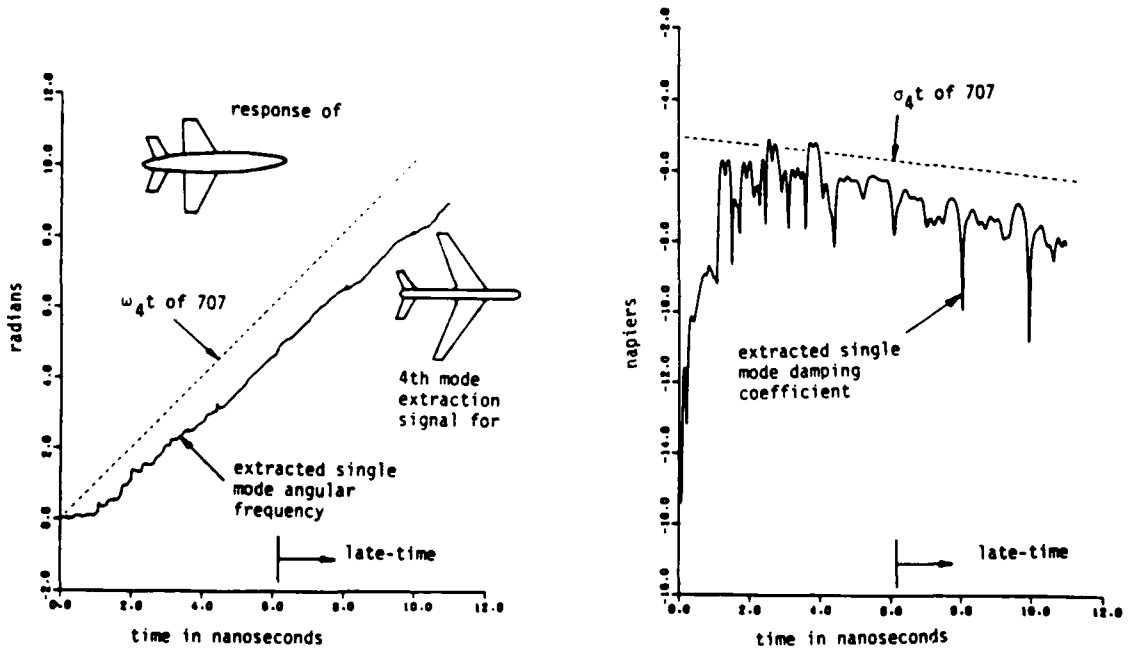

Fig. 6. Single mode angular frequency and damping coefficient extracted from the convolved outputs of the fourth mode extraction signals for the 707 target and the F-18 measured response.

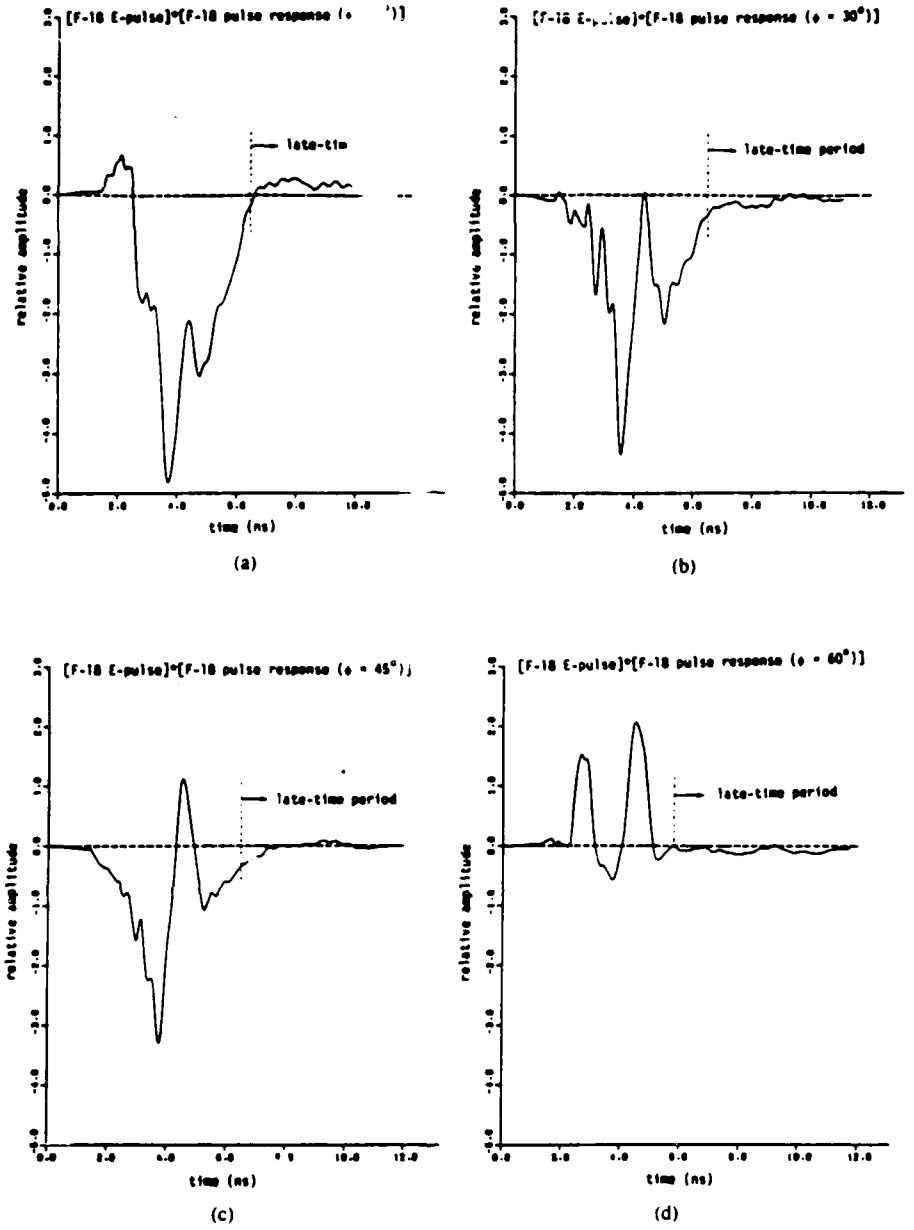

Fig. 7. Convolved outputs of F-18 *E*-pulse and pulse responses of F-18 model measured at (a) 0° aspect angle, (b) 30° aspect angle, (c) 45° aspect angle, (d) 60° aspect angle.

with both the 707 and F-18 responses. These frequency plots are obtained from the actual convolved waveforms by using (10). The dotted lines represent the slopes of the expected first or fourth mode frequencies. It is seen that the frequency plots for the expected target (Figs. 3 and 4) parallel the expected frequency lines in the late-time, while those for the unexpected target (Figs. 5 and 6) do not. Thus, the 707 and the F-18 are easily discriminated.

It is also quite important to verify experimentally the aspect independence of the *E*-pulse technique. To accomplish this, measurements have been made of the near-field pulse response of the 707 and F-18 models with the fuselage axes aligned at various angles with respect to the transmitting/receiving antenna configuration. Two natural rectangular pulse based *E*-pulses of minimum duration, one designed to eliminate all of the modes detected in the 707 responses and one designed to eliminate all the modes in the F-18 responses, are then constructed according to (28) and (29).

Convolution of the 707 and F-18 *E*-pulses with each of the measured aircraft responses yields the results shown in Figs. 7–10. It is apparent from Fig. 7 that convolving the F-18 *E*-pulse with the measured F-18 response gives a waveform with

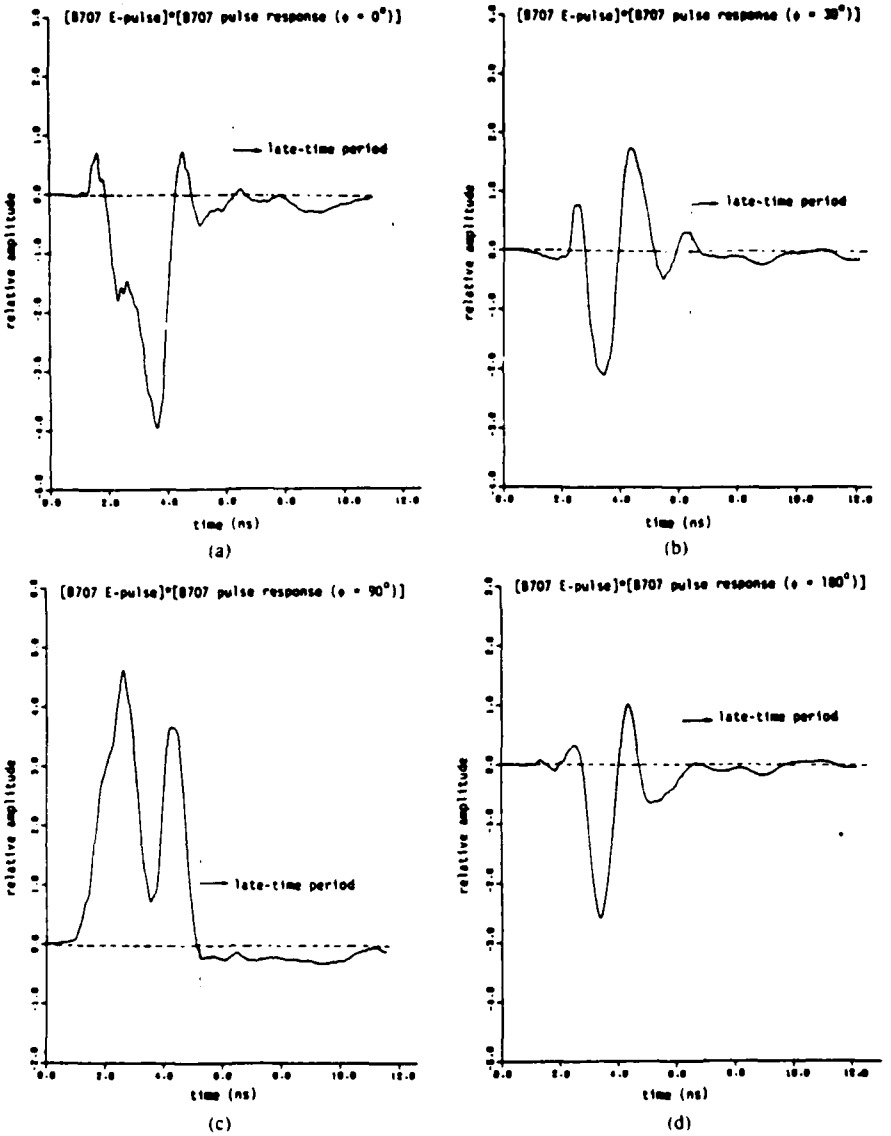

Fig. 8. Convolved outputs of B707 E-pulse and pulse responses of B707 model measured at (a) 0° aspect angle, (b) 30° aspect angle, (c) 90° aspect angle, (d) 180° aspect angle.

negligible amplitude in the late time, regardless of the aspect angle. Similar results are obtained in Fig. 8 when the 707 E-pulse is convolved with the 707 measured response. In contrast, Figs. 9 and 10 reveal that when the 707 E-pulse is convolved with any F-18 response, or when the F-18 E-pulse is convolved with any 707 response, the late-time portion of the resulting waveform has significant amplitude. Thus, discrimination between the two aircraft models is possible regardless of the target aspect.

The experimental results suggest the feasibility of an E-pulse target discrimination scheme which utilizes both a waveform designed to eliminate all the modes of a target and a set of waveforms designed to extract various individual target modes. This technique integrates the single mode extraction concept and the usual E-pulse technique into a scheme which has a greater potential for accurate target discrimination decisions.

VII. Conclusion

The E-pulse radar target discrimination concept has been expanded upon, incorporating single mode extraction waveforms into an integrated technique. Both time and frequency domain analyses have been included, and their equivalence demonstrated. The frequency domain viewpoint is helpful for interpreting E-pulse discrimination, and it has been applied to pulse basis function amplitude calculation.

Experimental results obtained using aircraft models have demonstrated the validity of radar target discrimination based on single mode extraction waveforms. Most importantly, experimental evidence has also shown the E-pulse technique to

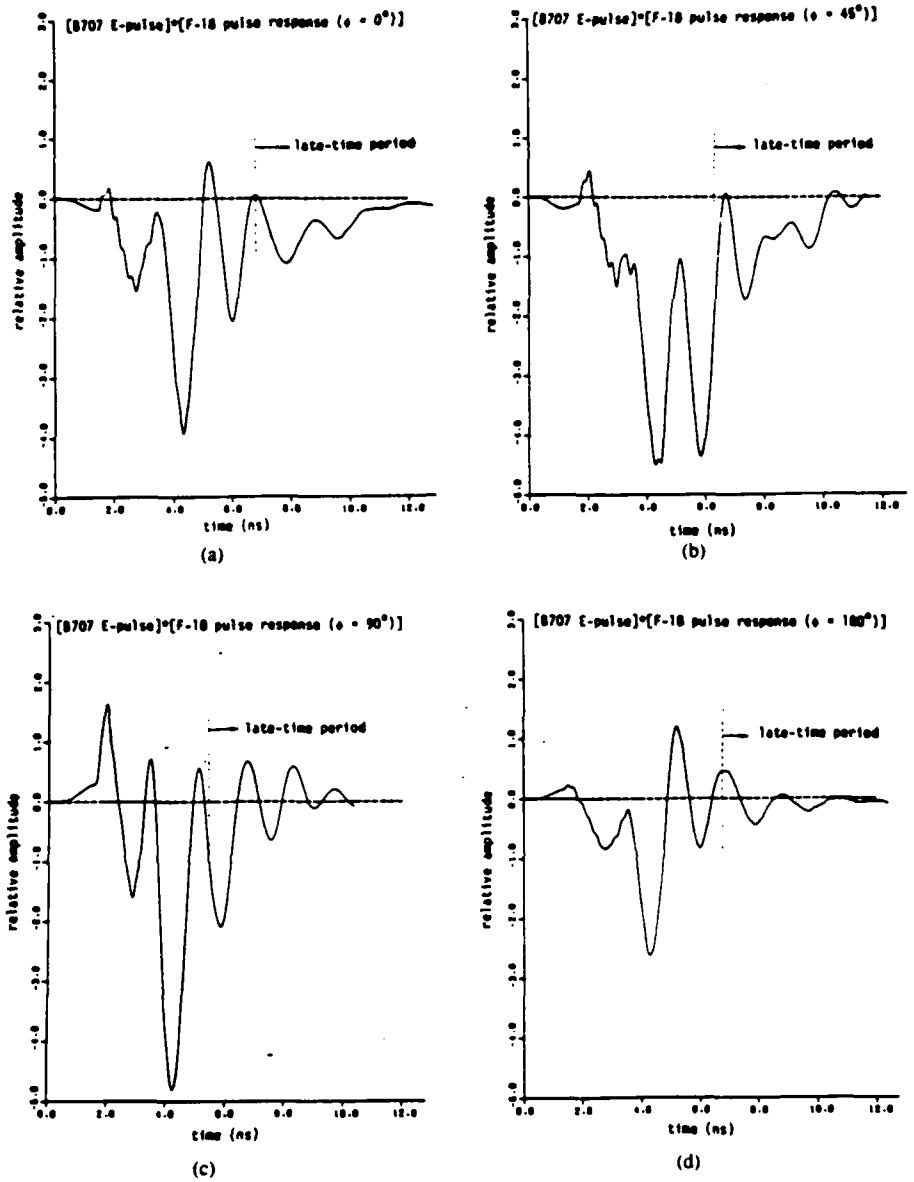

Fig. 9. Convolved outputs of B707 *E*-pulse and pulse responses of F-18 model measured at (a) 0° aspect angle, (b) 45° aspect angle (c) 90° aspect angle, (d) 180° aspect angle.

be successful regardless of target aspect angle. This aspect-independence of the *E*-pulse concept is fundamental for its application to practical situations.

References

[1] L. W. Pearson, "A note on the representation of scattered fields as a singularity expansion," *IEEE Trans. Antennas Propagat.*, vol. AP-32, pp. 520–524, May 1984.

[2] L. B. Felsen, "Comments on early time SEM," *IEEE Trans. Antennas Propagat.*, vol. AP-33, pp. 118–119, Jan. 1985.

[3] E. Rothwell, D. P. Nyquist, K. M. Chen, and B. Drachman, "Radar target discrimination using the extinction-pulse technique," *IEEE Trans. Antennas Propagat.*, vol. AP-33, pp. 929–937, Sept. 1985.

[4] E. Rothwell, "Radar target discrimination using the extinction-pulse technique," Ph.D. dissertation, Michigan State Univ., East Lansing, June 1985.

[5] K. M. Chen, D. Nyquist, E. Rothwell, L. Webb, and B. Drachman, "Radar target discrimination by convolution of radar return with extinction-pulses and single-mode extraction signals," *IEEE Trans. Antennas Propagat.*, vol. AP-34, pp. 896–904, July 1986.

[6] K. M. Chen and D. Westmoreland, "Radar waveform synthesis for exciting single-mode backscatters from a sphere and application for target discrimination," *Radio Sci.*, vol. 17, pp. 574–588, June 1982.

[7] K. M. Chen, D. P. Nyquist, D. Westmoreland, C. I. Chuang, and B. Drachman, "Radar waveform synthesis for single-mode scattering by a thin cylinder and application for target discrimination," *IEEE Trans. Antennas Propagat.*, vol. AP-30, pp. 867–880, Sept. 1982.

[8] P. H. Hanus, *Theory of Determinants*. Boston, MA: Ginn and Co., 1886.

[9] T. Muir, *A Treatise on the Theory of Determinants*. New York: Dover, 1960.

[10] B. Drachman and E. Rothwell, "A continuation method for identification of the natural frequencies of an object using a measured response," *IEEE Trans. Antennas Propagat.*, vol. AP-33, pp. 445–450, Apr. 1985.

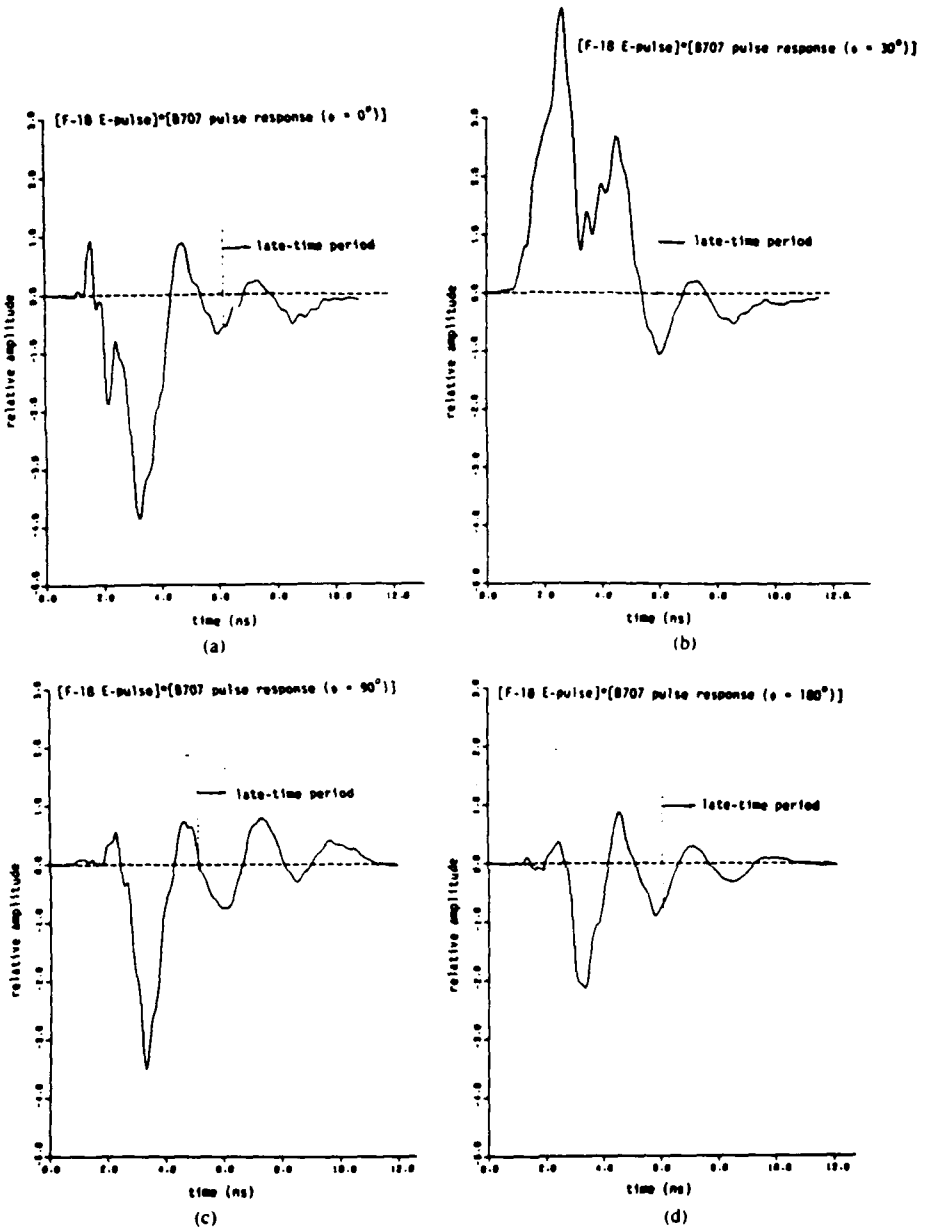

Fig. 10. Convolved outputs of F-18 E-pulse and pulse responses of B707 model measured at (a) 0° aspect angle, (b) 30° aspect angle, (c) 90° aspect angle, (d) 180° aspect angle.

Edward J. Rothwell (S'84-M'85), for a photograph and biography please see page 936 of the September 1985 issue of this TRANSACTIONS.

Kun-Mu Chen (SM'64-F'76), for a photograph and biography please see page 936 of the September 1985 issue of this TRANSACTIONS.

Dennis P. Nyquist (S'63-M'67), for a photograph and biography please see page 936 of the September 1985 issue of this TRANSACTIONS.

Weimin Sun was born in Jiangsu Province, China, on October 20, 1957. He received the B.S. degree in electrical engineering from Sichuan University, China, in 1982 and the M.S. degree in physics and electronics from Tsinghua University, Beijing, China, in 1984. He is currently a Ph.D. candidate in the Department of Electrical Engineering and Systems Science, Michigan State University, East Lansing.

From 1982-1984, his research was in the field of optical communications and integrated optics. His current research interests include radar target discrimination systems, and application of numerical methods for treating electromagnetic radiation and scattering problems.

Extraction of the Natural Frequencies of a Radar Target from a Measured Response Using *E*-Pulse Techniques

EDWARD J. ROTHWELL, MEMBER, IEEE, KUN-MU CHEN, FELLOW, IEEE, AND DENNIS P. NYQUIST, MEMBER, IEEE

Abstract—A new scheme is introduced for extracting the natural resonance frequencies of a radar target from a measured response. The method is based on the *E*-pulse technique and is shown to be relatively insensitive to random noise and to estimates of modal content. Verification of the technique is accomplished by comparing the natural frequencies extracted from the measured responses of a thin cylinder and a circular loop with those obtained from theory. The applicability of the technique to low-Q targets is also demonstrated, using the measured response of a scale model aircraft.

I. Introduction

MANY RECENT RADAR target discrimination schemes have utilized the late-time natural oscillation behavior of conducting targets [1]–[5]. These techniques are based upon the assumption that the late-time scattered field response of the target obeys the natural mode representation

$$E^s(t)=\sum_{n=1}^{N} a_n e^{\sigma_n t}\cos(\omega_n t+\phi_n), \qquad t>T_L \tag{1}$$

where $s_n = \sigma_n + j\omega_n$ is the aspect independent natural frequency of the nth target mode, a_n and ϕ_n are the aspect and excitation dependent amplitude and phase of the nth target mode, T_L describes the beginning of the late-time period, and the number of modes in the response N is determined by the finite frequency content of the waveform exciting the target.

Since the natural frequencies of the target are aspect independent, they form an ideal set of discriminants. Employing this set requires the knowledge of the natural frequencies of a wide variety of targets. As a theoretical determination of the natural frequencies of a complex target is impractical, it becomes necessary to develop a scheme for extracting the frequencies from a measurement of the response of the target.

A typical approach might use Prony's method [6], [7]. Although this technique is simple and efficient, it has been found to be overly sensitive to random noise and to the number of modes assumed to be present in the measured response. A nonlinear least squares curve-fitting scheme can overcome these drawbacks, but requires a time consuming minimization involving $4N$ variables [8].

Manuscript received February 12, 1986; revised June 2, 1986. This work was supported by the Naval Air Systems Command under Contract N00019-85-C-0411 and by the Office of Naval Research Grant N00014-87-K-0024.

The authors are with the Department of Electrical Engineering and Systems Science, Michigan State University, East Lansing, MI 48824.

IEEE Log Number 8714667.

In this paper an alternative scheme is proposed, utilizing *E*-pulse waveforms. It will be shown that this approach also overcomes the drawbacks of Prony's method, but is more efficient than nonlinear curve-fitting. The scheme was first introduced in [12] and [15], and is based on the frequency domain *E*-pulse concept first discussed in [14].

II. The *E*-Pulse Technique

An extinction-pulse (*E*-pulse) $e(t)$ is defined as a waveform of finite duration T_e which extinguishes $E^s(t)$ in the late time [1]. That is, convolution of $e(t)$ and $E^s(t)$ yields the null result

$$c(t)=e(t)*E^s(t)=\int_0^{T_e} e(t')E^s(t-t')\,dt'=0, \qquad t>T_L+T_e. \tag{2}$$

Using the natural mode representation for $E^s(t)$ allows (2) to be written as

$$c(t)=\sum_{n=1}^{N} |E(s_n)|a_n e^{\sigma_n t}\cos(\omega_n t+\psi_n)=0, \qquad t>T_L+T_e \tag{3}$$

where ψ_n is a new phase factor and $E(s)$ is the Laplace transform of $e(t)$

$$E(s)=\mathcal{L}\{e(t)\}=\int_0^{T_e} e(t)e^{-st}\,dt. \tag{4}$$

If the natural frequencies of a target are known, an *E*-pulse for that target can be synthesized by demanding

$$E(s_n)=E(s_n^*)=0, \qquad 1\le n\le N \tag{5}$$

and the convolution (3) will yield zero regardless of the aspect angle of the target for which $E^s(t)$ is measured.

Conversely, if the natural frequencies of a target are unknown, they can be extracted from the measured $E^s(t)$ by solving the integral equation given by (2). This equation can either be solved directly for the complex frequencies used to construct $e(t)$ or for $e(t)$ itself. If $e(t)$ is determined, the complex frequencies eliminated by $e(t)$ can be found by locating the roots to [12]

$$E(s)=0. \tag{6}$$

0018-926X/87/0600-0715$01.00

An E-pulse waveform can be represented as an expansion over a set of basis functions $\{f_k(t)\}$

$$e(t)=\sum_{k=1}^{K}\alpha_k f_k(t) \tag{7}$$

where α_k are the basis function amplitudes. Then, the requirements (5) result in a matrix equation for the real amplitude parameters α_k. Choosing $K = 2N$ results in a homogeneous equation which has solutions only at discrete values of T_e.

The difficulty associated with locating all the roots of (6) can be overcome by choosing subsectional basis functions in the E-pulse expansion

$$f_k(t)=\begin{cases} g(t-[k-1]\Delta), & (k-1)\Delta\le t\le k\Delta \\ 0, & \text{elsewhere}\end{cases} \tag{8}$$

resulting in the E-pulse shown in Fig. 1. Here $g(t)$ is any Laplace-transformable function. The E-pulse spectrum is then easily calculated as

$$E(s)=F_1(s)e^{s\Delta}\sum_{k=1}^{K}\alpha_k e^{-sk\Delta} \tag{9}$$

where $F_1(s)$ is the Laplace transform of the first basis function. Now the roots to $E(s)$ are easily found by solving the polynomial equation

$$\sum_{k=1}^{K}\alpha_k Z^k=0 \tag{10}$$

where

$$Z=e^{-s\Delta}. \tag{11}$$

This set of functions also allows a simple calculation of duration T_e when synthesizing E-pulses. It has been shown [9] that the solutions to the homogeneous matrix equation demanded by (5) are

$$\Delta=\frac{p\pi}{\omega_k}, \qquad 1\le k\le N, \quad p=1, 2, 3, \cdots. \tag{12}$$

III. Solutions to the Integral Equation

Solutions to the integral equation (2) have been obtained using two different methods. The first approach is to minimize

$$c^2(t)=[e(t) * E^s(t)]^2 \tag{13}$$

over the range of t corresponding to the late-time period of the convolution, $t > T_L + T_e$. This can be done either with respect to the complex frequencies used to construct the E-pulse via (5), or with respect to the basis function amplitudes used to construct $e(t)$ via (7). If minimization is done with respect to the complex frequencies, then the estimated values of the natural frequencies contained in $E^s(t)$ are available directly at the minimum point. If minimization is done with respect to the basis function amplitudes, then estimates of the natural frequencies in $E^s(t)$ are obtained by solving (6) or (10) using the values of α_k obtained at the minimum point. The latter minimization is computationally less intensive, since a new E-pulse need not be created at each step in the minimization, but it requires a normalization scheme to prevent the trivial solution $\alpha_k = 0$.

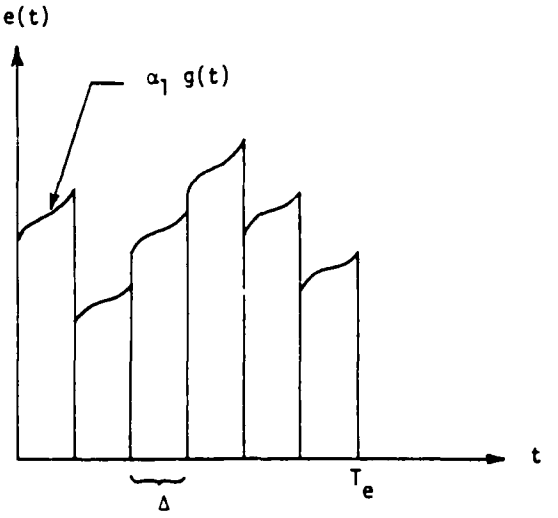

Fig. 1.

The integral equation can also be solved by using the method of moments [10]. The E-pulse is expanded as in (7) and moments are taken with a set of weighting functions $\{w_m(t)\}$

$$\left\langle w_m(t), \sum_{k=1}^{K}\alpha_k\int_0^{T_e} f_k(t')E^s(t-t')\,dt'\right\rangle=0$$
$$m=1, 2, \cdots, M \tag{14}$$

where the brackets $\langle\cdot\rangle$ indicate the inner product

$$\langle f(t), g(t)\rangle \int f(t)g(t)\,dt. \tag{15}$$

Choosing $K = M = 2N$ to reflect the number of modes believed to be in $E^s(t)$ results in a homogeneous matrix equation for the basis function amplitudes, a solution to which is possible only at discrete values of T_e which cause the determinant of the matrix of coefficients to vanish. By choosing subsectional basis functions (8) an estimate for the natural frequencies in $E^s(t)$ is found by solving (10).

With either of the two approaches, the amplitudes and phases of the natural modes comprising $E^s(t)$ can be found as a last step by using linear least squares.

IV. Discussion of the Methods

The major benefit of each of the two E-pulse methods is that they overcome the sensitivity of Prony's method to noise and to estimates of modal co . Although the minimization approach requires a compu nally time consuming multivariable minimization proce because the amplitudes and phases are not involved th number of parameters utilized is only $2N$, compared to r nonlinear curve-fitting, and only half the number of i guesses are needed for starting the minimization. On the ther hand, the moment method approach is extremely efficient; no minimization scheme is required, only a search for the single parameter T_e.

The insensitivity of these two approaches to the number of modes estimated to be present in $E^s(t)$ leads to a particularly useful scheme. Extraction of the frequencies in $E^s(t)$ may begin by assuming a small number of modes (usually one) to be present. For the methods requiring minimization, the frequencies extracted with a small number of modes assumed present prove to be very good initial guesses for the case when more modes are assumed present. For the moment method, because of the relationship (12), the value of T_e obtained allows an excellent estimate of the T_e to expect with more modes allowed.

The reasons for the success of the E-pulse method in the presence of random noise can be identified by investigating the relationship between Prony's method and the moment method approach to the E-pulse technique. By choosing impulses for both expansion and weighting functions in (14) and taking $K = M + 1$, an inhomogeneous matrix equation results. The matrix can be solved directly for α_k and the natural frequencies contained in $E^s(t)$ estimated by solving (10). Such an approach is found to be identical in all respects to Prony's method.

Because of the discrete nature of the convolution integral, each of the matrix entries and the right hand side vector elements are merely a single sampled value of the measured waveform. Thus, Prony's method is very sensitive to noise contamination of $E^s(t)$ and so is an inherently ill-conditioned algorithm (see [16]). The moment method approach can be viewed as a generalization of the basic Prony's method, where preprocessing of the measured data is naturally introduced. The preprocessing step can be incorporated in two places, individually or simultaneously, each of which works to reduce the noise sensitivity of the technique. First, by utilizing expansion functions which together span the E-pulse duration T_e (such as rectangular pulses), the convolution integral in (14) performs a moving window type smoothing of the measured data. Second, by using weighting functions which together span the late-time region of the convolution, the inner product integral (15) introduces additional smoothing. Although the numerical examples presented below utilize impulse functions for weighting, preliminary results using rectangular pulses indicate an additional reduction in noise sensitivity.

The result of preprocessing the measured data is matrix elements which are each a function of a large portion of the measured data. Consequently, solutions are less sensitive to the perturbation of individual sampled values of $E^s(t)$, and so the E-pulse technique is a better conditioned algorithm. Further noise reduction capabilities can be introduced by using basis functions that individually span T_e (such as Fourier cosines) and/or weighting functions that individually span the late-time of the convolution, involving even more of the measured data in each matrix element. However, choosing basis functions which are not subsectional complicates the search for zeroes of the E-pulse spectrum, since (10) can no longer be used.

One last distinction between Prony's method and the E-pulse techniques is the manner in which the E-pulse duration T_e is selected. Whereas in Prony's method T_e is determined solely by the sampling interval (so that discrete convolution may be performed), in the E-pulse technique T_e is linked directly to the natural frequencies contained in the measured response.

When minimizing with respect to the natural frequencies, the duration of the E-pulse convolved with the data is chosen to be the smallest allowed by (12). Note that this is given by

$$(T_e)_{\min} = 2N \frac{\pi}{\omega_h} \tag{16}$$

where ω_h is the largest value of ω present among the natural frequencies in the response. This choice results in the largest amount of the late-time convolved response used in minimizing $c^2(t)$. As the frequencies change during the minimization process the duration will change as well, but it is always related through (16).

When minimizing with respect to the basis function amplitudes, the E-pulse duration is allowed to be a free variable. However, at each step the basis function amplitudes represent an E-pulse which eliminates a certain set of natural frequencies, and the duration is tied to those frequencies via (12).

In employing the moment method, the E-pulse duration is the only free parameter. When a zero of the determinantal equation is located, it will again be tied to the natural frequencies eliminated by the E-pulse through (12). As before, it is prudent to search for the smallest value of T_e which satisfies the determinantal equation since this results in the longest late-time portion of the convolution.

As a last note, the E-pulse technique as a whole should not be considered just a generalization of Prony's method. For instance, the minimization with respect to natural frequencies approach completely avoids the second step in Prony's method—solving a polynomial equation for the natural frequencies (which itself can be an ill-conditioned problem). In the moment method approach a different choice of basis functions requires finding not the roots of a polynomial, but those of a sum of different functions altogether.

V. Examples

As a simple numerical example, Fig. 2 shows the theoretical impulse response of a thin cylinder oriented at 30° with respect to the incident field, constructed using the first eight natural frequencies of the cylinder [11]. An attempt will be made to extract these frequencies from the response using the E-pulse techniques.

To simulate a practical situation, this waveform is sampled at 500 points. The convolution indicated in (2) is then carried out by interpolating linearly between sampled points, and analytically integrating the product of the linear curve and the mathematical representation of the basis functions from (8). To keep the integrals simple, rectangular pulse basis functions are used throughout.

The minimization schemes utilize standard Newton's method and thus require initial guesses. For minimization with respect to the complex frequencies, initial guesses for σ_n and ω_n are required. These can often be obtained from the Fourier spectrum of $E^s(t)$ via the fast Fourier transform (FFT). For minimization with respect to the basis function amplitudes,

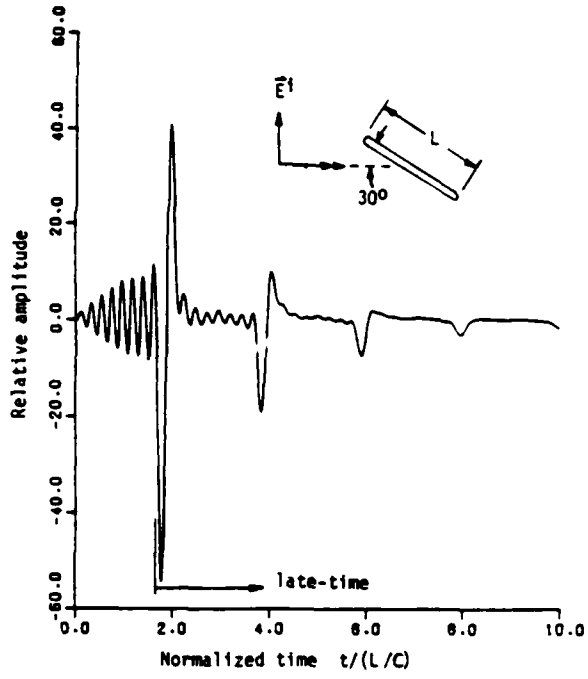

Fig. 2.

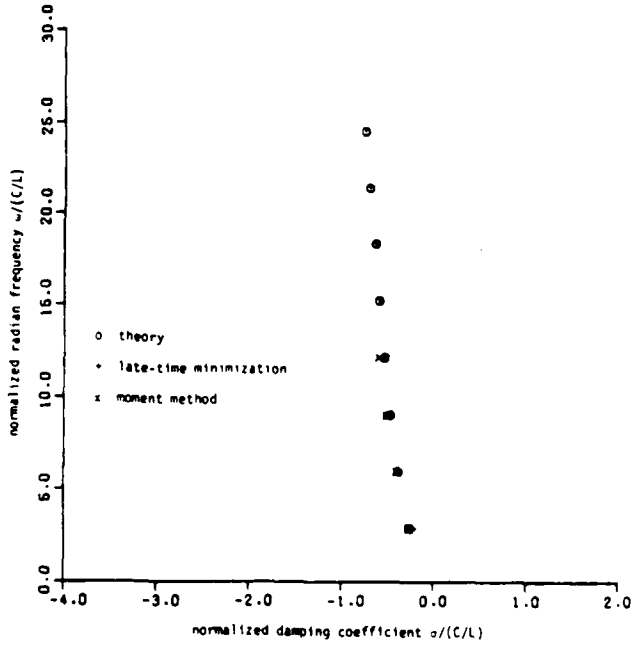

Fig. 3.

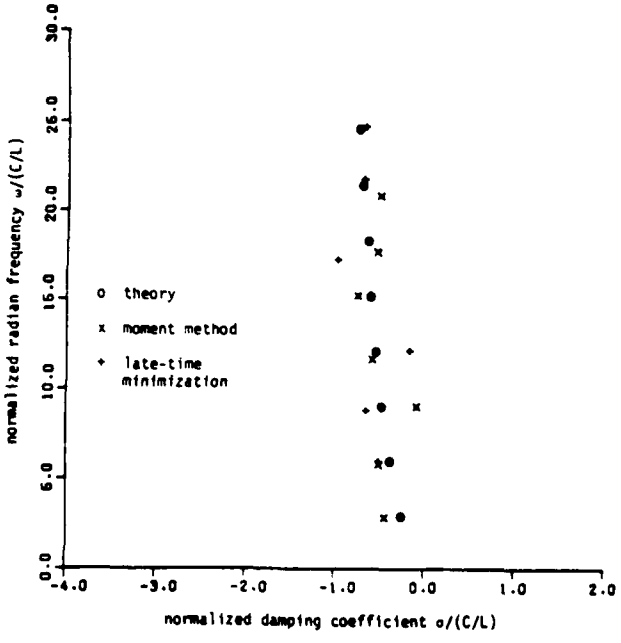

Fig. 4.

initial guesses are required for α_k. Anticipating these values is difficult, since intuition is lacking. However, a good guess for the amplitudes can be obtained by constructing at the first step an E-pulse based on guesses for σ_n and ω_n.

The number of basis functions chosen in the E-pulse expansion reflects the number of modes expected—two functions for each mode. If a dc component is present in $E^s(t)$ as an artifact of the measurement system, it can be effectively eliminated by utilizing an additional basis function [9].

To demonstrate the insensitivity of the E-pulse techniques to the number of modes assumed present in $E^s(t)$, an attempt will be made to extract four of the eight frequencies used to construct Fig. 2. Fig. 3 shows the results of using the moment method with impulse weighting functions, and minimization with respect to the complex frequencies. Obviously, the first four modes have been extracted with very good precision, even though the number of modes present has been drastically underestimated.

To demonstrate the insensitivity of the E-pulse techniques to the presence of random noise, an attempt will be made to extract the frequencies from a noisy version Fig. 2. The amplitude of the added noise is chosen to be 10 percent of the maximum value of the waveform. Fig. 4 shows the results of using the same moment method and minimization approaches, and the results are seen to be quite adequate. Note that the values of ω_n obtained are usually much better than the values of σ_n. As a direct comparison, [8, fig. 3(d)] shows the natural frequencies extracted from the noisy response using Prony's method. It is apparent that utilizing the E-pulse concept provides a decrease in the noise sensitivity of the extracted natural frequencies.

As a more practical example, Fig. 5 shows the measured surface current response of a thin cylinder to a nanosecond pulse excitation field (see [1] for a detailed description of the experiment). The measurement system has sampled this response at a total of 240 points. Fig. 6 shows the results of extracting the five dominant natural frequencies using minimization with respect to the complex frequencies. Rectangular pulse basis functions have been used again, and sampled point convolution performed as described above. The comparison of the extracted frequencies to those given by theory is excellent.

As a second practical example, Fig. 7 shows the measured late-time scattered field response of a thin wire circular loop to a nanosecond pulse excitation field. The measurement system has sampled this waveform at 1024 points. Fig. 8 shows the result of using minimization with respect to the complex frequencies to extract the six dominant natural frequencies. Also shown in Fig. 8 are the theoretical values calculated using a Fourier series type solution [13]. Again, the frequen-

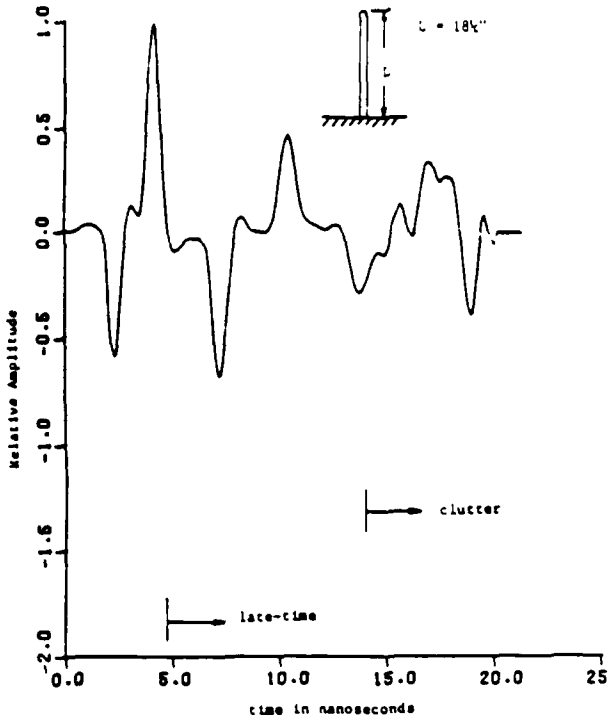

Fig. 5.

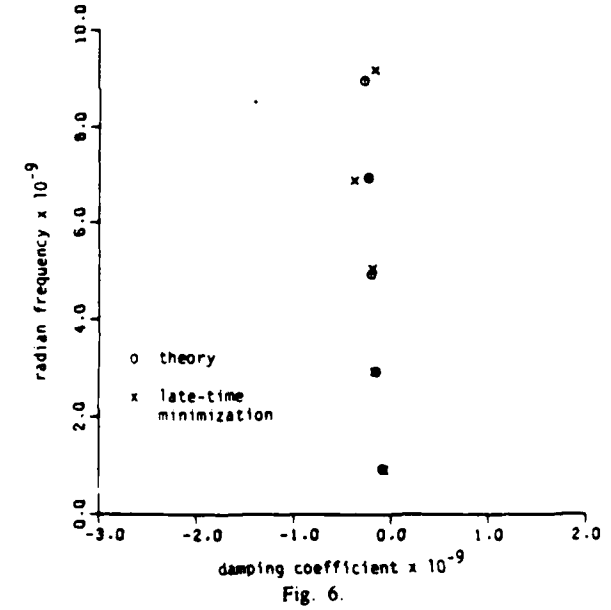

Fig. 6.

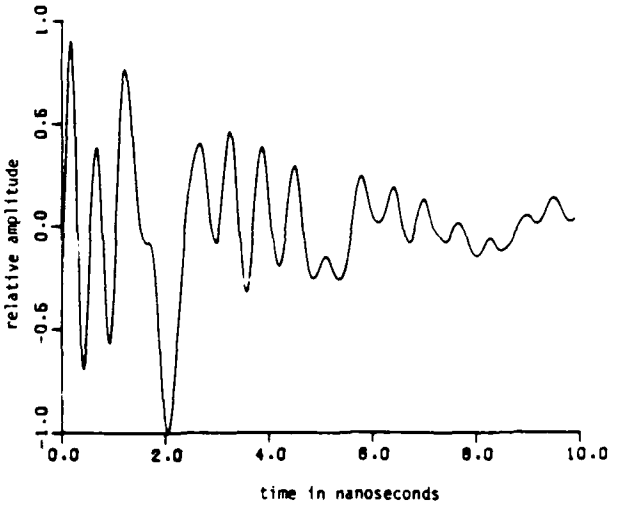

Fig. 7.

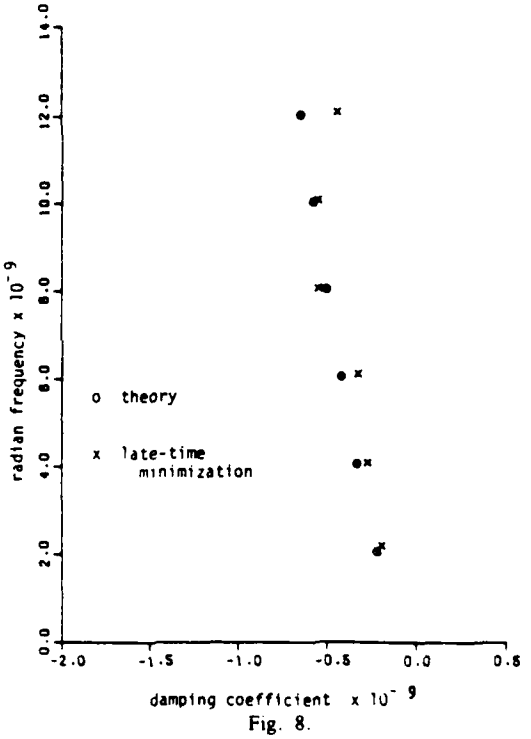

Fig. 8.

cies extracted from the measured waveform compare quite well with the theoretical values.

Lastly, it is important to demonstrate that the E-pulse technique will work successfully for low-Q type targets. In [1, fig. 11] the measured nanosecond pulse scattered field response of a Boeing 707 aircraft model is shown, sampled at 400 points. Although no theory is available for predicting the natural frequencies of this structure, they have been extracted from the measured response using a nonlinear least squares technique [8]. Fig. 9 shows the six dominant natural frequencies extracted using the least squares approach, and also those extracted using minimization of the late-time convolved response with respect to the complex frequencies (again, using rectangular pulse expansion functions). The agreement between the results obtained by these radically different methods is very good, verifying the usefulness of the E-pulse technique for low-Q structures.

VI. Conclusion

Two new approaches to extracting the natural frequencies of a radar target have been presented. They are based on the E-pulse technique, and have been shown to be relatively insensitive to random noise and to the number of modes assumed present in the measured response. They have also been shown to work in practical situations, accurately reproducing the expected natural frequencies of a thin cyclinder and a circular loop from measured values of their transient responses. Lastly, the new methods have been used to verify the values of the natural frequencies of a low-Q aircraft model obtained using a different approach.

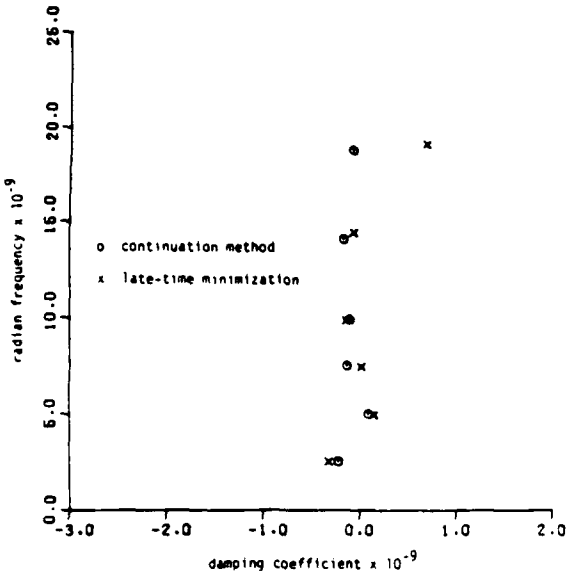

Fig. 9.

REFERENCES

[1] E. J. Rothwell, D. P. Nyquist, K. M. Chen, and B. Drachman, "Radar target discrimination using the extinction-pulse technique," *IEEE Trans. Antennas Propagat.*, vol. AP-33, pp. 929-937, Sept. 1985.

[2] C. Chuang and D. Moffatt, "Natural resonances of radar targets via Prony's method and target discrimination," *IEEE Trans. Aerospace Electron. Syst.*, vol. AES-12, pp. 583-589, Sept. 1976.

[3] A. Berni, "Target identification by natural resonance estimation," *IEEE Trans. Aerospace Electron. Syst.*, vol. AES-11, pp. 147-154, Mar. 1975.

[4] J. Auton *et al.*, "On the practicality of resonance-based identification of scatterers," presented at the IEEE Antennas Propagat. Soc. Symp. Nat. Radio Sci. Meet., Boston, MA, June 1984.

[5] E. Miller, "A study of target identification using electromagnetic poles," Lawrence Livermore Lab., Livermore, CA, Rep. UCRL-52685, 1979.

[6] M. Van Blaricum and R. Mittra, "A technique for extracting the poles and residues of a system directly from its transient response," *IEEE Trans. Antennas Propagat.*, vol. AP-23, pp. 777-781, Nov. 1975.

[7] A. Poggio *et al.*, "Evaluation of a processing technique for transient data," *IEEE Trans. Antennas Propagat.*, vol. AP-26, pp. 165-173, Jan. 1978.

[8] B. Drachman and E. Rothwell, "A continuation method for identification of the natural frequencies of an object using a measured response," *IEEE Trans. Antennas Propagat.*, vol. AP-33, pp. 445-450, Apr. 1985.

[9] E. Rothwell, K. M. Chen, and D. P. Nyquist, "Frequency domain *E*-pulse synthesis and target discrimination," *IEEE Trans. Antennas Propagat.*, vol. AP-35, pp. 426-434, Apr. 1987.

[10] R. F. Harrington, *Field Computation by Moment Methods*. New York: Macmillan, 1968.

[11] K. M. Chen *et al.*, "Radar waveform synthesis for single-mode scattering by a thin cylinder and application for target discrimination," *IEEE Trans. Antennas Propagat.*, vol. AP-30, pp. 867-880, Sept. 1982.

[12] E. Rothwell, "Radar target discrimination using the extinction-pulse technique," Ph.D. dissertation, Michigan State Univ., East Lansing, 1985.

[13] R. F. Blackburn and D. R. Wilton, "Analysis and synthesis of impedance-loaded loop antenna using the singularity expansion method," *IEEE Trans. Antennas Propagat.*, vol. AP-26, pp. 136-140, Jan. 1978.

[14] E. J. Rothwell, K. M. Chen, D. P. Nyquist, N. Gharsallah, and B. Drachman, "Frequency domain E-pulse synthesis and target discrimination," presented at North Am. Radio Sci. Meet. and Int. IEEE Antennas Propagat. Soc. Symp. Vancouver, BC, June 17-21, 1985.

[15] E. J. Rothwell, D. P. Nyquist, K. M. Chen, and W. M. Sun, "Identification of the natural frequencies of a target from a measured response using *E*-pulse techniques," presented at Nat. Radio Sci. Meet., Univ. Colorado, Boulder, Jan. 13-16, 1986.

[16] F. B. Hildebrand, *Introduction to Numerical Analysis*. New York: McGraw-Hill, 1956.

Edward J. Rothwell (S'84-M'85), for a photograph and biography please see page 936 of the September 1985 issue of this TRANSACTIONS.

Kun-Mu Chen (SM'64-F'76), for a photograph and biography please see page 936 of the September 1985 issue of this TRANSACTIONS.

Dennis P. Nyquist (S'63-M'67), for a photograph and biography please see page 936 of the September 1985 issue of this TRANSACTIONS.

Appendix 5

A Hybrid E-Pulse/Least Squares Technique for Natural Resonance Extraction

E. J. ROTHWELL AND K. M. CHEN

A new technique to extract the resonant frequencies of a radar target is presented. The scheme is completely automated, with only the number of natural modes expected and the beginning of late-time as inputs. Results using experimental data demonstrate the insensitivity of the method to random noise, and to estimates of modal content. Further, the technique is computationally efficient, taking only a few minutes to execute on a PC.

I. Introduction

Recent interest in using natural resonances in the discrimination of radar targets has prompted the introduction of several new schemes for extracting natural resonance frequencies from a measured transient response [1]–[5]. None of these has proven completely adequate. A truly useful numerical technique should have the following characteristics: 1) computational efficiency: can run on a microcomputer or work station in a short amount of time; 2) automatic operation: no need for user intervention during long iterative procedures, and no initial guesses required; 3) insensitivity to random noise and to estimates of the number of modes present.

This letter introduces a technique which will address all three requirements. The recently developed *E*-pulse scheme [1] was chosen as a starting point since it has been shown to meet the third provision.

II. Theory

Assume that the late-time measured response of a conducting radar target can be represented as a sum of natural modes

$$m(t) = \sum_{n=1}^{N} a_n e^{\sigma_n t} \cos(\omega_n t + \varphi_n), \qquad T_L < t < T_w \tag{1}$$

where $s_n = \sigma_n + j\omega_n$ is the natural frequency of the nth target mode, a_n and φ_n are the amplitude and phase of the nth mode, T_L describes the beginning of the late-time period, T_w describes the end of the measurement window, and the number of modes in the response, N, is determined by the finite frequency content of the waveform exciting the target.

An E-pulse, $e(t)$, is defined as a waveform of finite duration T_e

Manuscript received August 13, 1987. This work was supported by the Office of Naval Research under Contract N00014-87-K-0336.

The authors are with the Department of Electrical Engineering, Michigan State University, East Lansing, MI 48824, USA.

IEEE Log Number 8717956.

which satisfies [6]

$$c(t) = e(t)^* m(t) = \int_0^{T_e} e(t')\, m(t - t')\, dt' = 0,$$
$$t > T_t + T_e. \tag{2}$$

If this integral equation can be solved for the unknown E-pulse waveform, then the complex natural frequencies contained in $m(t)$ are the solutions $\{s_n\}$ to $E(s) = 0$, where $E(s)$ is the Laplace transform of $e(t)$ [6].

A solution to (2) can be obtained by using the method of moments. Expanding

$$e(t) = \sum_{k=1}^{K} \alpha_k f_k(t) \tag{3}$$

where $\{f_k\}$ is an appropriate set of basis functions, substituting into (2), and taking inner products with a set of weighting functions $\{w_m\}$ gives

$$\sum_{k=1}^{K} \alpha_k \int_{t'=0}^{T_e} \int_{T_t+T_e}^{T_w} f_k(t')\, m(t - t')\, w_m(t)\, dt\, dt' = 0,$$
$$m = 1, 2, 3, \cdots, M. \tag{4}$$

In the standard E-pulse technique, the selection of $M = K = 2N$, resulting in a "natural" E-pulse, makes (4) a homogeneous matrix equation. Solutions for $\{\alpha_k\}$ thus exist only for certain values of T_e which cause the matrix to be singular. An alternative approach is to choose $M = 2N$, $K = 2N + 1$, resulting in a "forced" E-pulse. Then (4) becomes an inhomogeneous matrix equation, with solutions corresponding to any choice of T_e which does not cause the matrix to be singular.

The natural frequencies in $m(t)$ can be found most easily by using subsectional basis functions of width Δ in (3), since $E(s) = 0$ then reduces to the polynomial equation [1]

$$\sum_{k=1}^{K} \alpha_k Z^k = 0 \tag{5}$$

where $Z = \exp(-s\Delta)$.

To maximize computational efficiency, rectangular basis functions are used in (3) while impulse functions are used for weighting (point matching). The integration on t in (4) is then trivial, while the integration on t' is done using the trapezoidal rule.

III. Discussion

In theory, these techniques should work for any choice of T_e. However, there are practical limitations on the range of T_e. It is bounded on the lower end by a time T_0 determined by the sampling interval used to measure $m(t)$, and on the upper end by $T_w - T_t$ from the limits of integration in (4). If natural E-pulses are used, then a solution for T_e might not exist inside this range of limits. Also, extraneous roots are possible, but there is no provision for describing the "quality" of a solution. Similarly, if forced E-pulses are used, either noise, or a poor estimate of N, or approximations used in calculating the integrals in (4), may result in one choice of T_e being "better" than another.

The most computationally efficient approach is to use forced E-pulses along with some method to determine the "best" T_e. An easily implemented scheme is to define the best T_e as that which *minimizes the squared error*

$$\epsilon = \|m(t) - \hat{m}(t)\|^2 = \sum_i [m(t_i) - \hat{m}(t_i)]^2 \tag{6}$$

where $\hat{m}(t)$ is the reconstructed waveform

$$\hat{m}(t) = \sum_{n=1}^{N} \hat{A}_n e^{\hat{\sigma}_n t} \cos(\hat{\omega}_n t + \hat{\varphi}_n) \tag{7}$$

and the sum is over sampled values between T_t and T_w. Here $\{\hat{s}_n = \hat{\sigma}_n + j\hat{\omega}_n\}$ are the solutions to (5), and $\{\hat{A}_n, \hat{\varphi}_n\}$ minimize ϵ with T_e and $\{\hat{s}_n\}$ fixed.

IV. Experimental Results

The pulse response of a thin wire circular loop has been publisned previously [1, fig. 7]. To test the sensitivity of the technique

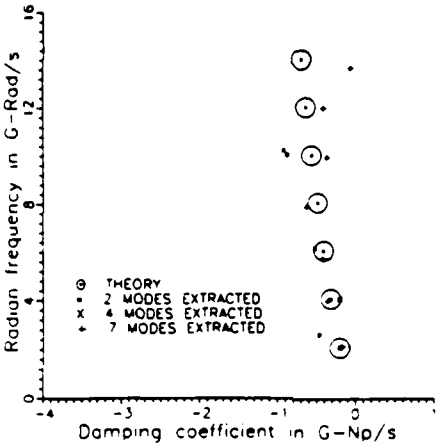

Fig. 1. Resonant frequencies of thin wire circular loop extracted from its transient pulse response, with various numbers of modes assumed present.

to the number of modes assumed present, the natural frequencies of the loop are extracted and compared in Fig. 1 to theory [7] for $N = 2$, 4, and 7. Here $T_t = 3$ and $T_w = 9$ ns have been used. Results are seen to compare quite well even for N as small as 2. Fig. 2 shows ϵ plotted versus T_e for $N = 7$. The global minimum is searched for

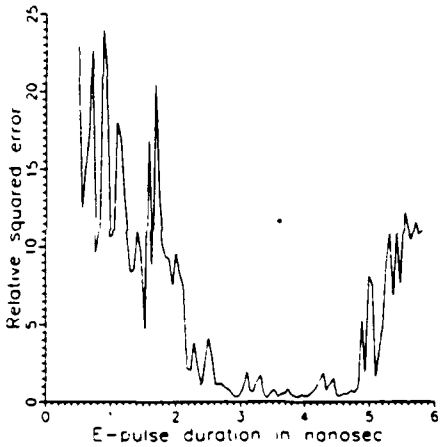

Fig. 2. Squared error versus T_e for circular loop, with seven modes assumed present.

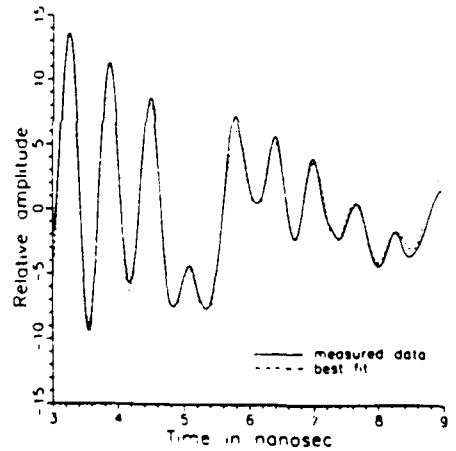

Fig. 3. Best fit waveform constructed from extracted natural frequencies of circular loop, with seven modes assumed present.

automatically between $T_0 = 0.5$ and $T_w - T_L = 6$ ns, and located at $T_e = 3.4$ ns. Note that reasonable results are expected over a fairly wide range of T_e where ϵ is small. The reconstructed waveform (7) is shown in Fig. 3 and is seen to faithfully reproduce the measured data.

To test the sensitivity of the scheme to random noise, the pulse response is contaminated by white Gaussian noise, with zero mean and standard deviation 3, 5, and 10 percent of the waveform maximum (15, 13, and 10 dB *S/N*). The frequencies extracted from the noisy waveform are shown in Fig. 4. Obviously, the presence of even 10 dB of Gaussian white noise has little effect on the results.

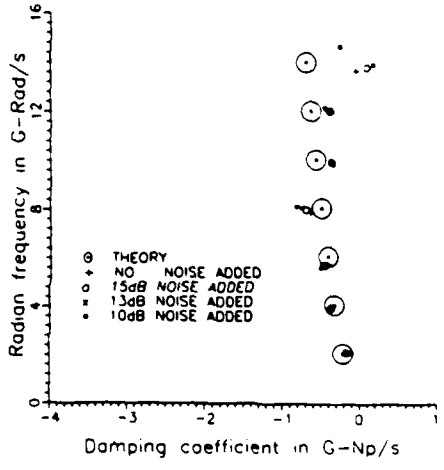

Fig. 4. Resonant frequencies of thin wire circular loop, extracted with various amounts of white Gaussian noise added, and seven modes assumed present.

Extracting seven modes from the above data took about 5 min on an IBM PC-XT microcomputer. Execution time depends on the number of data points used in (4) and (6) (1024 and 150 points, respectively, for the above data) and the number of iterations needed to locate the optimum T_e.

References

[1] E. J. Rothwell, K. M. Chen, and D. P. Nyquist, "Extraction of the natural frequencies of a radar target from a measured response using E-pulse techniques," *IEEE Trans. Antennas Propagat.*, vol. AP-35, pp. 715–720, June 1987.

[2] C. Chuang and D. Moffatt, "Natural resonances of radar targets via Prony's method and target discrimination," *IEEE Trans. Aerosp. Electron. Syst.*, vol. AES-12, pp. 583–589, Sept. 1976.

[3] A. G. Ramm, "Extraction of resonances from transient fields," *IEEE Trans. Antennas Propagat.*, vol. AP-33, pp. 223–226, Feb. 1985.

[4] A. J. Mackay and A. McCowen, "An improved pencil-of-functions method and comparison with traditional methods of pole extraction," *IEEE Trans. Antennas Propagat.*, vol. AP-35, pp. 435–441, Apr. 1987.

[5] B. Drachman and E. Rothwell, "A continuation method for identification of the natural frequencies of an object using a measured response," *IEEE Trans. Antennas Propagat.*, vol. AP-33, pp. 445–450, Apr. 1985.

[6] E. J. Rothwell, K. M. Chen, D. P. Nyquist, and W. Sun, "Frequency domain E-pulse synthesis and target discrimination," *IEEE Trans. Antennas Propagat.*, vol. AP-35, pp. 426–434, Apr. 1987.

[7] E. J. Rothwell and N. Gharsallah, "Determination of the natural frequencies of a thin wire elliptical loop," *IEEE Trans. Antennas Propagat.*, vol. AP-35, pp. 1319–1324, Nov. 1987.

0018-9219/88/0300-0298$01.00 © 1988 IEEE

Appendix 6

Radio Science, Volume 24, Number 3, Pages 369–380, May–June 1989

The natural oscillations of an infinitely long cylinder coated with lossy material

W. M. Sun, K. M. Chen, D. P. Nyquist, and E. J. Rothwell

Department of Electrical Engineering, Michigan State University, East Lansing

(Received August 18, 1988; revised January 30, 1989; accepted February 2, 1989)

Investigations are reported of the effects of lossy coatings on the natural frequencies of a perfectly conducting cylinder with TE excitation. A general characteristic equation for extraction of the natural frequencies of a cylindrical structure is developed. It is found that the natural frequencies are substantially shifted only when the coating thickness is comparable to the radius of the cylinder. When the conductivity of the coating material is high enough, the behavior of the natural modes of a coated cylinder is essentially the same as that of a perfectly conducting cylinder.

INTRODUCTION

The radar cross section of a metallic target can be greatly reduced by coating its surface with a layer of lossy material. When we wish to discriminate such a target with a target discrimination scheme, such as the E pulse technique [Chen et al., 1981, 1986; Rothwell et al., 1985], which is entirely based on the target natural frequencies, it is important to know the effects of lossy coatings on the natural frequencies of the target.

Since 1971, the singularity expansion method (SEM) [Baum, 1975] has been regarded as a powerful method to study the transient electromagnetic scattering from perfect conductors [Tesche, 1973; Marin, 1973]. Only in the last few years, the SEM analysis has been applied to a perfectly conducting thick cylinder [Chuang et al., 1985] and a radially inhomogeneous lossy cylinder [Tijhuis and Van der Weiden, 1986]. But considerably less attention has been devoted to the SEM analysis of a coated, perfectly conducting cylinder. The significance of this analysis is directly related to the available potential effectiveness of the E pulse technique in discrimination of targets coated with lossy material.

An infinitely long conducting cylinder coated with a layer of lossy material and an infinitely long lossy homogeneous cylinder are considered here. The natural modes identified numerically can be classified into "interior" and "exterior" types. The main difference between an exterior mode and an interior mode involves the radial behavior of the scattered field in the lossy region. The field distribution associated with an interior mode behaves as a standing wave in the lossy region, while the field associated with an exterior mode is attenuated into the center of the cylinder.

It is shown that the natural frequencies of exterior modes are substantially shifted on the complex plane only when the coating thickness is comparable with the radius of the cylinder. When the coating material is characterized by parameter $\sigma\eta a > 100$ (where σ is the conductivity, η is the wave impedance of free space and a is the radius of the cylinder), it has little effect on the natural frequencies of the exterior modes. In contrast, the natural frequencies of the interior modes, whose existence is attributed to the imperfect conducting properties of the cylinder or the lossy coating, are greatly dependent on coating thickness and parameters. They are shifted upward on the complex plane when the coating thickness is reduced, and they are shifted leftward when the conductivity is increased. As a rough estimation, the interior modes are no longer dominant when the conductivity satisfies $\sigma\eta a > 100$, or the coating thickness is less than 10% of the radius of the cylinder.

In this paper a generic characteristic equation for extraction of the natural frequencies of a coated cylinder is derived. The pole distributions and the pole trajectories of a number of dominant resonant modes are presented.

DERIVATION OF CHARACTERISTIC EQUATION

Consider a lossy cylinder coated with a lossy layer, with the geometry as shown in Figure 1. A cylindrical coordinate system is chosen with z axis in the axial direction, and the space is naturally divided into three regions.

Since we are interested most in the effect of lossy coatings on the natural frequencies, only natural modes associated with one polarization of electric field are considered. Assume the incident plane wave is cross polarized and strikes the coating

Paper number 89RS00245
0048-6604/89/89RS-00245$08.00

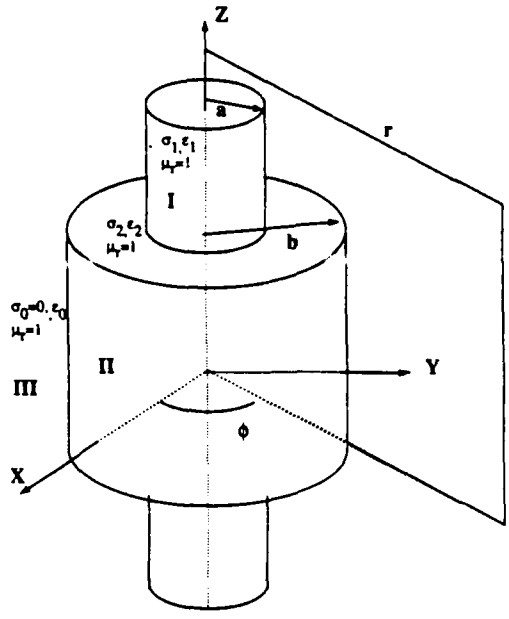

Fig. 1. Geometry of a lossy cylinder coated with a lossy layer.

surface at instant $t = 0$, then the waveform of incident electric field is written as:

$$\mathbf{E}^i(\mathbf{r},t) = \mathbf{y}\, U(t-(x+b)/c)\, F(t-(x+b)/c) \tag{1}$$

where $F(t)$ is the shape function of the incident waveform and $U(t)$ is the step function.

In the Laplace transform domain

$$\mathbf{E}^i(\mathbf{r},s) = \mathbf{y}\, F(s)\, e^{-\gamma_0(x+b)} \tag{2}$$

with $\gamma_0 = s/c$ and $F(s)$ the single-sided Laplace transform of $F(t)$.

In cylindrical coordinates, for TE-polarized excitation, the incident E field is decomposed into r and ϕ components:

$$\mathbf{E}^i(\mathbf{r},s) = \mathbf{r}\, E_r(r,\phi,s) + \boldsymbol{\phi}\, E_\phi(r,\phi,s)\,. \tag{3}$$

The H field has only a z component

$$\mathbf{H}^i(\mathbf{r},s) = \mathbf{z}\, H_z(r,\phi,s)\,. \tag{4}$$

Once the z component of the H field is known, the E field is recovered from

$$E_r = \frac{1}{\varepsilon^* s r}\frac{\partial}{\partial \phi} H_z \tag{5}$$

$$E_\phi = -\frac{1}{\varepsilon^* s}\frac{\partial}{\partial r} H_z \tag{6}$$

where

$$\nabla^2 H_z - \gamma^2 H_z = 0 \tag{7}$$

$$\gamma^2 = s^2 \mu \varepsilon^* \tag{8}$$

$$\varepsilon^* = \varepsilon + \frac{\sigma}{s} \tag{9}$$

The complex wave number γ and complex permittivity ε^* have been introduced.

In order to simplify matching boundary conditions, the incident plane wave fields are represented by infinite cylindrical wave expansions

$$E_\phi^i = -F(s) e^{-\frac{sb}{c}} \sum_{n=0}^{\infty} (-1)^n \varepsilon_n I'_n(\gamma_0 r)\cos(n\phi) \tag{10}$$

$$H_z^i = \frac{F(s)}{(\mu_0/\varepsilon_0)^{1/2}} e^{-\frac{sb}{c}} \sum_{n=0}^{\infty} (-1)^n \zeta_n I_n(\gamma_0 r)\cos(n\phi) \tag{11}$$

where the standard cylindrical wave expansion

$$e^{z\cos\theta} = I_0(z) + 2\sum_{k=1}^{\infty} I_k(z)\cos(k\theta) \tag{12}$$

has been used, where $I_n(s)$ denotes the first kind modified Bessel function, and Neumann's number is

$$\zeta_n = 1 \qquad n = 0$$

$$\zeta_n = 2 \qquad n > 0$$

The scattered fields in the several regions are expressed using the following cylindrical harmonic expansions:

Within region 3,

$$H_z^s = -\sum_{n=0}^{\infty} a_n(s)\, K_n(\gamma_0 r)\cos(n\phi) \tag{13}$$

$$E_\phi^s = \sqrt{\mu_0/\varepsilon_0} \sum_{n=0}^{\infty} a_n(s)\, K'_n(\gamma_0 r)\cos(n\phi) \tag{14}$$

where $K_n(s)$ is the second kind modified Bessel function.

Within region 2,

$$H_z^s = -\sum_{n=0}^{\infty} [b_n(s) I_n(\gamma_2 r)\cos(n\phi) + c_n(s) K_n(\gamma_2 r)\cos(n\phi)] \tag{15}$$

$$E_\phi^s = \frac{\gamma_2}{\varepsilon_2^* s} \sum_{n=0}^{\infty} [b_n(s) I'_n(\gamma_2 r)\cos(n\phi) + c_n(s) K'_n(\gamma_2 r)\cos(n\phi)] \tag{16}$$

Within region 1,

$$H_z^s = -\sum_{n=0}^{\infty} d_n(s)\, I_n(\gamma_1 r)\cos(n\phi) \tag{17}$$

$$E_\phi^s = \frac{\gamma_1}{\varepsilon_1^* s} \sum_{n=0}^{\infty} d_n(s)\, I'_n(\gamma_1 r)\cos(n\phi) \tag{18}$$

Here the complex wave numbers and complex permittivities are defined as

$$\varepsilon_2^* = \varepsilon_2 + \sigma_2/s \tag{19}$$

$$\gamma_2 = \sqrt{s^2\mu\varepsilon_2 + \mu\sigma_2 s} \tag{20}$$

$$\varepsilon_1^* = \varepsilon_1 + \sigma_1/s \tag{21}$$

$$\gamma_1 = \sqrt{s^2\mu\varepsilon_1 + \mu\sigma_1 s} \tag{22}$$

Four independent boundary conditions on the two interfaces require that

$$H_z^s(r = a^-) = H_z^s(r = a^+) \tag{23}$$

$$E_\phi^s(r = a^-) = E_\phi^s(r = a^+) \tag{24}$$

$$H_z^s(r = b^-) = H_z^s(r = b^+) + H_z^i(r = b^+) \tag{25}$$

$$E_\phi^s(r = b^-) = E_\phi^s(r = b^+) + E_\phi^i(r = b^+) \tag{26}$$

From equations (10)-(26), four simultaneous equations for the unknowns $a_n(s), b_n(s), c_n(s)$ and $d_n(s)$ are obtained by enforcing boundary conditions and using the orthogonality of the functions { $\cos(n\phi)$, n=0,1,2, ... }. The matrix form of these equations is

$$\begin{bmatrix} K_n(\gamma_0 b) & -I_n(\gamma_2 b) & -K_n(\gamma_2 b) & 0 \\ \sqrt{\mu_0/\varepsilon_0}K'_n(\gamma_0 b) & -\frac{\gamma_2}{\varepsilon_2 s}I'_n(\gamma_2 b) & -\frac{\gamma_2}{\varepsilon_2 s}K'_n(\gamma_2 b) & 0 \\ 0 & I_n(\gamma_2 a) & K_n(\gamma_2 a) & -I_n(\gamma_1 a) \\ 0 & \frac{\gamma_2}{\varepsilon_2 s}I'_n(\gamma_2 a) & \frac{\gamma_2}{\varepsilon_2 s}K'_n(\gamma_2 a) & -\frac{\gamma_1}{\varepsilon_1 s}I'_n(\gamma_1 a) \end{bmatrix}$$

$$\cdot \begin{bmatrix} a_n(s) \\ b_n(s) \\ c_n(s) \\ d_n(s) \end{bmatrix} = \begin{bmatrix} \frac{F(s)}{(\mu_0/\varepsilon_0)^{1/2}} e^{-\frac{sb}{c}} (-1)^n \varepsilon_n I'_n(\gamma_0 b) \\ F(s) e^{-\frac{sb}{c}} (-1)^n \varepsilon_n I_n(\gamma_0 b) \\ 0 \\ 0 \end{bmatrix} \tag{27}$$

The natural modes are contributed by s plane poles of $a_n(s), b_n(s), c_n(s)$ and $d_n(s)$ at points where $F(s)$ is regular. Natural frequencies consequently satisfy the determinantal equation:

$$\det \begin{bmatrix} K_n(\gamma_0 b) & -I_n(\gamma_2 b) & -K_n(\gamma_2 b) & 0 \\ \sqrt{\mu_0/\varepsilon_0}K'_n(\gamma_0 b) & -\frac{\gamma_2}{\varepsilon_2 s}I'_n(\gamma_2 b) & -\frac{\gamma_2}{\varepsilon_2 s}K'_n(\gamma_2 b) & 0 \\ 0 & I_n(\gamma_2 a) & K_n(\gamma_2 a) & -I_n(\gamma_1 a) \\ 0 & \frac{\gamma_2}{\varepsilon_2 s}I'_n(\gamma_2 a) & \frac{\gamma_2}{\varepsilon_2 s}K'_n(\gamma_2 a) & -\frac{\gamma_1}{\varepsilon_1 s}I'_n(\gamma_1 a) \end{bmatrix} = 0 \tag{28}$$

The expansion of the determinant leads to the general characteristic equation:

$$\begin{aligned} &[I_n(\gamma_2 b)\sqrt{\mu_0/\varepsilon_0}K'_n(\gamma_0 b) - \frac{\gamma_2}{\varepsilon_2 s}K_n(\gamma_0 b)I'_n(\gamma_2 b)] \\ &\cdot [I_n(\gamma_1 a)\frac{\gamma_2}{\varepsilon_2 s}K'_n(\gamma_2 a) - I'_n(\gamma_1 a)\frac{\gamma_1}{\varepsilon_1 s}K_n(\gamma_2 a)] \\ &-[\sqrt{\mu_0/\varepsilon_0}K'_n(\gamma_0 b)K_n(\gamma_2 b) - \frac{\gamma_2}{\varepsilon_2 s}K_n(\gamma_0 b)K'_n(\gamma_2 b)] \\ &\cdot [\frac{\gamma_2}{\varepsilon_2 s}I_n(\gamma_1 a)I'_n(\gamma_2 a) - \frac{\gamma_1}{\varepsilon_1 s}I_n(\gamma_2 a)I'_n(\gamma_1 a)] = 0 \end{aligned} \tag{29}$$

This equation characterizes a lossy cylinder coated with a lossy layer in free space. Some simplified expressions for special cases can be deduced by the selection of a specific parameter set.

Perfectly conducting infinite cylinder in free space

Letting $a = b$, $\sigma_1 = \sigma_2$ and $\sigma_1, \sigma_2 \to \infty$, the generic characteristic equation (29) gives rise to a very simple form:

$$K'_n(\gamma_0 a) = 0 \tag{30}$$

Infinitely long lossy cylinder in free space

Letting $a = b$, and $\sigma_1 = \sigma_2 \neq 0$, an equation characterizing a lossy cylinder is obtained by specialization of (29):

$$I_n(\gamma_2 a)\sqrt{\mu_0/\varepsilon_0}K'_n(\gamma_0 a) - \frac{\gamma_2}{\varepsilon_2 s}K_n(\gamma_0 a)I'_n(\gamma_2 a) = 0 \tag{31}$$

Perfectly conducting infinite cylinder coated with lossy material

Letting $a \neq b$, $\sigma_2 \neq 0$, and $\sigma_1 \to \infty$, the characteristic equation for this most interesting case is obtained:

$$\begin{aligned} &\frac{\gamma_2}{\varepsilon_2 s}K_n(\gamma_0 b)\,[-K'_n(\gamma_2 a)I'_n(\gamma_2 b) + I'_n(\gamma_2 a)K'_n(\gamma_2 b)\,] \\ &+\sqrt{\mu_0/\varepsilon_0}K'_n(\gamma_0 b)[K'_n(\gamma_2 a)I_n(\gamma_2 b) - I'_n(\gamma_2 a)K_n(\gamma_2 b)] = 0 \end{aligned} \tag{32}$$

NUMERICAL ALGORITHM

The root search for (32) has to be numerical owing to its complexity and nonlinearity. Special consideration is devoted in this section to the selection of the relevant branch cut, evaluation of Bessel fuctions with complex arguments, selection of a pole location algorithm, and numerical consistency checking.

The occurrence of the complex permittivity in parameters within the arguments of modified Bessel functions leads to branch points in the complex s plane. An examination of the complex wave number γ_2 suggests the existence of branch

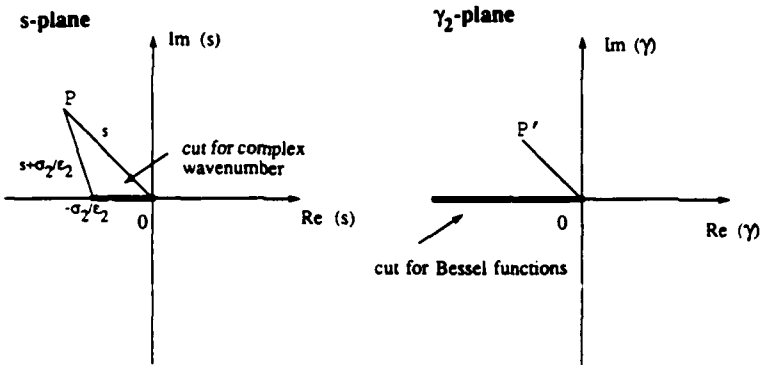

Fig. 2. The appropriate branch cuts for the complex wave number and Bessel functions.

points at $s = 0$ and $s = -\sigma_2/\varepsilon_2$. The associated branch cut extends from the origin to the point $s = -\sigma_2/\varepsilon_2$ along the negative real axis in the s plane [Giri and Tesche, 1981]. However, an appropriate branch cut for the modified Bessel function with a complex argument lies along the entire negative real axis in the γ_2 plane [Abramowitz and Stegun, 1972]. Figure 2 shows the mapping of the s plane to the γ_2 plane. As long as the point P does not move across the negative real axis beyond the point of $s = -\sigma_2/\varepsilon_2$ in the s plane, its image P' will not cross the negative real axis in the γ_2 plane. Thus the negative real axis in the s plane is selected as the branch cut, which is appropriate for evaluation of Bessel functions. By referring to Abramowitz and Stegun [1972], integer order Bessel functions are regular in the s plane cut along the negative real axis; this branch cut is also appropriate for the entire characteristic equation (32). The integration contour for the inverse Laplace transform will be closed on the principal Reimann sheet; consequently only poles residing on the first sheet are implicated. Since the conjugate symmetry of (32) gives rise to conjugate symmetry of the poles, the poles have to be located only within the second quadrant without crossing the cut.

An easy way to compute the modified Bessel functions with complex arguments is to represent them by their integral representations [Abramowitz and Stegun, 1972; Drachman and Chuang, 1981]. Since the numerical integration can be efficient and accurate, the calculation of the Bessel functions can be similarly accurate. An associated advantage with this approach is its capability of using a normalization procedure involved in the pole location. If an exponential function with a rather large argument needs to be computed, arithmetic overflows are easily encountered. The Bessel functions with complex arguments behave asymptotically as exponential functions when the argument is large. An investigation of the effects of lossy media parameters, varying over a considerably large range, upon the location of natural mode poles is impossible unless a prenormalization is attempted.

The prenormalization is performed by multiplying an exponential function into the pole-searched equation. The multiplied factor to the characteristic equation does not give rise to new extra poles, while the integral evaluation of the Bessel functions modulated by an exponential function is reduced computationally within arithmetic bounds.

The natural frequencies are identified by searching for the roots of a characteristic equation. The approximate location of the zeros is determined by using an algorithm which relates the argument change of an analytic function integrated along a closed contour to the number of the zeros and poles of the function within the contour [Singaraju et al., 1976]. When there are only zeros in the searched region, the algorithm can be mathematically described by

$$\frac{1}{2\pi i}\int_C s^m F'(s)/F(s)\,ds = \sum_n (s_n)^m \qquad (33)$$

where $F(s)$ is the function searched for zeros, C is the integration contour and s_n is the nth zero of the function $F(s)$ inside C.

After the approximate zeros are determined, they are improved in accuracy by calling the subroutine C05PBF, which is based on Powell's method, from the Library of the Numerical Algorithms Group (NAG). In the trajectory of a pole, Newton's method can even be applied as long as the variation rate of the parameters is slow enough.

Because of the numerical complexity of the characteristic equations, the numerical consistency has to be validated before any comprehensive root search is initiated. One easy numerical test is made by coating an air layer on a perfectly conducting cylinder. Evidently this coated cylinder is exactly the same as a perfectly conducting cylinder. As we expect, the poles located numerically for the air-coated cylinder are distributed precisely on the locations where the poles of a perfectly conducting cylinder are supposed to lie.

Another test involves varying the conductivity of the coating layer on a perfectly conducting cylinder from a finite

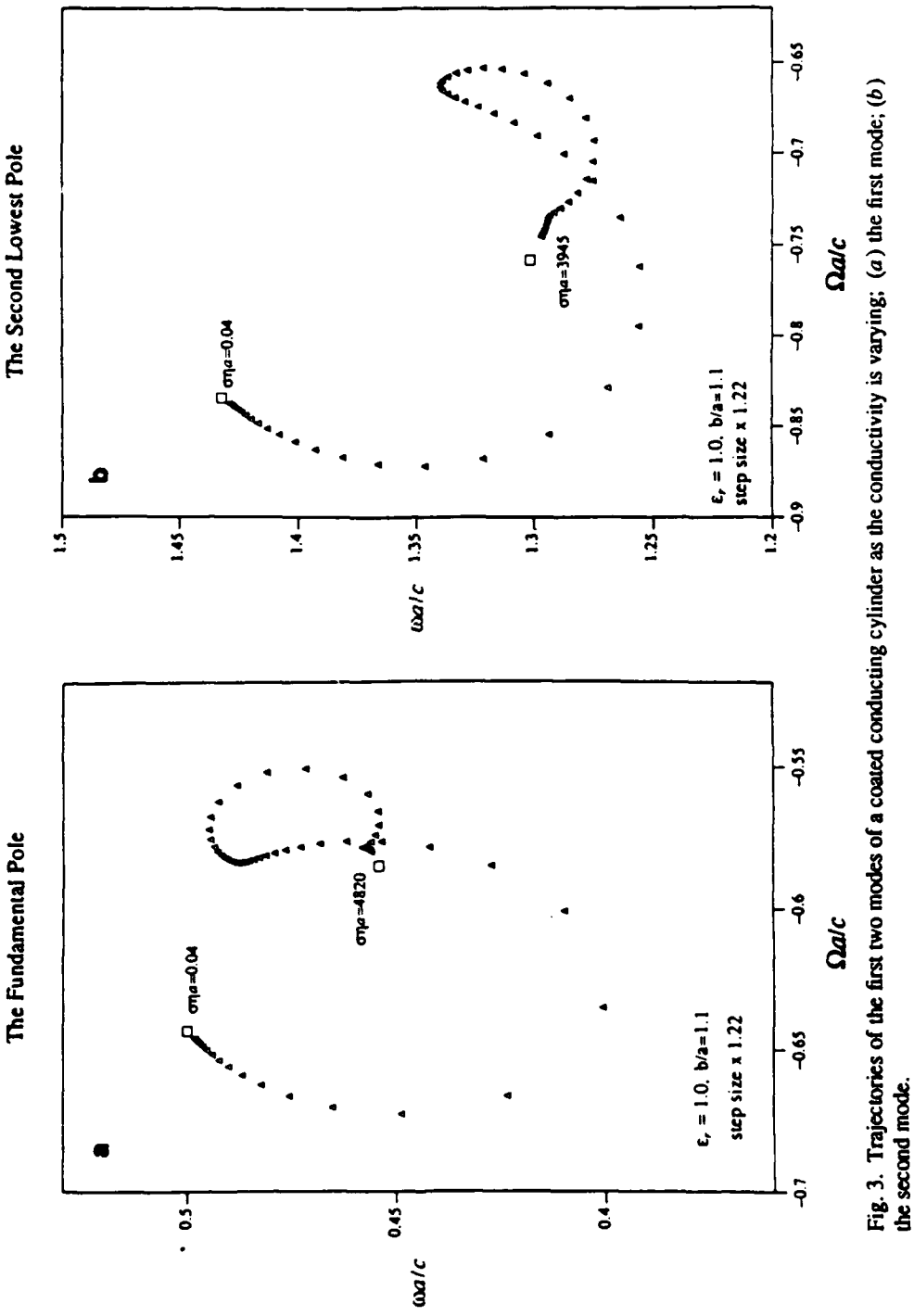

Fig. 3. Trajectories of the first two modes of a coated conducting cylinder as the conductivity is varying; (*a*) the first mode; (*b*) the second mode.

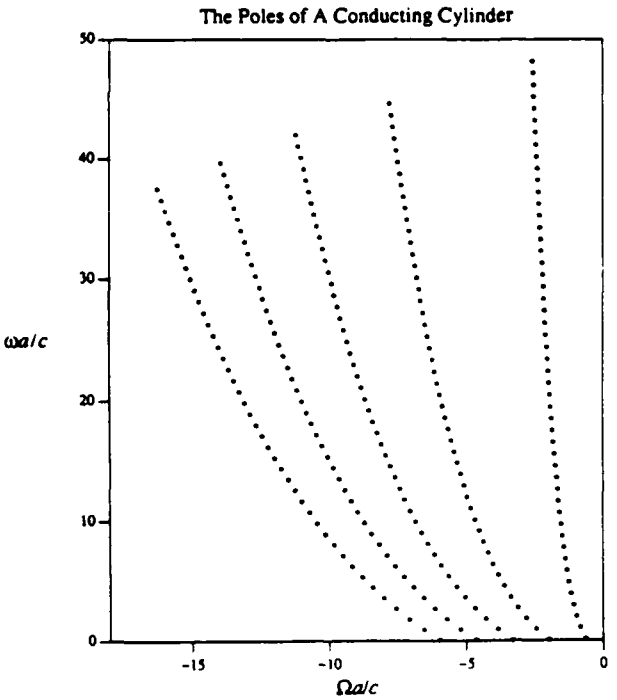

Fig. 4. The pole distribution of a perfectly conducting cylinder.

number to infinity. Physically, as the conductivity is increased to very large values, the coated cylinder approaches a good conducting cylinder with radius b. Figure 3a shows the trajectory of the first mode of a coated conducting cylinder with conductivity varying from a small to a quite large value. The conductivity is increased by a factor of 1.22 in each step. The upper square gives the location of the first mode of the perfectly conducting cylinder with radius a, and the lower square shows the position of the first mode of a perfectly conducting cylinder with radius b. It is observed that as the conductivity is enhanced, the pole is shifted toward the location of a thicker perfectly conducting cylinder. The looping phenomenon in Figure 3 reflects the fact that when the conductivity of the coated layer is gradually increased, the three-layer structure undergoes a transition to a two-layer structure, and the natural frequencies are not expected to shift along a simple trajectory. The test on the second mode is shown in Figure 3b.

NUMERICAL RESULTS OF THE POLE DISTRIBUTION

Based on the algorithm discussed above, the zeros of the characteristic equations (30)-(32) are located with a variety of parameter sets.

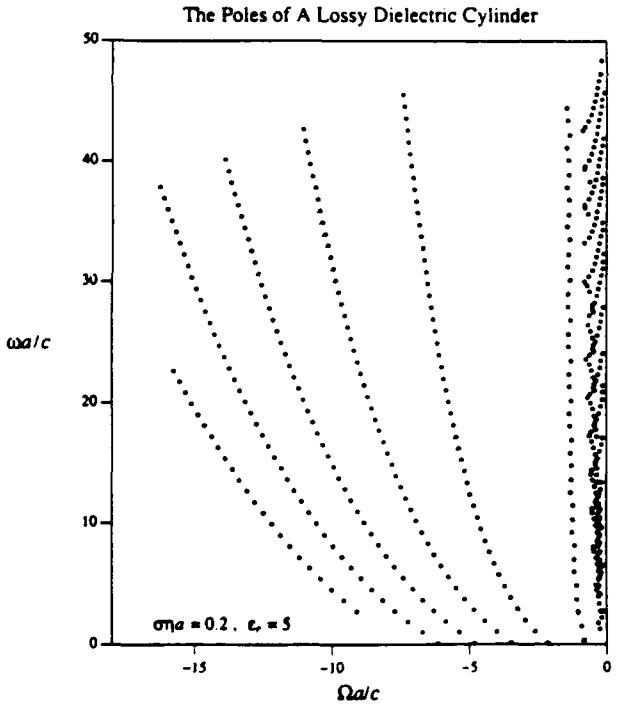

Fig. 5 . The pole distribution of a lossy dielectric cylinder (σ conductivity, ε_r relative permittivity, η wave impedance and a the radius of the cylinder), with $\sigma\eta a = 0.2$ and $\varepsilon_r = 5$.

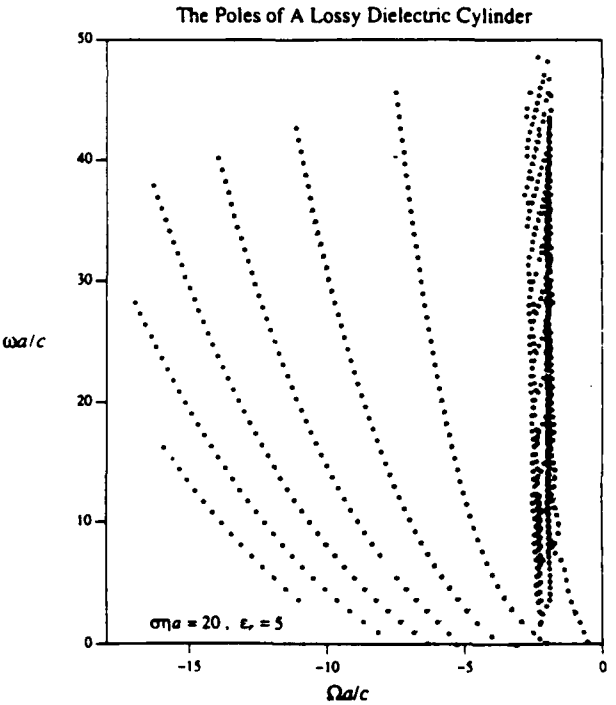

Fig. 6. The pole distribution of a lossy dielectric cylinder (σ conductivity, ε_r relative permittivity, η wave impedance and a the radius of the cylinder), with $\sigma\eta a = 20$ and $\varepsilon_r = 5$.

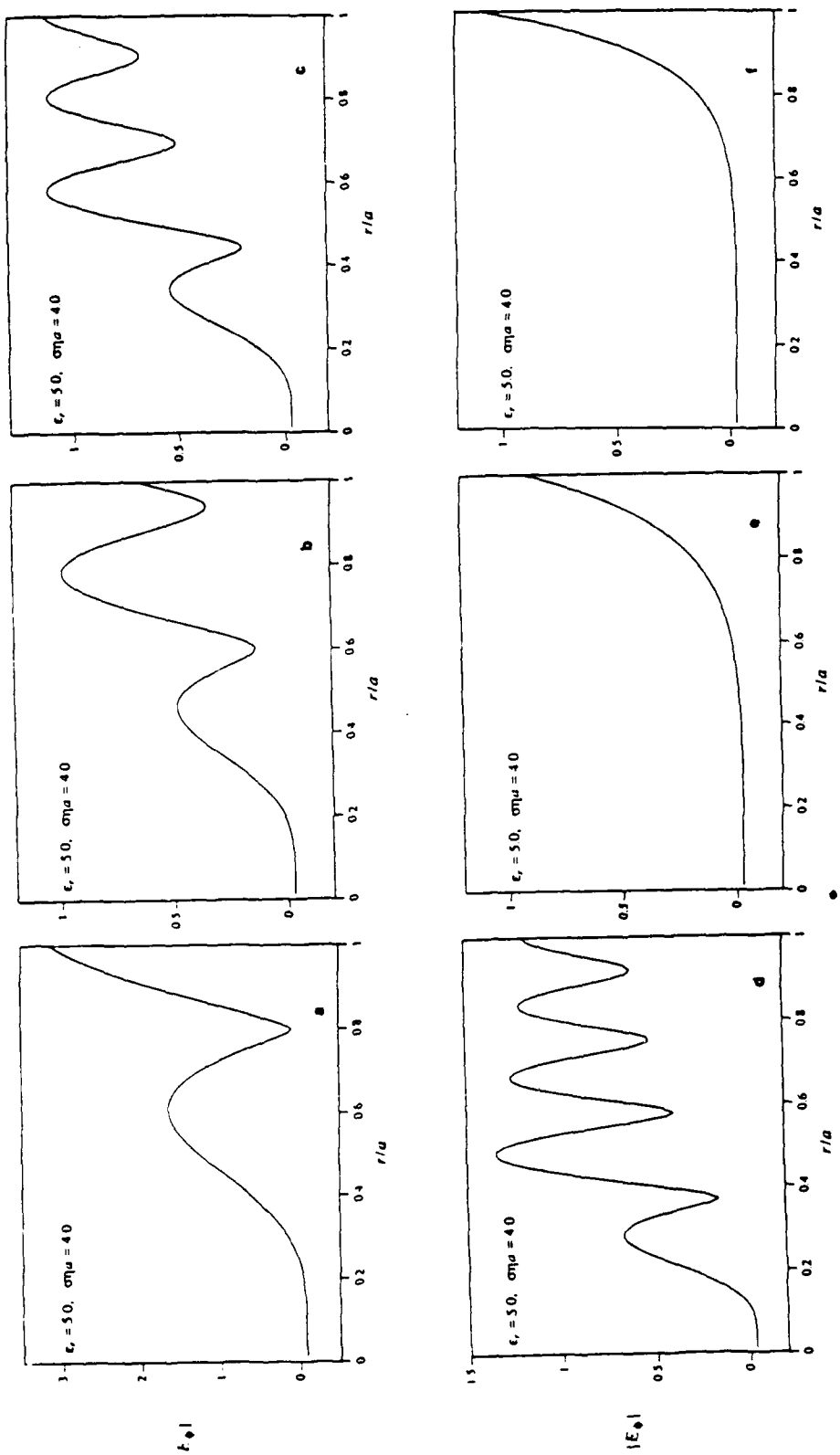

Fig. 7. The radial amplitude dependence of the ϕ component of the E field. Figure 7*a*-7*d* give the interior modes; Figure 7*e* and 7*f* give the exterior modes.

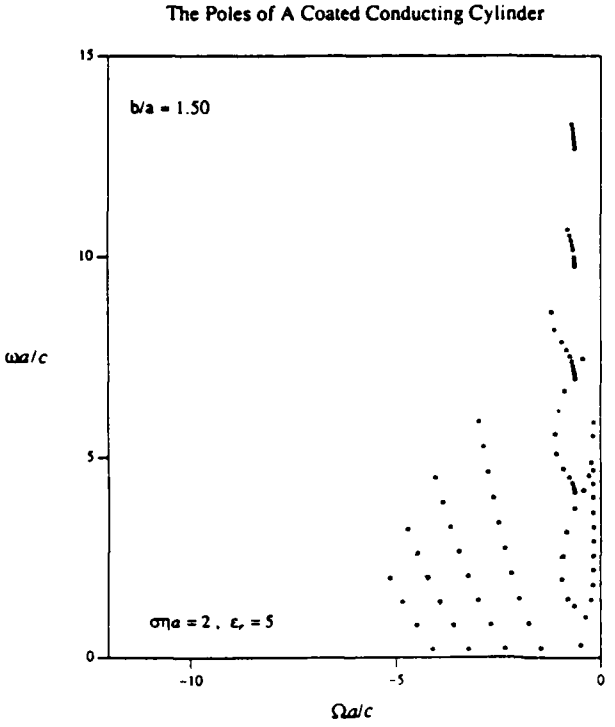

Fig. 8. The pole distribution of a coated perfectly conducting cylinder (σ conductivity, ε_r relative permittivity, η wave impedance and a the radius of the cylinder), with $b/a = 1.5$, $\sigma\eta a = 2$, and $\varepsilon_r = 5$.

The zeros of (30) are exactly the natural mode poles of a perfectly conducting cylinder. It is well known that the poles of a perfectly conducting cylinder are positioned in layers. Figure 4 shows the first 250 dominant poles. Later, these poles serve as a reference for the study of more complicated geometries.

The pole locations for a lossy cylinder are quite different. Figure 5 presents a typical pole distribution with a normal lossy parameter set. The dotted lines are drawn to show the positions where the poles of a perfectly conducting cylinder are located and to serve as the reference locations. It is seen that some poles are distributed in layers close to dotted lines, but some poles lying in arcs are close to the imaginary axis. We call those poles, close to the imaginary axis, interior modes, while we call those in layers exterior modes. Further study reveals that the fields of an exterior mode inside the cylinder attenuate radially from the cylinder surface to the center and the fields of an interior mode inside the cylinder behave radially as a standing wave. The physical insight to this difference is that the energy losses of an exterior mode are mainly attributed to the radiation of the surface current. In contrast, the energy losses of an interior mode are mainly attributed to the power loss inside the cylinder. This difference exists also in the case of a coated perfectly conducting cylinder.

Figure 6 shows the poles of a lossy cylinder with rather different parameters; compared to Figure 5 the normalized conductivity is changed from 0.2 to 20. The exterior modes have not been affected very much, but the interior modes are shifted significantly in the negative direction. Physically, the interior modes have increased power loss inside the cylinder with a higher conductivity.

Figure 7 illustrates the radial amplitude dependence of the ϕ component of the E field. The angular variation order is chosen as $n = 6$. The amplitudes of four interior modes and two exterior modes of the E field are plotted. The standing wave behavior of interior modes and the attenuation behavior of exterior modes are very clearly observed.

Figure 8 indicates the pole distribution of a coated perfectly conducting cylinder with a coating thickness equal to 50% of its radius. The dotted lines are still drawn here to serve as a reference. It is observed that the exterior modes are in layers, and interior modes are in arcs and close to the imaginary axis.

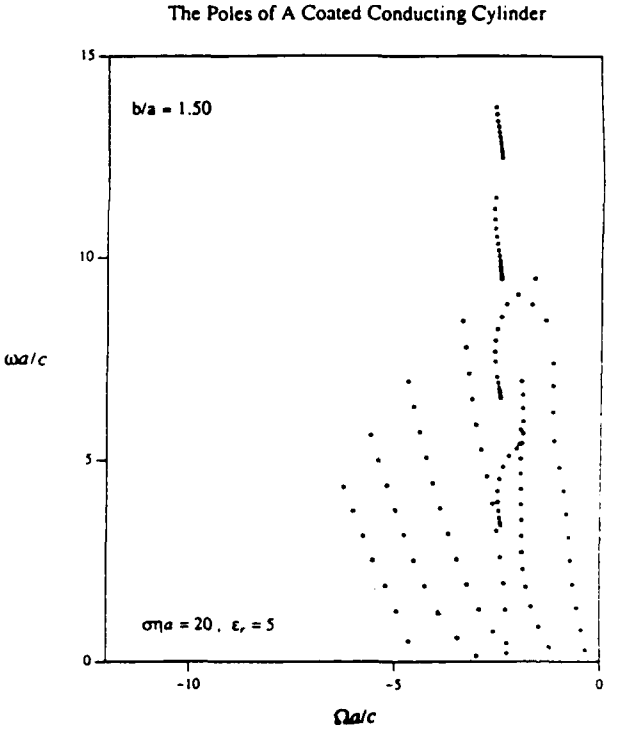

Fig. 9. The pole distribution of a coated perfectly conducting cylinder (σ conductivity, ε_r relative permittivity, η wave impedance and a the radius of the cylinder), with $b/a = 1.5$, $\sigma\eta a = 20$, and $\varepsilon_r = 5$.

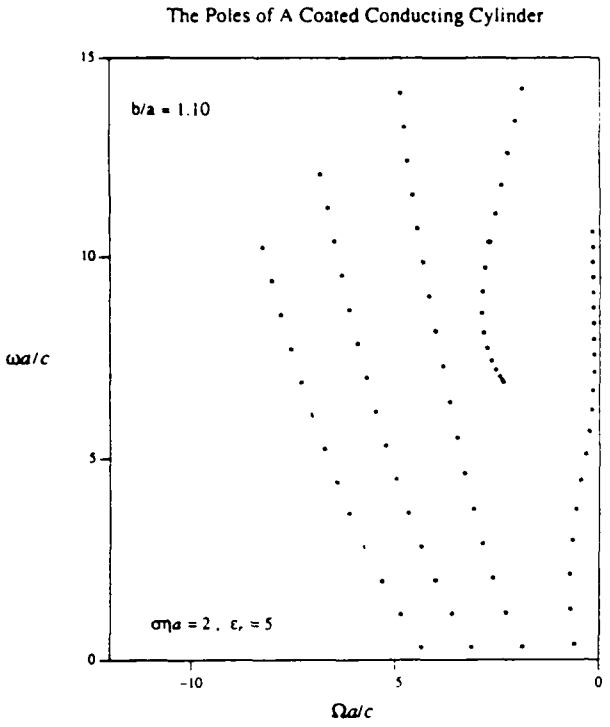

Fig. 10. The pole distribution of a coated perfectly conducting cylinder (σ conductivity, ε_r relative permittivity, η wave impedance and a the radius of the cylinder), with $b/a = 1.1$, $\sigma\eta a = 2$, and $\varepsilon_r = 5$.

Now examine the effects if the coating thickness is kept the same, but the normalized conductivity is changed. The result is shown in Figure 9. The interior modes are all shifted leftward. The exterior modes are dominant now, since they are lower in radian frequencies and smaller in damping coefficient. If the coating thickness is changed instead of the conductivity, the effect of the coating thickness on the interior modes is shown in Figure 10. The first arc of interior modes is moved far upward when the coating thickness is dropped to 10% of the radius. Once again the exterior modes are seen to be dominant.

Similar to a lossy cylinder in free space, a coated perfectly conducting cylinder has interior modes too. Their fields behave as standing waves in the cladding region. Figure 11 shows the amplitude of the ϕ component of the E field inside the cladding region. The angular order is selected with $n = 8$. Four interior modes and two exterior modes are illustrated. The differences of the field distributions inside the coating layer between the exterior modes and the interior modes are apparent. Furthermore it is seen that the E field amplitude of an exterior mode inside the coating layer is relatively very small. That is why the exterior mode is substantially affected only when the coating thickness is comparable to the radius.

EFFECTS OF LOSSY PARAMETERS ON AN EXTERIOR MODE

Since a perfectly conducting scatterer has only exterior modes and the normally coating layer used is not very thick, it is only necessary to investigate the effects of lossy parameters on the exterior modes. Extensive pole trajectories have been pursued by varying the lossy media parameters. Only a few examples are presented.

Figure 12 shows the trajectories of the second mode. The pole is traced as the coating thickness is increased with a step size of 0.04 starting from $b/a = 1$. The trajectories with four sets of parameters are shown here. The circle line, which presents an infinite conductivity in the coating layer, serves as the reference line to indicate the location of the second pole of a perfectly conducting cylinder with radius b. As the coating thickness is increased, the outer radius b of the layer is increased and the circle line locates the pole of a perfectly conducting cylinder which is increasing in radius. The star line corresponds to a normalized conductivity 80. After a few steps, the star line comes close to the perfectly conducting cylinder line, and in additional steps the triangle line, which corresponds to a conductivity of 15, follows. The last one to move toward reference is the square line with conductivity of 5. Figure 12 is interpreted as indicating that when the conductivity is greater, the pole of a coated cylinder behaves more like that of a perfectly conducting cylinder, and when the coating is thicker, the pole of a coated cylinder behaves more like that of a perfectly conducting cylinder.

Figure 13 presents the first pole traced by varying the permittivity. The pole is traced as the coating thickness is increased with a step size of 0.04 starting from $b/a = 1$. Three trajectories for three different parameter sets are given. It is seen that when the coating thickness is small the poles with different permittivities are located close to each other; however when the coating is thick, they are relatively separated.

CONCLUSION

The pole distribution of a coated cylinder structure has been investigated in this paper. Special attention has been directed to the effects of the lossy coatings on the dominant natural modes. It has been shown that the natural frequencies of exterior modes are substantially shifted on the complex plane only when the coating thickness is comparable with the radius of the cylinder. When the coating material has a parameter of $\sigma\eta a > 100$, it has little effect on the natural frequencies of the exterior modes. The natural frequencies of the interior modes are greatly dependent on coating thickness and parameters. As a rough estimation, the interior modes are no longer dom-

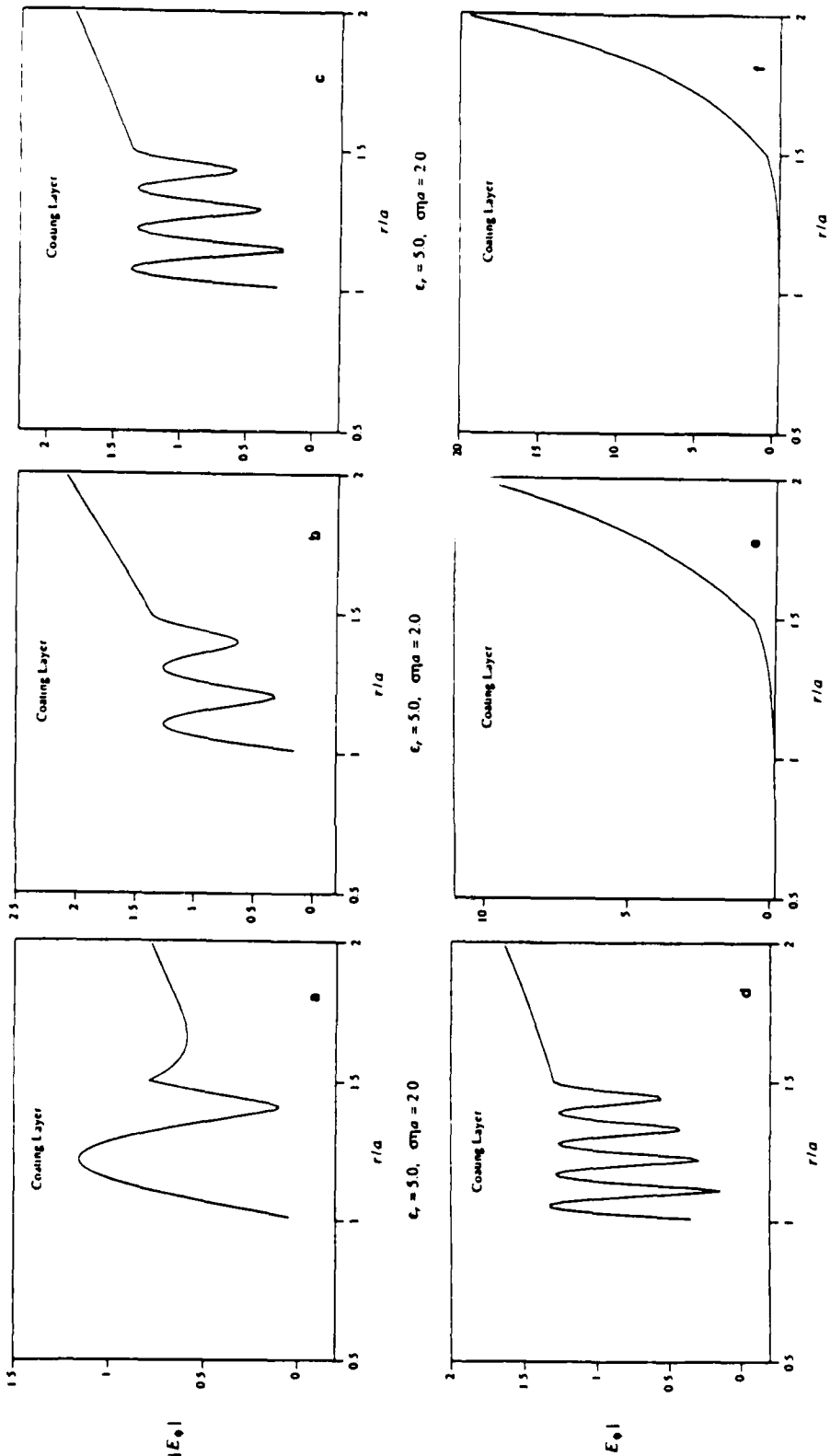

Fig. 11. The radial amplitude dependence of the ϕ component of the E field inside the cladding region. Figure 11*a*-11*d* give the interior modes; Figure 11*e* and 11*f* give the exterior modes.

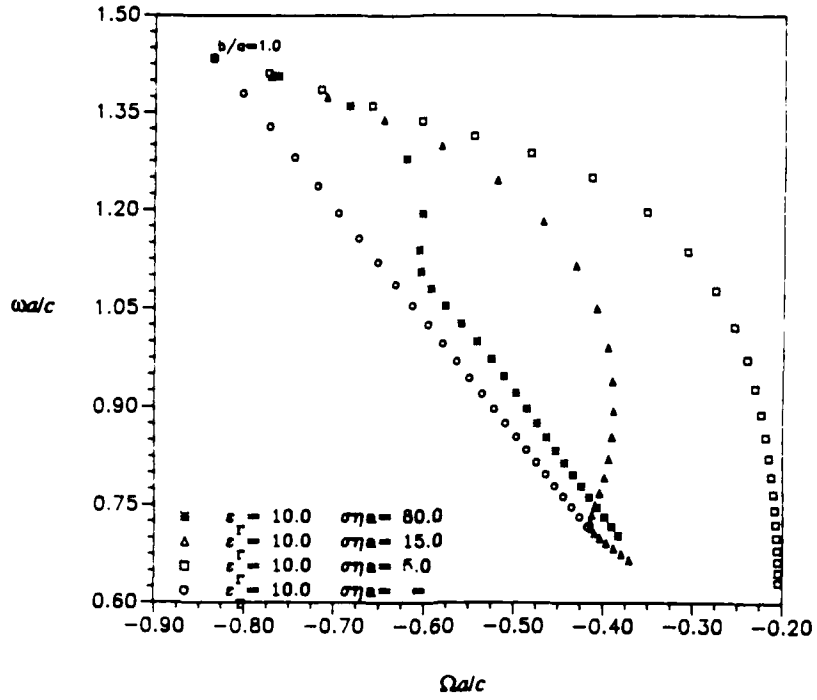

Fig. 12. Trajectories of the second exterior mode of a coated perfectly conducting cylinder as the coating thickness is varying.

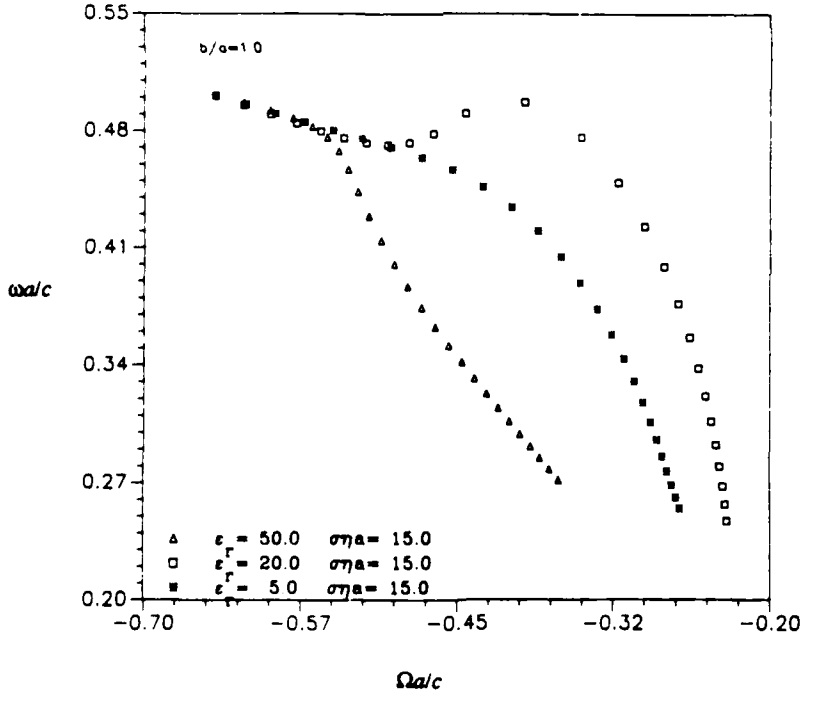

Fig. 13. Trajectories of the first exterior mode of a coated perfectly conducting cylinder as the coating thickness is varying.

inant when the conductivity satisfies $\sigma\eta a > 100$, or the coating thickness is less than 10% of the cylinder radius.

Acknowledgments. The work reported in this paper was supported by the Defence Advanced Research Project Agency and the Office of Naval Research under Contract N000-14-87-K-0336.

REFERENCES

Abr itz, M. and I. A. Stegun Eds., *Handbook of Mu atical Functions*, p. 374, Dover, New York, 1972.

Baur E., The singularity expansion method, in *Transient El omagnetic Fields*, edited by L. B. Felsen, pp. 130-176, Springer-Verlag, New York, 1975.

Chen, K. M., Radar waveform synthesis method -- A new radar detection scheme, *IEEE Trans. Antennas Propag., AP-29*, 553-566, 1981.

Chen, K. M., D. P. Nyquist, E. J. Rothwell, L. L. Webb, and B. Drachman, Radar target discrimination by convolution of radar returns with extinction-pulses and single-mode extraction signals, *IEEE Trans. Antennas Propag., AP-34*, 896-904, 1986.

Chuang, C. I., D. P. Nyquist, K. M. Chen, and B. C. Drachman, Singularity expansion method formulation for impulse response of a perfectly conducting thick cylinder, *Radio Sci.*, 20, 1025-1030, 1985.

Drachman, B. and C. I. Chuang, A table of two hundred zeros of the derivative of the modified Bessel function $K_n(z)$ and a graph of their distribution, *J. Comput. Appl. Math.*, 7, 167-171, 1981.

Giri, D. V. and F. M. Tesche, On the use of singularity expansion method for analysis of antennas in conducting media, *Electromagnetics*, 1, 455-471, 1981.

Marin, L., Natural-mode representation of transient scattered fields, *IEEE Trans. Antennas Propag., AP-21*, 809-818, 1973.

Rothwell, E. J., D. P. Nyquist, K. M. Chen, and B. Drachman, Radar target discrimination using the extinction-pulse technique, *IEEE Trans. Antennas Propag., AP-33*, 929-937, 1985.

Singaraju, B. K., D. V. Giri, and C. E. Baum, Further developments in the application of contour integration to evaluation of the zeros of analytic functions and relevant computer programs, *Math. Notes 42, AFWL*, 1976.

Tesche, F. M., On the analysis of scattering and antenna problems using the singularity expansion technique, *IEEE Trans. Antennas Propag., AP-21*, 53-62, 1973.

Tijhuis, A. G., and R. M. Van der Weiden, SEM approach to tramsient scattering by a lossy, radially inhomogeneous dielectric circular cylinder, *Wave Motion*, 8, 43-63, 1986.

W. M. Sun, K. M. Chen, D. P. Nyquist, and E. J. Rothwell, Department of Electrical Engineering, Michigan State University, East Lansing, MI 48824.

Appendix 7

Identification of the Natural Resonance Frequencies of a Conducting Sphere from a Measured Transient Response

NEILA GHARSALLAH, STUDENT MEMBER, IEEE,
EDWARD J. ROTHWELL, MEMBER, IEEE, KUN-MU CHEN,
FELLOW, IEEE, AND DENNIS P. NYQUIST, MEMBER, IEEE

Abstract—**The natural resonance frequencies of a conducting sphere are determined experimentally by using measured transient scattered field and surface charge responses. Comparison to theory is shown to be excellent for the imaginary parts of the complex frequencies.**

I. Introduction

The complex natural resonance frequencies of conducting radar targets form a useful set of aspect independent features, and have been employed recently in various radar target discrimination schemes [1], [2]. For geometrically complex targets these frequencies must be determined experimentally, from measurements of the targets' transient responses. It has been found that the natural frequencies of low-Q scatterers (those having relatively small late-time energy) are the most difficult to extract from measurement. By showing that the resonant frequencies of a sphere, a particularly low-Q structure, can be obtained accurately from experimental data, the plausibility of target classification using natural frequencies is enhanced greatly.

II. Theory

The late-time (unforced) transient response of a conducting sphere of radius a can be written as a series of natural oscillation modes

$$r(t) = \sum_{n=1}^{N} a_n e^{\sigma_n t} \cos(\omega_n t + \phi_n) \quad t > T_L \tag{1}$$

Manuscript received August 5, 1987; revised September 2, 1988. This work was supported by the Office of Naval Research under Contract N00014-87-K-0336.

The authors are with the Department of Electrical Engineering, Michigan State University, East Lansing, MI 48824.

IEEE Log Number 8929465.

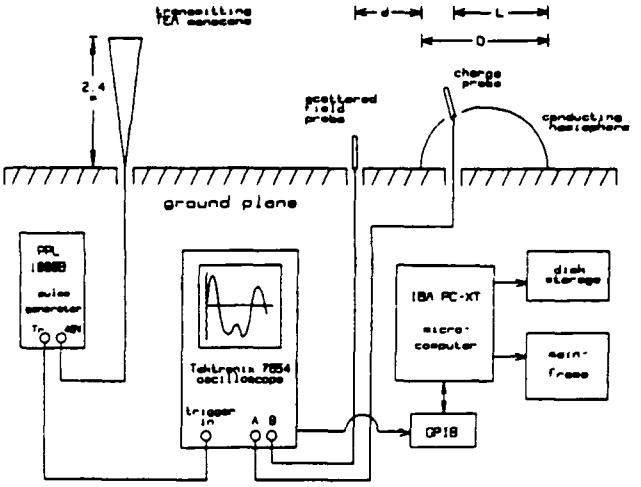

Fig. 1. Experimental facility used to measure transient scattered field and surface current responses of conducting sphere.

where $r(t)$ represents a measured quantity, such as the surface charge or scattered field response. Here T_L is the beginning of the late-time period, $s_n = \sigma_n + j\omega_n$ is the aspect and excitation independent natural frequency of the nth mode, a_n and ϕ_n are the aspect and excitation dependent amplitude and phase of the nth mode, and N is the number of modes excited by the incident illumination.

The natural frequencies of the sphere present in the measured response (1) can be calculated theoretically by using a frequency domain approach. If $R(s)$ represents the Laplace transform of $r(t)$, then

$$R(s) = F(s)H(s) \tag{2}$$

where $F(s)$ depends on the measurement and excitation systems, and $H(s)$ is the transfer function of the sphere [3]

$$H(s) = \sum_{n=1}^{\infty} \frac{(2n+1)\zeta^{2n}}{f_n(\zeta) g_n(\zeta)} \tag{3}$$

where

$$f_n(\zeta) = \sum_{\beta=0}^{n} \frac{(n+\beta)!}{\beta!(n-\beta)!} \frac{1}{2^\beta} \zeta^{n-\beta} \tag{4}$$

$$g_n(\zeta) = \sum_{\beta=0}^{n} \frac{(n+\beta)!}{\beta!(n-\beta)!} \frac{1}{2^\beta} (\beta+\zeta) \zeta^{n-\beta} \tag{5}$$

and $\zeta = (a/c)s$, with c the speed of light.

Since the natural frequencies are the poles of the transfer function, they can be calculated by locating the zeros of $f_n(\zeta)$ and $g_n(\zeta)$. Numerical values have been computed and are tabulated in [4]. It is found that the natural frequencies of the sphere are arranged along branches in the left half of the complex frequency plane. The frequencies of the first branch have the smallest real parts, and thus produce the most prominent resonances. These are the ones most easily distinguished in a measured response.

III. Experimental Set-Up

The transient electromagnetic response of the sphere is measured using the experimental facility shown in Fig. 1. Target excitation is provided by an incident electromagnetic wave radiated by a monocone

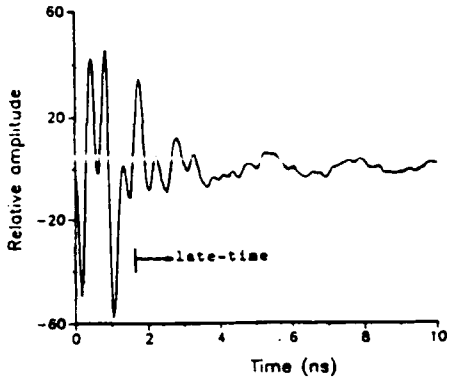

Fig. 2. Measured scattered field response of 30 cm diameter conducting sphere.

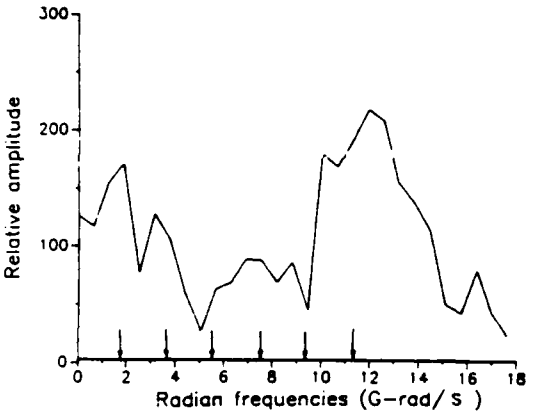

Fig. 3. Fourier spectrum of late-time portion of scattered field response of 30 cm diameter conducting sphere. Arrows indicate imaginary parts of theoretical natural frequencies.

antenna suspended over a conducting ground screen. The antenna has an axial height of 2.4 m, a polar angle of 8°, and a characteristic impedance of 160Ω. It radiates a spherical transverse electromagnetic (TEM) wave which approximates a plane wave polarized perpendicular to the ground screen at the position of the conducting hemisphere target. The ground screen consists of nine individual 4 × 8 ft aluminum sheathed modules, and has overall dimensions of 16 × 20 ft. This provides a window of approximately 14 ns in which to perform measurements, before reflections from the edges of the ground screen and the top of the antenna return.

The monocone antenna is driven by a Picosecond Pulse Labs model 1000B-01 pulse generator, providing quasi-rectangular pulses of duration 0.5 ns and amplitude 40 V. Both the resulting transient surface charge and scattered field pulse responses of the imaged sphere are measured, using short monopole probes coupled to a *Tektronix* 7854 waveform processing oscilloscope via S2 sampling heads (75 ps rise-time). Proper timing is accomplished using the variable trigger delay internal to the pulse generator.

Typically, 100 waveform measurements are taken and averaged in real time, using a pulse repetition rate of up to 1000 kHz. These measurements are then smoothed to reduce high frequency noise, and the dc level is removed. An additional measurement is obtained for the scattered field without the hemisphere present, and this clutter waveform is subtracted from the measured scattered field response. The resulting waveforms are then transfered via a general-purpose-interface-bus to an IBM PC microcomputer, where they are stored on floppy disk and later transmitted to a mainframe computer for further processing.

IV. Experimental Results

The measured scattered field response of a 30 cm diameter sphere is shown in Fig. 2. The monopole receiving probes are modeled as perfect differentiators, and thus Fig. 2 represents the derivative of the pulse response of the sphere. Since differentiation does not perturb the values of the natural frequencies contained in the scattered field response, no attempt is made to recover the pulse response via integration.

It is important that the beginning of the late-time period, during which the sphere oscillates in its natural modes, is carefully determined. Physically, the surface current in the early-time period should not exhibit resonance behavior because the induced surface current has not yet traversed the entire body. Resonance phenomena are determined by the global characteristics of the target, not by a fractional structure or local feature.

Michalski [6] has presented a theoretical study suggesting that the surface current response of a conducting target can be represented at all times purely in a set of its natural resonance modes (i.e., it has no early-time period). However, this representation is based on an *a priori* knowledge of the geometry of the scatterer (i.e., the early-time component is constructed based on the complete geometry of the target). However, in the "inverse" case, where natural frequencies are to be obtained based on an incomplete time history, it is contrary to physical reasoning to expect that the natural frequencies of a target can be retrieved from the early-time surface current response. For example, how can the early-time surface current response of a thin wire be interpreted as a pure set of its natural modes, when the early-time portion of the response of a shorter wire must be identical, but is comprised of an entirely different set of modes? It is not until the reflection from the end of the wire returns to the observation point that the responses will differ (and thus determine the beginning of the late-time period). *Obviously, it is impossible* to extract two different sets of natural frequencies from the same data, unless the additional knowledge of the complete geometry of the scatterer is available. Thus, it is assumed here that the late-time period begins only after the global characteristics of the target have been determined.

Although it may be possible to include the early-time component in the extraction process, it is now apparent that to use only this portion would be a disaster. To be safe, only the late-time portion is used here. At worst, this choice may be slightly conservative.

The first event recorded by the system occurs when the incident pulse interacts with the receiving probe. The late-time period (during which the sphere oscillates freely) begins a time $T_P + 2(d + D)/c$ later, where T_P is the duration of the pulse. By adjusting the time position control on the oscilloscope, most of the early-time period has been shifted out of the measurement window, resulting in a longer measured portion of the late-time period. Fig. 3 shows the spectrum of the late-time portion of the scattered field response, obtained via the fast Fourier transform (FFT). Arrows indicate the theoretical values of the imaginary parts of the first branch natural frequencies, obtained by solving for the roots of (4) and (5). It is seen that peaks in the Fourier spectrum correspond quite closely with predicted values.

Fig. 4 shows the measured surface charge response of the sphere. Here the late-time period begins a time $T_P + 2L/c$ after the first recorded event. Again, most of the early-time portion of the response has been shifted out of the measurement window. Fig. 5 shows the Fourier spectrum of the late-time portion of the surface charge response. Again, peaks in the spectrum correspond closely to the frequencies predicted.

Examining the Fourier spectra gives only a cursory estimate of the complex frequencies contained in the measured waveforms. More accurate techniques have been developed to extract the natural frequencies directly from the measured data. Fig. 6 shows the imaginary parts of the first six complex frequencies obtained from the late-time

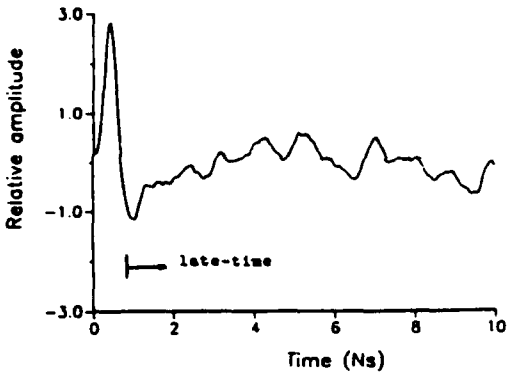

Fig. 4. Measured surface charge response of 30 cm diameter conducting sphere.

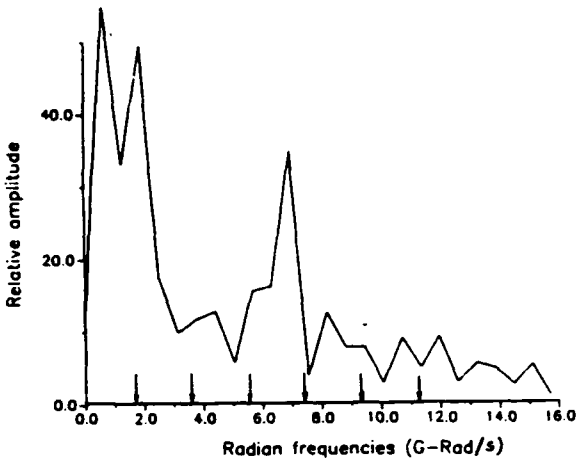

Fig. 5. Fourier spectrum of late-time portion of surface charge response of 30 cm diameter conducting sphere. Arrows indicate imaginary parts of theoretical natural frequencies.

portions of the measured waveforms using an E-pulse technique [5]. Agreement with theory is seen to be excellent. The results from the charge response are slightly better than those from the scattered field response, probably due to the more favorable S/N level.

The real parts of the first six natural frequencies were also extracted, but did not compare as well with theory. This is consistent with results obtained using high-Q targets—the real parts are rarely extracted with as great an accuracy as the imaginary parts.

V. Conclusion

It has been shown that the imaginary parts of the first six natural resonant frequencies of a spherical scatterer can be determined quite accurately from measurements of both its surface charge and scattered field responses. This is an important step in verifying the practicality of characterizing low-Q targets by means of their resonance frequencies. Results for the real parts of the natural frequencies are not highly accurate. However, these values do not need to be known with great precision, since radar target discrimination schemes can be geared to use information primarily from the imaginary parts.

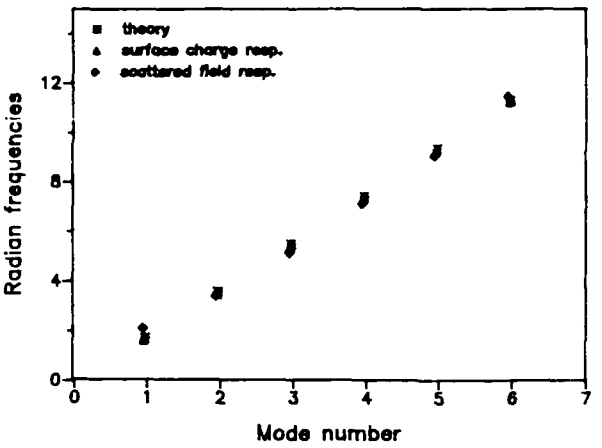

Fig. 6. Imaginary parts of natural frequencies of 30 cm conducting sphere extracted from measured surface charge and scattered field responses.

A recent theoretical study by Weyker and Dudley [7] on the identification of resonances of an acoustically rigid sphere painted a more pessimistic picture for the accurate extraction of resonance poles from a scattered response. The more optimistic results obtained here from experimental data are probably due to a more accurate pole extraction scheme, relative high signal-to-noise levels, and the presence of only the first few dominant modes (because of the finite bandwidth of the excitation pulse). It is important to note that target identification does not depend on the extraction of resonant frequencies in real time under adverse noise conditions. Rather, the resonance frequencies of the targets are assumed *a priori* knowledge, determined in a controlled, low-noise laboratory environment [1].

References

[1] E. J. Rothwell, K. M. Chen, D. P. Nyquist, and W. Sun, "Frequency domain E-pulse synthesis and target discrimination," *IEEE Trans. Antennas Propagat.*, vol. AP-35, no. 4, pp. 426–434, Apr. 1987.

[2] C. W. Chuang and D. L. Moffatt, "Natural resonances of radar targets via Prony's method and target discrimination," *IEEE Trans. Aerospace Electron. Syst.*, vol. AES-12, no. 5, pp. 583–589, Sept. 1976.

[3] K. M. Chen and D. Westmoreland, "Radar waveform synthesis for exciting single-mode backscatters from a sphere and application for target discrimination," *Radio Sci.*, vol. 17, no. 3, pp. 574–588, May-June 1982.

[4] K. M. Chen and D. Westmoreland, "Impulse response of a conducting sphere based on singularity expansion method," *Proc. IEEE*, vol. 69, no. 6, pp. 747–750, June 1981.

[5] E. J. Rothwell, K. M. Chen, and D. P. Nyquist, "Extraction of the natural frequencies of a radar target from a measured response using E-pulse techniques," *IEEE Trans. Antennas Propagat.*, vol. AP-35, no. 6, pp. 715–720, June 1987.

[6] K. A. Michalski, "On the class 1 coupling coefficient performance in the SEM expansion for the current density on a scattering object," *Electromagn.*, vol. 2, pp. 201–209, 1982.

[7] R. Weyker and D. G. Dudley, "Identification of resonances of an acoustically rigid sphere," *IEEE J. Oceanic Eng.*, vol. OE-12, pp. 317–326, Apr. 1987.

IEEE TRANSACTIONS ON ANTENNAS AND PROPAGATION, VOL. 38, NO. 5, MAY 1990

Determination of the Natural Modes for a Rectangular Plate

WEIMIN SUN, STUDENT MEMBER, IEEE, KUN-MU CHEN, FELLOW, IEEE,
DENNIS P. NYQUIST, MEMBER, IEEE, AND
EDWARD J. ROTHWELL, MEMBER, IEEE

Abstract—**A new coupled surface integral equation formulation for determination of natural frequencies of a rectangular plate is proposed. The method of moments (MM) solution to this formulation and the subsequent numerical results are presented. The natural frequencies predicted by the theory have been verified by an experiment. In comparison with the existing formulation of this problem, the present formulation predicts equally well for the first few dominant modes but better for the higher modes. Also, in the present formulation, no convergence problem has been encountered.**

I. Introduction

SUBSEQUENT TO THE introduction of the singularity expansion method (SEM) by Baum in 1971 [1], considerable attention has been devoted to the analysis of various perfectly conducting scatterers such as the sphere, prolate spheroid, and infinitely long cylinder and wire structures [2]–[4]. But the exploitation of SEM for the transient analysis of a rectangular plate has not received much attention. In fact, a thin rectangular plate structure is a very fundamental geometry for many realistic scatterers. The knowledge of its natural modes is thus of importance in the application of SEM to many transient scattering problems.

The natural modes of a perfectly conducting body can be obtained numerically by means of a method of moments (MM) solution to an electric field or magnetic field integral equation formulation. In early 1974, Rahmat-Samii and Mittra [5], [6] proposed an integral equation for formulating the scattering problem of a rectangular plate illuminated by a plane wave. Later, this integral equation was modified by Pearson [7] to extract SEM parameters of a plate in the complex domain. The formulation used by Pearson was essentially the same except the real frequency was directly replaced by a complex frequency.

It is well known that the singularity of the surface current occurs at all edges. A special numerical treatment, which uses basis functions containing the correct edge singularity in subdomains near an edge, can be used to represent the currents with singularity at edges [8]. However, to simplify the programming, uniform piecewise constant functions can also be employed as basis functions. The edge effects are shown to remain under this simpler treatment.

This paper proposes a new set of coupled electric field integral equations (EFIE) to determine the natural modes for a thin rectangular plate, and presents the numerical procedure and the results of a method of moments solution to the derived equation set. Special interest is focused on numerical convergence tests of the thin-strip limit and also on the solution with more basis functions.

A comparison is made between the natural frequencies predicted theoretically and those extracted from a real-time measured response. The agreement between theory and experiment is quite good.

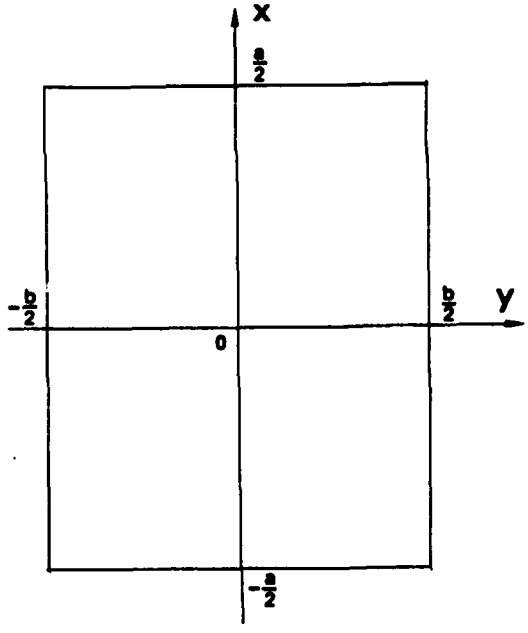

Fig. 1. Geometry of a rectangular plate.

II. The New Formulation of the EFIE

Consider a thin rectangular plate located in the xy plane, as shown in Fig. 1. A modal surface current on the plate obeys the homogeneous electric field integral equation in the complex domain

$$\int_{s'} [\nabla' \cdot \mathbf{K}(\mathbf{r}', s)\mathbf{t} \cdot \nabla - \gamma^2 \mathbf{t} \cdot \mathbf{K}(\mathbf{r}', s)] \frac{e^{-\gamma R}}{4\pi R} ds' = 0 \quad (1)$$

where

$$\gamma = \frac{s}{c}$$

$$R = |\mathbf{r}' - \mathbf{r}|.$$

Manuscript received August 22, 1988; revised April 11, 1989. This work was supported by DARPA and ONR under Contract N000-14-87-K-0336.

The authors are with the Department of Electrical Engineering and System Science, Michigan State University, East Lansing, MI 48824.

IEEE Log Number 9034570.

Here $\mathbf{r}'$ and $\mathbf{r}$ are the coordinates of the source point and the observation point, s is the natural frequency of a modal current, $\mathbf{K}$ is the modal surface current density and $\mathbf{t}$ is a unit vector in the tangential direction on the plate surface. For the geometry shown in Fig. 1, the surface current $\mathbf{K}$ is two-dimensional and it is natural to use a rectangular coordinate system. From (1), two decomposed coupled scalar equations result:

$$\int_{s'} \left\{ \left[\frac{\partial}{\partial x'} K_x(x', y', s) + \frac{\partial}{\partial y'} K_y(x', y', s) \right] \frac{\partial}{\partial x} - \gamma^2 K_x(x', y', s) \right\} \frac{e^{-\gamma R}}{4\pi R} ds' = 0 \quad (2a)$$

$$\int_{s'} \left\{ \left[\frac{\partial}{\partial x'} K_x(x', y', s) + \frac{\partial}{\partial y'} K_y(x', y', s) \right] \frac{\partial}{\partial y} - \gamma^2 K_y(x', y', s) \right\} \frac{e^{-\gamma R}}{4\pi R} ds' = 0. \quad (2b)$$

It is known that the normal components of the current need to be zero at all four edges, producing the four edge conditions:

$$K_x(-a/2, y, s) = 0 \quad (3a)$$

$$K_x(a/2, y, s) = 0 \quad (3b)$$

$$K_y(x, -b/2, s) = 0 \quad (3c)$$

$$K_y(x, b/2, s) = 0. \quad (3d)$$

Employing the edge conditions and integrating by parts on (2) yields a coupled partial differential equation set:

$$\left(\frac{\partial^2}{\partial x^2} - \gamma^2 \right) A_x + \frac{\partial^2}{\partial x \partial y} A_y = 0 \quad (4a)$$

$$\left(\frac{\partial^2}{\partial y^2} - \gamma^2 \right) A_y + \frac{\partial^2}{\partial x \partial y} A_x = 0 \quad (4b)$$

where the vector potentials are expressed as

$$A_x(x, y, s) = \mu_0 \int_{s'} K_x(x', y', s) \frac{e^{-\gamma R}}{4\pi R} ds' \quad (5a)$$

$$A_y(x, y, s) = \mu_0 \int_{s'} K_y(x', y', s) \frac{e^{-\gamma R}}{4\pi R} ds'. \quad (5b)$$

It can be proved that the complete homogeneous solution to equation set (4) is represented by

$$A_x(x, y) = W(y) \cosh \gamma x + B(y) \sinh \gamma x - \int_0^x \frac{\partial}{\partial y} A_y(x', y) \cosh \gamma (x' - x) dx' \quad (6a)$$

$$A_y(x, y) = C(x) \cosh \gamma y + D(x) \sinh \gamma y - \int_0^y \frac{\partial}{\partial x} A_x(x, y') \cosh \gamma (y' - y) dy' \quad (6b)$$

where the $W(y)$, $B(y)$, $C(x)$ and $D(x)$ are unknown coefficients, but functions of only one variable. The equation set (6) is the essential rigorous formulation applicable to extracting the natural frequencies of a rectangular plate for any mode. The x and y components of modal currents are closely coupled through the coupling integrals. This formulation is found to possess good numerical stability and convergence. The only sacrifice is the great number of computations for the evaluation of the coupling integrals. Details about the numerical properties will be discussed in the next section.

The natural frequencies are those complex frequencies s resulting in nontrivial currents of K_x and K_y, and the associated functions $W(y)$, $B(y)$, $C(x)$, and $D(x)$, which satisfy the excitation-free homogeneous equation set (6). The concomitant values of s are poles of a rectangular plate. The vanishing of excitation dependence and the symmetry of the geometry give rise to the symmetry of current distribution in (6). By bringing the symmetry relations into the solution procedure, significant computational savings in the numerical solution will be gained.

It is expected from the geometrical symmetry as shown in Fig. 1 that a modal current is symmetrically or antisymmetrically distributed with respect to the x- or y-axis. But the respective symmetries for K_x and K_y are not arbitrary. They must be compatible with each other since the current continuity equation has to be satisfied. The continuity equation in the complex frequency domain is

$$\frac{\partial}{\partial x} K_x(x, y, s) + \frac{\partial}{\partial y} K_y(x, y, s) = -\gamma c \rho(x, y, s). \quad (7)$$

From the right-hand side of (7), it is apparent that there are only four possible symmetries for charge ρ with respect to the x- and y-axes. Consequently, the symmetries for $(\partial/\partial x) K_x$ and $(\partial/\partial y) K_y$ are correspondingly limited to four cases. For example, if $\rho(x, y)$ is symmetric with respect to the x-axis and antisymmetric with respect to the y-axis, then the derivative of $(\partial/\partial x) K_x$ must be symmetric with respect to the x-axis and antisymmetric with respect to the y-axis. Therefore, the current K_x should be antisymmetric with respect to the x-axis and antisymmetric with respect to the y-axis. The same analysis results in the current K_y, which is symmetric with respect to the x-axis and symmetric with respect to the y-axis.

By means of this analysis, the information about possible symmetries can be used to reduce the complexity in numerical evaluation of the integral equation set (6). If $K_x(x, y)$ is symmetric with respect to the x-axis and symmetric with respect to the y-axis, $K_y(x, y)$ must be antisymmetric with respect to the x-axis and antisymmetric with respect to the y-axis. They are denoted as $K_x(x, y) = (e, e)$ and $K_y(x, y) = (o, o)$. All the other symmetry cases are denoted in a logically similar way. After the symmetry is specified, a simplified formulation is easily established. As an example, if $K_x(x, y) = (e, e)$ and $K_y(x, y) = (o, o)$, we have from (6):

$$A_x(x, y) = W(y)\cosh\gamma x - \int_0^x \frac{\partial}{\partial y} A_y(x', y)\cosh\gamma(x' - x)\,dx' \quad (8a)$$

$$A_y(x, y) = D(x)\sinh\gamma y - \int_0^y \frac{\partial}{\partial x} A_x(x, y')\cosh\gamma(y' - y)\,dy' \quad (8b)$$

Since equation set (8) is applied to the first quadrant only, the number of unknown coefficients is reduced by a factor of two.

III. Method of Moments Solution to the New EFIE

The integral equations for each of the four symmetry cases can be discretized by a method of moments. Here, two-dimensional subsectionally constant expansion functions are used with collocation testing. The zones are equally divided, respectively, along the x-axis and y-axis to simplify the programming procedure. A typical zoning scheme has 10×10 zones on the whole plate.

The unknown coefficients of $W(y)$, $B(y)$, $C(x)$ and $D(x)$ are also expanded with the pulse basis functions. Notice that the number of bases for these unknown coefficients is equal to the number of edge zones preassigned to zeros for the edge conditions to be enforced.

The major contribution to calculation efficiency by the use of pulse basis functions is that the evaluation of vector potentials need be performed once only. The individual kernel integral terms for all argument combinations, e.g., different distance combinations, are computed first. Then, subscript entries are chosen from a storage matrix to construct the matrix equation according to the symmetry conditions being assigned.

As one example of the implementation of the method of moments solution, the symmetry of $K_x = (e, e)$ and $K_y(o, o)$ is assumed. The currents are expanded in terms of pulse basis functions with widths Δx and Δy:

$$bK_x(x, y) = \sum_n \sum_m a_{nm} P_n(x) P_m(y) \quad (9a)$$

$$aK_y(x, y) = \sum_n \sum_m b_{nm} P_n(x) P_m(y) \quad (9b)$$

where

$$P_n(\eta) = \begin{cases} 1, & (n-1)\Delta\eta \le \eta \le n\Delta\eta \\ 0, & \text{elsewhere.} \end{cases}$$

The derivative of current K_y with respect to y is expanded as

$$\frac{\partial}{\partial y} K_y(x, y) = \frac{1}{a} \sum_n \sum_m b_{nm} P_n(x) \cdot [\delta(y - (m-1)\Delta y) - \delta(y - m\Delta y)] \quad (9c)$$

where a_{nm} and b_{nm} are coefficients to be determined, and a and b are the length and width of the plate. Thus, the discretized forms of the formulation (8) are created:

$$\sum_n \sum_m \frac{1}{b} a_{nm} f(x, y, n, m) = \sum_m W_m P_m(y)\cosh\gamma x - \sum_n \sum_m \frac{1}{a} b_{nm}[F_y(x, y, n, m-1) - F_y(x, y, n, m)] \quad (10a)$$

$$\sum_n \sum_m \frac{1}{a} b_{nm} f(x, y, n, m) = \sum_n D_n P_n(x)\sinh\gamma y - \sum_n \sum_m \frac{1}{b} a_{nm}[F_x(x, y, m, n-1) - F_x(x, y, m, n)] \quad (10b)$$

where

$$f(x, y, n, m) = \int_{(m-1)\Delta y}^{m\Delta y} \int_{(n-1)\Delta x}^{n\Delta x} \frac{e^{-\gamma[(x'-x)^2 + (y'-y)^2]^{1/2}}}{4\pi[(x'-x)^2 + (y'-y)^2]^{1/2}} dx'\,dy' \quad (11a)$$

$$F_x(x, y, n, m) = \int_0^x \cosh\gamma(x' - x)\,dx' \cdot \int_{(n-1)\Delta x}^{n\Delta x} F(x', x'', y, m)\,dx'' \quad (11b)$$

and

$$F(x', x'', y, m) = \frac{e^{-\gamma[(x'-x'')^2 + (y - m\Delta y)^2]^{1/2}}}{4\pi[(x'-x'')^2 + (y - m\Delta y)^2]^{1/2}}. \quad (11c)$$

By choosing matching points at the center of every partition zone, and shrinking the number of unknown amplitudes to one-quarter by using the symmetry properties of the currents, the following moment matrix equation is obtained

$$\begin{bmatrix} [G_{ij,nm}]_{qp \times qp} & [Q_{ij,nm}]_{qp \times qp} \\ [R_{ij,nm}]_{qp \times qp} & [T_{ij,nm}]_{qp \times qp} \end{bmatrix} \begin{bmatrix} [\tilde{a}_{nm}] \\ [\tilde{b}_{nm}] \end{bmatrix} = 0 \quad (12)$$

where $2q$ is the partition number along the x direction and $2p$ is the partition number along the y direction, with the restrictions $n, i \le q$, $m, j \le p$. The matrix entries are

$$G_{ij,nm} = \frac{1}{b}[f(x_i, y_j, n, m) + f(x_i, y_j, 2q - n, m) + f(x_i, y_j, n, 2p - m) + f(x_i, y_j, 2q - n, 2p - m)] \quad (13a)$$

$$T_{ij,nm} = \frac{1}{a}[f(x_i, y_j, n, m) - f(x_i, y_j, 2q-n, m) - f(x_i, y_j, n, 2p-m) + f(x_i, y_j, 2q-n, 2p-m)] \quad (13b)$$

$$Q_{ij,nm} = \frac{1}{a}[F_y(x_i, y_j, n, m-1) - F_y(x_i, y_j, n, m) - F_y(x_i, y_j, 2q-n, m-1) + F_y(x_i, y_j, 2q-n, m)] + [-F_y(x_i, y_j, n, 2p-m-1) + F_y(x_i, y_j, n, 2p-m) + F_y(x_i, y_j, 2q-n, 2p-m-1) - F_y(x_i, y_j, 2q-n, 2p-m)] \quad (13c)$$

$$R_{ij,nm} = \frac{1}{a}[F_x(x_i, y_j, m, n-1) - F_x(x_i, y_j, m, n) + F_x(x_i, y_j, m, 2q-n-1) - F_x(x_i, y_j, m, 2q-n)] + [F_x(x_i, y_j, 2p-m, n-1) - F_x(x_i, y_j, 2p-m, n) + F_x(x_i, y_j, 2p-m, 2q-n-1) - F_x(x_i, y_j, 2p-m, 2q-n)] \quad (13d)$$

$$\tilde{a}_{nm} = a_{nm} \quad (13e)$$

$$\tilde{b}_{nm} = b_{nm} \quad (13f)$$

$$x_i = 0.5a - (i-0.5)^*\Delta x \quad (13g)$$

$$y_j = 0.5b - (j-0.5)^*\Delta y. \quad (13h)$$

Note that when $n = 1$:

$$G_{ij,nm} = -P_m(y_j)\cosh\gamma x_i$$

$$R_{ij,nm} = 0$$

$$\tilde{a}_{nm} = W_m$$

while when $m = 1$:

$$T_{ij,nm} = -P_n(x_i)\sinh\gamma y_j$$

$$Q_{ij,nm} = 0$$

$$\tilde{b}_{nm} = D_n.$$

The matrix in (12) is a function of complex frequency, and a complex resonance occurs when this matrix has a zero determinant. The condition to guarantee the existence of natural resonances is therefore

$$\det\begin{bmatrix} [G_{ij,nm}]_{qp\times qp} & [Q_{ij,nm}]_{qp\times qp} \\ [R_{ij,nm}]_{qp\times qp} & [T_{ij,nm}]_{qp\times qp} \end{bmatrix} = 0. \quad (14)$$

It can be seen that this determinant is an analytic function in the complex plane, since the original integral equation is differentiable on the surface of the plate. Any standard root search algorithm can be used to locate the zeros of the determinant. The subroutine SEARCH [9] is called as a preliminary procedure to locate all dominant poles in the complex plane, and then the subroutine C05NBF in the NAG library is used to improve the accuracy of the pole locations. All symmetry cases can be handled in this manner.

A premium on computational efficiency has to be placed in the evaluation of the matrix and its determinant. Many such evaluations are required in the course of iterating the root locations. It is thus significant to have a good approximation to the coupling integrals and vector potentials.

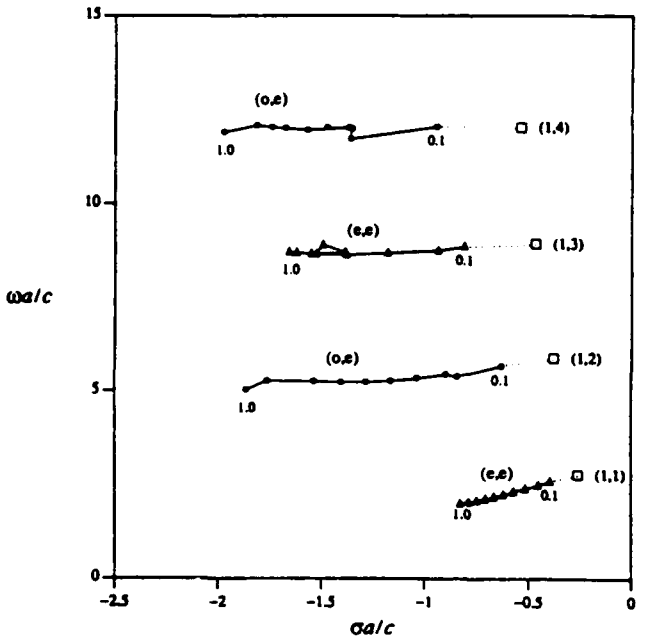

Fig. 2. Convergence of four natural modes to their thin-wire counterparts as aspect ratio is varying. The squares show the locations of the first four thin-wire modes selected from the first layer.

Different approximations are applied in the calculation of the interaction matrix. For the self-patches, i.e., the patch in which the match point is located, the integration is performed analytically after the exponential function is approximated by 1 in order to avoid the numerical singularity. For the patches adjacent to the matching patch, the integrals are well-behaved and are evaluated numerically.

IV. Numerical Convergence

The usefulness of the formulation (8) depends heavily on its numerical convergence properties. Two tests of convergence for the formulation are discussed in this section. One examines pole convergence in the thin-strip limit, and the other examines convergence as the number of basis functions is increased.

Intuitively, a rectangular plate approaches a thin strip when the aspect ratio, which is defined as the ratio of width to length, is very small. As is well know, a thin strip is related to an equivalent dipole. One test is performed by observing the trajectory of some typical poles when the aspect ratio is diminished. It is expected that the convergence of those poles to thin-wire modes should be apparent and uniform.

It is instructive to note that for the given coordinate system, only the modes with symmetries of $K_x = (e, e)$; $K_y = (o, o)$ and $K_x = (o, e)$; $K_y = (e, o)$ can reduce to thin-wire modes since it is nonphysical that the x-component of currents is antisymmetric with respect to the x-axis in the thin-strip limit.

Fig. 2 provides some insight into the convergence of poles to thin-wire counterparts for a range of aspect ratios. Two modes denoted by (e, e) result from the symmetry case of $K_x = (e, e)$; $K_y(o, o)$, while the other two denoted by (o, e) result from the symmetry case of $K_x = (o, e)$; $K_y = (e, o)$.

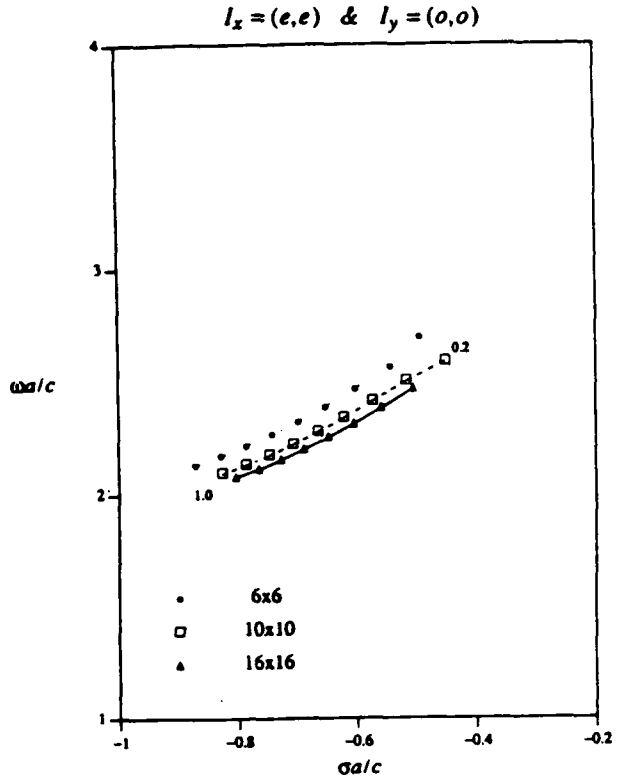

Fig. 3. Different partition schemes are applied to the first mode ($I_x = (e, e)$ and $I_y = (o, o)$) with various aspect ratios.

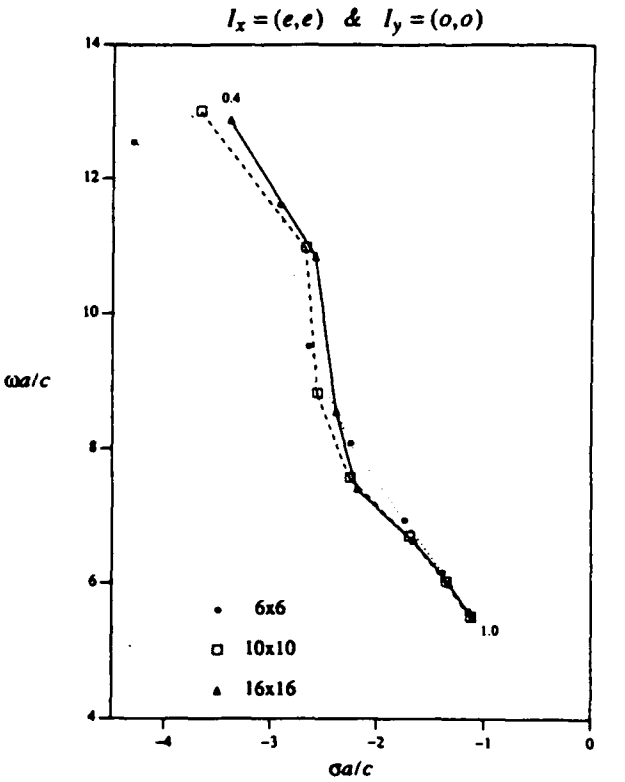

Fig. 4. Different partition schemes are applied to the second mode ($I_x = (e, e)$ and $I_y = (o, o)$) with various aspect ratios.

The first four thin-wire modes from the first layer of poles are displayed by small squares to serve as the limits of the trajectories. Each solid line is a trajectory of one mode. The trajectory is started with aspect ratio = 1 and stepped with a step size of 0.1. It is observed that the four poles converge apparently and uniformly to thin-strip limits.

An MM solution to the formulation (8) is the discretization of the electrical field integral equation. Mathematically, this procedure is an approximation with a finite-dimension space to an infinite-dimension space. The convergence of any numerical scheme implies that the error induced by finite-dimensional approximation is uniformly decreased as the dimensions, which are used to discretize the integral equation, are increased. A strong numerical verification of this convergence is beyond the available capability of any computer system, but convergence tests on a few dominant modes with a varying number of basis functions provide good insight into the convergent rate.

As typical examples, the first two modes with symmetry of $K_x = (e, e)$; $K_y = (o, o)$ are investigated with results shown in Figs. 3 and 4. Three different partition schemes are employed. They are identified as 6×6, 10×10, and 16×16 partition zones on the whole plate.

Fig. 3 shows the convergence of the first pole with various aspect ratios. The comparison with different partition zones is shown as the dotted line (6×6), dashed line (10×10), and solid line (16×16). Excellent agreement between the dashed line and the solid line is seen for varying aspect ratios. The trajectory with 10×10 partitions is very close to that with 16×16 partitions. Even with 6×6 partitions, the result is close enough to that with more partitions. It is seen that this special dominant mode converges very fast. Physically, such a convergent rate is expected as six, ten, and 16 pulses have been used within half a wavelength to present currents on the plate.

Fig. 4 shows the result of the second pole. The same notations are used as in Fig. 3. From Fig. 4, good agreement between the trajectories with 10×10 zones and that with 16×16 zones for a range of aspect ratios are again observed. It is also seen that the result with 6×6 partitions is less accurate as the aspect ratio decreases. This discrepancy is attributed to the fact that six pulses are not enough to present the currents within a range of one wavelength.

At this point the conclusion is made that for the first few dominant modes a 10×10 partition scheme is good enough to discretize the integral equation. As a rule of thumb, the applicability of a partition scheme could be estimated by the criteria that more than six pulses are required to present the currents in one wavelength range.

V. Numerical Results

Extensive computations have been conducted to locate all the dominant poles in the complex plane for each symmetry case and to solve for the current distributions for those natural modes. However, only representive natual modes for selected poles are presented here. This section provides the pole trajectories of the first few dominant modes for each symmetry case, and presents some typical modal current distributions.

It was stated previously that the pole location is found by the zero searching of the moment matrix determinant. The determinant is an analytic function in the complex plane, and thus the pole location is two dimensional. If a 10×10 partitioning is used to discretize the integral equation, a 50×50 moment matrix is created. To search for a zero on the complex

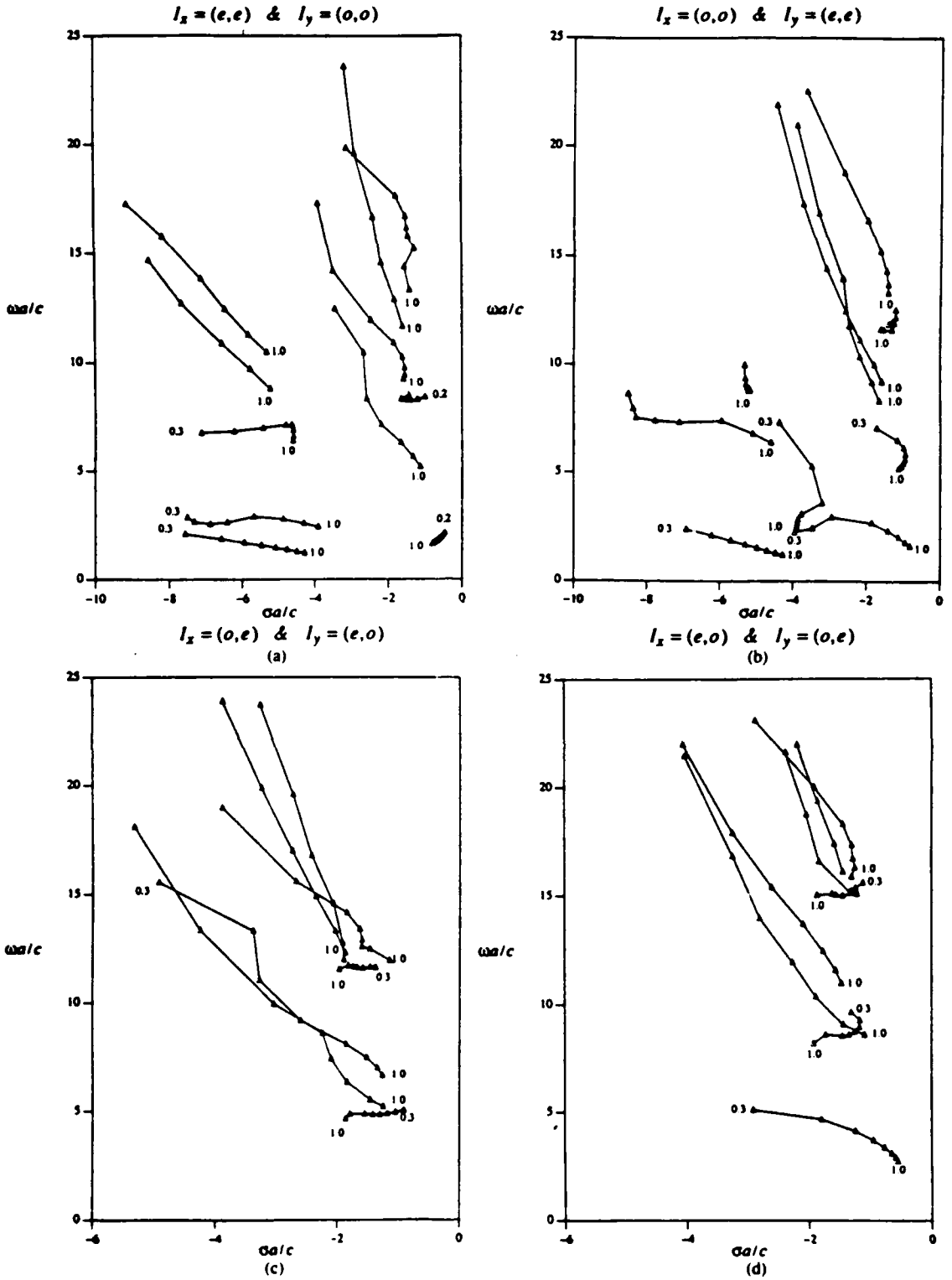

Fig. 5. Pole locations of four possible symmetry cases with various aspect ratios.

plane, the determinant of the 50 × 50 matrix is evaluated iteratively and thus the selection of an appropriate pole location algorithm is very important.

The method proposed by Singaraju, Giri, and Baum [9] is based on the theorem that relates the variation of the argument of a complex function integrated along a contour to the number of zeros and poles within the range bounded by the coutour. This approach is used conveniently and successfully in the present problem for the preliminary location of a pole before an iterative method is used to improve the precision. The applicability of the method is due to the analyticity of the moment matrix determinant and the locality of its poles.

Once the complex plane has been scanned for zeros by using the SEARCH subroutine which is the code of above algorithm, the output poles are served as initial guesses to be improved by calling the NAG library. The called NAG subroutine is named C05NBF, which is generated based on an iterative algorithm.

The locations of poles for a rectangular plate are given in Figs. 5(a)–5(d). Only poles in the third quadrant are displayed

since any physical pole has a negative real part, and all poles are arranged with conjugate symmetry, as deducted from the conjugate property of the integral equation formulation. The poles displayed are normalized by the length of the plate and the speed of light. Each solid line is a trajectory of one pole, the trajectory is initiated with aspect ratio of 1.0, and stepped with a size 0.1 in terms of aspect ratio.

Fig. 5(a) shows the pole trajectories with symmetry of $K_x = (e, e)$; $K_y = (o, o)$, where σ associated with the real axis is the damping coefficient, ω associated the imaginary axis is the radian frequency, and I_x and I_y are defined as $I_x = K_x \cdot b$, and $I_y = K_y \cdot a$. With this symmetry, the x-component of currents is symmetric with respect to both the x- and y-axes. The currents with this symmetry are easily excited on a plate placed on a ground plane, and illuminated by a normally incident pulse. This will be discussed further in the next section. Out of the 11 modes displayed, there are two special poles whose real parts are diminished as the aspect ratio is decreased. They are closely related to the thin-wire counterparts. In the thin-strip limit they go to the first and the third thin-wire modes. The physical significance of their behavior resides in their dominance over the other modes since they have smaller damping coefficients. In contrast, all the other modes move in the negative direction as the aspect ratio is decreased. In other words, these modes imply that the scattered field from the plate is reduced as the plate approaches a square. The unusual phenomenon is due to a complex induced current on the plate. Another interesting phenomenon is due to the fact the third mode has a "loop" trajectory. The same natural frequency is reached at two aspect ratios.

Fig. 5(b) shows the pole trajectory with symmetry of $K_x = (o, o)$; $K_y = (e, e)$. With this symmetry, the x-component of currents is antisymmetric with respect to both the x- and y-axes. It was mentioned previously that the modes with this symmetry cannot be related to any cylindrical wire modes since the antisymmetry of the x-component current with respect to the x-axis cannot be physical in the thin-strip limit. It is noted that modes belonging to symmetry $K_x = (e, e)$; $K_y = (o, o)$ are identical with those belonging to symmetry $K_x = (o, o)$; $K_y = (e, e)$ on a square plate. This identity is equivalent to the 90° rotation of the coordinate system.

Figs. 5(c) and 5(d) show the results of the other symmetry cases. The poles for these two cases are located within a less negative range as the dominant modes have smaller damping coefficients. The modes in "deeper" layers have not been determined.

Each natural mode is a two-component complex-valued vector function of two variables. Since the poles are distributed on the left-half complex plane with conjugate symmetry, any excited mode is accompanied by its conjugate mode. The pure contribution to the resonance comes from the real parts of complex-valued amplitudes of currents. Thus only the real parts of the complex currents solved from the moment matrix equation, are plotted in a three-dimensional format. The amplitude distributions displayed belong to a pair of conjugate modes.

The three-dimensional plots shown in Fig. 6 are the current distributions of the first dominant mode with the symmetry $K_x = (e, e)$; $K_y = (o, o)$. The current amplitudes of the two

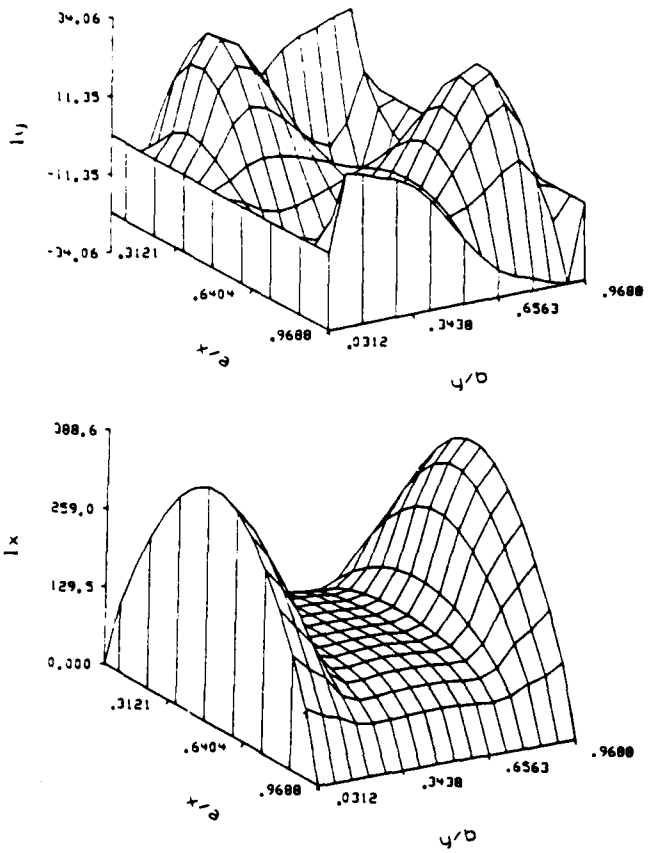

Fig. 6. Amplitude distributions of x- and y-components of surface currents associated with the first mode ($I_x = (e, e)$ and $I_y(o, o)$, $b/a = 0.75$ and $sa/c = -0.8087 + j2.511$).

components distributed on the whole plate are displayed along the z-axis, and the origin of the xy-plane has been displaced by one quadrant to make the plots clear. It is noted that the displayed amplitude values are normalized current densities, i.e., $I_x = K_x \cdot b$, and $I_y = K_y \cdot a$. The dominance of the x-component of the current is seen by comparing the amplitudes of two components of currents. The x-component is almost ten times larger. The symmetric shape and the edge effect at two edges of $y = 0$ and $y = 1$ are apparently manifested.

Fig. 7 gives the modal current distribution of the first mode with the symmetry $K_x = (e, o)$; $K_y = (o, e)$. Fig. 8 gives the modal current distribution of the second mode with the symmetry $K_x = (o, e)$; $K_y = (e, o)$. The one-cycle variation in both the x- and y-directions is very obvious here. The shape similarity is also observed.

The natural modes are characterized here by the trajectories and the current distributions. The modes are observed generally to be consistent with physical expectations. But a good theory should be consistent with experiment. The next section gives an experimental investigation into the extraction of natural modes from a measured response to verify the analytic results.

VI. Experimental Verification

The SEM analysis of transient scattering problems is based entirely on the conjecture that the late-time scattered field re-

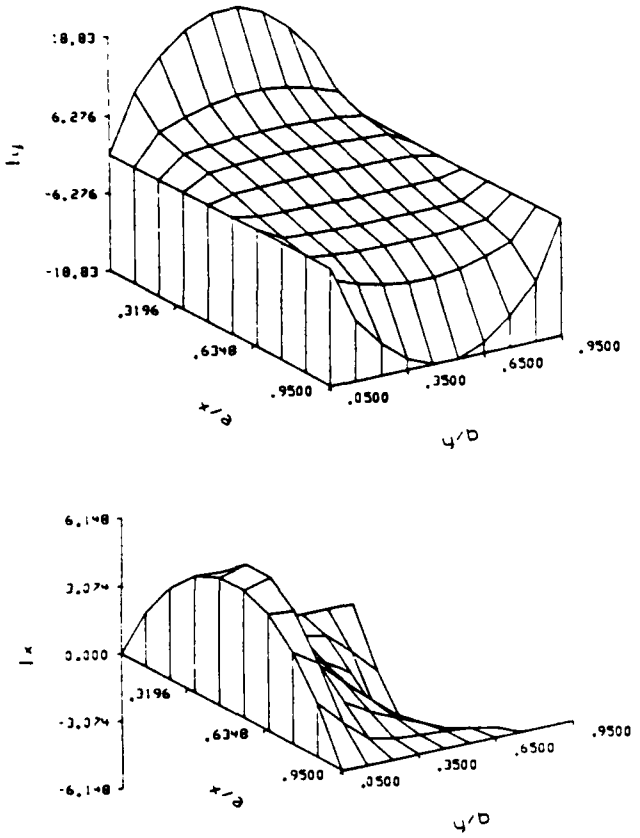

Fig. 7. Amplitude distributions of x- and y-components of surface currents associated with the first mode ($I_x = (e, o)$ and $I_y = (o, e)$, $b/a = 0.60$ and $sa/c = -1.073 + j4.739$).

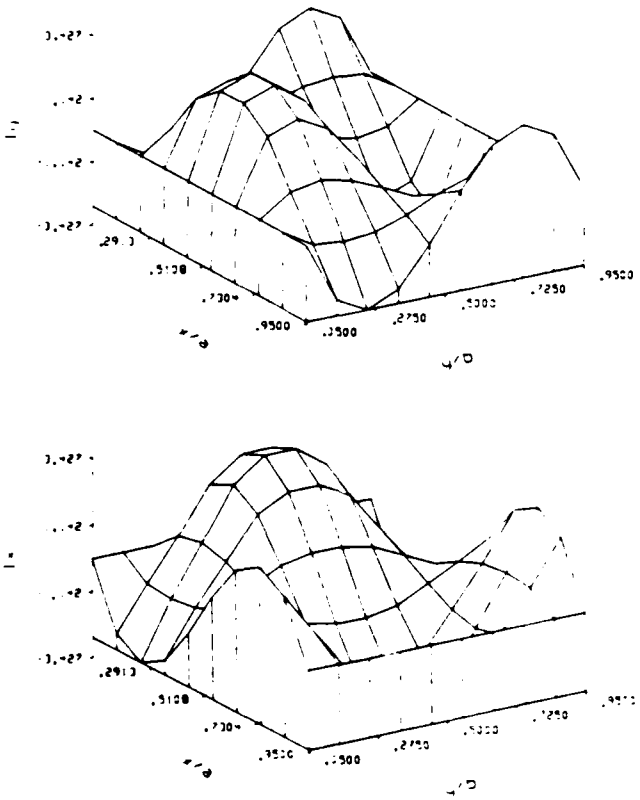

Fig. 8. Amplitude distributions of x- and y-components of surface currents associated with the second mode ($I_x = (o, e)$ and $I_y = (e, o)$, $b/a = 1.0$ and $sa/c = -1.409 + j7.985$).

sponse of a conducting target can be completely represented by a summation of damped sinusoid functions. It is thus extremely prudent to verify experimentally the natural resonance behavior of a rectangular plate, and at the same time to affirm the natural resonance obtained from theory by comparing them to those extracted from a measured response.

A striking confirmation of the theory is shown in Fig. 9. This shows the experimental geometry and the measured scattered response of a 4×16 in rectangular plate placed perpendicular to the ground plane, as received by a monopole. The coordinate system is chosen as indicated to align the x-axis along the longer dimension. The external exciting pulse is perpendicularly polarized. Due to the image effect of the ground plane, the equivalent dimension of this plate is 8×16 in. It is interesting to note that the image plane prevents the natural modes with symmetries of $K_x = (e, e)$; $K_y = (o, o)$ and $K_x = (o, e)$; $K_y = (e, o)$ from being excited. The dotted line indicates the beginning of the late-time portion of the measured response.

Five natural frequencies have been extracted from the late-time portion of the measured response using the continuation method [10], [11]. Out of the five modes, the first two are of symmetry $K_x = (o, o)$; $K_y = (e, e)$, and the other three are of symmetry $K_x = (o, o)$; $K_y = (e, e)$. In order to confirm the reliability of the experimental result, the late-time response is reconstructed by using the extracted five modes and compared to the original data. Fig. 9(a) provides a comparison between the natural frequencies experimentally extracted and those predicted from theory. The agreement of radian frequencies between experiment and theory is excellent. As we might expect, the agreement of damping coefficients is not satisfying since the experimental extraction of damping coefficients is very noise-sensitive. At the same time the available modes predicted from the existing formulation are listed in the table under Fig. 9(b) [8]. We can see that the existing formulation works equally well for the dominant modes, but there are two absent modes here which are experimentally measurable.

As the last example, Figs. 10(a) and 10(b) show the experimental results using a 10×4 in rectangular plate. Four natural modes are extracted from the measured response, and they are compared with theory. The comparison between the reconstructed late-time response and the received original response implies that more higher order modes are required to present this response. For the chosen coordinate, only the modes with symmetries of $K_x = (e, e)$; $K_y = (o, o)$ and $K_x = (e, o)$; $K_y = (o, e)$ are excited. The first mode is the dominant mode, and the consistency between theory and experiment is apparent. The fourth mode is actually the dominant mode with symmetry of $K_x = (e, o)$; $K_y = (o, e)$, as is also well verified by experiment.

VII. Conclusion

A new coupled surface integral equation formulation for determination of natural frequencies of a rectangular plate has been proposed. The numerical solutions to this formulation by the method of moments and extensive numerical results have been presented. An experiment has been conducted to verify the natural frequencies predicted by the theory. It seems

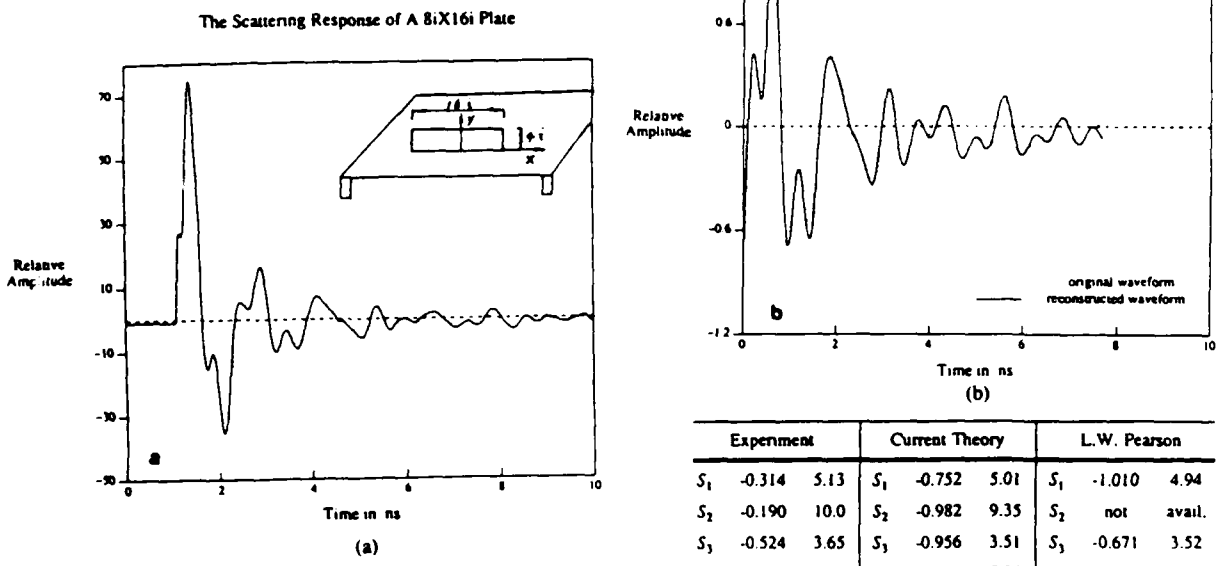

Experiment			Current Theory			L.W. Pearson		
S_1	-0.314	5.13	S_1	-0.752	5.01	S_1	-1.010	4.94
S_2	-0.190	10.0	S_2	-0.982	9.35	S_2	not	avail.
S_3	-0.524	3.65	S_3	-0.956	3.51	S_3	-0.671	3.52
S_4	-0.199	7.33	S_4	-0.876	7.07	S_4	-1.770	6.69
S_5	-1.060	12.7	S_5	-0.971	11.7	S_5	not	avail.

Fig. 9. Experimental measurement and natural mode extraction of the transient scattering response from a $4i \times 16i$ rectangular plate.

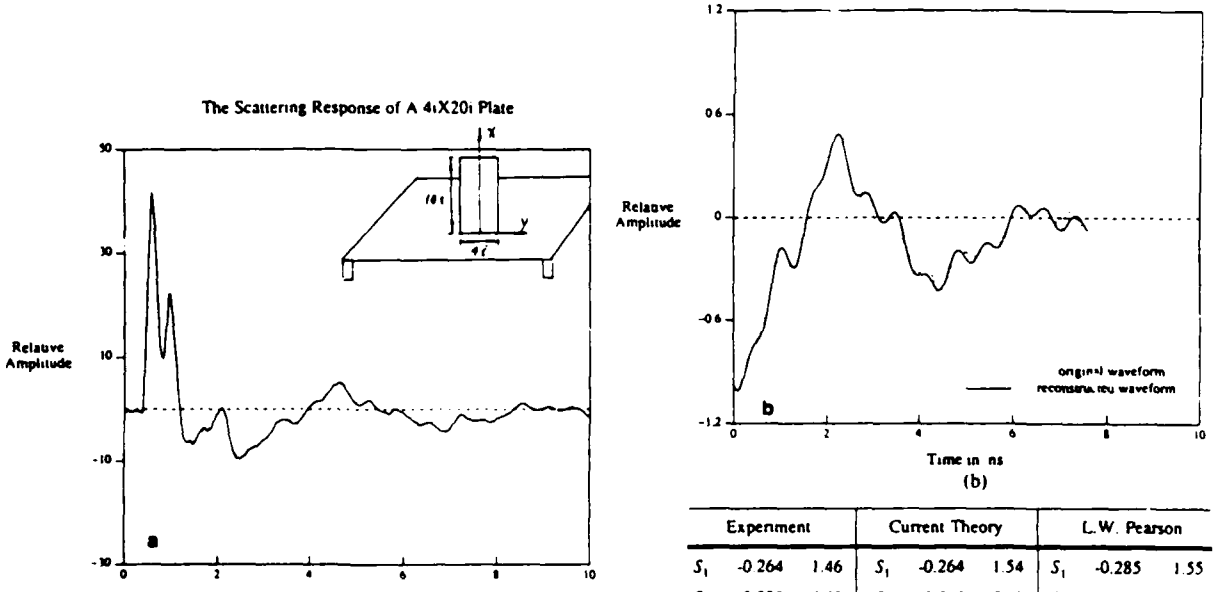

Experiment			Current Theory			L.W. Pearson		
S_1	-0.264	1.46	S_1	-0.264	1.54	S_1	-0.285	1.55
S_2	-0.228	4.59	S_2	-0.546	5.19	S_2	-0.590	5.01
S_3	-0.107	9.92	S_3	-0.609	9.61	S_3	not	avail
S_4	-1.130	6.19	S_4	-1.270	6.22	S_4	not	avail

Fig. 10. Experimental measurement and natural mode extraction of the transient scattering response from a $4i \times 10i$ rectangular plate.

that the present formulation can predict more higher natural modes, in addition to the dominant modes, than the existing formulation [8]. Also, no convergence problem was encounted in the present formulation.

Acknowledgment

The authors wish to acknowledge Dr. L. W. Pearson for his initial investigation of this topic and for his encouragement of our efforts.

References

[1] C. E. Baum, "On the singularity expansion method for the solution of electromagnetic interaction problems," AFWL, Interaction Notes 88, Dec. 1971.

[2] F. M. Tesche, "On analysis of scattering and antenna problems using the singularity expansion technique," *IEEE Trans. Antennas Propagat.*, vol. AP-21, no. 1, p. 53, Jan. 1973.

[3] K. R. Umashankar, "The calculation of electromagnetic transient currents on perfectly conducting bodies using singularity expansion method," Ph.D. dissertation, Univ. Mississippi, Oxford, MS, Aug 1974.

[4] L. Marin, "Natural-mode representation of transient scattering from rotationally symmetric bodies," *IEEE Trans. Antennas Propagat.*, vol. AP-22, no. 2, p. 266, Mar. 1974.
[5] Y. Rahmat-Samii and R. Mittra, "A new integral equation solution of electromagnetic aperture coupling and thin plate scattering problems," AFWL, Interaction Notes 224, Feb. 1975.
[6] ——, "Integral equation solution and RCS computation of a thin rectangular plate," *IEEE Trans. Antennas Propagat.*, vol. AP-22, p. 608, July 1974.
[7] L. W. Pearson and R. Mittra, "The singularity expansion representation of the transient electromagnetic coupling through a rectangular aperture," AFWL, Interaction Notes 296, June 1976.
[8] A. W. Glisson and D. R. Wilton, "Simple and efficient numerical methods for problems of electromagnetic radiation and scattering from surface," *IEEE Trans. Antennas Propagat.*, vol. AP-28, p. 593, 1980.
[9] B. K. Singaraju, D. R. Giri, and C. E. Baum, "Further developments in the application of contour integration to evaluation of the zeros of analytic functions and relevant computer programs," AFWL, Math. Notes 42, Mar. 1976.
[10] B. Drachman and E. Rothwell, "A continuation method for identification of the natural frequencies of an object using a measured response," *IEEE Trans. Antennas Propagat.*, vol. AP-33, p. 445, Apr. 1985.
[11] E. J. Rothwell, "Radar target discrimination using extinction-pulse technique," Ph.D. dissertation, Michigan State Univ., East Lansing, MI, 1985.

Weimin Sun (S'87) was born in Jiangsu Province, China, on October 20, 1957. He received the B.S. degree in electrical engineering from Sichuan University, China, in 1982, and the M.S. degree in physical electronics from Tsinghua University, China, in 1984. He is currently working toward the Ph.D. degree in the Department of Electrical Engineering, Michigan State University, East Lansing.

Prior to entering the Ph.D. program, he was engaged in a research program on optical communication and integrated optics at Tsinghua University, China. His current research interests include radar target discrimination with transient waveforms, interaction of electromagnetic waves with composite materials, and the application of numerical methods for treating electromagnetic radiation and scattering problems.

Mr. Sun is a member of Phi Kappa Phi. He was the recipient of the Outstanding Academic Award from the College of Engineering, Michigan State University, in 1988.

Kun-Mu Chen (SM'64–F'76) was born in Taipei, Taiwan, China, on February 3, 1933. He received the B.S.E.E. degree from the National Taiwan University, Taipei, Taiwan, in 1955, and the M.S. and Ph.D. degrees in applied physics from Harvard University, Cambridge, MA, in 1958 and 1960, respectively.

While at Harvard University, he held the C. T. Loo and the Gordon McKay Fellowships. From 1956 to 1957 he was a Teaching Assistant at the National Taiwan University, and from 1959 to 1960 he was a Research Assistant and Teaching Fellow at Harvard University. From 1960 to 1964 he was associated with the Radiation Laboratory, University of Michigan, Ann Arbor, where he was engaged in studies of electromagnetic theory and plasma. In 1962, while on leave from the University of Michigan, he was a Visiting Professor of Electronics at Chao-Tung University, Taiwan. Since 1964 he has been with Michigan State University, East Lansing, first as Associate Professor of Electrical Engineering, and since 1967 as Professor of Electrical Engineering. From 1968 to 1973 he was the Director of the Electrical Engineering program of the Department of Electrical Engineering and Systems Science. He has published numerous papers on electromagnetic radiation and scattering, plasmas, and the interaction of electromagnetic radiation with biological systems.

Dr. Chen is a fellow of the American Association for the Advancement of Science, a member of U.S. Commissions A, B, and C of the International Union of Radio Science, Sigma Xi, Phi Kappa Phi and Tau Beta Pi. He is the recipient of Distinguished Faculty Award from Michigan State University in 1976. He is also the recipient of Achievement Award in Science and Engineering from Taiwanese American Foundation in 1984.

Dennis P. Nyquist (S'63–M'67) was born in Detroit, MI, on August 18, 1939. He received the B.S.E.E. and M.S.E.E. degrees in 1961 and 1964, respectively, and the Ph.D. degree in electrical engineering from Michigan State University, East Lansing, in 1966.

Prior to obtaining the Ph.D. degree, he was a Research Engineer at the Ford Research Laboratories. He held an Engineering College Predoctoral Fellowship during his doctoral program at Michigan State University. He joined the Electrical Engineering Faculty at Michigan State University as an Instructor in 1966, became Assistant Professor in 1967, Associate Professor in 1970 and Professor in 1979. He has published a number of papers on electromagnetic radiation, antennas, and scattering. His current research interests include target discrimination with transient waveforms and guided-wave optics.

Dr. Nyquist is a member of Commission B of the International Union of Radio Science, the American Association for the Advancement of Science, Sigma Xi, and Phi Kappa Phi. He was the recipient of the Michigan State University Teacher-Scholar Award in 1969.

Edward J. Rothwell (S'84–M'85), for photograph and biography please see page 475 of the April 1990 issue of this TRANSACTIONS.

Appendix 9

The Singularity Expansion Method and its Application to Target Identification

C.E. Baum, Fellow, IEEE, E.J. Rothwell, Member IEEE
K.M. Chen, Fellow, IEEE and D.P. Nyquist, Member IEEE

Abstract:

The singularity expansion method (SEM) for quantifying the transient electromagnetic scattering from targets illuminated by pulsed EM radiation is reviewed. SEM representations for both induced currents and scattered fields are presented. Natural-resonance-based target identification schemes, based upon the SEM, are described. Various techniques for the extraction of natural-resonance modes from measured transient response waveforms are reviewed. Discriminant waveforms for target identification, synthesized based upon the complex natural-resonance frequencies of the relevant targets, are exposed. Particular attention is given to the aspect-independent (extinction) E-pulse and (single-mode) S-pulse discriminant waveforms which, when convolved with the late-time pulse response of a matched target, produce null or mono-mode responses, respectively, through natural-mode annihilation. Extensive experimental results for practical target models are included to validate the E-pulse target discrimination technique. Finally, anticipated future extensions and areas requiring additional research are identified.

This research was supported in part by DARPA through ONR Contract No. N00014-87-K-0336.

C.E. Baum is at Phillips Laboratory (AFSC), Kirtland AFB, NM 87117.

E.J. Rothwell, K.M. Chen and D.P. Nyquist are at Department of Electrical Engineering, Michigan State University, East Lansing, MI 48824

I. Introduction

The singularity expansion method (SEM) was introduced in 1971 as a way to represent the solution of electromagnetic interaction or scattering problems in terms of the singularities in the complex-frequency (s or two-sided-Laplace-transform) plane [3]. Particularly for the pole terms associated with a scatterer (natural frequencies), their factored form separates the dependencies on various parameters of the incident field, observer location, and scatterer characteristics, with equally simple form in frequency (poles) and time (damped sinusoids) domains. Besides the application to EMP (nuclear electromagnetic pulse) interaction problems, it was recognized from the beginning that SEM was useful for scatterer identification due to the aspect-independent nature of the pole locations in the complex frequency plane.

There has been quite a lot of work done on SEM since the basic structure was outlined in 1971 [45]. The complete bibliography is far too lengthy to be included here, but is included in [29]. There are several book chapters and review papers which summarize the major parts of SEM theory [17,19,23,24,45]; one of these summarizes numerical examples of surface currents [19]. Here we also mention the early papers which began SEM [3-5].

II. Singularity Expansion of Currents on Scatterers

As in Fig. 1, let there be some finite-size object in free space. While this is typically taken as a perfectly conducting object with only a surface current density on the surface S (with coordinate $\vec{r}_s$) the results are readily generalized to volume current density. The general coordinate $\vec{r}$ is chosen referenced to the center of the minimum circumscribing sphere (radius a) of the scatterer for optimum aspect-independent convergence of the poles series [30,57].

The incident field is taken as a plane wave with electric field

$$\tilde{\vec{E}}^{(inc)}(\vec{r},s) = E_o \tilde{f}(s)\vec{I}_p e^{-\gamma \vec{I}_1 \cdot \vec{r}}, \quad \vec{E}^{(inc)}(\vec{r},t) = E_o f(t - \frac{\vec{I}_1 \cdot \vec{r}}{c})\vec{I}_p \qquad (2.1)$$

$\gamma = \frac{s}{c}$, s = complex frequency (Laplace-transform variable)

$c = (\mu_o \epsilon_o)^{-1/2}$ = speed of light, $\vec{I}_1$ = direction of incidence

$\vec{I}_p$ = direction of polarization ($\vec{I}_p \cdot \vec{I}_1 = 0$)

$f(t)$ = waveform, $\tilde{\ }$ = Laplace transform (two sided)

The surface current density is related to the incident field via an integral equation

$$< \tilde{\bar{\bar{Z}}}_t(\vec{r}_s,\vec{r}'_s;s);\tilde{\vec{J}}_s(\vec{r}'_s,s) > = \tilde{\vec{E}}_t^{(inc)}(\vec{r}_s,s) = \tilde{\bar{\bar{I}}}_S(\vec{r}_s)\cdot\tilde{\vec{E}}^{(inc)}(\vec{r}_s,s) \qquad (2.2)$$

$$\bar{\bar{I}}_S(\vec{r}_s) = \bar{\bar{I}} - \vec{I}_S(\vec{r}_s)\vec{I}_S(\vec{r}_s), \qquad \bar{\bar{I}} = \text{identity} = \vec{I}_x\vec{I}_x + \vec{I}_y\vec{I}_y + \vec{I}_z\vec{I}_z$$

$\vec{I}_S(\vec{r}_s)$ = outward pointing normal to S.

Here we have taken the impedance or E-field integral equation. Any other such equation will also do since here we are concerned only with the general form of the solution, rather than numerical computations. The kernel $\tilde{\bar{\bar{Z}}}_t(\vec{r}_s,\vec{r}'_s;s)$ here is symmetric and involves the free-space dyadic Green's function [58]. Denote the symmetric product (no implied conjugation) as $< , >$ involving integration over the common coordinates.

The SEM form of the solution is

$$\tilde{\vec{J}}_s(\vec{r}_s,s) = E_o \sum_\alpha \tilde{f}(s_\alpha)\eta_\alpha(\vec{I}_1,\vec{I}_p)\vec{j}_{s_\alpha}(\vec{r}_s)[s-s_\alpha]^{-1}e^{-(s-s_\alpha)t_o} \qquad (2.3)$$

$$+ \text{ singularities of } \tilde{f}(s) + \text{possible entire function}$$

where only first-order poles have been included, but poles of higher order are possible in special circumstances [17,24]. We have the terms

$$< \tilde{\bar{\bar{Z}}}_t(\vec{r}_s,\vec{r}'_s;s_\alpha);\vec{j}_{s_\alpha}(\vec{r}'_s) > = \vec{0}$$

s_α = natural frequency, $\gamma_\alpha = \frac{s_\alpha}{c}$, $\vec{j}_{s_\alpha}(\vec{r}_s)$ = natural mode

$$\eta_\alpha(\vec{I}_1,\vec{I}_p) = \frac{\vec{I}_p\cdot<e^{-\gamma_\alpha\vec{I}_1\cdot\vec{r}'_s},\vec{j}_{s_\alpha}(\vec{r}'_s)>}{<\vec{j}_{s_\alpha}(\vec{r}_s);\ \frac{\partial}{\partial s}\tilde{\bar{\bar{Z}}}_t(\vec{r}_s,\vec{r}'_s;s)\Big|_{s=s_\alpha};\vec{j}_{s_\alpha}(\vec{r}'_s)>} \qquad (2.4)$$

= coupling coefficient.

In time domain the poles $[s-s_\alpha]^{-1}e^{-(s-s_\alpha)t_o}$ are replaced by $e^{s_\alpha t}u(t-t_o)$. Note the inclusion of a turn-on time t_o since the definition of t=0 is arbitrary (say-a/c, or first arrival at the scatterer) [30].

While we are not concerned here with numerical computations per se, it is instructive to think of the general integral equation (2.2) as a matrix equation (via the moment method) with N expansion and N testing functions [19] (here chosen symmetrically) as

$$(\bar{Z}_{t_{n,m}}(s))\cdot(\bar{J}_{s_n}(s)) = (\bar{E}^{(inc)}_{t_n}(s)) \tag{2.5}$$

Then (2.4) becomes

$$(\bar{Z}_{t_{n,m}}(s_\alpha))\cdot(\bar{j}_{s_n})_\alpha = (0_n), \qquad \det((\bar{Z}_{t_{n,m}}(s_\alpha))) = 0 \tag{2.6}$$

$$\eta_\alpha(\vec{I}_l,\vec{I}_p) = \frac{1}{E_o\bar{f}(s_\alpha)} \frac{(\bar{E}^{(inc)}_{t_n}(s_\alpha))\cdot(j_{s_n})_\alpha}{(j_{s_n})_\alpha\cdot\frac{\partial}{\partial s}(\bar{Z}_{t_{n,m}}(s))\Big|_{s=s_\alpha}\cdot(j_{s_n})_\alpha}$$

Since these terms are experimentally observable and can be obtained from scattering data [53], then all correct formulations (integral equations or other) must give the same results. As can be seen in these formulas the s_α are aspect independent (i.e. independent of the incident-field parameters), this being a powerful result which will be discussed later in the context of scatterer identification. In the context of computations, the determinant equation in (2.6) gives a means of calculating the s_α. While one can find the zeros of $\det((\bar{Z}_{t_{n,m}}(s)))$ by various iterative procedures, there are two powerful contour-integral techniques involving the argument number (generalized) and the residue theorem which rely on the property of the determinant as an analytic function in the complex s plane [24].

One of the important early SEM results was that the response (2.3) included no branch integrals provided we are dealing with a finite-size, perfectly-conducting (or suitable-simple-media) object and the exciting waveform had no branch cuts [3,4]. Two-dimensional objects (infinite in one direction), on the other hand, do have a branch contribution [19]. If the object is embedded in an infinite lossy medium, there is also a branch cut introduced [31]. Branch cuts are readily included in the SEM formalism when needed and can be thought of as a continuous distribution of poles [24].

There is the case of the elusive entire function (or singularity at ∞). While this is an area of continuing research, let us briefly summarize what is currently known. Assume that the turn-on time t_o in (2.3) is judiciously

chosen so that it is when or before the incident wave reaches the observation position on S [19], and no sooner than the earliest time that the pole series converges [30]. The numerical results for step-function incident waves ($\tilde{f}(s) = 1/s$) show that no entire function is required in this case for the various example problems [19]. Furthermore there is no pole at $s = 0$ due to the lack of scatterer response there [3]. The impulse (δ function) response is another matter. As discussed in [40] this leads to an "essential entire function" related to the physical optics terms. Similarly, if one considers an antenna (such as a gap in a wire), one can have such an entire function as a simple additive constant in the input admittance [24,27]. Asymptotic behavior as $s \to 0$ and $s \to \infty$ can help in establishing the best form to use [24]. Note that this entire-function determination is separate from what is the most efficient early-time representation. Instead of summing up a large number of poles, one can use a small number of high-frequency terms (GTD) involving physical optics and creeping waves [40].

Mentioning a few related topics, there is the eigenmode expansion method (EEM) in which the integral operator in (2.2) is diagonalized to give s-dependent eigenmodes which can be used to order the natural modes [17,24]. This is not unique in the sense that there are various integral equations that one can use, giving different sets of eigenmodes. The impedance integral equation is of interest, in that one can consider the synthesis of eigenimpedances (shifting natural frequencies by impedance loading of the scatterer). There is also the whole subject of synthesis of equivalent circuits from the SEM representation of antennas and scatterers [24].

III. Extension to Scattered Far Fields

Consideration of the currents on the scatterer has already led to the location of the s_α in the s plane (aspect independent) as a useful property for identification. Extending to the far fields one can ask if there are other potentially useful properties. Early considerations of this were in terms of far natural modes [6,15,17,19].

Recently a more complete theory has emerged [58]. The far scattered field is written in SEM form as

$$\vec{\tilde{E}}_f(\vec{r},s) = \frac{E_o}{4\pi r} e^{-\gamma r} \sum_\alpha \tilde{f}(s_\alpha) W_\alpha \vec{\vec{C}}_{f_\alpha}(\vec{1}_r,\vec{1}_l)\cdot\vec{1}_p [s-s_\alpha]^{-1} e^{-(s-s_\alpha)t_o}$$

$$W_\alpha = w_\alpha^2 = -s_\alpha \mu_o \left\langle \vec{j}_{s_\alpha}(\vec{r}_s); \frac{\partial}{\partial s} \vec{\vec{\tilde{Z}}}_t(\vec{r}_s,\vec{r}'_s;s)\Big|_{s=s_\alpha} ; \vec{j}_{s_\alpha}(\vec{r}'_s) \right\rangle^{-1}$$

$$\overset{\leftrightarrow}{C}_{f_\alpha}(\vec{I}_r,\vec{I}_1) = \vec{C}_{r_\alpha}(\vec{I}_r)\vec{C}_\alpha(\vec{I}_1) \tag{3.1}$$

$$\vec{C}_\alpha(\vec{I}_1) = \langle \overset{\leftrightarrow}{I}_1 e^{-\gamma_\alpha \vec{I}_1\cdot\vec{r}'_s}; \vec{J}_{s_\alpha}(\vec{r}'_s)\rangle, \quad \vec{C}_{r_\alpha}(\vec{I}_r) = \langle \overset{\leftrightarrow}{I}_r e^{\gamma_\alpha \vec{I}_r\cdot\vec{r}'_s}; \vec{J}_{s_\alpha}(\vec{r}'_s)\rangle$$

$$\overset{\leftrightarrow}{I}_1 = \overset{\leftrightarrow}{I} - \vec{I}_1\vec{I}_1, \quad \overset{\leftrightarrow}{I}_r = \overset{\leftrightarrow}{I} - \vec{I}_r\vec{I}_r \text{ (transverse identities)}$$

Note the reciprocity relationship

$$\vec{C}_{r_\alpha}(\vec{I}_r) = \vec{C}_\alpha(-\vec{I}_r), \quad \overset{\leftrightarrow}{C}_{f_\alpha}(\vec{I}_r,\vec{I}_1) = \overset{\leftrightarrow}{C}{}^{T}_{f_\alpha}(\vec{I}_1,\vec{I}_r) \tag{3.2}$$

The scattering residue for the s_α pole takes the form of a single dyad (for a single mode $\vec{J}_{s_\alpha}$ (non degenerate)) which, taken as a 2x2 matrix, has zero determinant, this property being observable in experimental scattering data. Note that for each pole the polarization of the far field is determined by the vector $\vec{C}_{r_\alpha}(\vec{I}_r)$, which in combination with the complex exponential $e^{s_\alpha t}u(t-t_o)$ gives what can be termed elliptical spiral polarization. This is a characteristic of the scatterer, not the incident field, and so can be termed a scatterer polarization vector (as seen at the observer). Referring to Fig. 1, one can interpret this scatterer polarization as the average direction of the natural mode currents ($_\perp\overset{\leftrightarrow}{I}_r$) as weighted by the integral with γ_α along the $\vec{I}_r$ direction. For long slender objects this gives a simple geometric interpretation.

Figure 1 gives the unit vectors for incident and far scattered fields. Note that in the far-field expansion one cannot in general let $|s| \to \infty$ since the transition from near to far field is in general a function of s. In time domain this appears in the form of errors in the expression for very small time changes which do not concern us here.

In terms of coupling coefficients (scalars) we have

$$\eta_{f_\alpha}(\vec{I}_r,\vec{I}_m;\vec{I}_1,\vec{I}_p) = W_\alpha \vec{I}_m\cdot\overset{\leftrightarrow}{C}_{f_\alpha}(\vec{I}_r,\vec{I}_1)\cdot\vec{I}_p = \text{far coupling coefficient}$$

$$= \eta_{r_\alpha}(\vec{I}_r,\vec{I}_m)\eta_\alpha(\vec{I}_1,\vec{I}_p) \tag{3.3}$$

$$\eta_\alpha(\vec{I}_1,\vec{I}_p) = -\frac{W_\alpha}{s_\alpha\mu_o}\vec{I}_p\cdot\vec{C}_\alpha(\vec{I}_1) = \text{coupling coefficient}$$

$$\eta_{r_\alpha}(\vec{I}_r,\vec{I}_m) = -s_\alpha\mu_o\vec{I}_m\cdot\vec{C}_{r_\alpha}(\vec{I}_r) = \text{recoupling coefficient}$$

If we normalize η_α so that it has value 1 (and peak magnitude) at $\vec{I}_1 = \vec{I}_{1_o}$, $\vec{I}_p = \vec{I}_{p_o}$, and similarly for η_{r_α}, then we can have

$$\vec{I}_{m_o} = \vec{I}_{p_o}, \quad \vec{I}_{r_o} = -\vec{I}_{1_o}, \tag{3.4}$$

which gives the reciprocity-related result

$$\eta_\alpha^{(n)}(\vec{I}_1,\vec{I}_p) = \eta_{r_\alpha}^{(n)}(-\vec{I}_1,\vec{I}_p) \tag{3.5}$$

with superscript n denoting the normalized coefficients. Then the normalized far coupling coefficient is

$$\eta_{f_\alpha}^{(n)}(\vec{I}_r,\vec{I}_m;\vec{I}_1,\vec{I}_p) = \eta_{r_\alpha}(\vec{I}_r,\vec{I}_m)\eta_\alpha(\vec{I}_1,\vec{I}_p) \tag{3.6}$$

For the case of backscattering with measurement parallel to the incident field we have

$$\eta_{b_\alpha}(\vec{I}_1,\vec{I}_p) = \eta_{r_\alpha}(-\vec{I}_1\ \vec{I}_p)\eta_\alpha(\vec{I}_1,\vec{I}_p) = W_\alpha \vec{I}_p\cdot\ddot{\vec{C}}_{b_\alpha}(-\vec{I}_1,\vec{I}_1)\cdot\vec{I}_p$$

$$\ddot{\vec{C}}_{b_\alpha}(-\vec{I}_1,\vec{I}_1) = \vec{C}_\alpha(\vec{I}_1)\vec{C}_\alpha(\vec{I}_1) \qquad \text{(symmetric dyad)} \tag{3.7}$$

In normalized form this is

$$\eta_{b_\alpha}^{(n)}(\vec{I}_1,\vec{I}_p) = \eta_{r_\alpha}^{(n)}(-\vec{I}_1,\vec{I}_p)\eta_\alpha^{(n)}(\vec{I}_1,\vec{I}_p) = [\eta_\alpha^{(n)}(\vec{I}_1,\vec{I}_p)]^2 \tag{3.8}$$

This is a powerful result in that it implies that one can measure either $\eta_{b_\alpha}^{(n)}$ (far field) or $\eta_\alpha^{(n)}$ (on S) and infer the other. Note that this applies for a case (typical) of non-degenerate modes.

If one has the various polarizations in transmission and reception available, then one can deal with the scattering residue dyadic. For backscattering, we have the usual (for radar) h,v coordinate orientations as in Fig. 1. Then it is convenient to introduce

$$\ddot{\vec{c}}_{b_\alpha}(\vec{I}_1) = W_\alpha \ddot{\vec{C}}_{b_\alpha}(\vec{I}_1) = \vec{c}_\alpha(\vec{I}_1)\vec{c}_\alpha(\vec{I}_1), \qquad \vec{c}_\alpha(\vec{I}_1) = w_\alpha \vec{C}_\alpha(\vec{I}_1) \tag{3.9}$$

In this form the $\overleftrightarrow{c}_{b_\alpha}$ is what is measurable in (3.1), the normalization constant being an artifice of scaling the natural mode. For non-degenerate modes this dyad is characterized by a single 2-component (transverse) complex vector. This is to be compared to the usual case of a backscattering dyad as a symmetric (due to reciprocity) 2x2 matrix characterized by three complex numbers.

If there is a modal degeneracy, the situation is a bit more complicated. This occurs for a body of revolution (C_∞ symmetry) which, it it has a symmetry plane containing the axis, gives a two-fold degeneracy with symmetric and antisymmetric parts with respect to the symmetry plane P through the observer. Then (3.9) generalizes to (5 real numbers)

$$\overleftrightarrow{c}_{b_\alpha}(\vec{I}_1) = \vec{c}_{sy,\alpha'}(\vec{I}_1)\vec{c}_{sy,\alpha'}(\vec{I}_1) + \vec{c}_{as,\alpha'}(\vec{I}_1)\vec{c}_{as,\alpha'}(\vec{I}_1)$$

$$= c_{b_{sy,\alpha'}}(\vec{I}_1)\vec{I}_{sy}(\vec{I}_1)\vec{I}_{sy}(\vec{I}_1) + c_{b_{as,\alpha'}}(\vec{I}_1)\vec{I}_{as}(\vec{I}_1)\vec{I}_{as}(\vec{I}_1) \quad (3.10)$$

In terms of h,v components the 2x2 matrix has (transverse components only)

$$\det(\overleftrightarrow{c}_{b_\alpha}(\vec{I}_1)) = \det((c^{(\alpha)}_{b_{n,m}}(\vec{I}_1))) = c^{(\alpha)}_{b_{h,h}}(\vec{I}_1)c^{(\alpha)}_{b_{v,v}}(\vec{I}_1) - c^{(\alpha)^2}_{b_{h,v}}(\vec{I}_1)$$

$$- c_{b_{sy,\alpha'}}(\vec{I}_1)c_{b_{as,\alpha'}}(\vec{I}_1) \quad (3.11)$$

$$\mathrm{tr}(\overleftrightarrow{c}_{b_\alpha}(\vec{I}_1)) = \mathrm{tr}((c^{(\alpha)}_{b_{n,m}}(\vec{I}_1))) = c^{(\alpha)}_{b_{h,h}}(\vec{I}_1) + c^{(\alpha)}_{b_{v,v}}(\vec{I}_1)$$

$$- c_{b_{sy,\alpha'}}(\vec{I}_1) + c_{b_{as,\alpha'}}(\vec{I}_1)$$

from which both eigenvalues are readily determined. The normalized eigenvectors are real unit vectors.

The various types of scattering residue dyadics treated in [58] are summarized in Table 1. Note that further reductions occur for cases where s_α is on the negative real axis of the s plane due to the real-valued nature of measurable parameters there.

In the context of the far field, the entire function contribution is further complicated due to the time derivative (or multiplication by s) in going from currents to far fields. This emphasizes the high-frequency or

fast-time-change (early-time plus possibly other times) part of the scattered field, where the entire function should contribute most. Appropriate choice of the incident-field waveform F(t) should suppress this somewhat, say by beginning the waveform as a ramp function. This requires further investigation. Note also that as $s \to \infty$ the far-field approximation breaks down, further complicating matters. In any event, the pole terms contain the information discussed here so our concern is being able to find these in the experimental data.

IV. Natural-Resonance-Based Target Discrimination

The SEM exposed in Sections II and III suggests that the late-time scattered field of a target, interrogated by pulsed EM radiation, can be represented as a sum of natural-resonance modes. Since the excitation-independent natural frequencies depend upon the detailed size and shape of the target, then the full complement of those frequencies is unique to a specific target and provides a potential basis for its identification. A prominent early effort to approximate the transient and impulse response of a target was that of [2]. Here the emphasis was on the early-time (profile function) and late-time ramp response (polarizability), while the presence of a resonance region was recognized. This was followed by attempts [8,9,11,12,64] to identify and discriminate targets by examination of the natural-frequency content in their pulse-response waveforms. Other efforts on target imaging [10,16,20] were based upon the broadband transient responses of those targets. These methods are limited by the low energy content in the late-time transient responses of practical low-Q targets.

Identification of targets based upon their natural resonances precipitated extensive research on the extraction of natural frequencies from measured target pulse responses. The first such efforts [13,18] were based upon Prony's method, but in the practical low signal-to-noise environment only one or several modes could be reliably extracted using that inherently ill-conditioned algorithm. Various improvements to Prony's method included [26], where an effort was made to identify and exclude non-physical "curve-fitting" poles. Finally, efforts to overcome the ill-conditioned nature of natural-frequency extraction from noisy measured data [35,54] exploited the use of multiple data sets.

Various discriminant waveforms, synthesized to identify a specific target response from among an ensemble of such returns, have emerged. These are linear time-domain filters which, when convolved with the target responses to

which they are matched, annihilate pre-selected natural-frequency content of those responses. The excitation-independent natural frequencies of the relevant target can be measured in the laboratory using scale-model targets in an optimal low-noise environment. The first such synthesized signal was Kennaugh's K-pulse [28], defined as that waveform of minimal duration which would "kill" all the natural modes in the resulting target response. More recent discrimination waveforms [44,49] are the (extinction) E-pulse and (single-mode) S-pulse, which are detailed below. The E-pulse is synthesized to annihilate, when convolved with a band-limited late-time target pulse response, all natural modes present in that response. The S-pulse is an E-pulse synthesized to annihilate all but one natural mode of a target, so when it is convolved with that target response a single natural mode emerges. Characteristics of the K-pulse and the E-pulse have recently [52] been compared. A similar discriminant pulse [55], based upon natural-mode annihilation, has been conceptualized using a different synthesis scheme. Parametric modeling methods have also been exploited [25] to identify targets from their transient electromagnetic returns. Discriminant waveforms for any number of targets can be synthesized, based upon natural frequencies measured in the laboratory, and stored in disk files for subsequent convolution with a measured target return to discriminate that target. The most recent efforts on discriminant waveform synthesis [50,53,60,65] have resulted in methods to construct those signals directly from measured target response data, without a-priori knowledge of the natural frequencies. Each of those techniques ultimately yields the natural frequencies from zeros of the corresponding discriminant signal spectrum. Synthesis of the E-pulse is detailed below, as well as its implementation for natural-mode extraction and target discrimination.

Synthesis conditions for an E-pulse waveform can be easily established. It has been shown that the scattered field response of a conducting object can be written in the late-time as a sum of damped sinusoids

$$r(t) = \sum_{n=1}^{N} a_n e^{\sigma_n t} \cos(\omega_n t + \phi_n) \qquad t > t_L \tag{4.1}$$

where T_L is the beginning of the late-time response, a_n and ϕ_n are the aspect dependent amplitude and phase of the nth mode, $s = \sigma + j\omega$, and only N modes are assumed excited by the incident field waveform. The convolution of an E-pulse waveform e(t) having duration T_e switch the above response is given by

$$c(t) = \sum_{n=1}^{N} a_n |E(s_n)| e^{\sigma_n t} \cos(\omega_n t + \psi_n) \tag{4.2}$$

where ψ_n is dependent on e(t) and

$$E(s) = L\{e(t)\} = \int_0^{T_e} e(t) e^{-st} dt \tag{4.3}$$

is the Laplace transform of the E-pulse. Constructing an E-pulse to produce a null late-time convolved response, c(t) = 0, is seen to require

$$E(s_n) = E(s_n^*) = 0 \qquad 1 \le n \le N \tag{4.4}$$

A single-mode extraction signal necessitates the same except for $n \neq m$ to leave the mth mode "unextinguished" in the convolved response.

The E-pulse is represented as

$$e(t) = e^f(t) + e^e(t) \tag{4.5}$$

where $e^f(t)$ is a forcing component which excites the target's response, and $e^e(t)$ is an extinction component which extinguishes the response due to $e^f(t)$. The forcing component is chosen freely, while the extinction component is expanded in a set of basis functions

$$e^e(t) = \sum_{m=1}^{M} \alpha_m f_m(t) \tag{4.6}$$

and the synthesis conditions are applied. For an E-pulse designed to extinguish all the modes of a target response, (4.4) results in a matrix equation for the basis function amplitudes

$$\begin{bmatrix} F_1(s_1) & F_2(s_1) \cdots F_M(s_1) \\ \vdots & \\ F_1(s_N) & F_2(s_N) \cdots F_M(s_N) \\ F_1(s_1^*) & F_2(s_1^*) \cdots F_M(s_1^*) \\ \vdots & \\ F_1(s_N^*) & F_2(s_N^*) \cdots F_M(s_N^*) \end{bmatrix} \begin{bmatrix} \alpha_1 \\ \alpha_2 \\ \vdots \\ \alpha_n \end{bmatrix} = - \begin{bmatrix} E^f(s_1) \\ \vdots \\ E^f(s_N) \\ E^f(s_1^*) \\ \vdots \\ E^f(s_N^*) \end{bmatrix} \tag{4.7}$$

where

$$F_m(s) = L\{f_m(t)\}, \quad E_f(s) = L\{e^f(t)\}$$

and $M = 2N$ is chosen to make the matrix square. Note that if a DC offset artifact is present in the measured response the E-pulse can be synthesized to remove the DC by demanding, in addition to the above requirements, E(s=0) = 0.

The matrix equation (4.7) has a solution for any choice of E-pulse duration. However, for some choices of T_e the determinant of the matrix vanishes, and (4.7) has a solution only if $e^f(t) = 0$. This type of E-pulse is termed a "natural" E-pulse, while all others are called "forced" E-pulses.

A variety of basis functions have been used in the expansion (4.6), including δ-functions [44,51], Fourier cosines [39], damped sinusoids [33], and polynomials [42,43]. While each choice has its own important motivation, perhaps the most versatile expansion is in terms of subsectional basis functions [49]

$$f_m(t) = \begin{cases} g(t-[m-1]\Delta) & (m-1)\Delta \le t \le m\Delta \\ 0 & \text{elsewhere} \end{cases} \tag{4.8}$$

so that $T_e = 2N\Delta$ and

$$F_m(s) = Z^m F_1(s) e^{s\Delta}, \qquad Z = e^{-s\Delta} \tag{4.9}$$

giving a matrix of the Vandermonde type. The determinant of this matrix is zero when

$$\Delta = \frac{p\pi}{\omega_k}, \qquad p = 1,2,3,\ldots, \qquad 1 \le k \le N \tag{4.10}$$

revealing that the duration of a natural E-pulse is only dependent upon the imaginary part of one of the natural frequencies. The minimum natural E-pulse duration is just

$$T_e = 2N \frac{\pi}{\omega_{max}} \tag{4.11}$$

where ω_{max} is the largest radian frequency among the modes.

Early researchers interested in experimentally determining natural frequencies concentrated on Prony's method [13,21,46] but soon found the technique to be highly sensitive to both random noise and estimates of the number of poles present in the data [22,25]. In its basic form, Prony's method is inherently an ill-conditioned algorithm [1], but several recent improvements have made the scheme more robust [52] while techniques have also been devised for estimating pole content [37,61]. A variety of other techniques for resonance extraction have been introduced, including the pencil-of-function methods [34,48,59] and several nonlinear [38,47,58] and combined linear-non-

linear [7,14] least square approaches. In addition, Ksienski [41] has outlined the benefits of using multiple data sets, while Baum has stressed the importance of incorporating a priori information about the scatterer [36].

Particularly suited for radar target applications are a group of resonance extraction techniques which synthesize the discriminant waveform directly from the measured data, and provide the natural resonance frequencies as a by-product of the algorithm. Several authors have developed algorithms around this approach [50,60,65] and typical is the E-pulse mode extraction scheme described as follows.

Let $r_k(t)$ represent the scattered field, current or charge response of a target to an interrogating waveform, measured at aspect angle k, $k = 1,\ldots,K$. The convolution of an E-pulse for the target with the measured response will be zero at each aspect angle. Writing the convolution in the time domain and using the expansion (4.6) gives

$$\sum_{m=1}^{2N} \alpha_m \int_0^{T_e} f_m(t')r_k(t - t')dt' = -\int_0^{T_e} e^f(t')r_k(t - t')dt' \qquad (4.12)$$

$$k = 1,2,\ldots,K, \qquad t > T_{L_k} + T_e$$

where T_{L_k} is the beginning of late-time for the kth measurement and N is the number of modes expected. Matching both sides of the equation at discrete times t_ℓ, $\ell = 1,2,\ldots,L$, yields a matrix equation for the E-pulse amplitudes (α_m). Generally the product KL is chosen to be greater than 2N, so that the matrix equation is overdetermined, and a solution is obtained using least squares and the singular-value decomposition. Once the E-pulse waveform is determined, the natural frequencies in the measured response can be determined by solving for the roots (s_n) to $E(s) = 0$. That is, if the convolution of $r_k(t)$ and $e(t)$ is zero, $E(s)$ must be zero at the complex frequencies comprising $r_k(t)$. If subsectional basis functions are used in the E-pulse expansion, and the forcing function is chosen to be an identical subsectional function, then by (4.9) the solutions to $E(s) = 0$ are merely the roots of a polynomial equation

$$\sum_{m=1}^{2N+1} \alpha_m Z^m = 0 \qquad (4.13)$$

where α_{2N+1} is the amplitude of the forcing pulse.

The above scheme is found to be quite insensitive to both the presence of random Gaussian noise and to estimates of the modal content of the measured

data, if the proper E-pulse duration is used. See [53] for typical results using measured data. Incorporating multiple aspect data is important, as the modal amplitudes (α_n) are highly aspect dependent--some modes may not be excited at certain aspects.

Empirical results show that if T_e is chosen to be less than the minimum natural E-pulse duration (4.11) the resulting E-pulse is highly oscillatory with a majority of its energy above ω_{max} [42] and poor results are obtained in the presence of random noise. It is tempting to solve (4.12) in the least squares sense and choose the E-pulse duration which produces a minimum error, but this approach is often misleading. For certain values of T_e a good solution to (4.12) may produce solutions to (4.13) which are poor approximations to the actual resonant frequencies present in $r_k(t)$. This dilemma can be resolved by choosing the value of T_e which results in the solution to (4.13) which best reproduces the measured data; i.e., T_e is chosen to minimize

$$\epsilon = \sum_k \epsilon_k = \sum_k \frac{1}{\epsilon_k} ||r_k(t) - \hat{r}_k(t)||^2 \tag{4.14}$$

where ϵ_k is the late-time energy in $r_k(t)$, $\hat{r}_k(t)$ is the reconstructed waveform

$$\hat{r}_k(t) = \sum_{n=1}^{N} \hat{a}_{nk} e^{\hat{\sigma}_n t} \cos(\hat{\omega}_n t + \hat{\phi}_{nk}) \tag{4.15}$$

and the norm is over the late time $t > T_{L_k} + T_e$. Here $(\hat{s}_n = \hat{\sigma}_n + j\hat{\omega}_n)$ are the solutions to (4.13) while (a_{nk}, ϕ_{nk}) minimize ϵ_k with T_e and $(\hat{s}_n)$ fixed. Interestingly, an E-pulse duration found in this manner very often approaches that of a natural E-pulse (4.10), suggesting that the natural E-pulse is optimum for target discrimination in the presence of random noise.

V. Experimental Validation of the E-pulse Method

The E-pulse radar target discrimination scheme has been successfully demonstrated on numerous occasions using measurements taken on a ground plane range [44,49,63]. Recently, a time domain anechoic chamber has been implemented at Michigan State University for the purpose of demonstrating the E-pulse technique in a free field environment. The chamber allows a simulation of the free-space radar environment where realistic scale-model targets can be illuminated at arbitrary aspect and polarization.

The chamber is 24' long by 12' wide by 12' high and is lined with 12" pyramid absorber. A pulse generator provides a half nanosecond duration pulse to an American Electronic Laboratories model H-1734 wideband horn (0.5-6

GHz) which has been resistively loaded to reduce inherent oscillations, and the field scattered from a radar target is received by an identical horn. A waveform processing oscilloscope is used to acquire the received signal and the data is then passed to a microcomputer for processing and analysis.

Accurate discrimination among eight different target models at a variety of aspects has been demonstrated using the free field range. The targets, shown in Fig. 2, include simple aluminum models as well as detailed cast-metal models, and range in fuselage length of from six to eighteen inches. Fig. 3 shows the responses of the big F-15 and A-10 target models measured at a 45° aspect angle (0° aspect is nose-on to the horns), with the early and late-time portions of the responses indicated. Note that the late-time period begins at different times for the two targets, due to their dissimilar sizes. E-pulse waveforms have been constructed to eliminate all the modes of each target using the E-pulse mode extraction scheme with measurements from five different aspect angles. These waveforms are shown in Fig. 4.

Discrimination between the big F-15 and the A-10 can be accomplished by convolving the E-pulses with the measured responses, and observing which E-pulse produces the smallest late-time output. First assume the 45° response of the big F-15 is from an unknown target. Figure 5a shows the convolutions of the two E-pulses with this response. Clearly the big F-15 E-pulse produces the smaller late-time signal, and thus the response is identified as coming from a big F-15 aircraft. For the complementary situation, assume the 45° response of the A-10 is from an unknown target. Figure 5b shows the convolutions of the E-pulses with this response. In this case the A-10 E-pulse produces the smaller late-time signal, indicating the response is from an A-10 aircraft.

As the number of prospective targets becomes large, a visual inspection of the convolved outputs becomes more subjective, and eventually impractical. A scheme has therefore been devised to automate the discrimination decision. Ideally, if the E-pulse convolutions were uncorrupted, the energy ratio

$$E = \frac{\int_{T_{LES}}^{T_{LEE}} c^2(t)dt}{\int_0^{T_e} e^2(t)dt} \qquad (5.1)$$

would be zero only for the correct E-pulse. Here c(t) is the convolution of the E-pulse e(t) with the measured response, and T_{LES} is the earliest time at

which the unknown target convolution is CERTAIN to be a unique series of natural modes

$$T_{LES} = T_e + 2T_r \tag{5.2}$$

where T_r is the one-way transit time of the largest dimension of the target corresponding to the E-pulse. (The largest dimension must be used since the target aspect is unknown.) The end of the energy window, T_{LEE}, is chosen so that the window width, T_{LEE}-T_{LES}, is the same for all convolutions.

To show that successful discrimination is possible regardless of target aspect, E-pulses for the eight targets have been convolved with the responses of the big F-15 measured at five different aspect angles from 0° (nose-on) to 90° (broadside). The energy ratio (5.1) has been plotted as a function of aspect angle in Fig. 6 for each expected target. It is obvious that for all aspects tested the big F-15 produces the smallest late-time convolved response, with a minimum 10 dB difference in late-time energy. Thus, the big F-15 is identified from among all the possible targets at each aspect angle.

Finally, discrimination among all eight targets can be demonstrated when any of the eight is the unknown target. Table 2 shows the energy ratios (5.1) obtained by assuming that each target in turn is the unknown target and convolving the E-pulses for each of the eight expected targets with the response of the unknown target. Here the target responses were all measured at 45° aspect. Accurate discrimination for each target is indicated by the minimum energy ratio being due to the E-pulse of the unknown target. For example, the convolution of the F-18 E-pulse with the F-18 response produces a late-time energy 29.8 dB below that produced by the convolution of the medium 707 E-pulse with the F-18 response, and 15.3 dB below that produced by the convolution of the B-1 bomber E-pulse with the F-18 response.

VI. Extensions and Implementation

The theoretical basis for the application of SEM concepts to aspect-independent target identification/discrimination is rather well established and the feasibility of the E-pulse scheme has been well verified in the laboratory with scale models of various aircraft as described in this paper. A possible radar system based on the E-pulse techniques has been discussed previously [44]. To advance this scheme to practical application, there remain some major tasks to be investigated: (1) the design of optimal transmitting and receiving antennas and associated optimal waveforms, (2) the

generation of high power EM pulses, and (3) the refinement of the E-pulse synthesis technique.

Concerning the first task of the antenna and waveform design for this system, there is very little work done. Considering various aircraft targets, major resonant mode frequencies are of the order of a few to tens of MHz, implying pulse widths in the range of ten to a hundred or so nanoseconds to maximize energy content at these frequencies. To radiate and receive this pulse waveform, various antenna elements such as tapered and resistively loaded dipoles, radiating transmission line antennas and TEM horn antennas, etc. should be investigated. An array of these elements could be used to increase the signal strength and provide some beam steering capability. Two or more such arrays, sufficiently separated, might be used to give more accurate location of the target. Alternatively, one might combine such an array with a more traditional radar designed for high spatial resolution. It is also worthwhile to look into the possibility of modifying the antenna systems of existing radar systems such as over-the-horizon radars which utilize a similar frequency band.

There are other types of transmitted waveforms which may warrant consideration for the E-pulse radar discrimination scheme. Since the transmitted radar signal is intended to excite the resonant modes of the target, a waveform comprising a set of damped sinusoids resembling the target's resonance modes may be transmitted instead of a pulse. Another interesting waveform may be a set of cw sinusoids of different frequencies and finite durations to be transmitted simultaneously to excite a set of selected resonant modes of the target. Of course, the antenna design will be affected by the type of transmitted waveform.

Regarding the second task of the generation of high power EM pulses, there are indications that some types of high power EM pulse sources are already available, developed in other fields such as for the electromagnetic pulse.

Finally, the task of refining the E-pulse synthesis technique seems a never ending effort. Even though we and other researchers have studied this topic for many years, an optimal synthesis technique has yet to be developed. The synthesis technique includes an accurate extraction of the natural frequencies of the target from its measured pulse response, and the synthesis of an optimal E-pulse waveform which provides the most sensitive discrimination capability as well as the most robust noise tolerance.

Before ending this paper, two questions raised by a reviewer are answered: (1) The E-pulse technique is designed for non-cooperative target recognition. When it is used for IFF purpose, some unfriendly targets with unknown structure information can only be identified as unknown targets, (2) the E-pulse technique will be affected by a shift in the target's resonance frequencies. However, the shift due to target motion is extremely small (in the order of v/c where v is the target speed and c the speed of light) and that due to target deformation can be taken into account for if the type of deformation is known beforehand.

References

[1] F.B. Hildebrand, Introduction to Numerical Analysis, McGraw-Hill, New York, 1956.

[2] E.M. Kennaugh and D.L. Moffatt, "Transient and impulse response approximations," Proc. IEEE, vol. 53, pp. 893-901, Aug. 1965.

[3] C.E. Baum, "On the singularity expansion method for the solution of electromagnetic interaction problems," Interaction Note 88, Airforce Weapons Lab, 1971.

[4] L. Marin and R.W. Latham, "Analytical properties of the field scattered by a perfectly conducting, finite body," Interaction Note 92, Air Force Weapons Lab, 1972, and L. Marin, Natural-Mode Representation of Transient Scattered Fields, IEEE Trans. Antennas and Propagation, 1973, pp. 809-818.

[5] F.M. Tesche, "On the singularity expansion method as applied to electromagnetic scattering from thin-wires," Interaction Note 102, Air Force Weapon Lab, 1972, also as F.M. Tesche, On the Analysis of Scattering and Antenna Problems using the Singularity Expansion Technique, IEEE Trans. Antennas and Propagation, 1973, pp. 52-63.

[6] C.E. Baum, "Singularity expansion of electromagnetic fields and potentials radiated from antennas or scattered from objects in free space," Sensor and Simulation, Note 179, Air Force Weapons Lab, 1973.

[7] G.H. Golub and V. Pereyra, "The differentiation of pseudo-inverse and nonlinear least squares problems whose variables separate," SIAM Journal of Numerical Analysis, vol. 10, pp. 413-432, 1973.

[8] A.J. Berni, "Target identification by natural resonance estimation," IEEE Trans. Aerospace Elect. Sys., vol. AES-11, pp. 147-154, March 1975.

[9] L.W. Pearson, M.J. VanBlaricum and R. Mittra, "A new method for radar target recognition based upon the singularity expansion method," Record of IEEE International Radar Conference, Arlington, VA, pp. 452-457, April 1975.

[10] A.G. Repjar, A.A. Ksinski and L.J. White, "Object identification from multi-frequency radar returns," Radio Electronic Eng., vol. 45, pp. 161-167, April 1975.

[11] D.L. Moffatt and R.K. Mains, "Detection and discrimination of radar targets," IEEE AP-S Trans., vol. AP-23, pp. 358-367, May 1975.

[12] F.D. Deadrick, H.G. Hudson, E.K. Miller, J.A. Landt and A.J. Poggio, "Object identification via pole extraction from transient fields," USNC/URSI Meeting, University of Illinois, Urbana, IL, p. 67, June 1975.

[13] M.L. VanBlaricum and R. Mittra, "A technique for extracting the poles and residues of a system directly from its transient response," IEEE AP-S Trans., vol. AP-23, pp. 777-781, Nov. 1975.
[14] L.C. Kaufman, "A variable projection method for solving separable nonlinear least squares problems," BIT, vol. 15, pp. 49-57, 1975.
[15] F.M. Tesche, "The far-field response of a step-excited linear antenna using SEM," IEEE Trans. Antennas and Propagation, 1975, pp. 834-838.
[16] J.D. Young, "Radar imaging from ramp response signatures," IEEE AP-S Trans., vol. AP-24, pp. 276-282, May 1976.
[17] C.E. Baum, "Emerging technology for transient and broad-band analysis and synthesis of antennas and scatterers," Proc. IEEE, pp. 1598-1616, 1976
[18] C.W. Chuang and D.L. Moffatt, "Natural resonance of radar target via Prony's method and target discrimination," IEEE Trans. Aerospace Elect. Sys., vol. AES-12, pp. 583-589, 1976.
[19] C.E. Baum, "The singularity expansion method," in L.B. Felsen (ed.), Transient Electromagnetic Fields, Springer Verlag, 1976, pp. 129-179.
[20] K.A. Shubert, J.D. Young and D.L. Moffatt, "Synthetic radar imagery," IEEE AP-S Trans., vol. AP-25, pp. 477-483, July 1977.
[21] A.J. Poggio, M.L. VanBlaricum, E.K. Miller and R. Mittra, "Evaluation of a processing technique for transient data," IEEE AP-S Trans., vol. AP-26, pp. 165-173, 1978.
[22] M.L. VanBlaricum and R. Mittra, "Problems and solutions associated with Prony's method for processing transient data," IEEE AP-S Trans., vol. AP-26, pp. 174-182, 1978.
[23] C.L. Dolph and R.A. Scott, "Recent developments in the use of complex singularities in electromagnetic theory and elastic wave propagation," in P.L.E. Uslenghi (ed.), Electromagnetic Scattering, Academic Press, 1978, pp. 503-570.
[24] C.E. Baum, "Toward an engineering theory of electromagnetic scattering: The singularity and eigenmode expansion methods," in P.L.E. Uslenghi (ed.), Electromagnetic Scattering, Academic Press, 1978, pp. 571-651.
[25] D.G. Dudley, "Parametric modelling of transient electromagnetic systems," Radio Science, vol. 14, pp. 387-396, 1979.
[26] J.N. Brittingham, E.K. Miller and J.L. Willows, "Pole extraction from real frequency information," Proc. IEEE, vol. 68, pp. 263-273, Feb. 1980.
[27] C.E. Baum and B.K. Singaraju, "The singularity and eigenmode expansion methods with application to equivalent circuits and related topics," in V.K. Varadan and V.V. Varadan, Acoustic, Electromagnetic and Elastic Wave Scattering - Focus on the T-Matrix Approach, Pergamon, 1980, pp. 431-452.
[28] E.M. Kennaugh, "The K-pulse concept," IEEE AP-S Trans., vol. AP-29, pp. 327-331, March 1981.
[29] K.A. Michalski, "Bibliography of the singularity expansion method and related topics," Electromagnetics, pp. 493-511, 1981.
[30] C.E. Baum and L.W. Pearson, "On the convergence and numerical sensitivity of the SEM pole-series in early-time scattering response," Electromagnetics, pp. 209-228, 1981.
[31] D.V. Giri and F.M. Tesche, "On the use of singularity expansion method for analysis of antennas in conducting media," Electromagnetics, pp. 455-471, 1981.

[32] L.W. Pearson and L. Marin (eds.), "Special issue on the singularity expansion method," Electromagnetics, vol. 1, No. 4, 1981.
[33] K.M. Chen, D.P. Nyquist, D. Westmoreland, C.I. Chuang and Byron Drachman, "Radar waveform synthesis for single-mode scattering by a thin cylinder and application for target discrimination," IEEE AP-S Trans., vol. AP-30, pp. 867-880, September 1982.
[34] V.K. Jain, T.K. Sarkar and D.D. Weiner, "Rational modeling by pencil-of-function methods," IEEE Trans. on Acoustics, Speech and Signal Processing, vol. ASSP-31, pp. 564-573, June 1983.
[35] D.A. Ksienski, "Pole and residue extraction from measured data in the frequency domain using multiple data sets," Radio Science, vol. 20, pp. 13-19, Jan.-Feb. 1985.
[36] C.E. Baum, "A priori application of results of electromagnetic theory to the analysis of electromagnetic interaction data," Interaction Note 444, Air Force Weapons Laboratory, February 1985.
[37] A.G. Ramm, "Extraction of resonances from transient fields," IEEE AP-S Trans., vol. AP-33, pp. 223-226, February 1985.
[38] B. Drachman and E. Rothwell, "A continuation method for identification of the natural frequencies of an object using a measured response," IEEE AP-S Trans., vol. AP-33, pp. 445-450, April 1985.
[39] E. Rothwell, D.P. Nyquist, K.M. Chen and B. Drachman, "Radar target discrimination using the extinction-pulse technique," IEEE AP-S Trans., vol. AP-33, pp. 929-937, September 1985.
[40] E. Heyman and L.B. Felsen, "A wavefront interpretation of the singularity expansion method," IEEE Trans. Antennas and Propagation, pp. 706-718, 1985.
[41] D.A. Ksienski, "Pole and residue extraction from measured data in the frequency domain using multiple data sets," Radio Science, vol. 20, No. 1, pp. 13-19, 1985.
[42] E. Rothwell, "Radar target discrimination using the extinction-pulse technique," Ph.D. dissertation, Michigan State University, 1985.
[43] G. Turhan and D. Moffatt, "Expansion of K-pulses in terms of Legendre polynomials for an arbitrary target," National Radio Science Meeting, June 10, 1986.
[44] K-M Chen, D.P. Nyquist, E.J. Rothwell, L.L. Webb and B. Drachman, "Radar target discrimination by convolution of radar returns with extinction pulses and single-mode extraction signals," IEEE AP-S Trans., vol. AP-34, pp. 896-904, July 1986.
[45] C.E. Baum, "The singularity expansion method: background and developments," Electromagnetics, 1981, pp. 351-360, and updated in IEEE Antennas and Propagation Newsletter, pp. 15-23, August 1986.
[46] C.W. Chuang and D.L. Moffatt, "Natural resonances of radar targets via Prony's method and target discrimination," IEEE Trans. Aerospace Elect. Sys., vol. AES-12, pp. 583-589, September 1986.
[47] D.G. Dudley and D.M. Goodman, "Transient identification and object classification," in Time-Domain Measurements in Electromagnetics, E.K. Miller, Ed., Van Nostrand Reinhold, New York, pp. 456-497, 1986.
[48] A.J. Mackay and A. McCowen, "An improved pencil-of-function method and comparisons with traditional methods of pole extraction," IEEE AP-S Trans., vol. AP-35, pp. 435-441, April 1987.
[49] E.J. Rothwell, K.M. Chen, D.P. Nyquist and W. Sun, "Frequency domain E-pulse synthesis and target discrimination," IEEE AP-S Trans., vol. AP-35, pp. 426-434, April 1987.

[50] E. Rothwell, K.M. Chen and D.P. Nyquist, "Extraction of the natural frequencies of a radar target from a measured response using E-pulse techniques," IEEE AP-S Trans., vol. AP-35, pp. 715-720, June 1987.
[51] F.Y.S. Fok, D.L. Moffatt and N. Wang, "K-pulse estimation from the impulse response of a target," IEEE AP-S Trans., vol. AP-35, pp. 926-933, August 1987.
[52] F.Y.S. Fok and D.L. Moffatt, "The K-pulse and the E-pulse," IEEE AP-S Trans., vol. AP-35, pp. 1325-1326, Nov. 1987.
[53] E.J. Rothwell and K.M. Chen, "A hybrid E-pulse/least squares technique for natural resonance extraction," Proc. IEEE, pp. 296-298, March 1988.
[54] S-W Park and J.T. Cordaro, "Improved estimation of SEM parameters from multiple observations," IEEE Trans. Aerospace Elect. Sys., vol. 30, pp. 145-153, May 1988.
[55] M.A. Morgan, "Scatterer discrimination based upon natural resonance annihilation," Journal of Electromagnetic Waves and Applications, vol. 2, pp. 481-502, May/June 1988.
[56] C.E. Baum, "On the eigenmode expansion method for electromagnetic scattering and antenna problems, part II: asymptotic expansion of eigenmode-expansion parameters in the complex-frequency plane," Interaction Note 1472, Air Force Weapons Laboratory, 1988.
[57] C.E. Baum, "SEM and EEM scattering matrices, and time-domain scatterer polarization in the scattering residue matrix," in W.-M. Boerner (ed.), Proceedings of NATO-ARW-DIMRP 1988, Reidel, Dordrecht (in publication).
[58] S. Al Khouri-Ibrahim, R. Gomez-Martin, F.J. Munoz-Delgado and V. Ramirez-Gonzalez, "Extraction of the poles of noisy rational signals by the continuation method," IEE Proceedings, Part F, pp. 57-62, February 1989.
[59] Y. Hua and T. Sarkar, "Generalized pencil-of-function method for extracting poles of an EM system from its transient response," IEEE AP-S Trans., vol. AP-37, pp. 229-234, February 1989.
[60] G. Turhan-Sayan and D.L. Moffatt, "Substructure-related K-pulse estimation for an aircraft from full-scale radar data," URSI Radio Science Meeting, Syracuse University, Syracuse, NY, June 1989.
[61] Y. Hua and T.K. Sarkar, "A discussion of E-pulse method and Prony's method for radar target resonance retrieval from scattered field," IEEE AP-S Trans., vol. AP-37, pp. 944-946, July 1989.
[62] G. Majda, W. Strauss and M. Wei, "Computation of exponentials in transient data," IEEE AP-S Trans., vol. AP-37, pp. 1284-1290, October 1989.
[63] W. Sun, "Scattering of transient electromagnetic waves and radar target discrimination," Ph.D. dissertation, Michigan State University, 1989.
[64] W.E. Howell and H. Uberall, "Selective observation of resonances via their ringing in transient radar scattering, as illustrated for conducting and coated spheres," IEEE AP-S Trans., vol. AP-38, pp. 293-298, March 1990.
[65] J-P.R. Bayard and D.H. Schaubert, "Target identification using optimization techniques," IEEE AP-S Trans., to appear.

E-Pulse / Target Response	BF15	MB707	B1B	SB707	F18	TB747	SF15	A-10
BF15	**-25.7 dB**	-11.8	-11.0	- 6.9	- 8.5	- 0.8	- 3.1	0
MB707	-20.0	**-32.0**	-16.9	- 9.1	- 9.6	- 3.3	- 4.8	0
B1B	-11.2	0	**-23.4**	- 7.7	- 7.0	- 4.5	- 3.1	- 1.3
SB707	-16.7	- 0.8	-20.1	**-25.1**	- 8.0	0	- 2.5	- 3.8
F18	- 7.1	0	-14.5	- 2.6	**-29.8**	-11.8	- 1.9	- 4.6
TB747	-10.5	- 0.1	- 5.0	0	- 6.0	**-21.5**	- 3.0	- 1.5
SF15	-4.5	- 1.7	- 6.2	- 4.3	- 5.5	- 2.2	**-11.4**	0
A-10	-9.2	-2.9	- 0.8	0	- 4.9	-10.9	- 6.8	**-17.6**

Table 2. Late-time energy in the convolutions of various E-pulses with responses of various targets at 45° aspects.

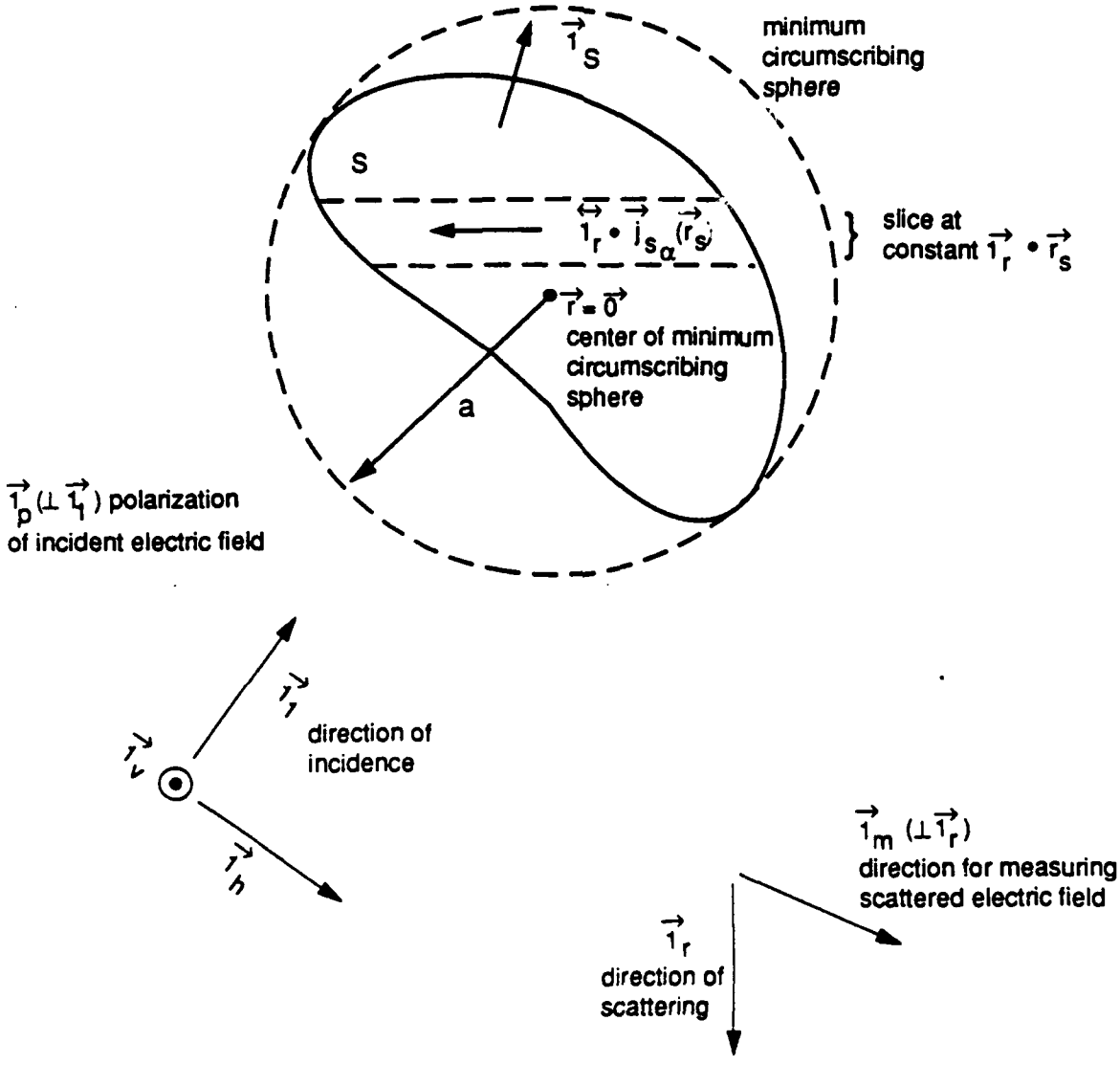

Fig. 1. Finite-Size Object in Free Space Illuminated by Plane Wave

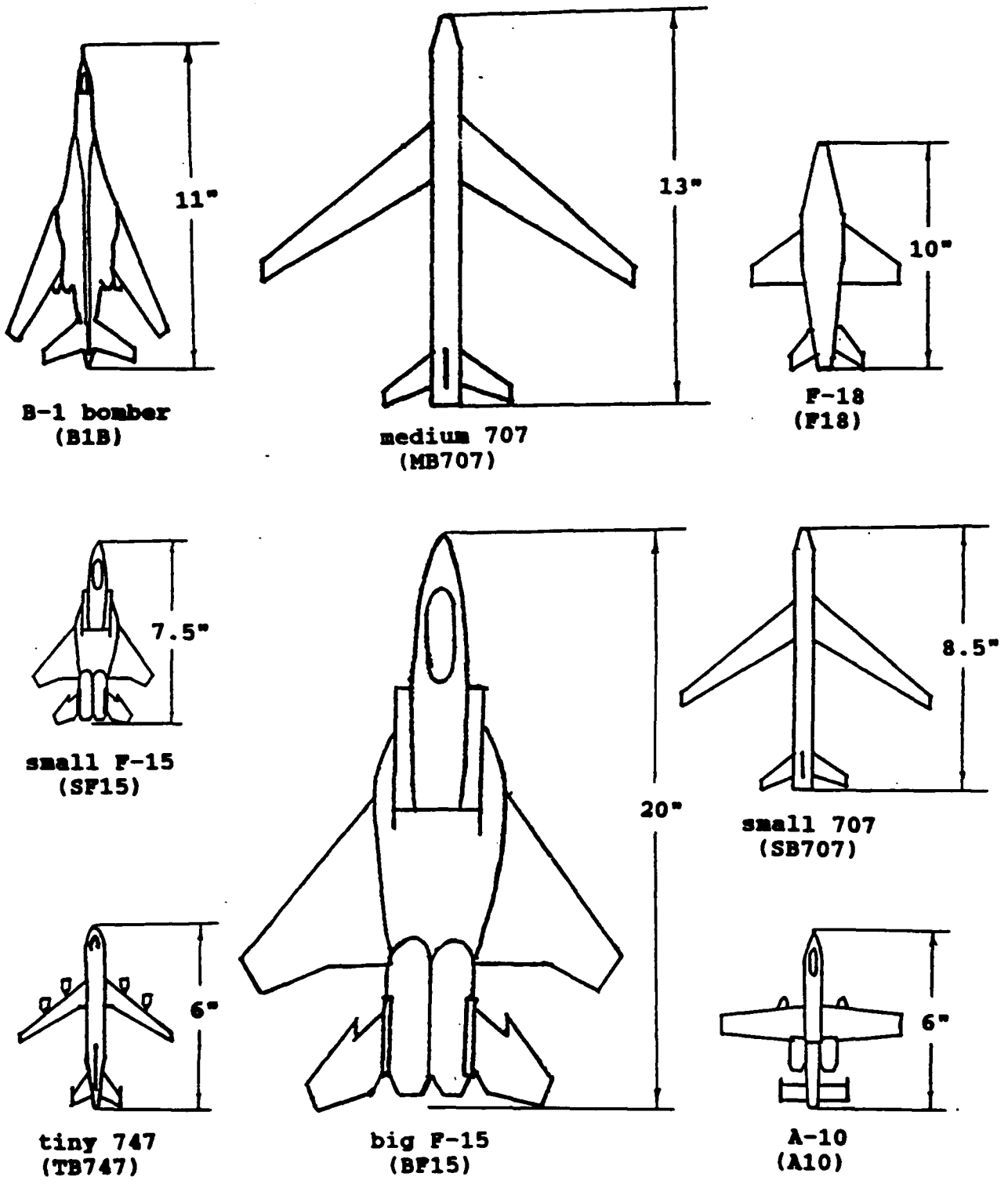

Figure 2. Eight target models used in discrimination experiments in the free-field chamber scattering range.

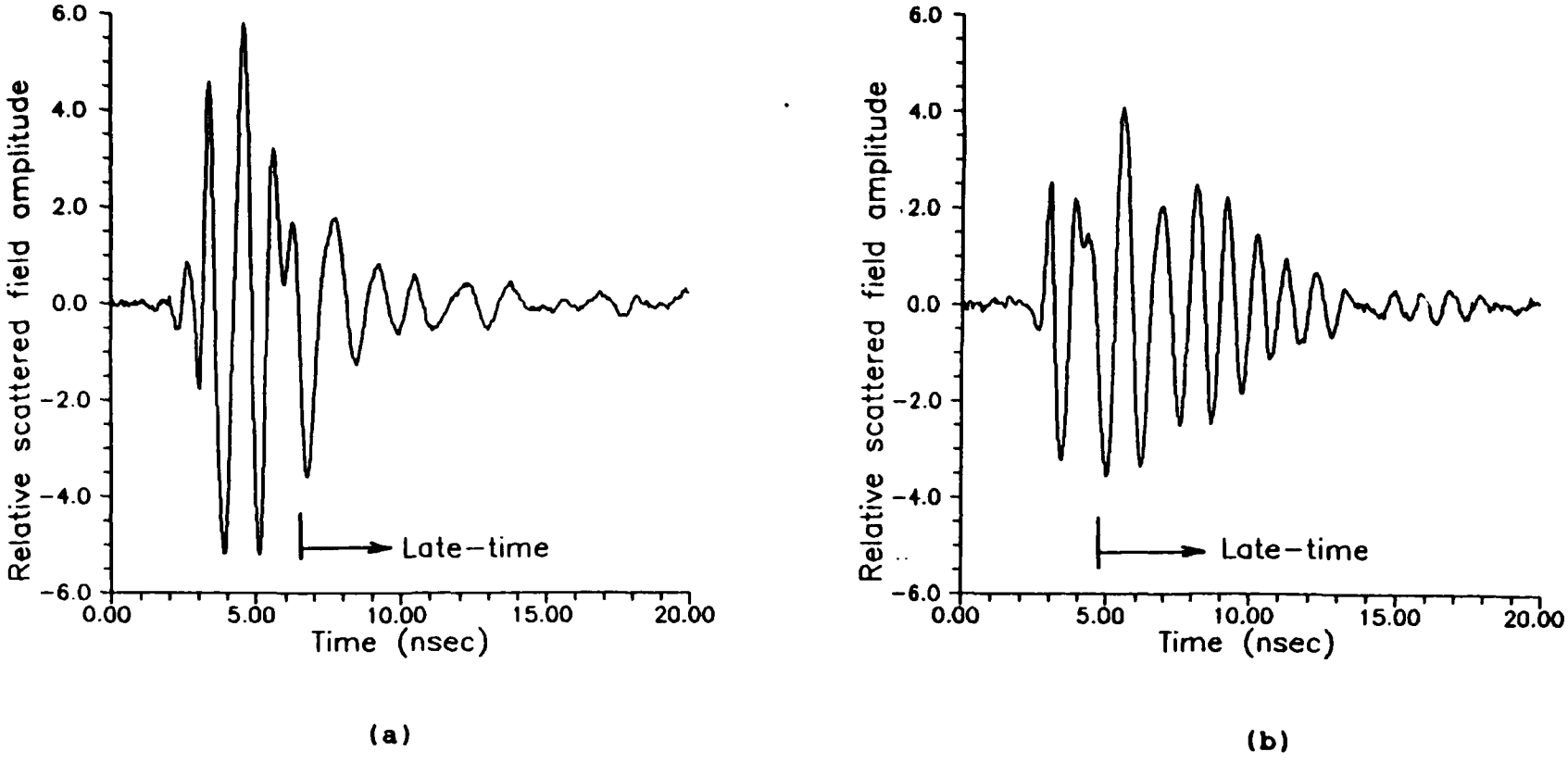

Figure 3. Scattered field pulse responses of (a) big F-15 and (b) A-10 target models measured at 45° aspect.

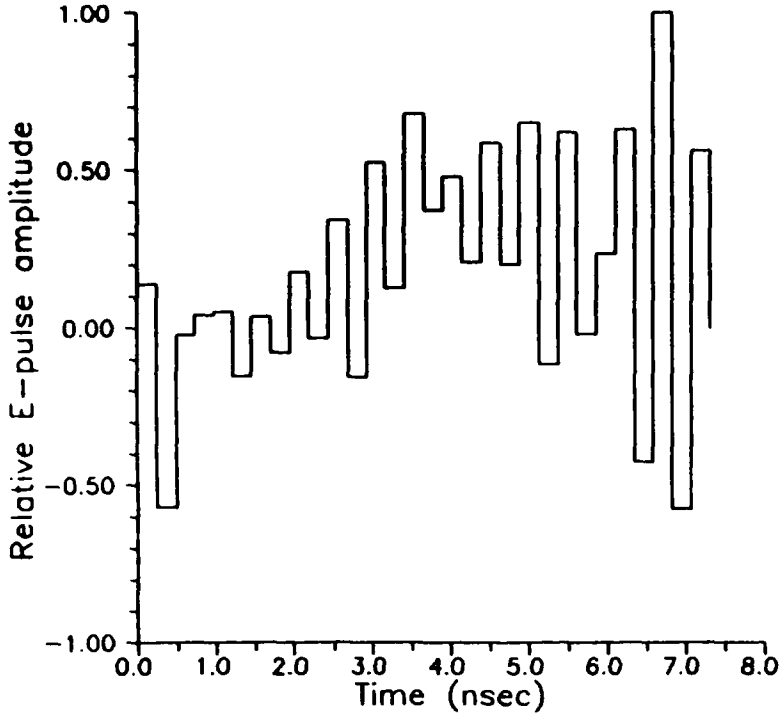

(a)

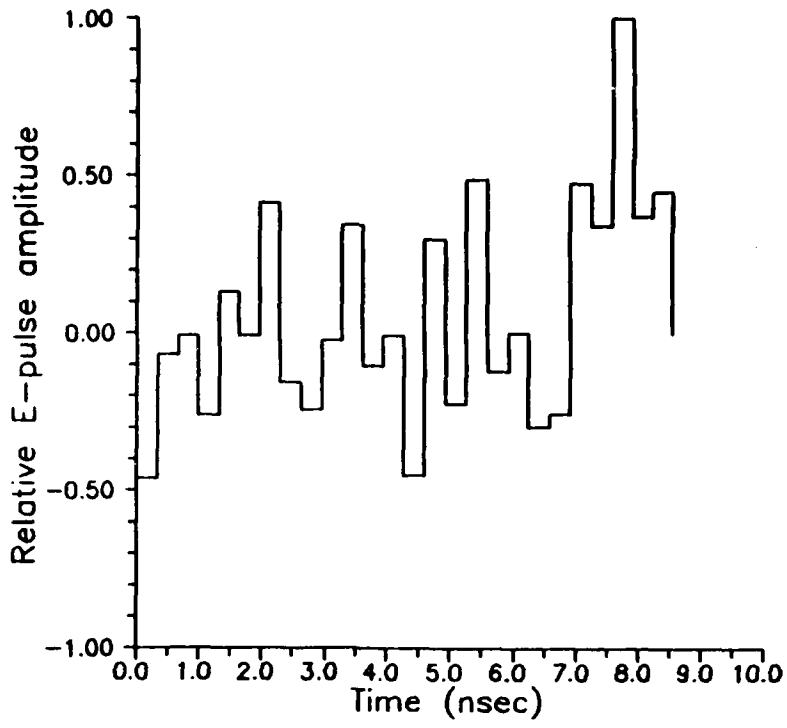

(b)

Figure 4. **E-pulses constructed to eliminate the modes of the (a) big F-15 and (b) A-10.**

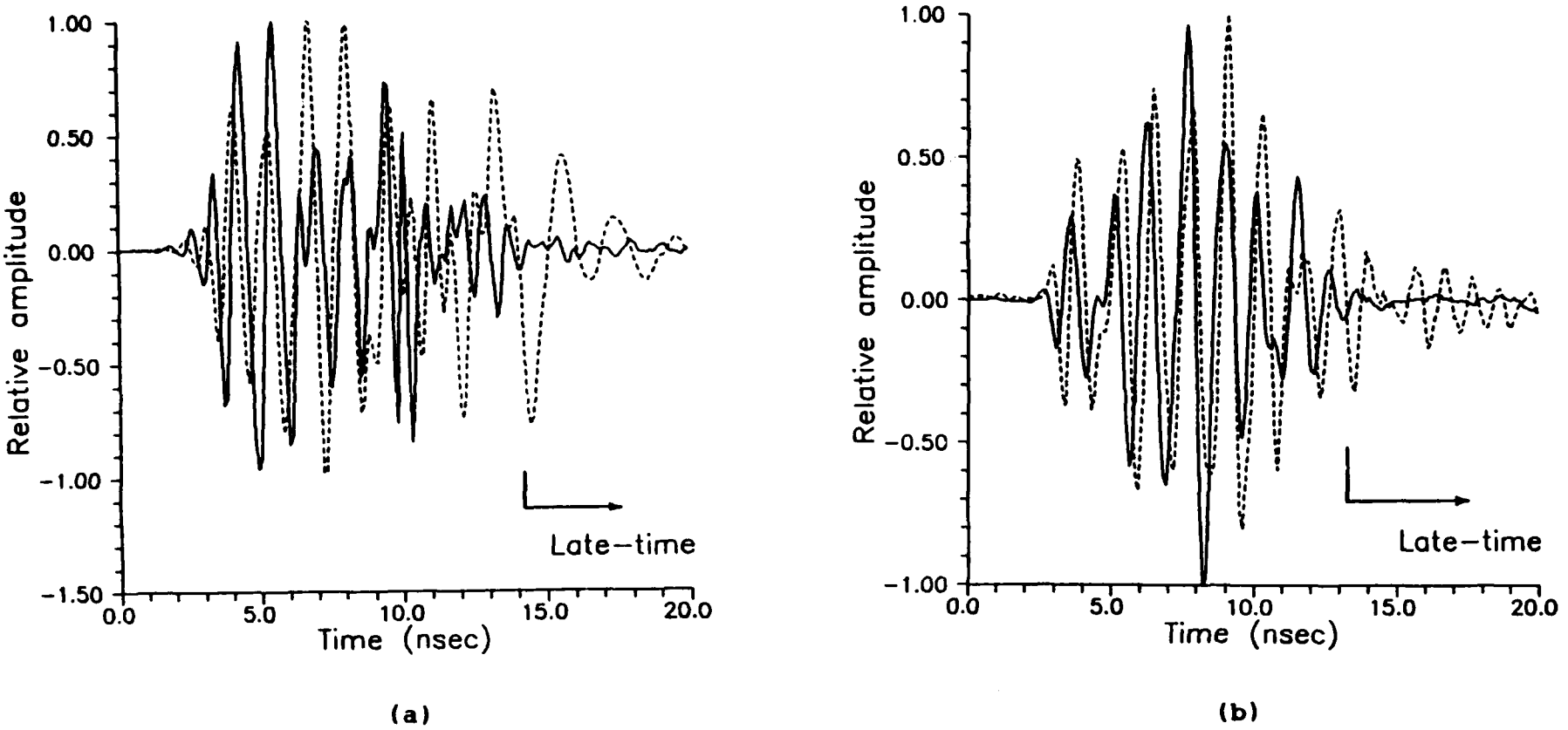

Figure 5. a) Convolution of the big F-15 E-pulse (solid line) and the A-10 E-pulse (dashed line) with the 45^0 response of the big F-15. b) Convolution of the big F-15 E-pulse (dashed line) and the A-10 E-pulse (solid line) with the 45^0 response of the A-10.

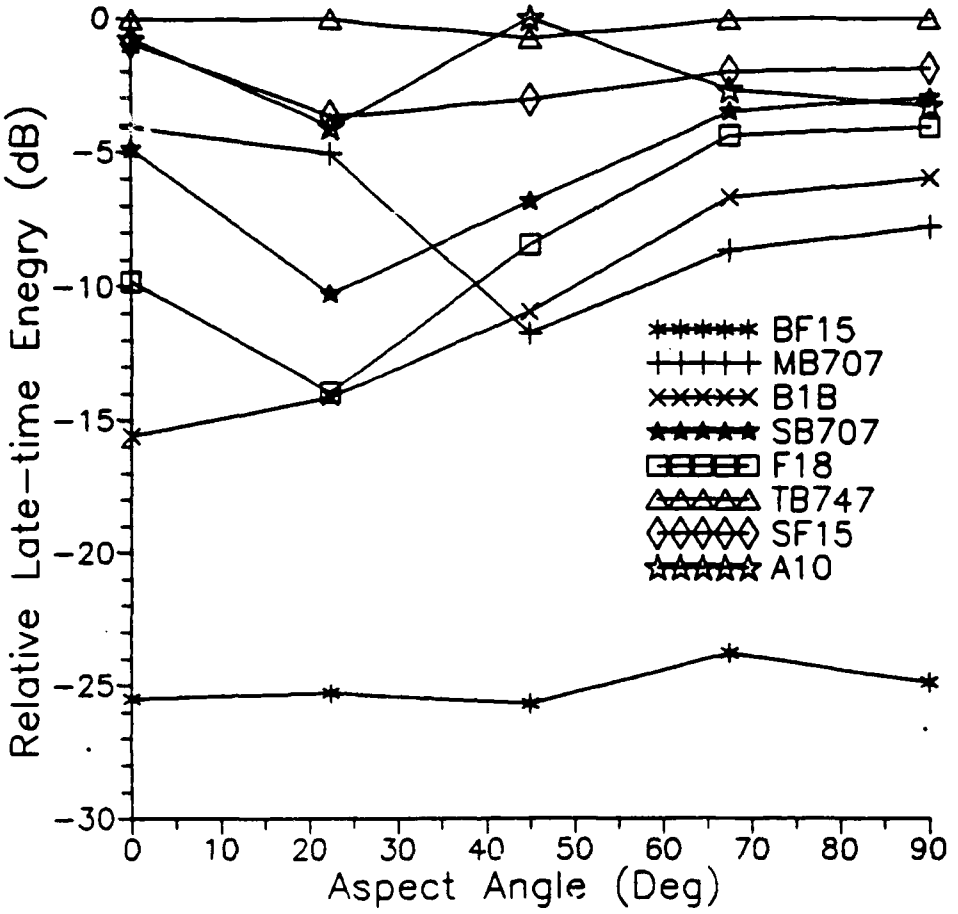

Figure 6. **Late-time energy from convolution of eight target E-pulses with responses of big F-15 measured at various aspect angles.**

geometrical properties	scattering residue dyadic $\overleftrightarrow{C}_{f_\alpha}(\vec{1}_r, \vec{1}_1)$ (bistatic) - properties of $\vec{C}_{r_\alpha}(\vec{1}_r)$ ($\vec{C}_\alpha(\vec{1}_1)$ similar)	backscattering residue dyadic $\overleftrightarrow{c}_{b_\alpha}(\vec{1}_1)$ (monostatic)
non-degenerate modes, no special symmetry	$\vec{C}_{r_\alpha}(\vec{1}_r)$: 2 complex numbers - excitation independent $\vec{C}_{r_\alpha}(\vec{1}_r)/\lvert\vec{C}_{r_\alpha}\rvert_{max}$ = scatterer polarization - 3 real numbers	$\overleftrightarrow{c}_{b_\alpha}(\vec{1}_1) = \vec{c}_\alpha(\vec{1}_1)\vec{c}_\alpha(\vec{1}_1)$ - 2 complex numbers Test by $\det(\overleftrightarrow{c}_{b_\alpha}(\vec{1}_1)) = 0$ (2×2 sense)
non-degenerate modes, symmetry plane P through observer	$\vec{C}_{r_\alpha}(\vec{1}_r)$: symmetric (//P) or antisymmetric ($\perp$P) - complex number times real unit vector (3 real numbers)	$\overleftrightarrow{c}_{b_\alpha}(\vec{1}_1) = c_{b_\alpha}\vec{1}_{sy}\vec{1}_{sy}$ or $c_{b_\alpha}\vec{1}_{as}\vec{1}_{as}$ - 3 real numbers
body of revolution with symmetry plane P containing axis: $C_{\infty a}$	$\overleftrightarrow{C}_{f_\alpha}(\vec{1}_r, \vec{1}_1) = \vec{C}_{r_{sy,\alpha'}}(\vec{1}_r)\vec{C}_{sy,\alpha'}(\vec{1}_1) + \vec{C}_{r_{as,\alpha'}}(\vec{1}_r)\vec{C}_{as,\alpha'}(\vec{1}_1)$	$\overleftrightarrow{c}_{b_\alpha}(\vec{1}_1) = \vec{c}_{sy,\alpha'}(\vec{1}_1)\vec{c}_{sy,\alpha'}(\vec{1}_1) + \vec{c}_{as,\alpha'}(\vec{1}_1)\vec{c}_{as,\alpha'}(\vec{1}_1)$ - 5 real numbers Test by $\det(\overleftrightarrow{c}_{b\alpha}(\vec{1}_1)) \neq 0$ (2×2 sense)
body with C_N symmetry, N≥3, axis through observer		$\overleftrightarrow{c}_{b_\alpha}(\vec{1}_1) = c_{b_\alpha}\overleftrightarrow{1}_1$ - 1 complex number

Table 1. Properties of Scattering Residue Dyadic

NOISE CHARACTERISTICS OF THE E-PULSE TECHNIQUE FOR TARGET DISCRIMINATION

W. M. Sun, K. M. Chen, D. P. Nyquist, and E. J. Rothwell

Department of Electrical Engineering
Michigan State University, East Lansing, MI 48824

Abstract--In previous papers, the E-pulse technique for radar target discrimination has been proposed and shown to be aspect independent. This paper presents the results of investigation on the noise characteristics of the E-pulse technique. An error estimate is derived for extracting natural frequencies from measured responses by a least-squares formulation. The signal-to-noise ratios of a target response before and after the E-pulse convolution is analyzed. It is shown that the S/N ratios of a response can be enhanced about 20 dB by the E-pulse convolution. Also presented is the experimental verification of the large enhancement of S/N ratios after the E-pulse convolution by using scale airplane models.

I. Introduction

The development of new radar target discrimination schemes has received considerable attention recently [1-4]. In previous papers, the E-pulse technique has been proposed and applied successfully to various simulated targets, such as wire structures [3,5], conducting plates [6] and scale airplane models [3,4,7]. One of the most encouraging attributes of the technique is its aspect independence, as demonstrated by experiments [7]. But before the scheme is put into practice, its noise performance has to be considered.

This work was supported by DARPA and ONR under Contract N000-14-87-K-0336.

The E-pulse technique consists of synthesizing discriminant signals, including the Extinction-pulse (E-pulse) and single-mode extraction pulses (S-pulses), based on the natural frequencies of a target, and convolving those signals with radar returns from the targets to be discriminated [4]. When the discriminant signals of a target are numerically convolved with the late-time response of the expected target, zero or single-mode late-time responses are produced in the convolved outputs. However, when the discriminant signals of a target are convolved with radar return from a different target, the convolved outputs are significantly different from zero or single-mode responses in the late-time period.

This paper explores several aspects of noise characteristics of the E-pulse technique for target discrimination. First, a fairly good error estimate is sought for extracting the natural frequencies from a measured target response by a least-squares method. This estimation is based on a small perturbation model. Then the convolution of a target's response with its corresponding E-pulse, which is synthesized based on the noise perturbed natural frequencies, is evaluated. The visible variation of the E-pulse waveform to the perturbation of the natural modes reflects the E-pulse's potential in discrimination between similar sized targets, and it suggests the necessity for extraction of natural frequencies from scale models in a laboratory environment. Thereafter the analysis on the signal-to-noise ratios is performed for a target's response before and after the E-pulse convolution. A more than 20 dB enhancement of S/N ratio results from the E-pulse convolution. The last section presents the experimental verification of the noise performance of the E-pulse convolution.

II. Error Estimation on the Extraction of Natural Modes

The implementation of the E-pulse target discrimination scheme, which is based on natural resonances of the target, needs accurate information about the natural frequencies of a target. Unfortunately, for most realistic targets, theoretical and numerical determination of the natural resonances is impossible. Thus, the determination of natural modes requires extracting the natural frequencies from measured responses of a scale model. Since no experimental measurement can avoid envirenmental noise, it is

prudent to obtain an error estimate of the natural frequencies extracted from the noise contaminated measured responses.

Various numerical algorithms have been reported to extract the natural frequencies of a target from measured responses [8-10]. The most popular technique is the least-squares formulation, including minimization of a regularized ill-conditioned least-squares equation [9] and minimization of the energy [10] in the late-time portion of the convolution between the measured response and the E-pulse waveform. The least-squares problem is a nonlinear one, so a strict error estimation is rather difficult. To make the problem easier, only a linearized error estimation is pursued.

A fundamental assumption regarding a transient response of a target is that the late-time part of the response can be represented by a sum of damped sinusoids [11]. The target response can consequently be modelled by the fitting function

$$g(\mathbf{x}, t) = \sum_{n=1}^{N} a_n e^{\sigma_n t} \cos(\omega_n t + \phi_n) \tag{1}$$

where x is the vector of fitting parameters

$$\mathbf{x} = [a_1,\ldots,a_N;\ \sigma_1, \ldots ,\sigma_N;\ \omega_1, \ldots ,\omega_N;\ \phi_1, \ldots ,\phi_N]^T \tag{2}$$

The measured time-sampled data is written in a vector form

$$F = \begin{bmatrix} f_1 \\ f_2 \\ \vdots \\ f_M \end{bmatrix} \tag{3}$$

and the fitting function is sampled into a vector at the same time instants as the measured data

$$G(\mathbf{x}) = \begin{bmatrix} g(\mathbf{x},t_1) \\ \vdots \\ g(\mathbf{x},t_M) \end{bmatrix}. \tag{4}$$

The function to be minimized is given by the sum of the squared residues

$$h(\mathbf{x}) = \frac{1}{2}\sum_{i=1}^{M}|f_i - g(\mathbf{x},t_i)|^2 = \frac{1}{2}(F-G)^T(F-G) \tag{5}$$

where T denotes the transposition of a matrix, and the derivative of (5) is denoted as

$$Dh(\mathbf{x}) = \begin{bmatrix} \frac{\partial}{\partial x_1}h(\mathbf{x}) \\ \vdots \\ \frac{\partial}{\partial x_{4N}}h(\mathbf{x}) \end{bmatrix}. \tag{6}$$

The j'th component of (6) can be written in an explicit form as

$$(Dh(\mathbf{x}))_j = \frac{\partial}{\partial x_j}h(\mathbf{x}) = \sum_{i=1}^{M}(f_i - g(\mathbf{x},t_i))(\frac{\partial}{\partial x_j}g(\mathbf{x},t_i))$$

so that

$$Dh(\mathbf{x}) = DG^T(\mathbf{x})\,(G(\mathbf{x}) - F) \tag{7}$$

The requirement for minimization of the function $h(\mathbf{x})$ is thus

$$Dh(\mathbf{x}) = DG^T(\mathbf{x})\,(G(\mathbf{x}) - F) = 0 \tag{8}$$

Now if an error is somehow introduced in the sampled data, the regression parameters of $\mathbf{x}$ will be slightly different. Assuming that $\mathbf{x}_1$ is the solution with sampled data F_1 and that $\mathbf{x}_2$ is the solution with sampled data F_2, (8) is satisfied for both $\mathbf{x}_1$ and $\mathbf{x}_2$.

$$Dh(\mathbf{x}_1) = DG^T(\mathbf{x}_1)\,(G(\mathbf{x}_1) - F_1) = 0 \tag{9}$$

$$Dh(\mathbf{x}_2) = DG^T(\mathbf{x}_2)\,(G(\mathbf{x}_2) - F_2) = 0. \tag{10}$$

Subtracting (10) from (9) yields

$$DG^T(\mathbf{x}_1)\,(G(\mathbf{x}_1) - F_1) - DG^T(\mathbf{x}_2)\,(G(\mathbf{x}_2) - F_2) = 0 \tag{11}$$

An equivalent form is provided by

$$[DG^T(\mathbf{x}_1) - DG^T(\mathbf{x}_2)][G(\mathbf{x}_1) - F_1] + DG^T(\mathbf{x}_2)[G(\mathbf{x}_1) - G(\mathbf{x}_2) + F_2 - F_1] = 0. \tag{12}$$

An exact estimate of the difference between $\mathbf{x}_1$ and $\mathbf{x}_2$ is difficult, but if the perturbation of the sampled data is small, an approximate estimate based on (12) can be constructed. Now the second-order derivative of the fitting function vector is used to represent the differences of both the fitting function and its first order derivative

$$DG^T(\mathbf{x}_1)-DG^T(\mathbf{x}_2) = D^2G^T(\mathbf{x}_2)\ (\mathbf{x}_1 - \mathbf{x}_2) \tag{13}$$

where D^2G is a three-dimensional matrix and

$$G(\mathbf{x}_1) - G(\mathbf{x}_2) = D^TG(\mathbf{x}_2)\ (\mathbf{x}_1 - \mathbf{x}_2) + \frac{1}{2}\ DD^TG(\mathbf{x}_2)(\mathbf{x}_1 - \mathbf{x}_2)(\mathbf{x}_1 - \mathbf{x}_2) \tag{14}$$

Then, (12) results in

$$D^2G^T(\mathbf{x}_2)\ (\mathbf{x}_1 - \mathbf{x}_2)(G(\mathbf{x}_1) - F_1) + DG^T(\mathbf{x}_2)[\ D^TG(\mathbf{x}_2)(\mathbf{x}_1 - \mathbf{x}_2)$$

$$+ \frac{1}{2}\ DD^TG(\mathbf{x}_2)(\mathbf{x}_1 - \mathbf{x}_2)(\mathbf{x}_1 - \mathbf{x}_2) + F_2 - F_1] = 0 \tag{15}$$

It is assumed that the perturbation of sampled data is small, that is

$$\frac{\|F_1 - F_2\|}{\|F_1\|} \ll 1$$

By ignoring the higher order perturbations, (15) is linearized into a form

$$DG^T(\mathbf{x}_2)[\ D^TG(\mathbf{x}_2)(\mathbf{x}_1 - \mathbf{x}_2) + F_2 - F_1] = 0 \tag{16}$$

An estimate for $\mathbf{x}_1$–$\mathbf{x}_2$ is thus given by

$$\mathbf{x}_1 - \mathbf{x}_2 = [DG^T(\mathbf{x}_2)\ D^TG(\mathbf{x}_2)]^{-1}\ DG^T(\mathbf{x}_2)(F_1 - F_2) \tag{17}$$

It should be pointed out that (17) is created based on the squared-error function (5), but the function often used in numerical algorithms is a regularized cost fuction $h(\mathbf{x})$, defined as

$$h(\mathbf{x}) = \frac{1}{2}\ \tau \sum_{i=1}^{M} |f_i - g(\mathbf{x},t_i)|^2 + \frac{1}{2}\ (1 - \tau) \sum_{i=1}^{M} |x_i - x_i^0|^2$$

$$= \frac{1}{2}\ \tau\ (F - G)^T(F - G) + \frac{1}{2}\ (1 - \tau)\ (\mathbf{x} - \mathbf{x}_0)^T(\mathbf{x} - \mathbf{x}_0) \tag{18}$$

where $\mathbf{x}_0$ is a known vector. Here $\tau = 1$ gives the original minimization problem, while $\tau \leq 1$ provides a better conditioned, regularized problem. Solving a series of problems with τ progressing from 0 to 1 is called a continuation method. It is easy to show the error estimate of (18) is

$$\|\mathbf{x}_1 - \mathbf{x}_2\| \leq \|\tau[DG^T(\mathbf{x}_2)\, D^T G(\mathbf{x}_2) + (1-\tau)I\,]^{-1}\, DG^T(\mathbf{x}_2)\| \;\; \|(F_1 - F_2)\|$$

$$= \|S\|\, \|F_1 - F_2\| \tag{19}$$

with I the unit matrix and S defined as:

$$S = \tau\, [DG^T(\mathbf{x}_2)\, D^T G(\mathbf{x}_1) + (1-\tau)\, I\,]^{-1}\, DG^T(\mathbf{x}_2) \tag{20}$$

Fig. 1 shows the norm of the matrix S when the $G(\mathbf{X})$ is a three-mode fitting function for the impulse response of a 30 cm thin wire. The impulse response is constructed based on the first five natural modes of the thin wire which has a 60^0 aspect angle w.r.t. the direction of the incident wave. The M associated with the x axis is the length of the vector F. Fig. 2 is the same plot as Fig. 1 except five natural modes are sought in the fitting function of $G(\mathbf{x})$. It is seen that the norm of the matrix S is increased as τ approaches unity. The norm of S is much bigger when five modes are expected. This implies that when more than a resonable number of modes are expected we may have poor results with some bad modes, though the rest are quite accurate. The oscillations of the curves with τ close to 1 reflect the ill-conditioned nature of the original least-squares problem since when $\tau = 1$, while the regularized equation reduces to the original least-squares problem. The norm of S is only the maximum error estimate for the extracted natural frequencies. The practical application of the least-squares method to (5) can result in much smaller error.

To see how the extracted natural frequencies can be shifted when the sampled data is perturbed, Table 3.1 lists the first five natural frequencies of a 30 cm thin wire extracted from an impulse response of the thin wire by means of a continuation method. The impulse response is constructed based on the first five natural nodes. It is seen that when the standard deviation of the added white uniform noise is less than 10% of the maximum amplitude of the data, the extracted modes are fairly close to the true values.

III. The E-Pulse Convolution With Natural Modes Perturbed

As most practical E-pulses are synthesized based on the extracted natural frequencies, it is appropriate to ask the question of whether the E-pulse can eliminate the natural resonances of late-time response scattered from an expected target, or how the E-pulse convolution will be affected by the shifting of the expected natural frequencies.

The convolution of an E-pulse of duration T_e with the scattered field response from a target is represented by [7]

$$c(t) = \sum_{n=1}^{N} a_n |E(s_n)| e^{\sigma_n t} \cos(\omega_n t + \psi_n) \qquad t > T_L \tag{21}$$

where the $E(s)$ is the spectrum of the E-pulse given by

$$E(s) = \int_0^{\infty} e(t) e^{-st} dt = \int_0^{T_e} e(t) e^{-st} dt \tag{22}$$

and $E(s_n)$ is $E(s)$ evaluated at s_n where s_n is the n'th natural frequency of the target. Now assume that a target is characterized by the natural frequencies $s_1, \cdots, s_N$, while the extracted natural frequencies from its scattered response are $s_1^0, \cdots, s_N^0$. The E-pulse synthesized for this target satisfies

$$E(s_n^0) = \int_0^{T_e} e(t) e^{-s_n^0 t} dt = 0 \qquad (n=1,2,\ldots,N) \tag{23}$$

But the spectrum of the E-pulse is not zero at frequencies of $s_1, \cdots, s_N$. Consequently the late-time convolution of $c(t)$ of (19) is not zero. The error can be estimated as follows. Define

$$s_n = s_n^0 + \Delta s_n \qquad (n=1,2,\ldots,N) \tag{24}$$

and suppose that the extracted s_n^0 is very close to the true value of s_n. If the relationship

$$\Delta s_n T_e \ll 1 \qquad (n=1,2,\ldots,N) \tag{25}$$

holds, then (22) can be approximated as

$$E(s_n) \approx E(s_n^0) + \Delta s_n \frac{\partial}{\partial s} E(s)|_{s_n^0}$$

$$\approx \Delta s_n \frac{\partial}{\partial s} E(s_n^0) \tag{26}$$

Thus the convolution of the E-pulse with a late-time scattered response from an expected target has a nonzero amplitude of

$$c(t) = \sum_{n=1}^{N} a_n |\Delta s_n \frac{\partial}{\partial s} E(s_n^0)| \, e^{\sigma_n t} \cos(\omega_n t + \psi_n) \qquad t > T_L \tag{27}$$

If the differences of $\Delta s_1, \ldots, \Delta s_N$ are sufficiently small, the late-time convolved output is negligible.

In the preceeding section, it is shown that the extracted natural frequencies will be perturbed if the experimental data is contaminated by noise. Since the synthesis of the E-pulse is based on the natural frequencies extracted from measured responses, the extracted frequencies are always perturbed from the exact frequencies. To view the tolerable range of the perturbation on the natural frequencies, a numerical experiment is performed on the impulse response of a thin wire.

Fig. 3 shows the backscattered impulse response of a thin wire oriented 45^0 w.r.t. the incident wave. The impulse response is constructed with the first five modes. It is observed that the early-time part of the impulse response is oscillatory. This early-time response is faulty because an early-time response of a target can not be constructed with a sum of natural modes with the second-kind coupling coefficients. We have ignored this faulty early-time response, since only the late-time response, which is correct as depicted in Fig. 3, is needed for our analysis.

The first five natural frequencies are then perturbed by white Gaussian noise with various deviations. This perturbation is directly applied to the narural frequencies. Subsequently, the E-pulses are synthesized based on the noise perturbed natural frequencies. Thereafter, the synthesized E-pulses are convolved respectively with the impulse response of the thin wire shown in Fig. 3. The convolution result is shown in Fig. 4. It is obvious that when the noise perturbation is more than 5%, the

convolved responses in the late time are significantly different from the expected null response. Fig. 5 shows the various E-pulses which are synthesized based on the noise perturbed natural frequencies of the thin wire.

It is observed that the E-pulse synthesis and the E-pulse convolution are quite sensitive to the perturbation of the natual frequencies. These results consequently suggest that the natual frequencies must be extracted from scale-model targets in a noise-controlled laboratory envirenment. However, it should be remembered that this sensitivity of the E-pulse to the perturbation of the natural modes provides the E-pulse technique with the potential to discriminate two similar sized targets.

It is interesting to note that if the natural frequencies of a target are assigned to be second order zeros of $E(s)$, so the derivative of the E-pulse complex spectrum is also zero at any natural frequency of the target, then the convolved output of (27) will remain zero. However when discrimination between two targets whose natural frequencies are located close to each other in the complex plane is desired, the difference between two late-time convolved outputs may not be large enough.

IV. Noise Performance of The E-Pulse Convolution

This section is devoted to identifying a statistical noise estimate when the E-pulse technique is applied to the scattered response contaminated by noise. As a preliminary analysis, only white additive stationary noise is considered.

When zero-mean stationary white noise of $\mathbf{n}(t)$ is considered, it is mathematically implied that [12]

$$E_n[\mathbf{n}(t)] = 0 \tag{28}$$

$$R_n(\tau) = \frac{N_0}{2}\delta(\tau) \tag{29}$$

and

$$S_n(f) = \frac{N_0}{2} \tag{30}$$

where E denotes the mean, R denotes the autocorrelation function, S denotes the power spectrum of the noise and N_0 is the amplitude of the power spectrum. Now a target's response contaminated by noise is assumed to be

$$r(t) = r_0(t) + \mathrm{n}(t) \tag{31}$$

with $r_0(t)$ being its uncontaminated response. The convolution of the response (31) with an E-pulse waveform is given by

$$c(t) = \int_0^{T_e} e(t')\, r(t - t')\, dt'$$

$$= \int_0^{T_e} e(t')\, r_0(t - t')\, dt' + \int_0^{T_e} e(t')\, \mathrm{n}(t-t')dt' = c_0(t) + \int_0^{T_e} e(t')\, \mathrm{n}(t-t')dt' \tag{32}$$

The mean of the E-pulse convolved response is given by

$$E[c(t)] = E[c_0(t)] + E[\int_0^{T_e} e(t')\, \mathrm{n}(t-t')dt'] = c_0(t) \tag{33}$$

and the autocorrelation function is evaluated as

$$R_c(t_1, t_2) = E[\, c(t_1)c(t_2)\,]$$

$$= c_0(t_1)c_0(t_2) + c_0(t_1)\int_0^{T_e} e(t')\, E[\mathrm{n}(t_2-t')]\, dt'$$

$$+ c_0(t_2)\int_0^{T_e} e(t')\, E[\mathrm{n}(t_1-t')]\, dt' + \int_0^{T_e} e(t')\, dt' \int_0^{T_e} e(\tilde{t})\, E[\mathrm{n}(t_1-t')\, \mathrm{n}(t_2-\tilde{t})]\, d\tilde{t} \tag{34}$$

Using (28) and (29) leads to

$$R_c(t_1, t_2) = c_0(t_1)c_0(t_2) + \frac{N_0}{2}\int_0^{T_e} e(t')\, dt' \int_0^{T_e} e(\tilde{t})\, \delta(t_1-t' - t_2+\tilde{t})\, d\tilde{t}$$

$$= c_0(t_1)c_0(t_2) + \frac{N_0}{2}\int_0^{T_e} e(t')\, e(t_2-t_1+t')\, dt' \tag{35}$$

The variance of the E-pulse convolved response takes the value of

$$\sigma^2(t) = R_c(t, t) - E^2[c(t)]$$

$$= \frac{N_0}{2}\int_0^{T_e} e^2(t')\,dt' = \frac{N_0}{2}\,P_e \tag{36}$$

where P_e is the energy contained in the E-pulse waveform.

The noise model used here is an ideal one. More practical would be white noise band limitted by the band-width of the system being considered. As an example, an ideal low-pass system is considered. Its transfer function is

$$W(f) = \begin{cases} 1 & |f| < W \\ 0 & \textit{elsewhere} \end{cases} \tag{37}$$

Then, the power spectrum of the noise output from system is

$$S_n(f) = \frac{N_0}{2}\,|W(f)|^2 \tag{38}$$

and the associated autocorrelation function is

$$R_n(\tau) = \frac{N_0}{2}\int_{-\infty}^{\infty} |W(f)|^2 exp(-j2\pi f\tau)\,df$$

$$= WN_0\frac{\sin 2\pi W\tau}{2\pi W\tau} \tag{39}$$

while the variance of the noise is obtained by

$$\sigma_n^2 = R_n(0) - E[n(t)] = R_n(0) = WN_0 \tag{40}$$

With (34), the autocorrelation function of the E-pulse convolved response for the case of band-limited white noise can be shown to be

$$R_c(t_1, t_2) = c_0(t_1)c_0(t_2) + WN_0\int_0^{T_e} e(t')\,dt'\int_0^{T_e} e(\bar{t})\,\frac{\sin 2\pi W(t_1-t_2+t'-\bar{t})}{2\pi W(t_1-t_2+t'-\bar{t})}\,d\bar{t} \tag{41}$$

The variance is deduced from (41) as

$$\sigma_c^2 = R_c(t,t) = WN_0\int_0^{T_e} e(t')\,dt'\int_0^{T_e} e(\bar{t})\,\frac{\sin 2\pi W(t'-\bar{t})}{2\pi W(t'-\bar{t})}\,d\bar{t} \tag{42}$$

If the noise is specified with a standard deviation, then the parameter N_0 can be obtained with the help of (40) as long as the system bandwidth is given. The signal-to-noise ratio before the E-pulse convolution is provided by

$$(S/N)_0 = 10\log_{10}\frac{\overline{|r^2(t)|}}{WN_0} \tag{43}$$

while the signal-to-noise ratio after the E-pulse convolution can be evaluated from

$$(S/N)_1 = 10\log_{10}\frac{\overline{|c_0^2|}}{WN_0\int_0^{T_e} e(t')\,dt'\int_0^{T_e} e(\tilde{t})\,\frac{\sin 2\pi W(t'-\tilde{t})}{2\pi W(t'-\tilde{t})}\,d\tilde{t}} \tag{44}$$

where the bar denotes the average in a time period.

The behavior of the noise performance of the E-pulse convolution is described by Figure 6 in which the signal-to-noise ratios are compared before and after the convolution of the noise-contaminated impulse responses of a thin wire with its E-pulses. The signal-to-noise ratios for different aspect angles are evaluated with (43) and (44). The noise deviation associated with the x axis is the percentage of the maximum amplitude in an impulse response. The θ is the angle between the wave incident direction and the thin wire axis. An ennhancement of about 20 dB after the E-pulse convolution has been achieved.

V. Noise-Testing on Experimental Data

In the preceeding analysis, only the constructed thin wire responses are used as examples. But the analysis is applicable to any response. To show the applicability, extensive experiments with measured responses from airplane models have been conducted. However only a few examples can be shown.

In the experiments conducted, very noisy radar responses are created by adding extra white Gaussian noise to the measured responses of the targets. These noisy responses are then convolved with the E-pulses of the targets. It is found that the E-pulses are still effective in smothering the noise and are capable of discriminating

between the expected and unexpected targets from these noisy responses.

Fig. 7.a shows the pulse response (the response excited by an incident Gaussian pulse) of a B-707 aircraft model [3] measured at 90^0 aspect angle, without extra noise added. Fig. 7.b is the convolved output of the pulse response of Fig. 7.a with the E-pulse synthesized for the B-707 model. As expected, a very small output is produced in the late-time portion of the convolved response. This identifies the pulse response of Fig. 7.a to be from the expected B-707 model target.

Subsequently, a noisy response is generated by purposely adding Gaussian white noise to the measured pulse response of the B-707 model shown in Fig. 7.a. The standard deviation of the noise is as large as 20% of the maximum amplitude of the measured response. The noise contaminated response is shown in Fig. 8.a. When this noisy pulse response of Fig. 8.a is convolved with the E-pulse waveform of a B-707 model, a satisfactory convolved output, as shown in Fig. 8.b, is obtained. This convolved output resembles that of Fig. 7.b. The late-time response still remains small. The signal-to-noise ratio is enhanced from -1.12 dB to 23.7 dB after the E-pulse convolution. This confirms that the B-707 model may be identified from the noisy pulse response of Fig. 8.a.

Next, an attempt is made to discriminate an unexpected F-18 target model by applying the E-pulse for the B-707 model to the noisy pulse responses of the wrong target. Fig. 9.a is the pulse response of the F-18 model measured at the same aspect angle of 90^0 without extra noise added. When the response of Fig. 9.a is convolved with the E-pulse of the B-707 model, the convolved output is shown in Fig. 9.b. It is seen that a relatively large late-time response is obtained. This is the indication of the wrong target.

As done previously for the response of the B-707 model, the pulse response of an F-18 model is contaminated with white Gaussian noise. The standard deviation is kept to be 20% of the maximum amplitude of the measured response of the F-18 model. Fig. 10.a shows the resulting waveform. The noisy pulse response of Fig. 10.a is subsequently convolved with the E-pulse of the B-707 model. The convolved output is shown in Fig. 10.b. As compared to the result of Fig. 9.b, the convolved output

of Fig. 10.b presents a relatively unchanged early-time response followed by a still large and somewhat noisy late-time response. This late-time response is sufficiently large to indicate that the noisy pulse response of Fig. 10.a is scattered from an unexpected target other than the B-707 model. In this case the signal-to-noise ratio is enhanced from -2.43 dB to 30.1 dB after the E-pulse convolution.

VI. Conclusion

Several aspects concerning the noise characteristics of the E-pulse technique for radar target discrimination have been investigated. An error estimate on the extraction of the natural frequencies of a target from measured responses has been given. It has been shown that if a set of natural modes of a target is perturbed more than 5%, the corresponding E-pulse waveform and the consequent convolution are significantly different. This property provides the E-pulse with the potential to discriminate two similar sized targets, and strongly suggests that the extraction of the natural frequencies from measured responses must be done on a scale model in the laboratory environment. Also, the signal-to-noise ratio of a response has been demonstrated to be enhanced 20 dB by the E-pulse convolution. Thus the noise insensitivity of the E-pulse convolution has been demonstrated.

Experimental results with the measured responses from scale airplane models have verified the analysis in the paper. The scattered responses from two similar sized airplane models with 20% extra white noise added can be used to discriminate the targets.

References

[1] K.M. Chen, "Radar waveform synthesis method--a new radar detection scheme," IEEE Trans. Antennas and Propagation, Vol. AP-29, no.4, 553-566, July, 1981.

[2] E.M. Kennaugh, "The K-pulse concept," IEEE Trans. Antennas and Propagation., Vol. AP-29, no.2, 327-331. Mar., 1981.

[3] E.J. Rothwell, D.P. Nyquist, K.M. Chen and B. Drachman, "Radar target discrimination using Extinction-pulse technique," IEEE Trans. Antennas and Propagation., Vol. AP-33, no.9, 929-937, Sept., 1985.

[4] K.M. Chen, D.P. Nyquist, E.J. Rothwell, L.L. Webb and B. Drachman, "Radar target discrimination by convolution of radar returns with extinction-pulses and single-mode extraction signals," IEEE Trans. Antennas and Propagation, Vol. AP-34, no.7, 896-904, July, 1986

[5] K.M. Chen, et.al., "Radar waveform synthesis for single-mode scattering by a thin cylinder and application for target discrimination," IEEE Trans. Antennas and Propagation, Vol. AP-30, no 3, 867-880, May, 1982.

[6] W.M. Sun, K.M. Chen, D.P. Nyquist and E.J. Rothwell "Discrimination of conducting plates by E-pulse technique" 1988 National Radio Science Meeting, Boulder, Colorado, January, 1988.

[7] E.J. Rothwell, K.M. Chen, D.P. Nyquist and W. Sun, "Frequency domain E-pulse synthesis and target discrimination," IEEE Trans. Antennas and Propagation, Vol. AP-35, no.4, 426-434, Apr., 1987.

[8] C.W. Chuang and D.L. Moffatt, "Natural resonances of radar targets via Prony's method and target discrimination," IEEE Trans. Aerospace Electron. Syst., vol. AES-12, no.5, 583-589, Sept. 1976.

[9] B. Drachman, and E. Rothwell, " A continuation method for identification of the natural frequencies of an object using a measured response," IEEE Trans. Antennas and Propagation., Vol. AP-33, no.4, 445-450, Apr., 1985.

[10] E.J. Rothwell, K.M. Chen and D.P. Nyquist, "Extraction of the natural frequencies of a radar target from a measured response using E-pulse techniques," IEEE Trans. Antennas and Propagation., Vol. AP-35, no.6, 715-720, June, 1987.

[11] C.E. Baum, " The Singularity Expansion Method," *Transient Electromagnetic Fields*, L.B. Felsen Ed., Springer-Verlag, New York, 130-176, 1975.

[12] J.M. Wozencraft and I.M., Jacobs *Principles of Communication Engineering* John Wiley & Sons, 188-192, 1965

Table 1 The first five natural frequencies of a 30 cm thin wire extracted from its impulse response via a continuation method. The impulse response is constructed with the first five modes and is contaminated with an uniform white noise.

Fig. 1 The norm of the matrix S ($\log_{10}$) when three modes are extracted from an impulse response of a 30 cm thin wire ($\theta = 60^0$)

Fig. 2 The norm of the matrix S ($\log_{10}$) when five modes are extracted from an impulse response of a 30 cm thin wire ($\theta = 60^0$)

Fig. 3 The impulse response of a 30 cm thin wire with a 45^0 angle w.r.t. to the incident direction of the exciting wave.

Fig. 4 The impulse response of a 30 cm thin wire ($\theta = 45^0$) is convolved with the E-pulses which are synthesized based on the noise-perturbed natural frequencies of the thin wire.

Fig. 5 The E-pulse waveforms synthesized for a 30 cm thin wire based on its first five natural frequencies. The five natural frequencies are perturbed with Gaussian white noise.

Fig. 6 Comparison of the signal to noise ratios before and after the impulse responses of a 30 cm thin wire are convolved with its E-pulse. The first five natural frequencies are used to construct the impulse responses and to synthesize the E-pulses of the thin wire.

Fig. 7 (a) The measured scattered waveform of B-707 model at aspect angle of 90^0; (b) its convolved response with the E-pulse waveform of B-707 model

Fig. 8 (a) The noise contaminated (20% of maximum amplitude) scattered waveform of B-707 model at aspect angle of 90^0; (b) its convolved response with the E-pulse waveform of B-707 model

Fig. 9 (a) The measured scattered waveform of F-18 model at aspect angle of 90^0; (b) its convolved response with the E-pulse waveform of B-707 model

Fig. 10 (a) The noise contaminated (20% of maximum amplitude) scattered waveform of F-18 model at aspect angle of 90^0; (b) its convolved response with the E-pulse waveform of B-707 model

mode #	theory	no noise	5% noise	10% noise
S_1	-0.2601+j2.906	-0.2601+j2.906	-0.2595+j2.901	-0.2667+j2.894
S_2	-0.3808+j6.007	-0.3808+j6.007	-0.3862+j6.051	-0.3912+j5.988
S_3	-0.4684+j9.060	-0.4684+j9.060	-0.4136+j8.960	-0.2322+j9.193
S_4	-0.5381+j12.17	-0.5415+j12.17	-1.1178+j12.02	-0.4702+j13.40
S_5	-0.5997+j15.24	-0.5997+j15.25	-0.4716+j14.98	-0.6789+j15.09

Table 1 The first five natural frequencies of a 30 cm thin wire extracted from its impulse response via a continuation method. The impulse response is constructed with the first five modes and is contaminated with an uniform white noise.

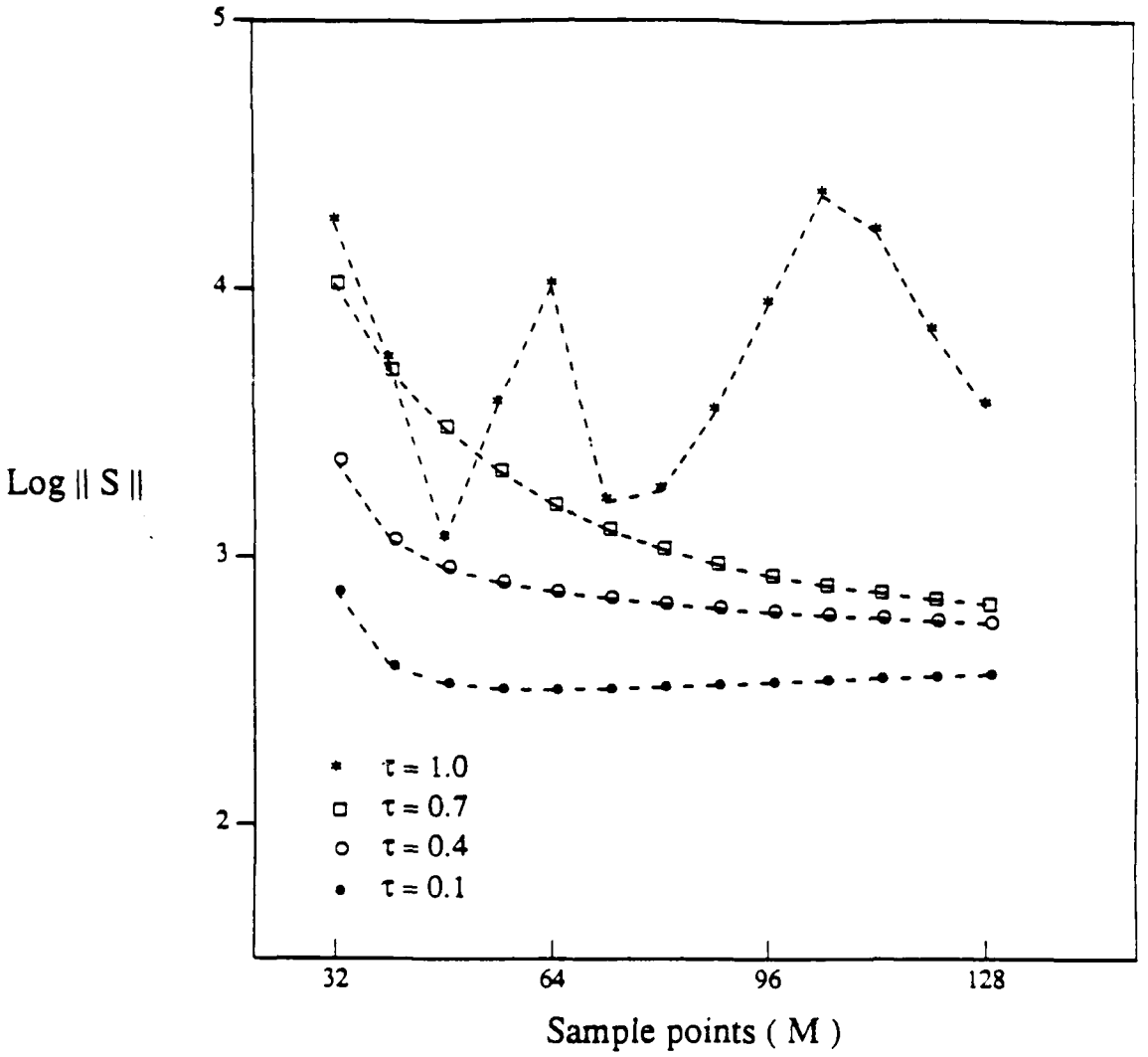

Fig. 1 The norm of the matrix S ($\log_{10}$) when three modes are extracted from an impulse response of a 30 cm thin wire ($\theta = 60^0$)

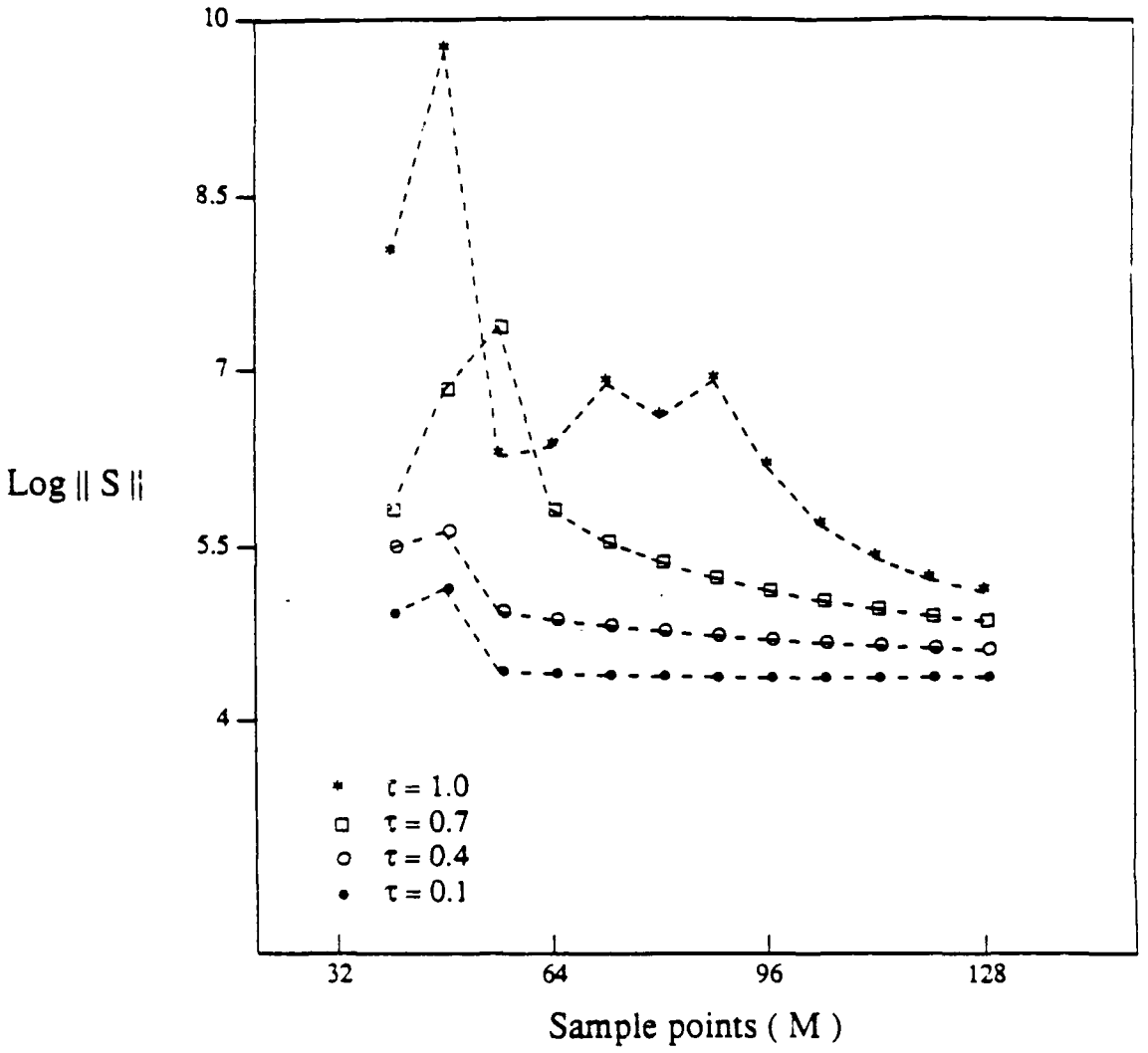

Fig. 2 The norm of the matrix S ($\log_{10}$) when five modes are extracted from an impulse response of a 30 cm thin wire ($\theta = 60^0$)

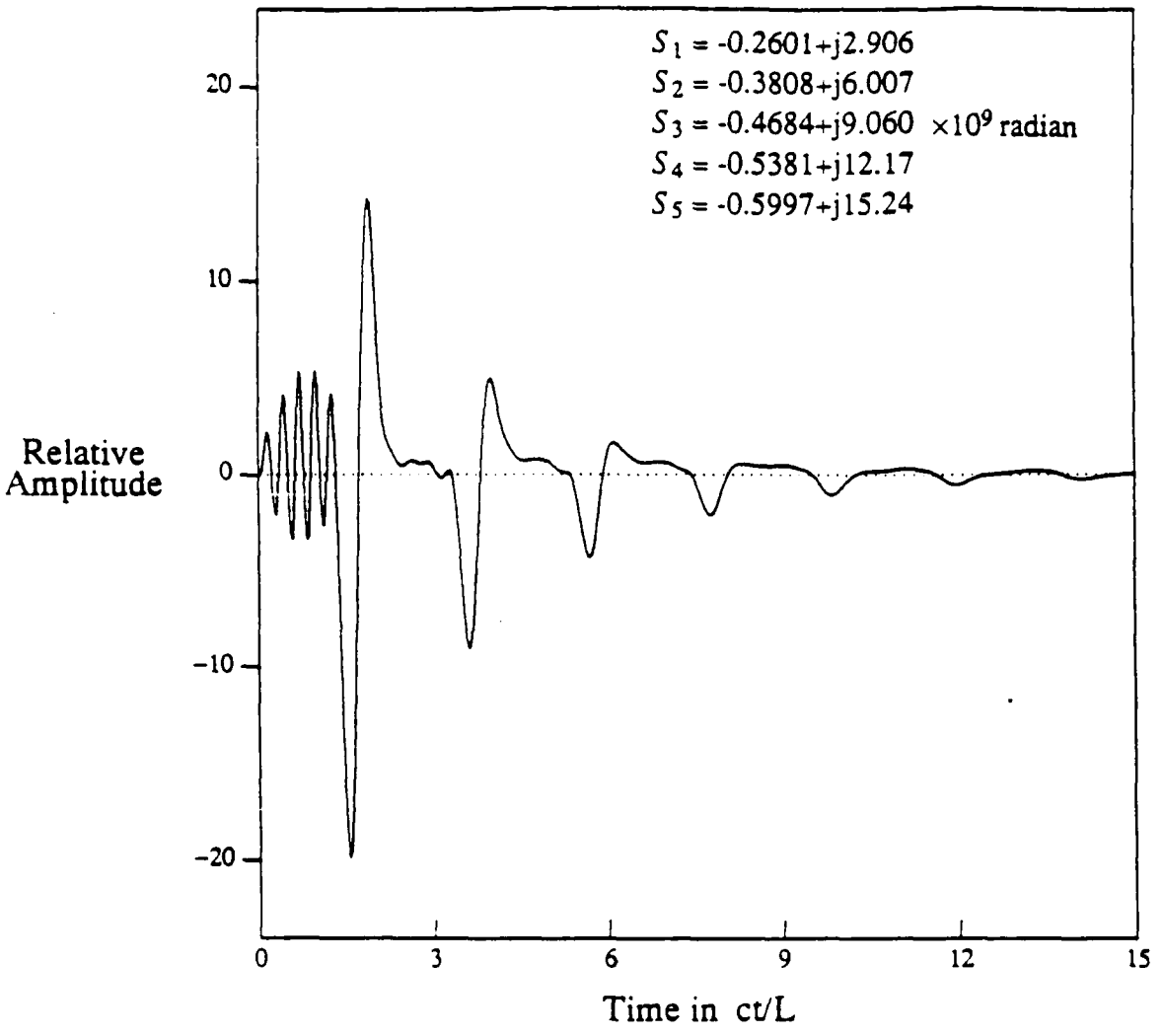

Fig. 3 The impulse response of a 30 cm thin wire with a 45^0 angle w.r.t. to the incident direction of the exciting wave.

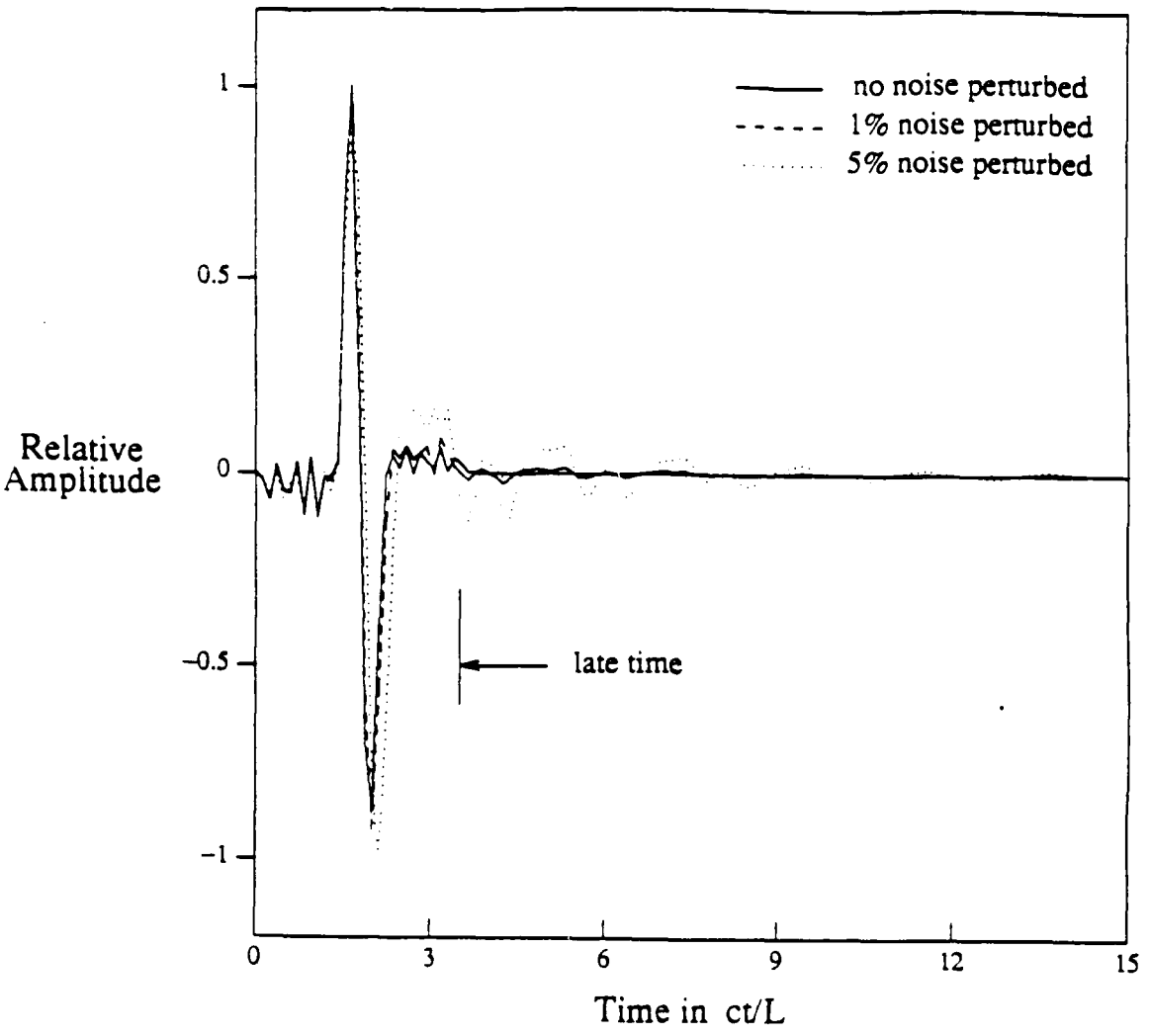

Fig. 4 The impulse response of a 30 cm thin wire ($\theta = 45^0$) is convolved with the E-pulses which are synthesized based on the noise-perturbed natural frequencies of the thin wire.

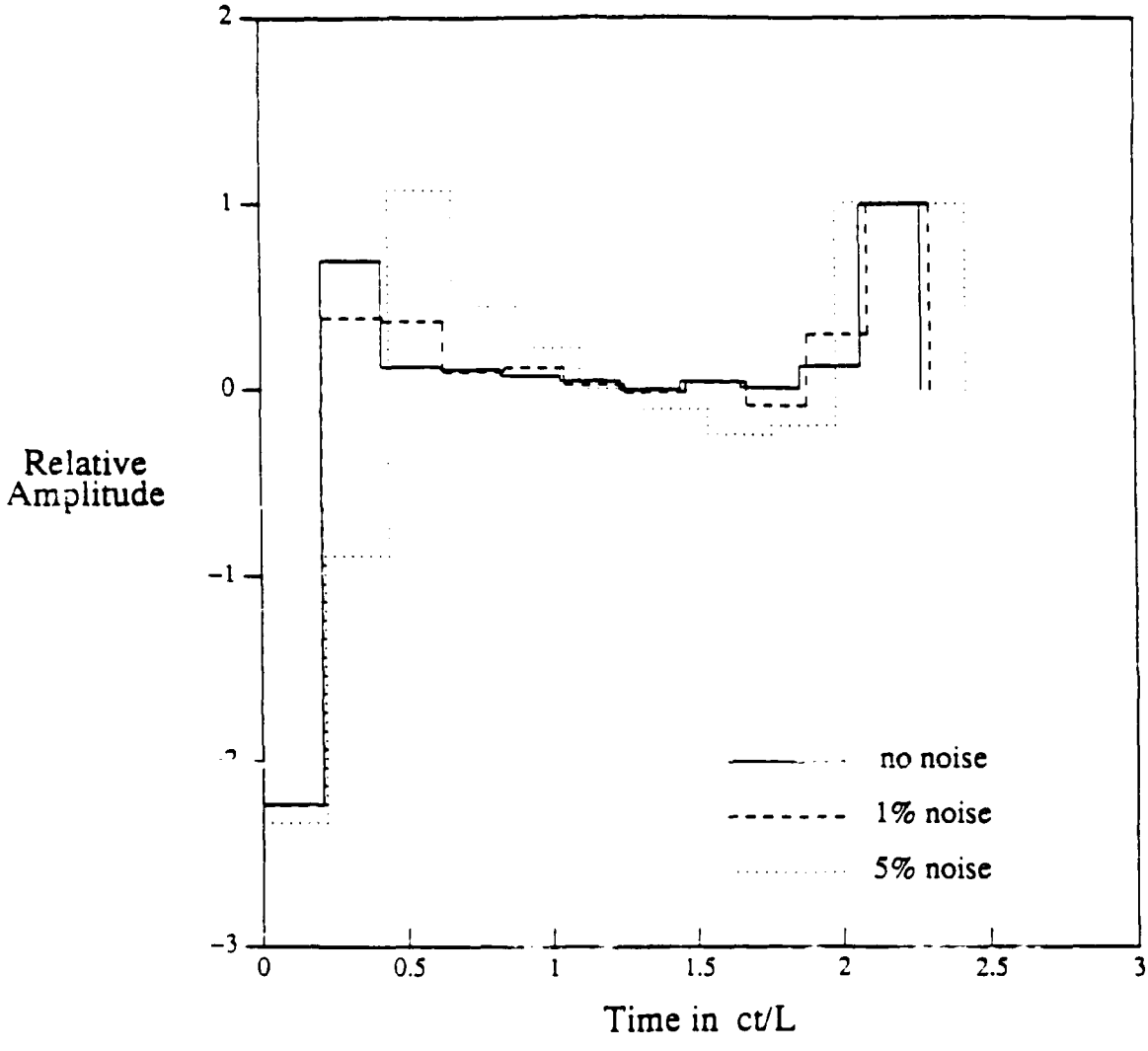

Fig. 5 The E-pulse waveforms synthesized for a 30 cm thin wire based on its first five natural frequencies. The five natural frequencies are perturbed with Gaussian white noise.

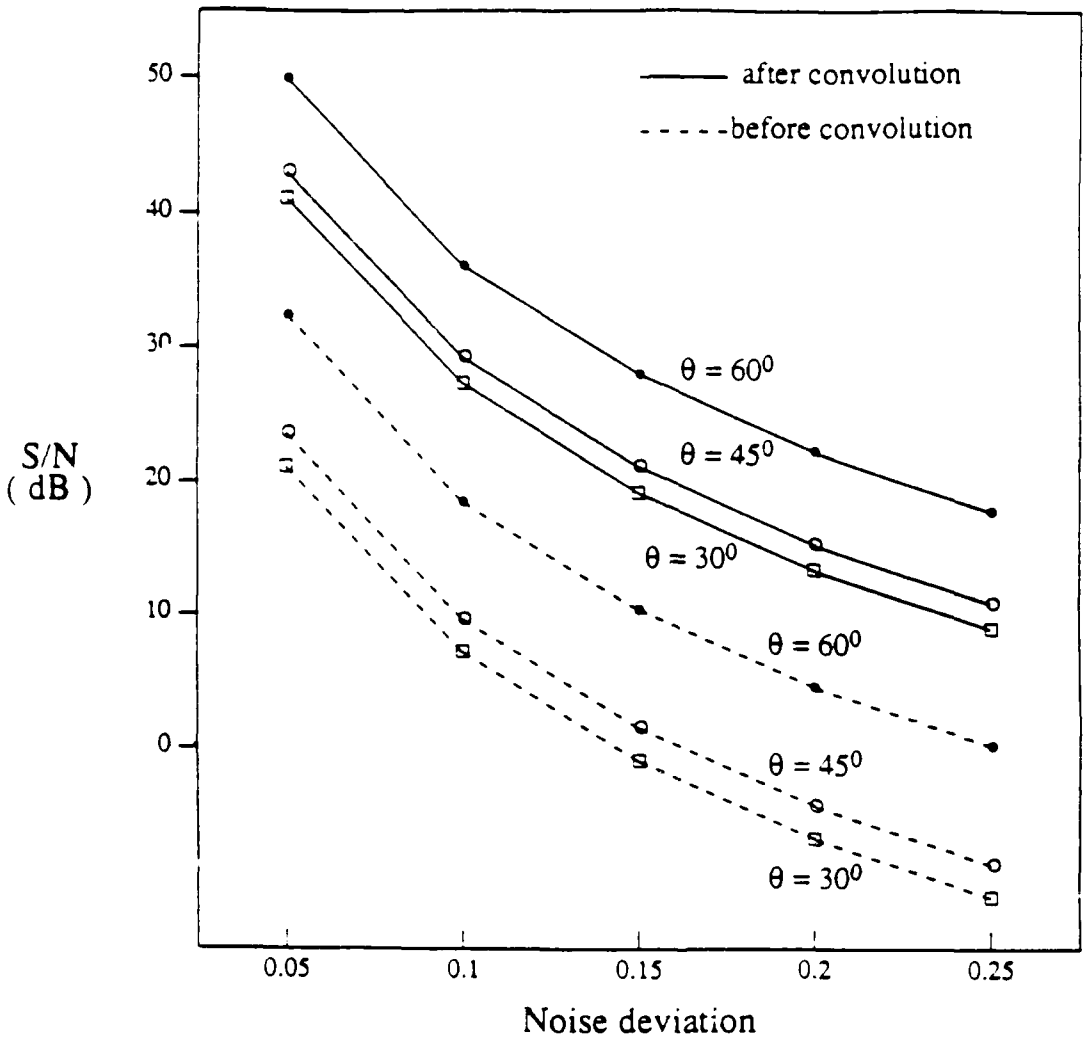

Fig. 6 Comparison of the signal to noise ratios before and after the impulse responses of a 30 cm thin wire are convolved with its E-pulse. The first five natural frequencies are used to construct the impulse responses and to synthesize the E-pulses of the thin wire.

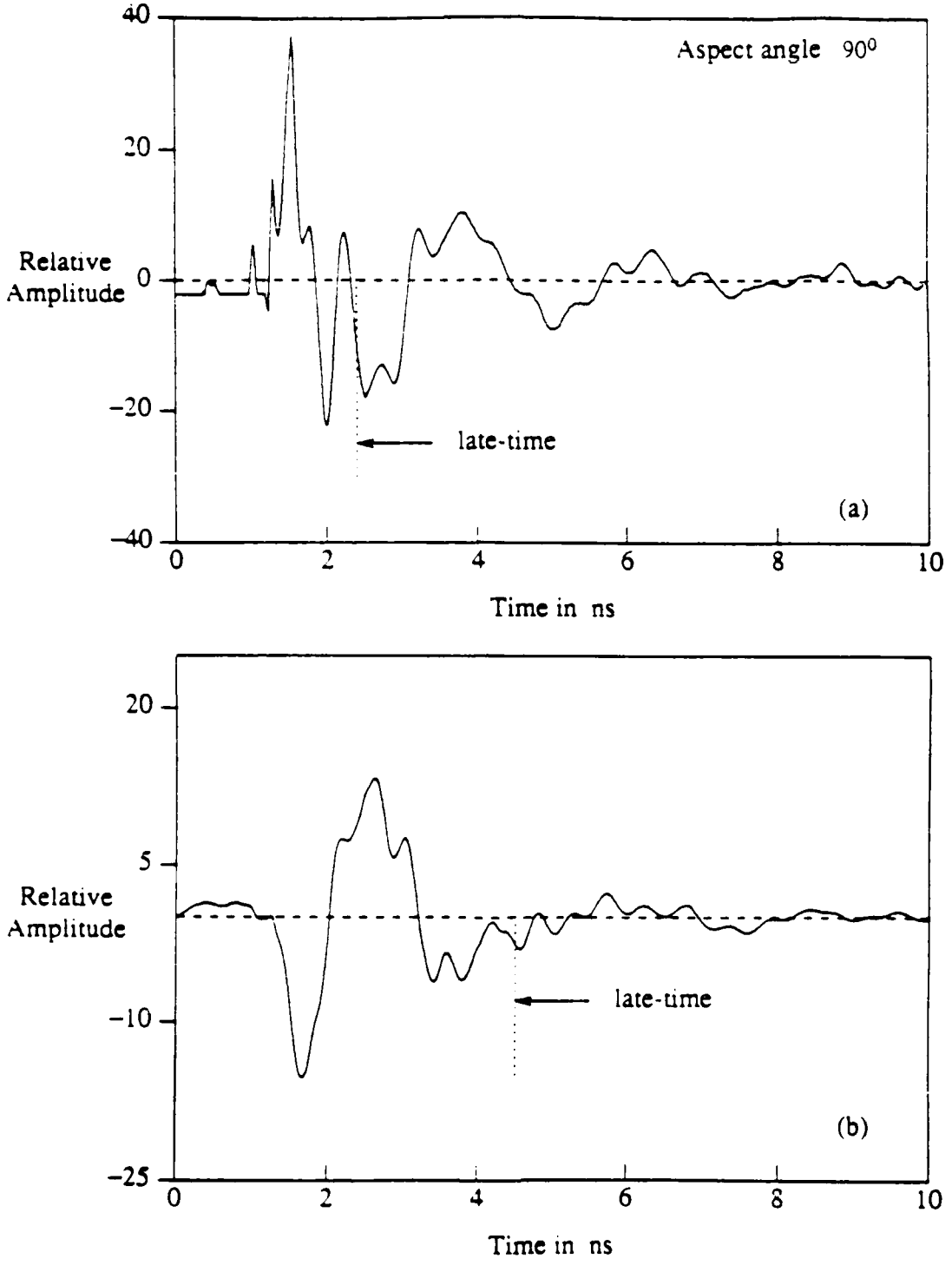

Fig. 7 (a) The measured scattered waveform of B-707 model at aspect angle of 90^0; (b) its convolved response with the E-pulse waveform of B-707 model

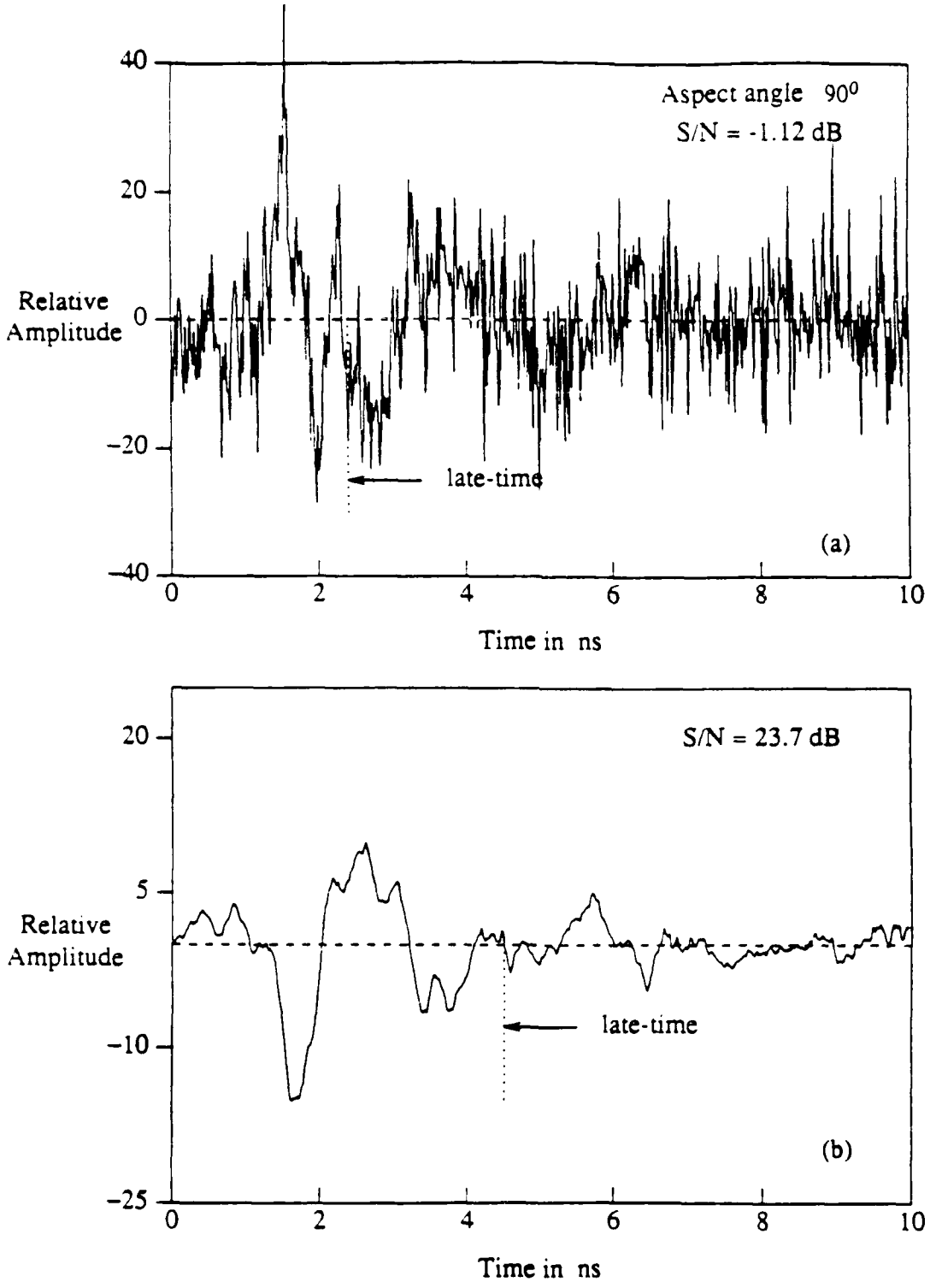

Fig. 8 (a) The noise contaminated (20% of maximum amplitude) scattered waveform of B-707 model at aspect angle of 90^0; (b) its convolved response with the E-pulse waveform of B-707 model

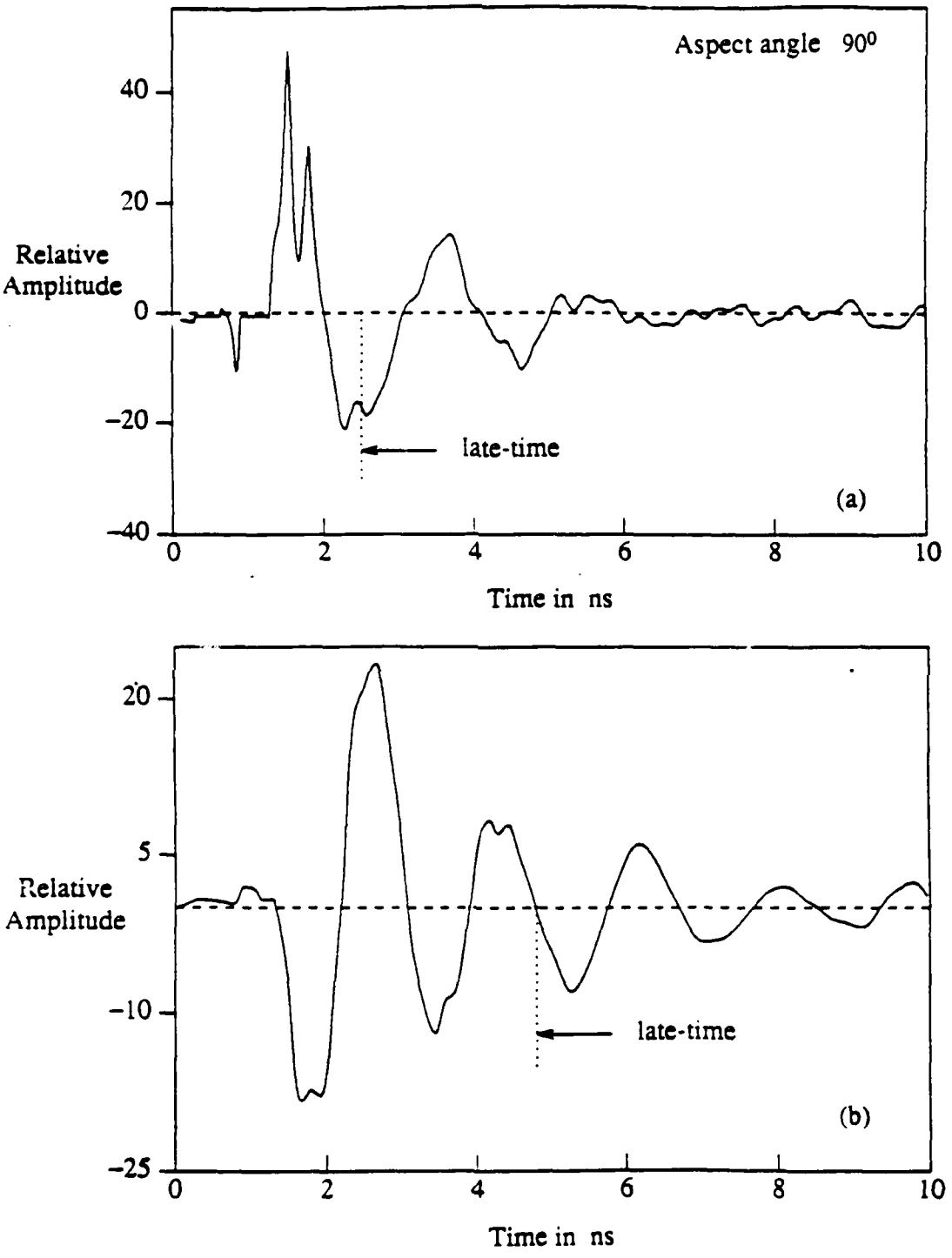

Fig. 9 (a) The measured scattered waveform of F-18 model at aspect angle of 90^0; (b) its convolved response with the E-pulse waveform of B-707 model

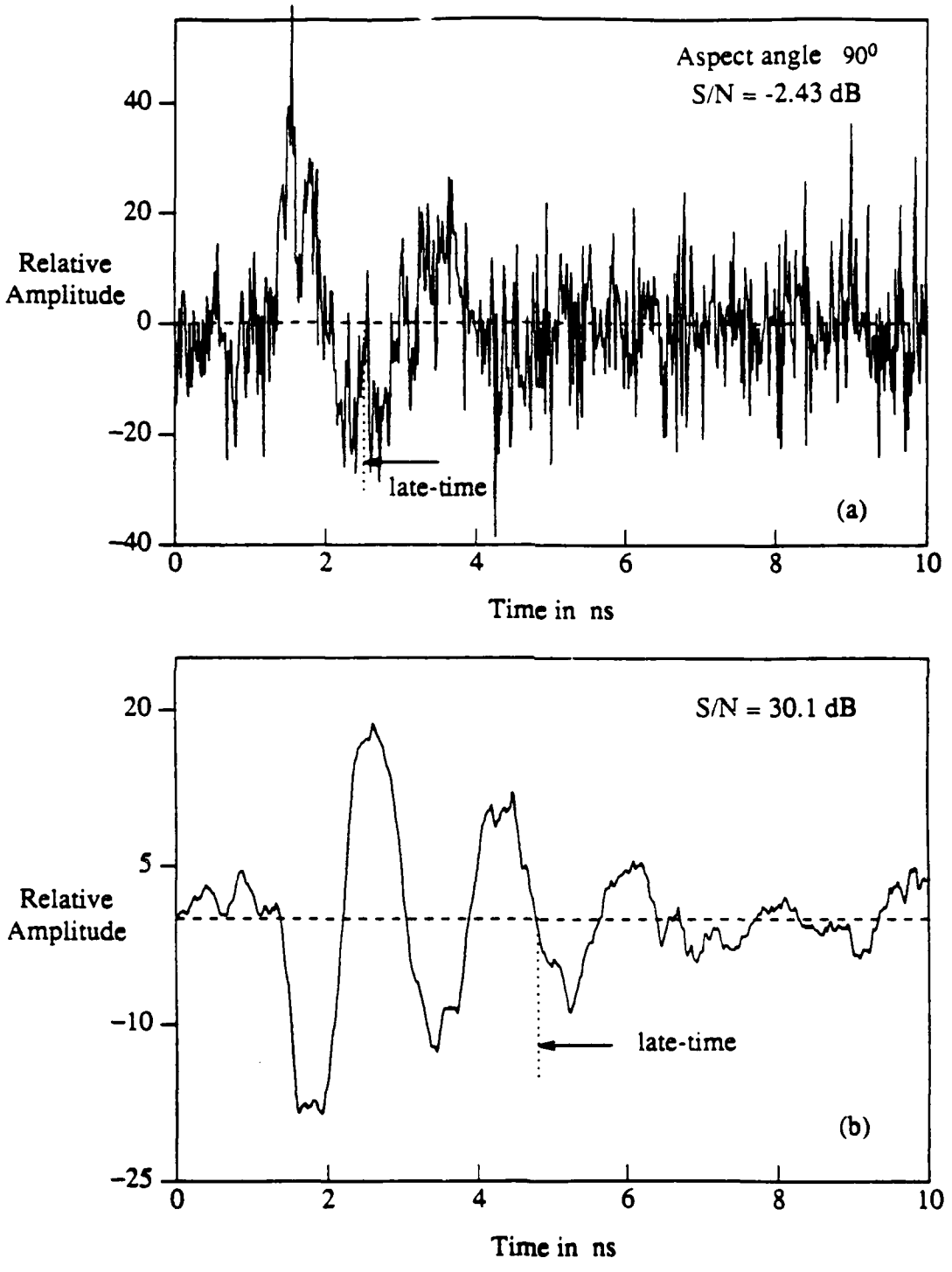

Fig. 10 (a) The noise contaminated (20% of maximum amplitude) scattered waveform of F-18 model at aspect angle of 90^0; (b) its convolved response with the E-pulse waveform of B-707 model

Appendix 11

APPROXIMATE NATURAL RESPONSE OF AN ARBITRARILY SHAPED THIN WIRE SCATTERER

E. J. Rothwell, Member IEEE, J. Baker, Student Member IEEE,
K. M. Chen, Fellow IEEE and D. P. Nyquist, Member IEEE

Department of Electrical Engineering
Michigan State University

ABSTRACT

This paper introduces an approximate but computationally simple technique for calculating the natural current and backscattered field response of an arbitrarily shaped thin wire scatterer. A simple one-term resonant current approximation is shown to yield excellent results for the natural frequencies of perturbed straight wires and circular loops. Comparison with the measured current response of a compound wire target validates the simple theory.

This work was supported by DARPA and ONR under contract N000-14-87-K-0336.

I. INTRODUCTION

The introduction of the singularity expansion method (SEM) by Baum [1] renewed interest in transient electromagnetic scattering by providing a simple means of characterizing the response of a scatterer in terms of its natural resonances. SEM concepts are actively employed in radar target identification, where natural resonances are used as aspect-independent target features [2]. An important facet of target identification is the ability to discriminate targets with subtle differences in geometry, such as aircraft wing angle and length. Since a theoretical study of the effect of slight shifts in resonant frequencies requires the calculation of a large number of sets of frequencies, simple targets such as wires are often employed to minimize computational effort.

To fully understand the effects of small shifts in target geometry on target discrimination it is not necessary to precisely determine the natural frequencies, but rather to accurately quantify their change. To that end, this paper introduces a simple technique for approximating the natural frequencies of an arbitrarily shaped thin wire, providing an efficient means to test target discrimination algorithms.

A straight thin cylinder was one of the first structures to be analyzed using the SEM [3]. It was found that the dominant natural mode currents (those with the smallest temporal damping rates) were nearly sinusoidal, each representing a standing wave due to reflections from the ends of the wire. This simple picture is equally valid for a thin wire bent into an arbitrary shape, and so a sinusoidal current distribution remains a valid approximation for the resonant current. A transcendental equation for the natural frequencies based on this approximation is introduced, and the coupling coefficients for the

current and backscattered field response are specified. Comparison with moment method solutions reveals that the approximate resonant frequencies are quite accurate for modest perturbations from a straight wire or circular loop.

II. TRANSCENDENTAL EQUATION FOR APPROXIMATE NATURAL FREQUENCIES

Consider a thin wire of radius a and length L arranged along an arbitrary axial path Γ in free space, as shown in Fig. 1. The arc length along the wire axis is measured by the variable u with its origin chosen, for convenience, at the origin of coordinates. The wire is illuminated by a transient plane wave field travelling in the direction $\hat{w}$ with time history f(t) and polarization $\hat{v}$. In the Laplace frequency domain this field is

$$\vec{E}^i(\vec{r},s) = \hat{v}E_0F(s)e^{-\gamma w} \tag{1}$$

where

$$w(\vec{r}) = \vec{r}\cdot\hat{w} \tag{2}$$

$$\gamma = \frac{s}{c} \tag{3}$$

and F(s) is the Laplace spectrum of f(t).

Using the thin wire approximation, the current induced on the surface of the wire is replaced by an equivalent axial current I(u). The field produced by

the induced current is then, adopting the approach by Mie [1]

$$\vec{E}(\vec{r},s) = \frac{1}{4\pi\epsilon_0 s}\int_\Gamma \left[\frac{\partial I(u')}{\partial u'}\nabla - \gamma^2 \hat{u}' I(u')\right]\frac{e^{-\gamma R}}{R}du' \tag{4}$$

where

$$R = |\vec{r}-\vec{r}'| \tag{5}$$

and $\hat{u}$ is the unit tangent to the wire axis at the axial point u. Applying the boundary condition on the surface of the wire that the total tangential field must be zero leads to the electric field integral equation (EFIE) for the current induced in the wire

$$\int_\Gamma \left[\frac{\partial I(u')}{\partial u'}\frac{\partial}{\partial u} - \gamma^2 \hat{u}\cdot\hat{u}' I(u')\right]\frac{e^{-\gamma R}}{R}du' = -4\pi\epsilon_0 s\hat{u}\cdot\hat{v}E_0 F(s)e^{-\gamma w} \quad \text{all } u\in\Gamma \tag{6}$$

Here, by the thin wire approximation, R is the distance from an axial source point at axial position u' to a field point on the wire surface at axial position u.

The natural resonances of the wire are defined through the unforced solutions to (6). Spatially weighting (6) by the natural mode current distribution gives a transcendental equation for the natural frequencies of the wire $\{s_n\}$

$$\int_\Gamma I(u)\int_\Gamma\left[\frac{\partial I(u')}{\partial u'}\frac{\partial}{\partial u} - \gamma^2\hat{u}\cdot\hat{u}'I(u')\right]\frac{e^{-\gamma R}}{R}du\,du' = 0 \tag{7}$$

which could be solved if I(u) were known. Integrating by parts, and using the boundary condition that the current must be zero at the ends of an open wire, or continuous on a closed loop, gives the more stable equation

$$\int_\Gamma\int_\Gamma\left[\frac{\partial I(u)}{\partial u}\frac{\partial I(u')}{\partial u'} + \gamma^2\hat{u}\cdot\hat{u}'I(u)I(u')\right]\frac{e^{-\gamma R}}{R}du\,du' = 0 \tag{8}$$

where the derivative has been removed from the Green's function.

A typical approach to determining the natural frequencies is to solve the homogeneous version of (6) for the natural mode current distribution and the natural frequencies simultaneously. This requires a tedious moment method solution, where the wire is discretized and a large matrix equation is solved repeatedly during a root search [2]. Since there is no way of predetermining the current distribution, the resulting natural frequencies are often hard to separate.

A much simpler approximate solution for the natural frequencies can be obtained by solving (8) with an appropriate approximation of the natural current. It is well known that the dominant (first layer) resonant modes of a thin wire are highly sinusoidal such that a satisfactory approximation for the nth mode current distribution is

$$I(u) = I_n(u) \sim \sin\left(n\pi\frac{u}{L}\right) \qquad n = 1,2,... \tag{9}$$

with an appropriate phase factor included for closed loop wires. Substituting (9) into (8) gives a simple transcendental equation for the nth mode natural frequencies of the wire

$$F^+(s) - F^-(s) = 0 \tag{10}$$

where

$$F^{\pm}(s) = \int_\Gamma \int_\Gamma \left[\left(\frac{n\pi}{L}\right)^2 \pm \gamma^2 \hat{u}\cdot\hat{u}'\right] \frac{e^{-\gamma R}}{R} \cos\frac{n\pi}{L}(u \mp u')\, du\, du' \tag{11}$$

It is interesting to note that a zeroth order solution for the natural frequencies can be obtained using the crude approximation

$$\frac{e^{-\gamma R}}{R} \sim \delta(u-u') \tag{12}$$

which yields

$$F^{\pm}(s) \sim \left[\left(\frac{n\pi}{L}\right)^2 \pm \gamma^2\right] \int_\Gamma \cos\frac{n\pi}{L}(u \mp u)\, du \sim \begin{cases} L\left(\frac{n\pi}{L}\right)^2 + L\gamma^2 \\ 0 \end{cases} \tag{13}$$

Using (10) then gives

$$s_n = \pm j\frac{n\pi c}{L} \tag{14}$$

which are the expected simple non-radiating resonant mode natural frequencies.

III. CALCULATION OF LATE-TIME TRANSIENT CURRENT INDUCED ON WIRE

The approximate late-time transient current induced in the thin wire can be written as a singularity expansion over the dominant natural mode current distributions [1]. In the frequency domain this expansion is

$$I(u,s) = \sum_{n=1}^{2N} a_n(s_n)(s-s_n)^{-1} I_n(u) \tag{15}$$

where N is the number of dominant modes excited by the incident pulse waveform f(t), $a_n(s_n)$ is the class-1 coupling coefficient for the nth mode and $I_n(u)$ is given by (9). Note that both the coupling coefficients and the natural frequencies appear in complex conjugate pairs; i.e., $s_k = s_{k+N}^*$, where * denotes the complex conjugate.

The coupling coefficients are excitation dependent and can be computed as follows. Substituting the singularity expansion (15) into the integral equation (6), multiplying both sides by the current distribution of the mth mode and integrating gives

$$\sum_{n=1}^{2N} a_n(s_n)(s-s_n)^{-1} \int_\Gamma du I_m(u) \int_\Gamma \left[\frac{\partial I_n(u')}{\partial u'} \frac{\partial}{\partial u} - \gamma^2 \hat{u} \cdot \hat{u}' I_n(u') \right] \frac{e^{-\gamma R}}{R} du' - \\ = -4\pi s \varepsilon_0 E_0 F(s) \int_\Gamma I_m(u) \hat{u} \cdot \hat{v} e^{-\gamma w} du \tag{16}$$

Integrating by parts twice and using the boundary conditions on current at the ends of the wire allows the roles of I_n and I_m to be swapped. Using reciprocity of the Green's function then gives

$$\sum_{n=1}^{2N} a_n(s_n)(s-s_n)^{-1} \int_\Gamma du I_n(u) \int_\Gamma \left[\frac{\partial I_m(u')}{\partial u'} \frac{\partial}{\partial u} - \gamma^2 \hat{u} \cdot \hat{u}' I_m(u') \right] \frac{e^{-\gamma R}}{R} du' - \\ = -4\pi s \varepsilon_0 E_0 F(s) \int_\Gamma I_m(u) \hat{u} \cdot \hat{v} e^{-\gamma w} du \tag{17}$$

Now, taking the limit as $s \to s_m$, the left hand side is seen to be zero by virtue of the definition of a natural mode (7) for all terms in the sum except n=m. The n=m term produces an indeterminate form which can be evaluated using l'Hopital's rule to yield the class-1 coupling coefficient. Substituting the approximate current distribution (9) gives the approximate class-1 coupling coefficients for the dominant (first layer) modes

$$a_n(s_n) = -\frac{4\pi s_n \epsilon_0 E_0 F(s_n)}{C_n} Q_n(s_n) \tag{18}$$

where

$$Q_n(s_n) = \int_\Gamma \sin\left(n\pi \frac{u}{L}\right) \hat{u}\cdot\hat{v} e^{-\gamma_n w} du \tag{19}$$

Here C_n is a normalization coefficient given by

$$C_n = C_n^+ - C_n^- \tag{20}$$

where

$$C_n^\pm = \frac{1}{2c}\int_\Gamma\int_\Gamma \left[R\left(\frac{n\pi}{L}\right)^2 \mp \hat{u}\cdot\hat{u}'\gamma_n(2-R\gamma_n)\right]\cos\frac{n\pi}{L}(u\mp u')\frac{e^{-\gamma_n R}}{R} du\,du' \tag{21}$$

The late-time current response of the thin wire can now be evaluated by inverting (15)

$$I(u,t) = \sum_{n=1}^{N} \sin\left(n\pi \frac{u}{L}\right)\left[a_n(s_n)e^{s_n t} + a_n^* e^{s_n^* t}\right] \tag{22}$$

IV. CALCULATION OF BACKSCATTERED FIELD

Once the transient current on the wire has been found, the far zone backscattered field is easily calculated by integrating over the current distribution. The far zone field scattered by the wire can be calculated by keeping terms only to 1/R in the general formulation for the transient field radiated by a current source [6]. This gives

$$\vec{E}(\vec{r},s) = \frac{\mu_0}{4\pi}\int_\Gamma \hat{R}\times\hat{R}\times\hat{u}'\frac{I'\left(u',s-\frac{R}{c}\right)}{R}du' \tag{23}$$

Using the standard far zone approximations that

$$R \approx r-\hat{r}\cdot\vec{r}' \tag{24}$$

in the time shift factor while

$$R \approx r \tag{25}$$

in the denominator, and

$$\hat{R} \approx \hat{r} \tag{26}$$

leads to

$$\vec{E}(\vec{r},s) = \frac{\mu_0}{4\pi}\hat{r}\times\hat{r}\times\int_\Gamma \hat{u}'I'\left(u',s-\frac{r}{c}+\frac{\hat{r}\cdot\vec{r}'}{c}\right)du' \tag{27}$$

as the far-zone scattered field.

Substituting the current expansion (22) into the scattered field formula (27) and noting that in the backscattered direction

$$\hat{r} = -\hat{w}\hat{r} = -w \tag{28}$$

gives the backscattered field

$$\vec{E}(r,t) = \frac{\mu_0}{4\pi r}\sum_{n=1}^{N}\int_{\Gamma}(\hat{w}\times\hat{w}\times\vec{u})\sin\left(n\pi\frac{u}{L}\right)\left[s_n a_n e^{s_n\tau}e^{-\gamma_n w} + s_n^* a_n^* e^{s_n^*\tau}e^{-\gamma_n^* w}\right]du \tag{29}$$

where $\tau = t - r/c$. Finally, remembering that the field polarization of the incident field $\hat{v}$ must be orthogonal to the direction of propagation $\hat{w}$ leads to

$$E_v(r,t) = \hat{v}\cdot\vec{E}(r,t) = -\frac{\mu_0}{4\pi r}2\sum_{n=1}^{N} Re\left\{s_n a_n(s_n)Q_n(s_n)e^{s_n\tau}\right\} \tag{30}$$

for the polarization matched component of the far-zone backscattered field, where $Q_n(s_n)$ was defined in (19), and Re indicated the real part.

V. EXAMPLES

As a simple first example, consider a plane wave with a unit step time history incident on a straight thin wire as shown in Fig. 2. The natural frequencies $s_n = \sigma_n + j\omega_n$ obtained by solving (10) are shown in the figure for the

first ten dominant modes of the wire, along with the natural frequencies obtained by solving the homogeneous version of (6) using the method of moments [3]. Agreement is seen to be excellent for the imaginary parts, with a maximum error of less than one per cent. The real parts are less accurate, showing a maximum error of about 12%. Both these errors increase with modal index, as expected, since the resonant current approximation (9) is most accurate for modes with the least spatial variation of current.

Also shown in Fig. 2 is the current response to the incident step plane wave, calculated at u=0.75L using (18) in (22) and the first ten dominant modes. A comparison with the moment method results of Michalski [4, Fig. 3] shows excellent agreement, suggesting that the relatively high error in the real parts of the natural frequencies does not lead to an equivalently high error in predicting the current response. This is not surprising. Based on experience in mode extraction, accurate modelling of a response with natural modes is highly insensitive to variations in the real parts of the natural frequencies, making them difficult to extract from data [5].

Note that the time origin for the current response is at the first moment the incident wave strikes the cylinder. Thus, the response should be zero until t=0.65L/c, the time the incident field reaches the observation point at u=0.75L. That this is not so is a reflection of the inability of the class-1 coupling coefficients to accurately represent the early-time response of the wire. However, as explained in [4], the causal portion of the response is adequately modelled using class-1 coefficients.

The backscattered field step response of the cylinder shown in Fig. 2 has also been calculated. Using (30) with the first ten approximate natural frequencies yields the electric field waveform shown in Fig. 3. Note that since

the early-time current response was not accurately modelled using class-1 coefficients, the early-time of the backscattered field response will also be inaccurate. However, the late-time portion, beginning at t=1.73L/c, a time equal to the two-way transit time of the cylinder times the cosine of the incidence angle, should be well approximated. Note that it is this late-time period which is needed in the study of radar target discrimination schemes such as the E-pulse and K-pulse methods [6].

As a second example, consider a thin wire elliptical loop, as shown in Fig. 4. The natural mode current distributions on the loop demonstrate two types of symmetry, corresponding to either the sinusoidal or cosinusoidal distributions in a circular loop. The current for sine modes is approximated using (9) while cosine modes require a 90^0 phase shift. The n=1 natural frequencies found by solving (10) are compared in Fig. 4 with those found using a moment method solution [7], as a function of ellipse eccentricity. Again, agreement is seen to be very good, with the best results coming for the smallest eccentricity. This is expected, since zero eccentricity corresponds to a circular loop, which in fact has true sinusoidal natural mode current distributions [8].

Similar results are obtained for segmented wires as shown in Fig. 5. Here a thin wire has been bent at its midpoint through a series of angles and the n=1 natural frequency has been calculated by solving (10). A comparison with results obtained using the moment method for a right angle bend [9] shows reasonable agreement.

As a last example, a compound bent wire has been constructed and its current response to a one-nanosecond-pulse wavefront has been measured above a conducting ground plane. The result is shown in Fig. 6. (Only one half of the target was actually used, and only the odd modes were excited, due to the image

effect. For a description of the MSU transient measurement range, see [10]). A small circular loop current probe was used to sample the magnetic field near the surface of the wire, and thus the measured response is proportional to, by Faraday's law, the derivative of the current response. The natural frequencies of the wire were extracted from the late-time portion of the measured response using an E-pulse technique [11] and are compared in Fig. 6 to those calculated by solving (10). Agreement between the approximate theory and experiment is seen to be excellent for the imaginary parts.

The current response of the compound wire has also been calculated, by first finding the impulse response using $F(s)=1$ in (18) and then convolving with the measured incident pulse waveform. Rather than attempting to integrate the measured data to compare to the theory (an often difficult task, due to a pesky DC offset present in the measured data), the theoretical current distribution (22) has been analytically differentiated and the result plotted in Fig. 6. Agreement during the late-time period is seen to be quite good.

VI. DISCUSSION

This paper has introduced a simple approximation for the portion of the natural response of an arbitrarily shaped thin wire scatterer that results from the dominant (first layer) modes. Numerical and experimental results show that the approximation is quite good. It is important to note that while modes of higher complexity have been ignored in this simple analysis, they are not often of practical value. The real parts of the simple first layer resonant modes are usually much smaller (in magnitude) than those of more complex modes, and thus

dominate the response. This is especially true of measured responses, where modes of higher complexity fall beneath the noise level. Thus, good agreement was seen between the measured and approximate responses of the compound wire target of Fig. 6, even though higher complexity modes were ignored in the analysis.

The benefits of using the approximate approach are twofold. First, by specifying the order of the resonance (i.e., picking n) the complexity of solving for the natural frequencies is reduced compared to the moment method. When using the moment method, all the frequencies are determined from the same homogeneous matrix equation, and their existence depends on the level of discretization of the wire or representation of the current. (That is, if the current is not allowed sufficient freedom to oscillate, higher order frequencies cannot be obtained).

Second, the simple transcendental equation (10) is very stable (i.e., not highly sensitive to integration accuracy), and allows for a rapid solution for the natural frequencies. Many frequencies of a quite complicated wire can be obtained in just a few minutes on an ordinary PC. This is extremely valuable when the transient responses of several similar targets are needed for a parametric analysis. For instance, it is possible to generate a large amount of data for wire targets with slightly different geometries for use in evaluating radar target identification schemes. In fact, since the change in natural frequency is what affects the ability to discriminate, the approximate frequencies are often sufficiently accurate.

As a last note, it is straightforward to generalize this approach to arrays of thin wires of arbitrary shape. The natural frequencies are then obtained by solving a determinental equation of order equal to the number of wires involved.

REFERENCES

[1] C.E. Baum, "The singularity expansion method," Transient Electromagnetic Fields, L.B. Felsen Ed. New York: Springer-Verlag, 1975.

[2] E. Rothwell, K.M. Chen, D.P. Nyquist and W.M. Sun, "Frequency domain E-pulse synthesis and target discrimination," IEEE Transactions on Antennas and Propagation, vol. AP-35, pp. 426-434, April 1987.

[3] F.M. Tesche, "On the analysis of scattering and antenna problems using the singularity expansion method," IEEE Transactions on Antennas and Propagation, vol. AP-21, pp. 53-62, Jan. 1973.

[4] K.A. Michalski, "On the class 1 coupling coefficient performance in the SEM expansion for the current density on a scattering object," Electromagnetics, vol. 2, pp. 201-209, 1982.

[5] E. Rothwell, K.M. Chen and D.P. Nyquist, "Extraction of the natural frequencies of a radar target from a measured response using E-pulse techniques," IEEE Transactions on Antennas and Propagation, vol. AP-35, pp.715-720, June 1987.

[6] F.Y.S. Fok and D.L. Moffatt, "The K-pulse and the E-pulse," IEEE Transactions on Antennas and Propagation, vol. AP-35, pp. 1325-1326, Nov. 1987.

[7] E. Rothwell and N. Gharsallah, "Determination of the natural frequencies of a thin wire elliptical loop," IEEE Transactions on Antennas and Propagation, vol. AP-35, pp. 1319-1324, Nov. 1987.

[8] R.F. Blackburn and D.R. Wilton, "Analysis and synthesis of impedance-loaded loop antenna using the singularity expansion method," IEEE Transactions on Antennas and Propagation, vol. AP-26, pp. 136-140, Jan. 1978.

[9] K. Umashankar and D. Wilton, "Transient scattering of an L-shaped wire using the singularity expansion method," IEEE Transactions on Antennas and Propagation, vol. AP-23, pp. 838-841, Nov. 1975.

[10] N. Gharsallah, E. Rothwell, K.M. Chen and D.P. Nyquist, "Identification of the natural resonances of a conducting sphere from a measured response," IEEE Transactions on Antennas and Propagation, vol. AP-38, pp. 141-143, Jan. 1990.

[11] E.J. Rothwell and K.M. Chen, "A hybrid E-pulse/least squares technique for natural resonance extraction," Proceedings of the IEEE, pp. 296-298, March 1988.

FIGURE CAPTIONS

Fig. 1. Geometry of an arbitrarily shaped thin wire scatterer.

Fig. 2. First ten natural frequencies s_nL/c of a thin cylinder, and surface current step response at u=0.75L calculated using first ten frequencies of approximate theory.

Fig. 3. Backscattered field step response of a thin cylinder, calculated using first ten frequencies of approximate theory.

Fig. 4. Variation of the n=1 sine and cosine mode resonant frequencies with eccentricity for a thin wire elliptical loop.

Fig. 5. Variation of the n=1 resonant frequency with bend angle for a bent wire.

Fig. 6. First six odd mode frequencies s_nx10^{-9} of a compound wire, and comparison of measured current pulse response with response calculated using first six odd modes of approximate theory.

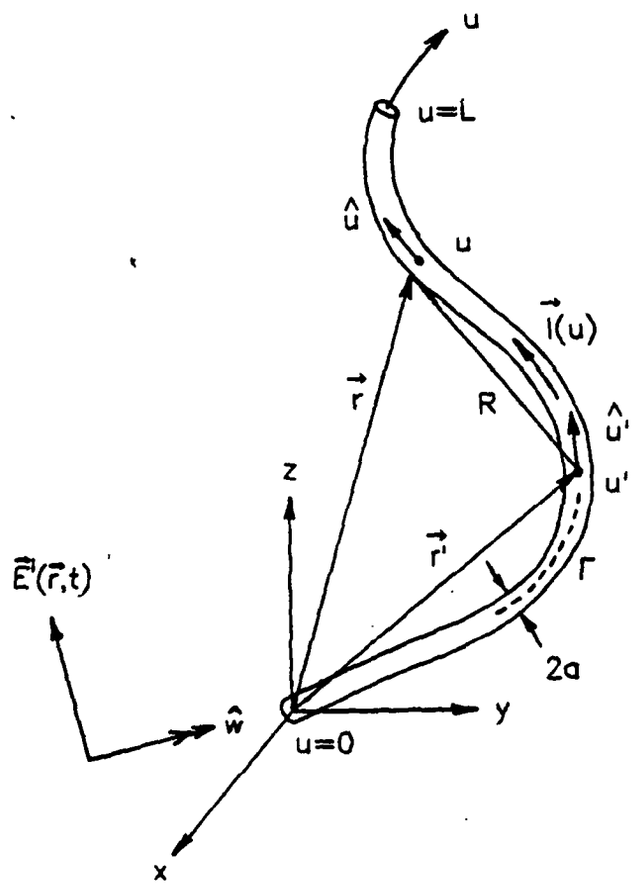

Fig. 1. Geometry of an arbitrarily shaped thin wire scatterer.

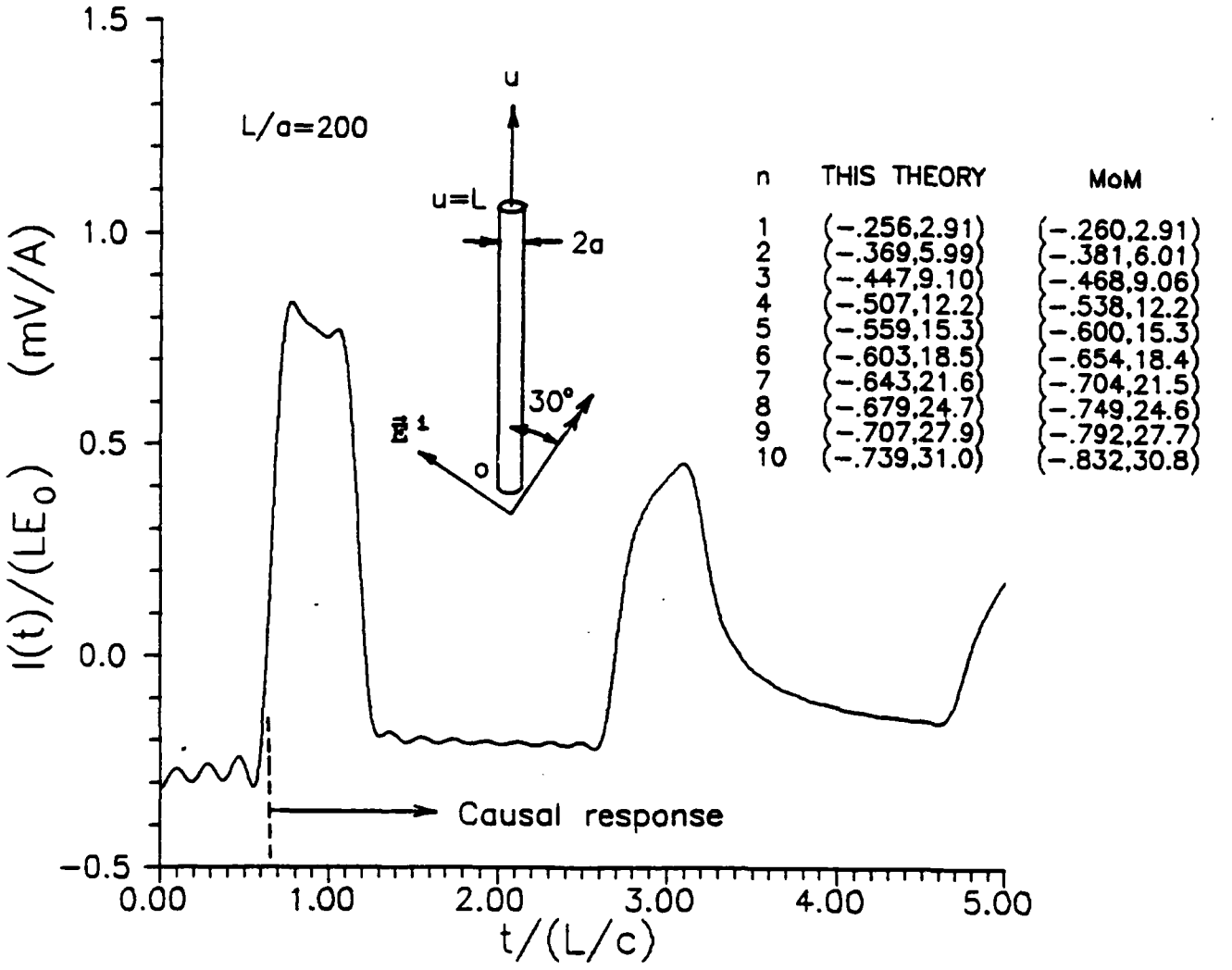

Fig. 2. **First ten natural frequencies s_nL/c of a thin cylinder, and surface current step response at u=0.75L calculated using first ten frequencies of approximate theory.**

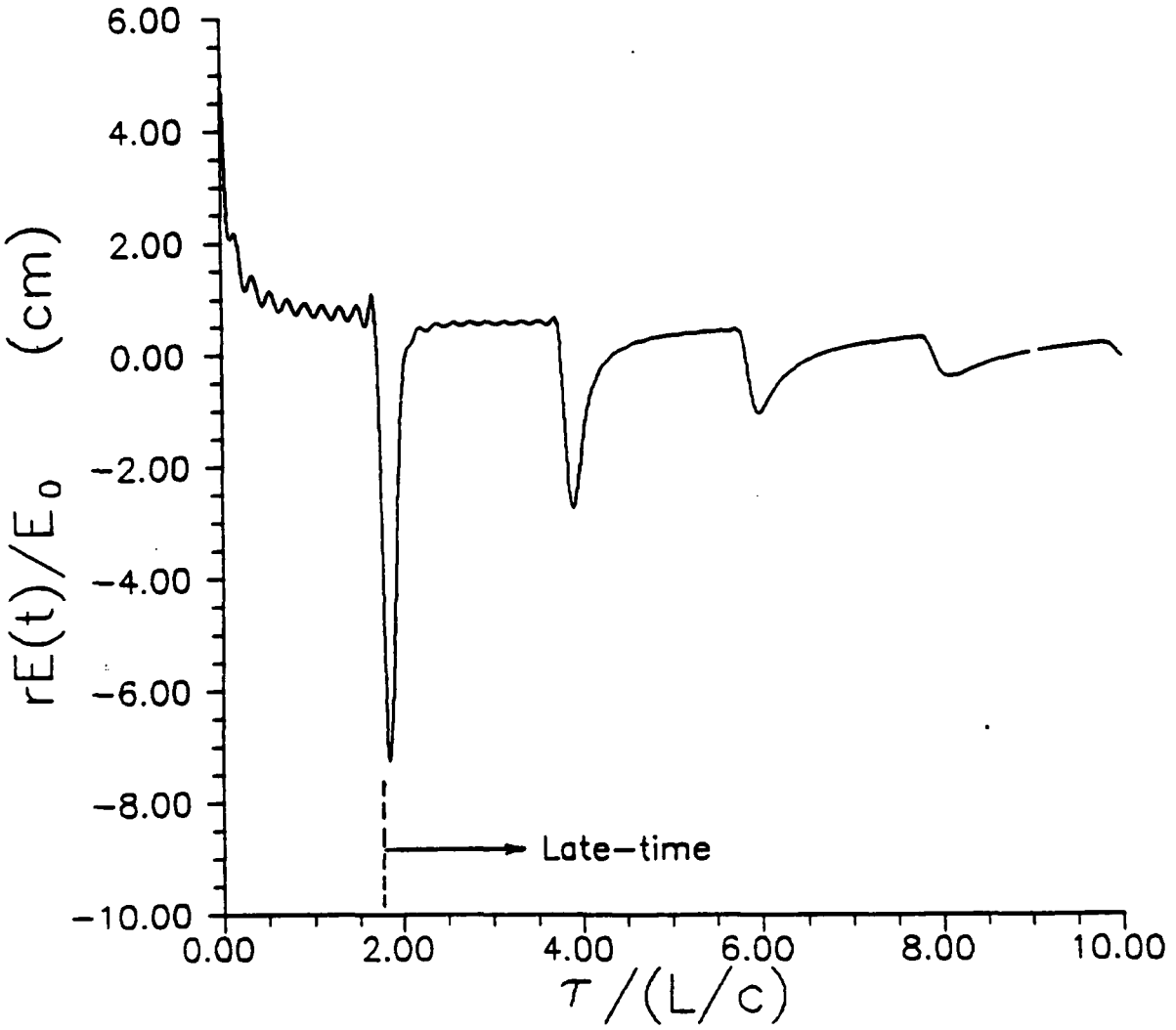

Fig. 3. **Backscattered field step response of a thin cylinder, calculated using first ten frequencies of approximate theory.**

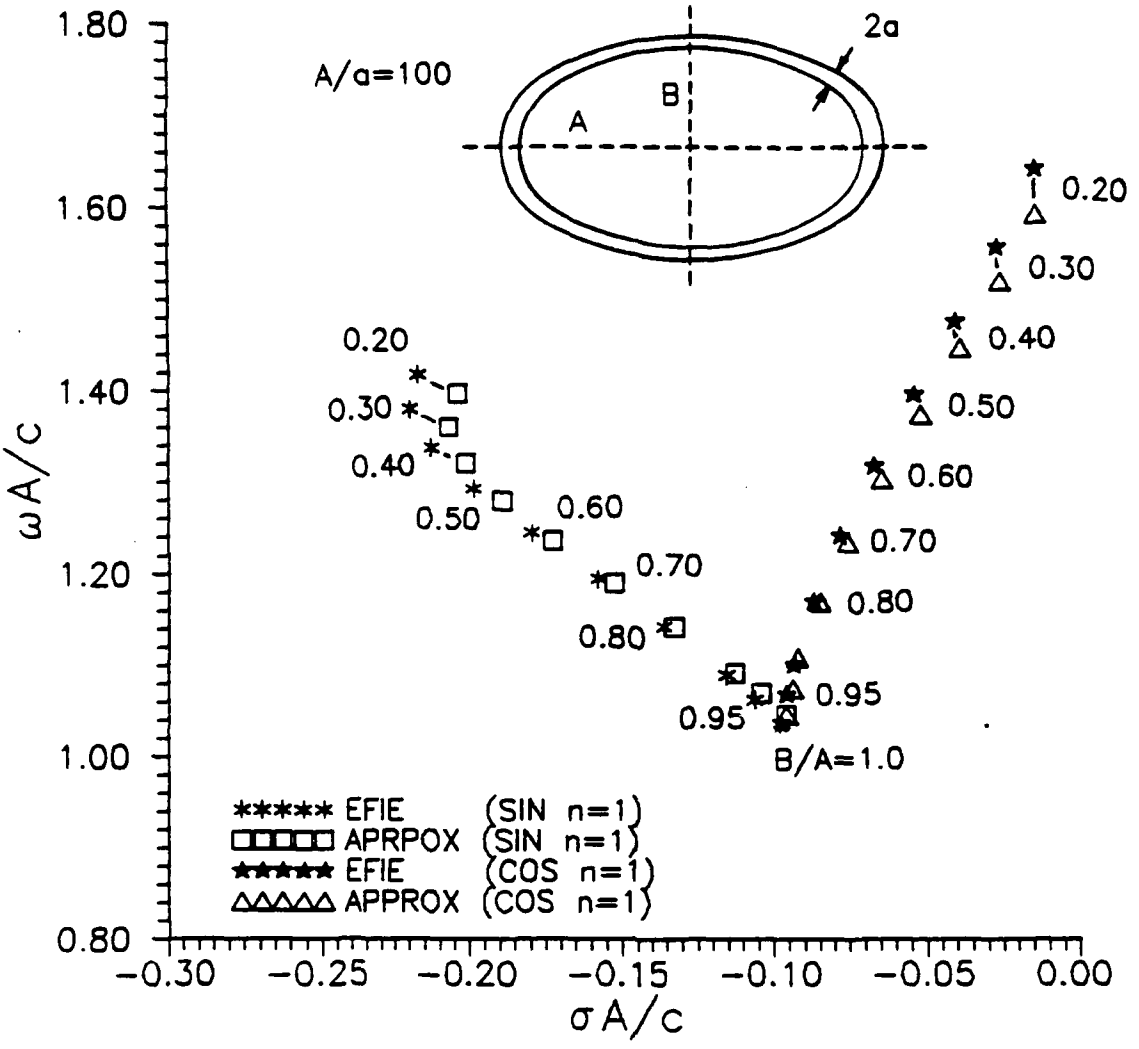

Fig. 4. **Variation of the n=1 sine and cosine mode resonant frequencies with eccentricity for a thin wire elliptical loop.**

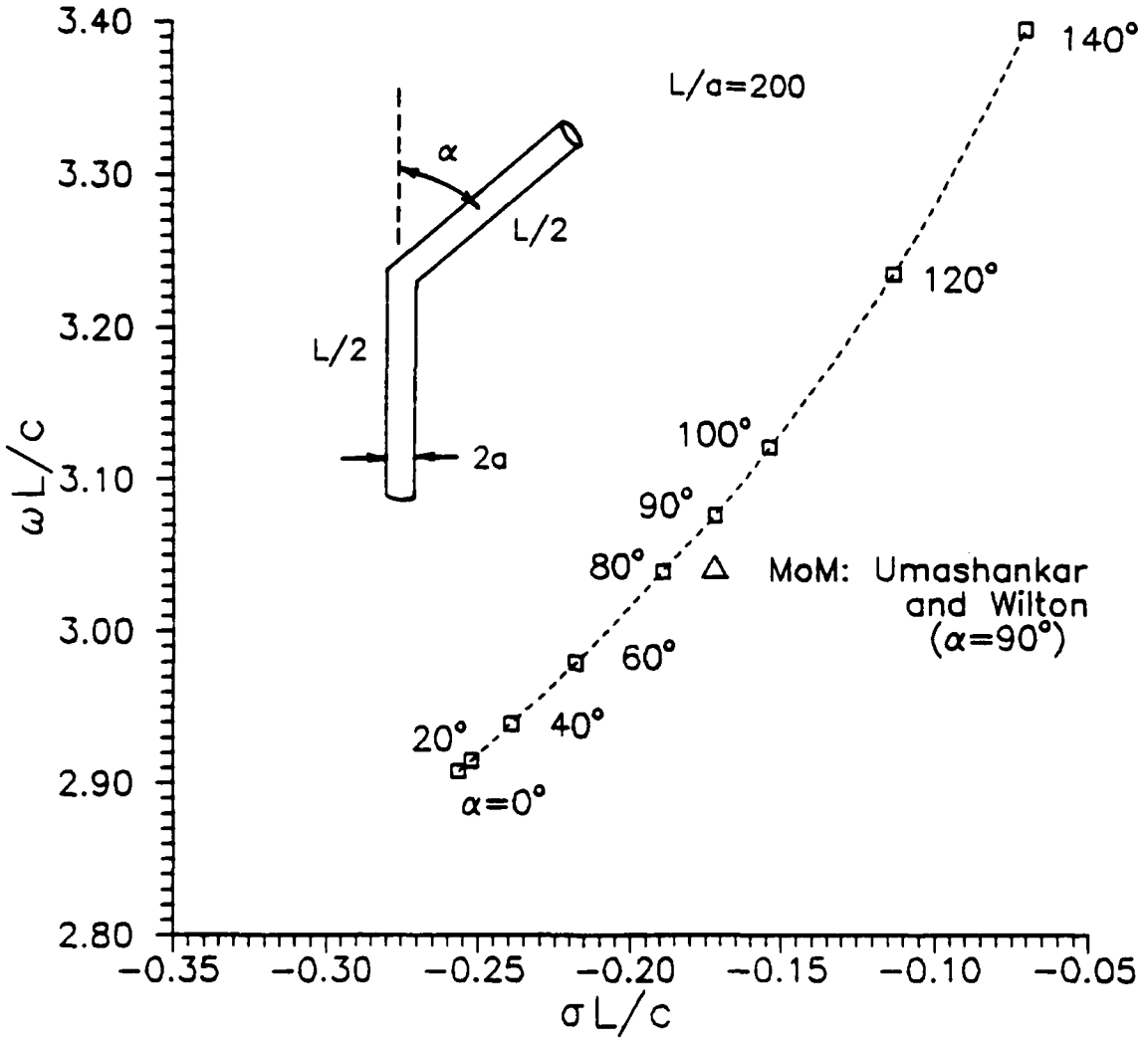

Fig. 5. **Variation of the n=1 resonant frequency with bend angle for a bent wire.**

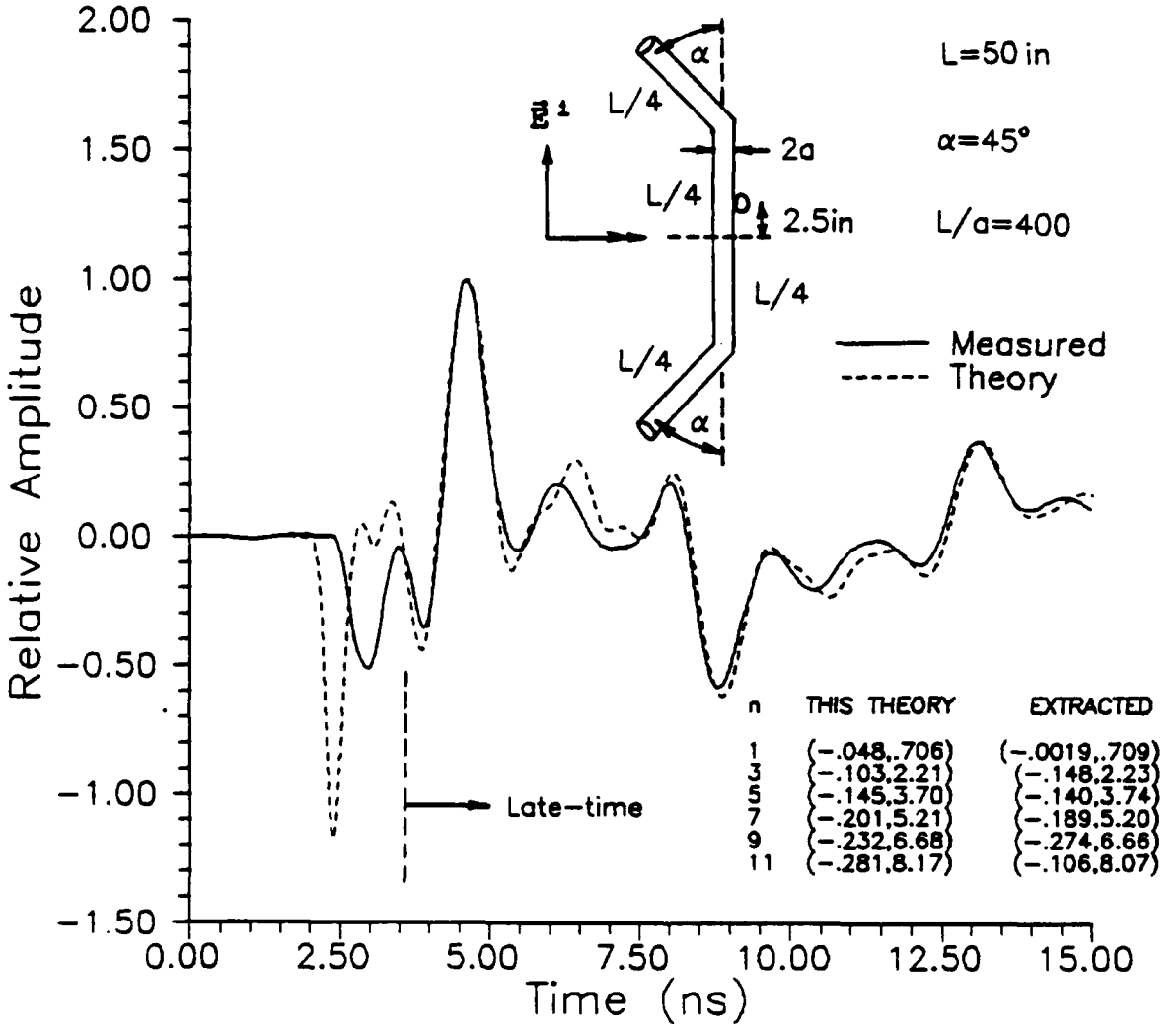

Fig. 6. First six odd mode frequencies $s_n x10^{-9}$ of a compound wire, and comparison of measured current pulse response with response calculated using first six odd modes of approximate theory.